Characterization of seismic sources using sequential spatial clustering and fractal dimension

by

Donna Marie Cortolezzis

A thesis submitted in partial fulfillment of
the requirements for the degree of
Doctor of Philosophy (PhD) in Natural Resources Engineering

The Faculty of Graduate Studies
Laurentian University
Sudbury, Ontario, Canada

THESIS DEFENCE COMMITTEE/COMITÉ DE SOUTENANCE DE THÈSE
Laurentian Université/Université Laurentienne
Faculty of Graduate Studies/Faculté des études supérieures

Title of Thesis Titre de la thèse	Characterization of seismic sources using sequential spatial clustering and fractal dimension
Name of Candidate Nom du candidat	Cortolezzis, Donna Marie
Degree Diplôme	Doctor of Philosophy Science
Department/Program Département/Programme	Natural Resource Engineering
Date of Defence Date de la soutenance	July 30, 2018

APPROVED/APPROUVÉ

Thesis Examiners/Examinateurs de thèse:

Dr. Marty Hudyma
(Supervisor/Directeur de thèse)

Dr. Dougal McCreath
(Committee member/Membre du comité)

Dr. Ming Cai
(Committee member/Membre du comité)

Dr. Phil Dirige
(Committee member/Membre du comité)

Dr. Phil Dight
(External Examiner/Examinateur externe)

Dr. Mostafa Nagizadeh
(Internal Examiner/Examinateur interne)

Approved for the Faculty of Graduate Studies
Approuvé pour la Faculté des études supérieures
Dr. David Lesbarrères
Monsieur David Lesbarrères
Dean, Faculty of Graduate Studies
Doyen, Faculté des études supérieures

ACCESSIBILITY CLAUSE AND PERMISSION TO USE

Abstract

Despite years of research, unexpected seismic events in mines continue to cause damage and loss to people, equipment, infrastructure, and reserves. This research uses novel approaches to characterize the locations, times, and intensity of seismic events for four known seismic sources. The seismic source case studies are the development of a ramp, the abutments around a zone of stopes, a failing stope pillar, and a shear zone adjacent to an orebody. Each seismic source is characterized by sequential spatial clustering, and the fractal dimension of the seismic source parameters of location, time and intensity. The novel application of sequential spatial clustering preserves the sequence of events within a cluster. The method can be used at any point in time which means as a rock mass changes the seismic response is expressed and identified very early on. Once identified, it allows the opportunity for investigation and decision making to take place as the rock mass changes in an unexpected manner. The application of fractal dimension to seismic source parameters revealed that the fractal nature of a parameter is not infinite but exists within a range. The fractal range reflects the character of a seismic source. If some events occur outside the fractal range they also provide important information about the history of the seismic source that occur less often than the fractal range but are still possible. This research has expanded the knowledge of when, where, and how intense seismic events can be expected for four seismic sources using a new sequential spatial clustering method and fractal dimension characterization.

Keywords

mining, seismicity, fractal dimension, sequential spatial clustering

Acknowledgments

This thesis would not have been possible without the support and guidance of my supervisor Dr. Martin Hudyma. Thank you Marty, it has been a privilege to work with you and I am very grateful for this opportunity. I also appreciate the time and support provided by the committee members Drs. Dougal McCreath, Ming Cai, Phil Dirige, Phil Dight, and Mostafa Naghizadeh. Your questions and suggestions are much appreciated. No research is possible without funding. The financial support provided by Laurentian University, NSERC, CAMIRO, and MINERVA have made this research possible. Finally I would like to thank my family for finding humor in every situation; including all the late nights and number of hours I spent on this thesis. You have made me a better person.

Table of Contents

List of Appendices

List of Figures

List of Tables

List of Equations

Glossary

C	-	Cluster
CR	-	Correlation Integral
DBE	-	Distance Between Events
DBNN	-	Distance Between Nearest Neighbours
E	-	Event
IE	-	Inter-Event
M_L	-	Local Magnitude Scale
M_N	-	Nuttli Magnitude Scale
M_R	-	Magnitude Richter Scale
M_W	-	Moment Magnitude
MS	-	Micro Seismic
NN	-	Nearest Neighbour
PDF	-	Probability Density Function
SE	-	Single Events
SGM	-	Strong Ground Motion
SR	-	Source Radius
TBE	-	Time Between Events
TBNN	-	Time Between Nearest Neighbours

Chapter 1

1 Introduction

Seismicity in mines and the hazard it poses to workers has been present and a research topic since the 1930's in Canada. The level of understanding into what causes seismicity in mines has increased tremendously since that time. However, there are still seismic events that occur cannot be anticipated or explained using the existing body of research. This thesis approaches the problem in a new way by characterizing four seismic sources using a new method of sequential spatial clustering and an expanded use of fractal dimension. These methods provide a different approach and new insight into seismic sources in mines that otherwise may go unnoticed until a damaging event occurs.

1.1 Mining Induced Seismicity

Seismic events in a mine are common and result as rock is removed and voids are created. A seismic event is a dynamic stress wave that takes place when a rock mass deforms inelastically. For example, voids created by mining activity leave the rock around it unconfined. As ground stresses act on the rock, it can deform into a void. The complexity of geological structures, different rock mass properties, a changing stress environment, blasting, void size, void shape, stope sequence, mining rate and whether or not backfill is placed in voids all effect how and when a rock mass will fail. The combination of these factors makes the seismic response to mining complex to understand.

1.2 Unexpected Seismic Events

Seismic analysis methods have improved the understanding of the seismic response to mining activity over the last twenty five years. However, not everything is known and unexpected seismic events continue to cause injury, damage, and loss to personnel, equipment, and reserves. The unexpectedness of these events tends to occur either at an unexpected location, time or intensity.

1.2.1 Location

As mining progresses, the seismic events generally locate in the area of mining. From a day to day perspective, the seismic response of the rock mass will shift and follow the progression of mining. However, it is the events that occur in anomalous areas – further away from the active mining area that are of particular cause for concern. Such a scenario is presented in Barrett and Player (2002). In this case, two large seismic events occurred in locations previously thought to be relatively inactive. Figure 1 is a plan view of a level in the mine where one of the events occurred (local magnitude 2.1).

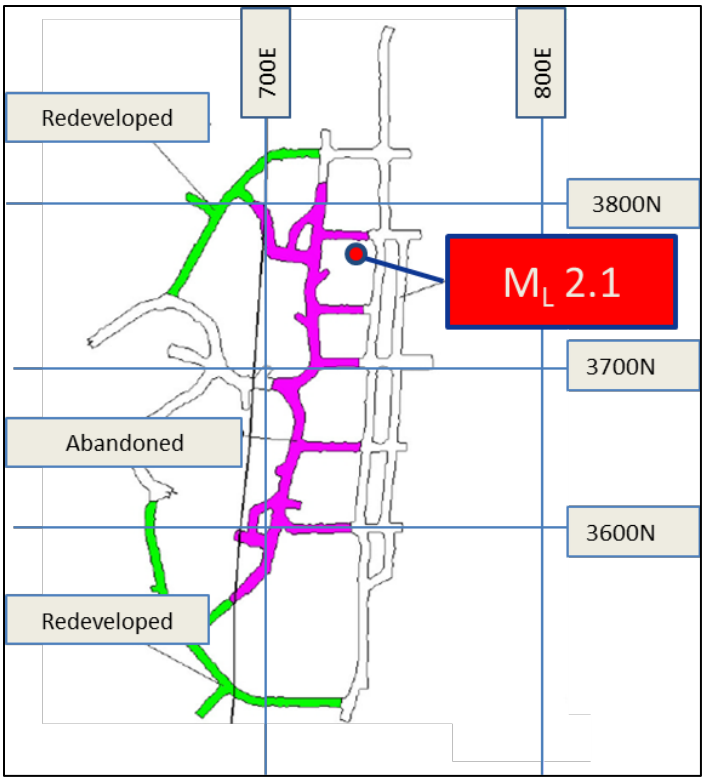

Figure 1: Seismic event in unexpected location (after Barrett and Player, 2002)

This event was the largest magnitude ever experienced at the mine and was located in the footwall beside the orebody. The damage was significant with hundreds of metres of development having to be abandoned and then redeveloped for mining to continue.

1.2.2 Time

There are examples in which seismic events occur at a time that does not seem to be connected to the mining activity at the time. Perhaps it is because the perception of when seismic events should occur as by Mendecki and Lotter (2011).

> *"Given some short time delay for rock mass excitation and relaxation, the bulk of seismic activity in mines starts with rock extraction, increases with the extraction ratio of the orebody and stops with cessation of mining."*

This was certainly not the case at the Longshaft mine in Australia, where the largest seismic events occurred well after mining stopped during a care and maintenance period (Mollison *et. al*., 2003). Not only did the events continue for over a year, the intensity of the events increased as time progressed Table 1.

Table 1: Seismic events that occurred during an extended care and maintenance period with no mining activity (after Mollison *et. al*., 2003)

Source	Date	Time After Mining Cessation	Released Energy (J)
Fault	26-Jun-1999	~4 months	84,800
Aqua Porphyry	19-Aug-1999	5½ months	111,000
Pink Porphyry	March 4, 2000	1 year	224,000

The post-mining experience at Longshaft mine is not unique. It appears that the perception of what timeframe a seismic source is active may not be as straightforward as is sometimes thought. It could be that seismic sources are active over longer periods of time such as weeks, months or years. A different approach to how time of seismic sources is studied is needed.

1.2.3 Intensity

Along with the unexpected location of the seismic events described in Barrett and Player (2002), the events also were unexpected in terms of the intensity (M_L 2.1 and M_L 2.3) – the largest events in the history of the mine at that point. Figure 2 shows the magnitude time history of the events at the mine. It can be seen that prior to June 14th, the seismic events were well under magnitude 1.

The first large event on June 14th and the second large event on July 9th were out of character to the magnitude previously experienced at the mine.

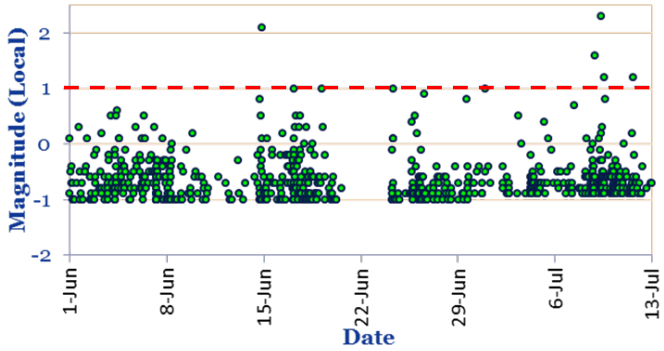

Figure 2: Unexpected magnitude event

The damage to the infrastructure caused by the events was significant (Player and Barrett, 2002). However it is only one consequence of seismic events that are unexpected in terms of intensity, location and/or time.

1.2.4 Consequences

The consequences of unexpected seismic events are significant and can include loss of life, near miss incidents, significant damage to infrastructure/equipment, loss of reserves, which can ultimately lead to a mine having to suspend operations. Loss of life is by far the most important loss such as the fatalities at the Big Bell mine in 2000 (Barrett and Player, 2002) or at the Beaconsfield mine in 2006 (Hills, 2012). More recently, two near miss events occurred at the Westwood mine in January and May of 2015 (Kalenchuk *et al.*, 2017). On each occasion, miners were trapped behind a fall of ground. Fortunately there were no injuries, however the potential for harm was high. The Kidd mine received significant damage to infrastructure after a M_N 3.8 event in January, 2009 (Duan *et al.*, 2015). It is these types of losses that make it hard for mines to recover from, which can force the suspension of operations such as the Macassa mine in 2000

(Blake and Hedley, 2001), Thayer-Lindsley in 2009, (Carmichael, 2009), and the Perseverance mine in 2013 (BHP, 2014). Despite the wealth of research into rockbursting and mining-induced seismicity world-wide, the occurrence of unexpected events is still a problem in mines.

1.3 Seismic Analysis Techniques - Retroactive

Previous research into mine seismicity has developed analysis methods that have helped understand various seismic sources. These methods are primarily retrospective analyses where often the large, unexpected events have to occur before they can be studied. A list of many seismic parameters and analysis techniques that have been developed and are currently in use are shown in Figure 3.

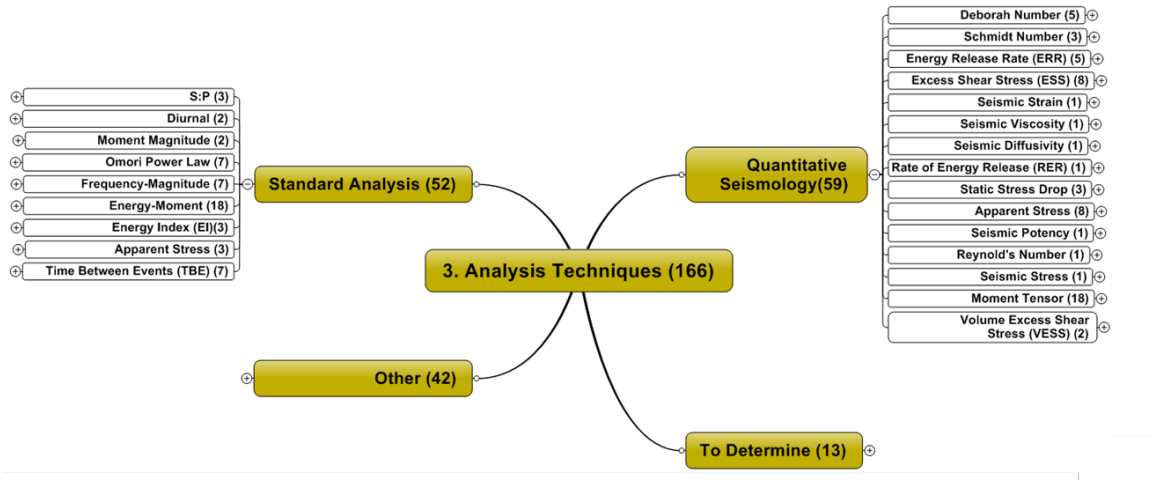

Figure 3: Sample of current seismic analysis techniques

Clustering seismic events using seismic source locations brought new insight into a rock mass' seismic response to changing stresses or mining activity. These methods rely on a large number of events to create the clusters prior to analysis and no not preserve the time sequence of the events. A different approach to clustering seismic events is needed to overcome these limitations.

Seismic activity in mines is complex, constantly changing and can be scale invariant. Previous research applied fractal dimension to the study of seismicity for this reason. The difficulty with the studies did not lie in the application of fractal dimension but more to do with the seismic population chosen that often contained multiple seismic sources. One of the conclusions in the application of fractals to seismic events at the Strathcona mine (Trifu *et al.*, 1993) was that different mechanisms might be involved in the earthquake generation process at the smaller magnitudes found in mines. The study in this paper used 1503 seismic events from an area 1000 metres x 1000 metres x 1000 metres of space so it is reasonable to expect multiple seismic sources in such a large space. Similar large volumes within mines were also studied in Eneva and Young (1993) and Mortimer and Lasocki (1996a) which also likely contained more than one seismic source. Since the primary focus of research at that time was focused on studying fractal dimension before and/or after large events, the fractal dimensions were often calculated using very short time periods of data (Lu, 2013; Xie and Pariseau, 1993; Gibowicz, 1997). The opportunity to apply fractal dimension to a statistically proven single source was a logical approach that had not been attempted.

1.4 Thesis Objective

Seismic analysis methods have improved the understanding of the seismic response to mining activity over the last twenty five years. However additional research is still needed as injury to personnel, damage to equipment and loss of ore reserves in mines caused by unexpected seismic events continues to hinder the mining industry. The objective of this thesis is to examine four known seismic sources differently by using a new clustering method called sequential spatial clustering. Fractal mathematics will be used to characterize each seismic source by determining

the fractal dimension of the nearest neighbour distances, the time between nearest neighbours and the range of distance/time for which the fractal dimension is valid.

1.5 Research Scope

This thesis examines four seismic sources of a developing ramp, abutments around a mining zone, a failing pillar, and a shear adjacent to an orebody using sequential spatial clustering and fractal dimension of the seismic source parameters of location, time and intensity. The results of the methods are used to characterize each seismic source, creating a benchmark for each seismic source. The characterizations help to remove the unexpected nature of a seismic event by describing how far events can be expected from other events, and the time frame over which a seismic source demonstrates activity. When combined with seismic intensity, new information about the range of time, location and intensity becomes available. The data used in this thesis does not have waveforms. Therefore a discussion of system sensitivity, moment tensor or seismic source mechanism is out of the scope of this research.

1.6 Research Approach

The distribution of the distances between nearest neighbour seismic events is determined along with the mode and mean distances. A nearest neighbour event is not the event that is closest to another event at any point in time. Instead, when an event occurs the event that is closest to it at that point in time is its nearest neighbour. The distribution of nearest neighbour distances is a reflection of the data itself so the mode or mean distance from a cumulative distribution graph can be used to as the clustering distance. Since the nearest neighbour distance reflects the data set, the resulting clusters can be used as a characterization of a seismic source.

The second approach is to use the correlation method to determine the fractal dimension of the seismic source parameters of location, distance, and intensity. Each source is described by the fractal dimension, the range in which the data is fractal and the range in which it is not fractal, if one exists. The results of each fractal dimension determination are added to the cluster characterization for each seismic source to create a more robust description.

1.7 Thesis Structure

A review of the relevant literature to gain knowledge of the subject matter as well as determine the course of needed research is covered in Chapter 2. An explanation of the methods developed and used to analyze the seismic data is presented in Chapter 3. The results of the data analysis are presented in Chapter 4. Chapter 5 is a summary and discussion of the results, their significance and other learnings from the application of the methods to each case study. The final Chapter 6 summarizes the motivation and originality of this thesis. The contributions of this work to the understanding of what is an expected seismic event are described. The creation of these benchmark cases may be used to reduce the “unexpectedness” of seismicity in mines.

Chapter 2

2 Literature Review

A review of academic research has been concluded to gain knowledge pertaining to the fundamental concepts of seismicity encountered in mines. This knowledge is necessary in order to understand the research that has already taken place. The need for continued research will be described based on the limitations of existing research and the opportunities that exist to address remaining problems associated with mining induced seismicity.

2.1 Seismicity in Mines

In January, 1928, the first rockburst in Ontario was recorded at the Frood Mine in Sudbury. Subsequently, this phenomenon continued to occur in other Canadian mines – initiating the study of mine seismicity in Canada. This research both in Canada and abroad, most notably in South Africa and more recently in Australia, has made mines safer but has not yet fully identified the underlying causes of some large, unexpected seismic events. These events still occur with devastating results in the form of fatalities (Kiirunavaara Mine 2008, Beaconsfield Mine 2006, Big Bell Mine 2000), miners trapped on two occasions (Westwood Mine 2015), workers injured (Eloise Copper Mine 2012), and mine closures (Perseverance Mine 2013, Thayer-Lindsley 2009, and Macassa Mine 2000). Many more mines around the world have experienced large, unexpected seismic events, fortunately without significant loss. However, further research is warranted to identify the cause of these large, unexpected events so that the hazard they present can be quantified and mitigation strategies developed.

2.1.1 Introduction

Mining has become increasingly deeper over the last twenty years. A review of *in situ* ground stresses in Canada determined that all three principal tresses ($\sigma_1, \sigma_2, and\ \sigma_3$) increase in depth (Arjang and Herget, 1997). Additional research confirmed this finding and revealed that stress increases are not linear with depth, as presented in 1997, but increase in three distinct domains (Maloney *et al.*, 2006). The Canadian Shield can be characterized as follows: Domain 1 (0 -300 metres-Figure 4); Domain 2 (300-600 metres-Figure 5), and Domain 3 (600-2400 metres-Figure 6).

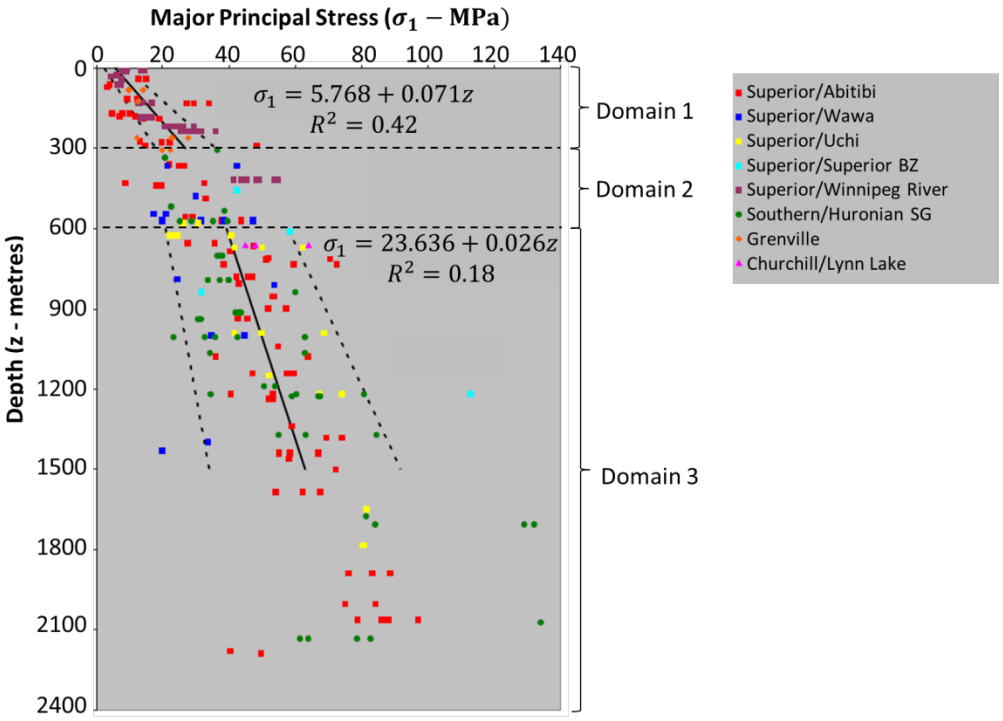

Figure 4: Increase in the major principal stress (σ_1) with depth for various geologic regions in Canada

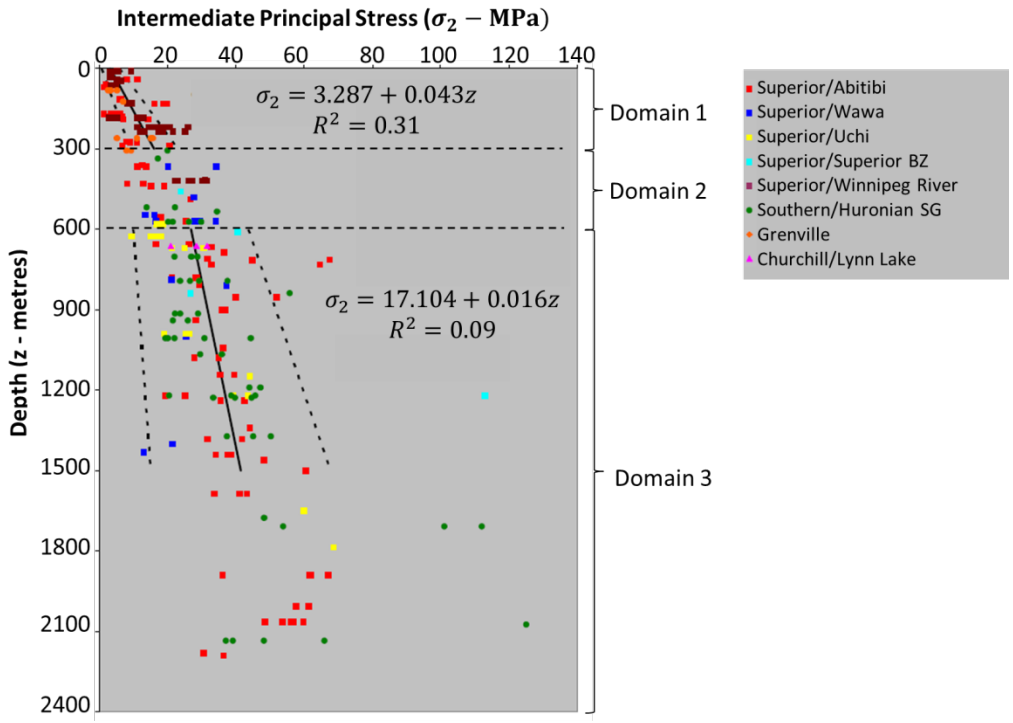

Figure 5: Increase in the intermediate principal stress (σ_2) with depth for various geologic regions in Canada

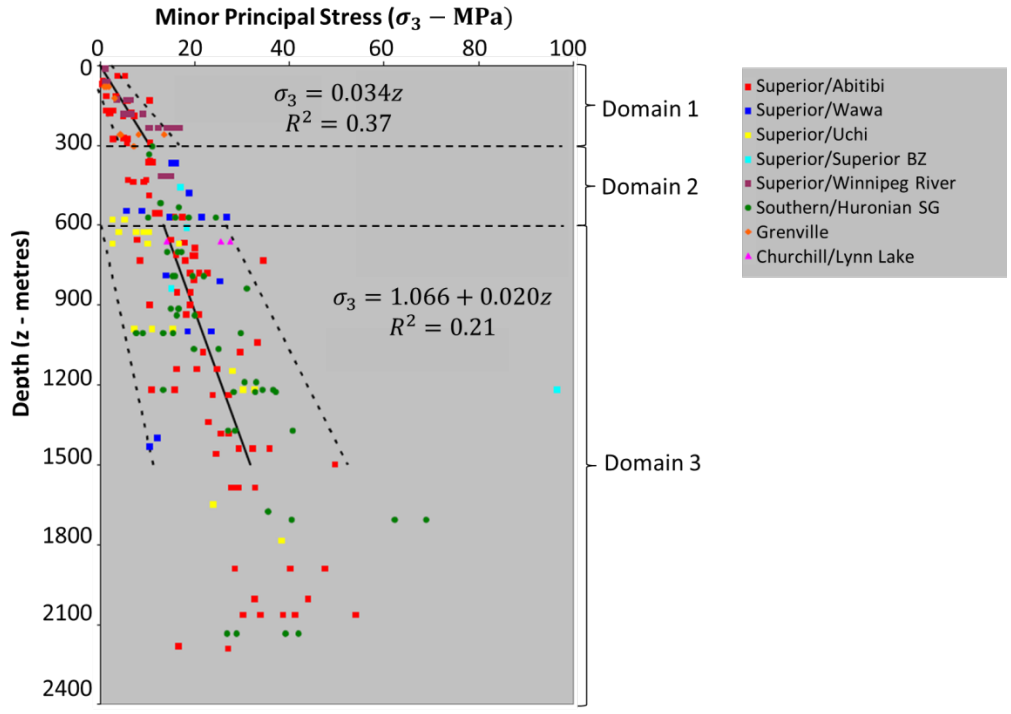

Figure 6: Increase in the minor principal stress (σ_3) with depth for various geologic regions in Canada

The challenge for mines is to estimate rock mass behavior at unprecedented depths. An increase in stress becomes problematic if it reaches the unconfined compressive strength (UCS) of the rock. Figure 7 compares the ground stresses at various Canadian mines to the rock strength. The blue-yellow boundary indicates a transition from low to high stress. The yellow-red boundary depicts the depth at which a transition from high to very high stress may occur (after Swan *et al.*, 2005).

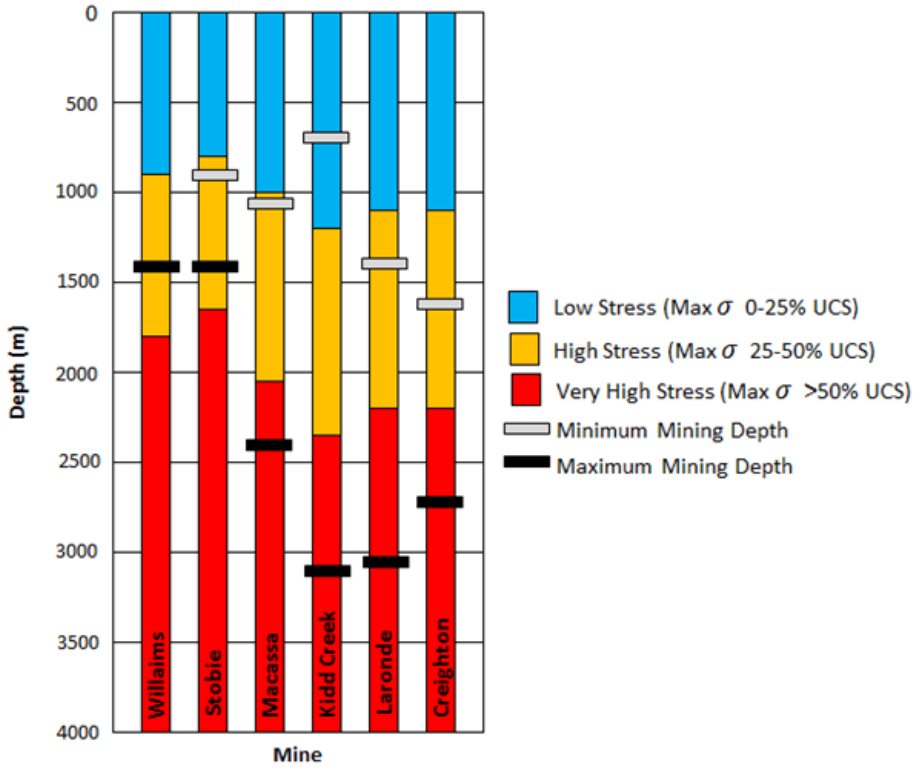

Figure 7: Ground stress compared to rock strength for the deepest mines in Canada

Figure 4 and Figure 7 show Canadian mines will also face new challenges as they mine deeper and in unprecedented higher ground stresses. This increasingly challenging problem has been recognized and was found to be one of the highest safety risks in the 2015 Mining Health, Safety and Prevention Review in Ontario (Ministry of Labour, 2015). The Ultra Deep Mining Network was created in 2014 to address the challenges of deep mining below 2.5km. The network is comprised of government, industry and academic groups that have also recognized that new tools

and technology are needed to deal with the issues of progressively deeper mining. The academic community has also created a biannual conference in 2002 dedicated to topics related only to deep and high stress mining. The eighth conference took place in March 2017.

One of the most important tools used to understand changing ground conditions is a seismic monitoring system. This type of system is commonly used in mines – seventy percent of underground, hardrock mines in Ontario have a system. Currently twenty five such systems are installed in mines in Ontario and Quebec – seven of which have been installed in the last four years (Hudyma *et al.*, 2016). A seismic monitoring system is a key component to managing seismic risk in a mine and keeping personnel safe.

2.1.2 Seismic Monitoring

Seismic systems installed today in underground mines are readily available, reliable and provide full waveform analysis (Collins *et al.*, 2014). A typical seismic system arrangement in a mine is shown in Figure 8.

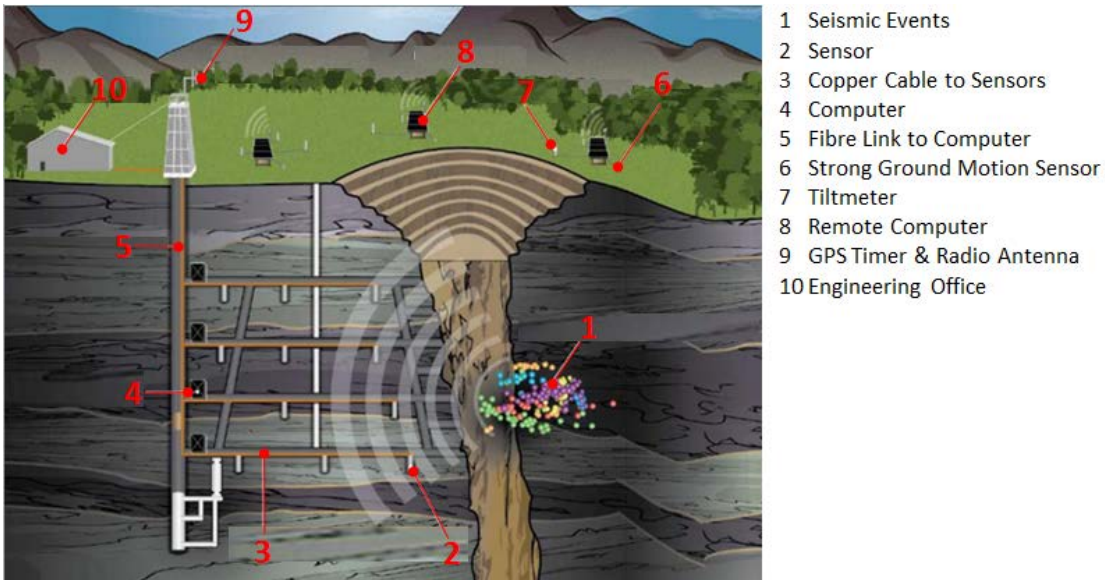

Figure 8: Example of a microseismic monitoring system setup (after Collins *et al.*, 2014)

Sensors are installed in holes drilled into the rock. The sensor information is sent via copper wire to a digitizing computer. Each computer links to an acquisition computer on surface via a fibre optic cable. The acquisition computer software allows for the data to be processed and analyzed by mine personnel. While there is a slight delay of a minute or two for data to be received and transmitted, seismic events in a mine are essentially available in quasi-real time. Current technology allows for thousands of events per day to be recorded and available for analysis.

The type of sensor installed underground or on surface determines the size of seismic event that can be recorded (Figure 9). Three types of sensors (1-30V/g Accelerometers, 15 Hz Geophones, and 4.5 Hz Geophones) allow the system to be sensitive to seismic events that range from moment magnitude M_w -3 to 3.

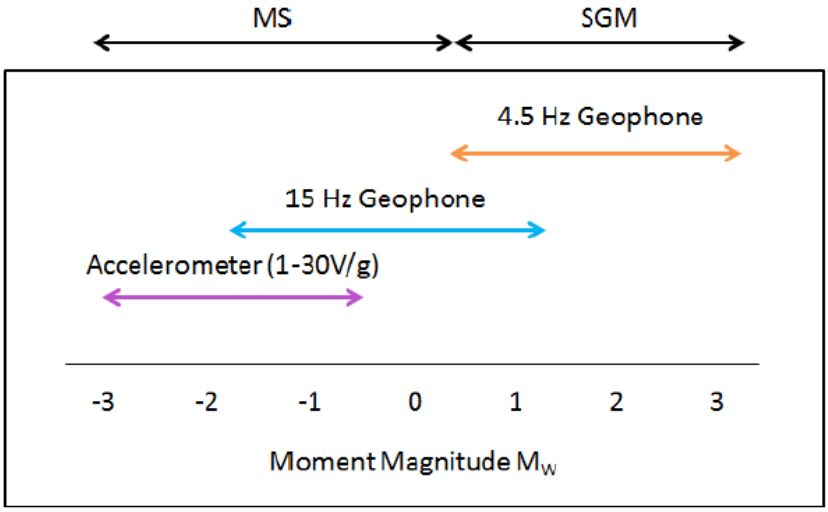

Figure 9: Recommended monitoring range for underground seismic systems (Collins *et al.*, 2014)

Strong ground motion sensors (SGM) are usually located on surface about 1-2 kilometres away from the mine. They record the low frequency events (moment magnitude greater than 0). The microseismic sensors (MS) record the higher frequency events (moment magnitude less than 0).

2.1.3 Seismic Source Parameters

When stress applied to a rock reaches the rock strength, the rock fractures and releases a dynamic stress wave. The sensors in a mine's microseismic system measures the stress wave and a computer records the ground motion and the time at each sensor. The shock wave hits the sensor twice – the primary ("*p*") is a compressional wave and the second a shear wave ("*s*"). The seismic system records the *p* and *s* wave arrival times as well as the amplitude of each wave for each sensor the seismic wave passes. The waveform (shown at the top of the image in Figure 10) is transformed mathematically using a fast Fourier transform algorithm. The result is then plotted on the spectral graph that is shown below the waveform. On the spectral graph the fourier transform of the s-wave is shown by the red line and the pre-event noise by the black line. The two asymptotes are fit using the Brune model to determine the spectrum model (red line). The usable frequency bandwidth is in the range where signals are not dominated by noise (~1-70 Hz) (after Baig *et al.*, 2012).

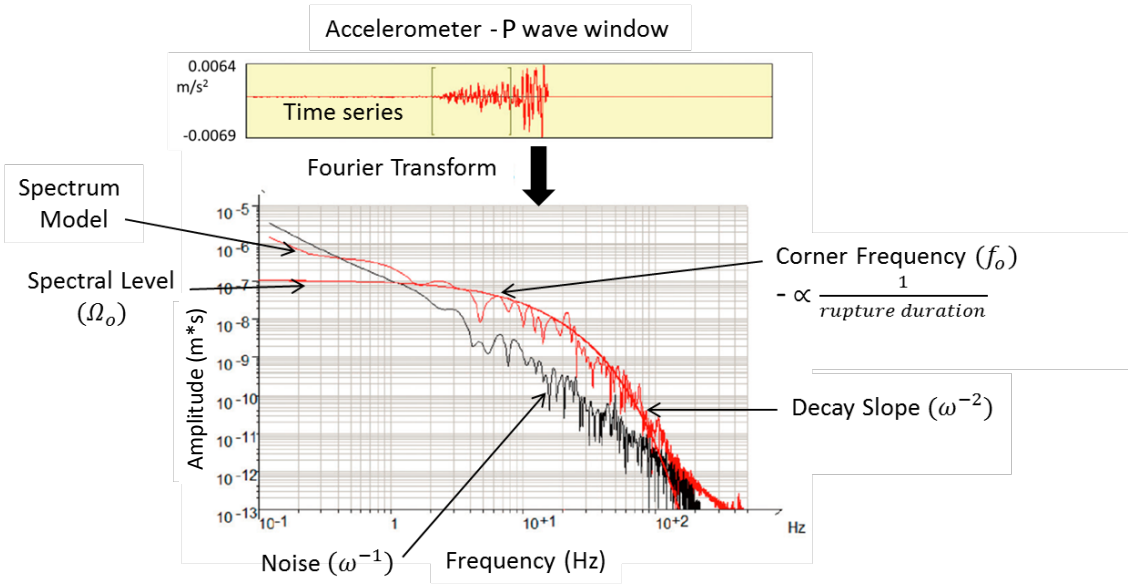

Figure 10: Attenuation-corrected amplitude displacement source spectrum of a seismic event

The spectral graph is used to characterize a seismic event by its corner frequency ($\boldsymbol{f_o}$), and the low-frequency or spectral level ($\boldsymbol{\Omega_0}$).

Initially, spectral analysis was empirically related to earthquakes to quantify the magnitude of an event. The Richter scale was created to describe the relative strength of earthquakes in California (Richter, 1935). Using mechanically recorded waveforms on a seismograph, an earthquake 100km away recorded a 1mm amplitude height and was assigned a magnitude of zero. Nomograms were created using this empirical data, enabling the magnitude of subsequent earthquakes to be quantified. However, the Richter scale was found to be limited to that region of California. It was determined that seismic body waves and surface wave attenuation in Eastern North America were found to be significantly smaller than those west of the Rocky Mountains (Evernden, 1967; Nuttli, 1973). The Nuttli scale was also empirically derived to describe earthquakes in eastern North America (Nuttli, 1973). However these models were not based on a physical model, until one was proposed by Brune (1970). Based on the shear movement of a planar fault, the model described the spectral shape by Equation 1:

$$\Omega(f) = \frac{\Omega_o}{1+(f/f_o)^2} \qquad \text{(Equation 1)}$$

Where:
$\Omega(f)$ - spectral shape (m/s)
Ω_o - long period amplitude (m/s)
f_o - corner frequency (Hz)
f - frequency (Hz)

Modifications and improvements to Brune's model have taken place such as, but not limited to, Boatwright (1980), Abercrombie (1995), Andrews (1986), and Madariaga (1976) to create a general model for both *p* and *s* waves that fits the displacement spectra as a function of frequency (Mendecki, 1997) (Equation 2).

$$\boldsymbol{\Omega(f) = \frac{\Omega_o e^{-[\frac{\pi f R}{V_c Q}]}}{[1+(f/f_o)^{\gamma n}]^{1/\gamma}}} \quad \text{(Equation 2)}$$

Where:
$\Omega(f)$ - spectral shape (m/s)
Ω_o - long period amplitude (m/s)
f_o - corner frequency (Hz)
R - hypocentral distance (m)
V_c - velocity of the body waves (m/s)
n - the high frequency fall off rate on a log-log plot (Hz/s)
γ - controls the sharpness of the corner
Q - attenuation

Equation 2 reduces to Equation 1 when R =0, n=2, and γ = 1. The significance of this model is that three independent source parameters (seismic moment (M), radiated energy (E), and corner frequency(f_o)) can be calculated, and empirical waveforms can be compared to the model. How this is accomplished is described in Hanks and Kanamori (1979).

Confidence in the method using spectral data for seismic analysis can be seen in Figure 11. This figure shows the results from a number of studies in the literature at a range of seismic event size moment magnitudes (Goodfellow and Young, 2014).

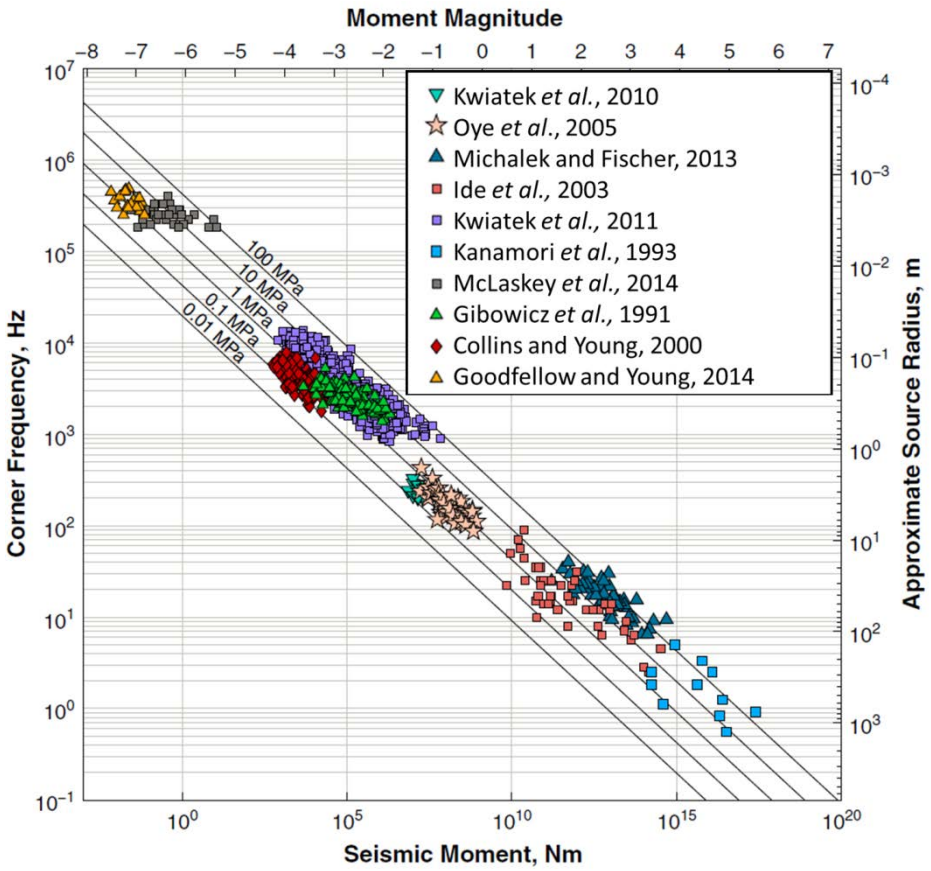

Figure 11: The relation between seismic moment and corner frequency for mine-by acoustic emission data in comparison with human and natural seismicity (summarized in Goodfellow and Young, 2014).

The moment magnitude scale was developed by Hanks and Kanamori (1979) after it was determined that earthquakes larger than magnitude 7 could not be calculated using the Richter scale. Thus, instead of estimating radiated energy from Richter magnitude (Gutenberg and Richter, 1956), Kanamori (1977) uses the independent parameters of seismic moment and the area of a fault plane from spectra to develop the moment magnitude scale (Hanks and Kanamori, 1979).

Local magnitude is a scale used that has been customized to a particular region. For meaningful use of a local scale, it must be calibrated to another scale such as moment magnitude. Seismic data from mines in Australia and Canada that is used in this thesis have been recorded on different seismic systems, using one of the magnitude definitions just described. Since most mines develop

an approximation of their local magnitude scale to the Richter scale, Richter magnitude (noted as M_R) approximations will be used in this thesis. In this thesis the word "magnitude" used on its own will imply Richter magnitude. If another magnitude scale is used it will be described with the type of scale along with the word magnitude.

2.1.3.1 Energy

A seismic event is a release of energy from a source location that has built of stress over time. Radiated seismic energy is only a small portion of the total energy released (McGarr, 1976); however it is the fraction of energy that is radiated as seismic waves (*p* and *s* waves). The remainder of the energy released (strain energy) in faults dissipates as heat and as microstructural defects for a crush mechanism (Gibowicz and Kijko, 1994). Radiated energy is calculated by the following equation:

$$\boldsymbol{E = \frac{4\pi\rho c R^2 J_c}{f_c^2}} \qquad \text{(Equation 3)}$$

Where:
E - radiated energy (joules)
ρ - rock density (kg/m^3)
c - velocity of either the p wave or s wave (m/s)
R - distance from the source (m)
J_c - integral of the square of the ground velocity
f_c - radiation pattern coefficient

2.1.3.2 Location

The location of a seismic event is an independent parameter that is fundamental to understanding the source mechanism of a seismic event. Methods used to calculate the locations are described in Ge and Kaiser (1990) and Gibowicz and Kijko (1994) and a sample calculation in Bolt (1993). The arrival time at each sensor for a seismic event and the velocity at which the *p* and *s* waves

move through the rock mass are needed to calculate the event location. The arrival time of the *p* and *s* waves are available from the waveform and rock mass velocities are usually calibrated by firing a blast at a known time and known coordinates. In order to calculate the location it is important that the sensor array has enough sensors, the locations of the sensors are accurate, the waveform time is synchronized for each of the sensors throughout the system, accurate arrival times must be picked, the velocity model must be accurate and up to date and there should be a small time residual between the theoretical and actual arrival times (Collins, 2012). Current research is improving event location algorithms to reduce the attenuation of the waves by the presence of voids or complex media (i.e. backfill) that may occur between a seismic event and a sensor. The attenuation affect in a simple velocity model often over estimates the distance of the source location because of the increased time it takes for a wave to reach the sensor if it travels through a medium with a different velocity or if it has to travel around a void. The three dimensional velocity model in Collins *et al.*, (2014), describes this concept and model well. The research in this thesis is not about improving seismic locations, but rather uses the distance between nearest neighbour events as a basis to identify seismic sources. This differs from principal component analysis (PCA) in two ways. First, PCA incorporates inter-event distance and time (Hedley, 1992), while this research only calculates inter-event distances. Secondly, the inter-event distance considers only events within a defined radius. This research does not limit an event to a prescribed distance but rather considers the distance between each event and all other events.

2.1.3.3 Time

The time at which a seismic event occurs is recorded when the stress wave hits a sensor with the *p* wave hitting first and then the *s* wave. It is a parameter that reflects the moment the rock mass

failed and propagated a stress wave. Event times are most commonly used in relation to other event times and blast times to indicate how a rock mass is changing over time. The difficulty with studying event times is not with the time itself but with which events are chosen to be compared. For example, a magnitude time history chart (Figure 12) is useful to show how event magnitudes increase/decrease with time. The maximum magnitude of seismic events is lower as the cave zone begins to be established at the end of February 2007(M <0). Magnitudes steadily increase to Magnitude 1.8 in September 2007. This example is fairly straight forward because the rock mass is failing under the influence of gravity, unconfined, and without the influence of blasting. However, it offers no explanation why other seismic analysis techniques are required to further interpret the data.

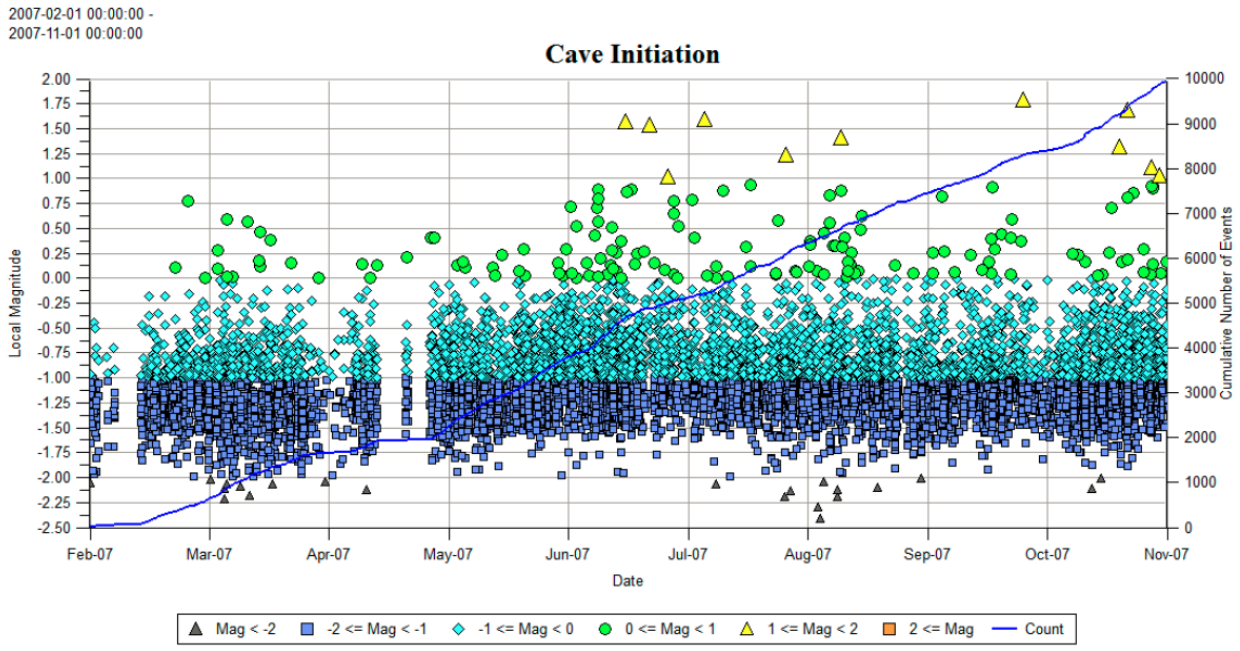

Figure 12: Magnitude time history of a cave zone initiation (Abolfazlzadeh, 2013)

In Beneteau (2012), five patterns were identified when the time between events (TBE) was studied for a number of data sets which could be used to indicate the seismic source mechanism. For example Pattern 1 had one TBE-rate, one b-value on a frequency magnitude graph, and one

consistent seismic source mechanism; Pattern 2 had two TBE-rates, one b-value indicating the onset of different seismic source mechanisms for large events; Pattern 3 had two TBE-rates, two b-values and different seismic source mechanisms for small and large events; and Pattern 4 which had two TBE-rates, two b-values in sequence indicating there are different seismic source mechanisms for large and small events; and Pattern 5 includes all other events that are not in Pattern one to four. Beneteau (2012) also acknowledges that the time between events cannot be solely used to identify seismic source mechanisms and needs to be used in conjunction with other seismic analysis techniques. While it is the objective of many seismologists to use the time history of previous events to estimate when the next large event will occur, the existence of multiple mechanisms in a data set as identified in the TBE patterns in Beneteau (2012), makes it a difficult objective to achieve. The populations of seismic events studied need to be meaningful and of a single seismic source in order to completely understand a rock mass through the failure process and the amount of time it takes.

Acoustic emission (AE) studies give some insight into why the study of time and seismic events is problematic. Lockner and Byerlee (1992) used AE to follow the failure process in a laboratory sample of granite that subjected to pressure. During a creep experiment where a stress level of ~70-90% of the granite's short term failure strength is applied, they were able to locate micro-fracture events in three dimensions up to the point of failure. They could not follow the development of the fault once failure was initiated because it occurred catastrophically. They modified their experiment to include a constant AE rate feedback system that would reduce the loading system during fault propagation. With reduced load, the fault propagation continued to develop such that it could be recorded and analyzed (Figure 13).

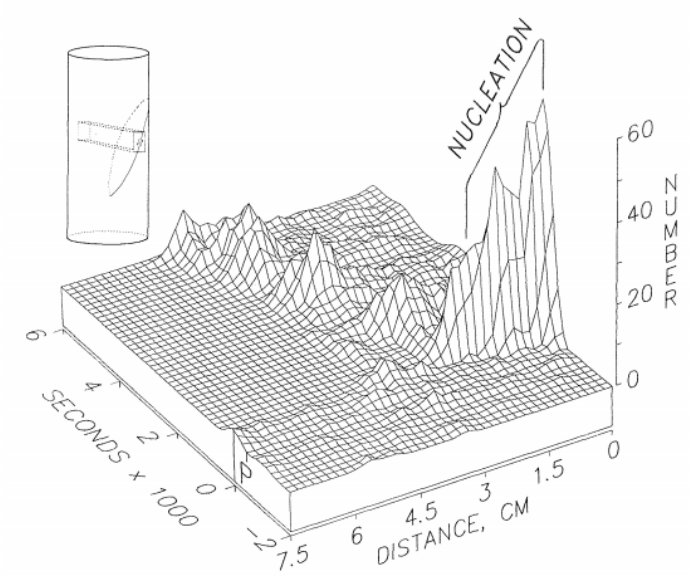

Figure 13: Fault growth. Each time step represents 80 seconds (Lockner and Byerlee, 1992)

The paper demonstrates two points – first that the rate of failure can change depending on the seismic source mechanism. If seismic events are studied on a prescribed time scale (weeks, days, hours, etc.) the lead up to rock mass failure can be missed. Back analysis on the same time scale could also miss the variable nature of the failure propagation. The second point is that when the stress applied to the sample was changed, the time to failure also changed. The failure timeline of a rock mass in a mine will also change if the stresses around it change. Thus, if stresses are pushed onto an abutment by the mining of an adjacent stope, this may accelerate the failure process of the abutment. The opposite can also be true – if stresses are reduced on an abutment by not mining the adjacent stope, the failure of the abutment will take on a different time frame. Stresses are constantly shifting in a mine depending on where the mining front is taking place, the size and frequency of blasts, changing rock types and location of geologic structures. What is known for sure is that as the stresses on a rock mass change, so too will the time to failure if the stress exceeds the strength of the rock mass. This thesis will not study seismic events on prescribed time frames but rather observe seismic sources (locations) to see when the rock mass is seismically active. The

active periods can then be compared to the current beliefs of how long a rock mass is seismically active in different failure scenarios (failing pillar, relaxation of a rock mass around a drift, fault failure).

2.1.4 Using Seismic Monitoring to Define Normal/Abnormal Seismic Response

Beneteau (2012) lists the qualitative characteristics based on the location, time and relative size for a normal and abnormal seismic response to mining. A normal response occurs in close proximity to the blast site, within hours of the blast at a rate that diminishes with time, and has a small magnitude, often less than Richter 0. An abnormal seismic response is distant to the blast location, and appears to not be related to the time of a blast and has a magnitude greater than 0.

Underground mining changes the stresses acting on a rock mass by the creation of voids and by adding dynamic stress to the rock by blasting. Seismic events have been used to help quantify how far the rock mass is disturbed from the void, by delineating the damage to the rock mass immediately adjacent to the excavation. McGarr (1976) found that seismicity could be as much as ten metres ahead of an advancing stope with uncontrolled blasting, (1.25m H x 10m W). Kuzyk and Martino (2008) conducted a blast damage assessment at the Underground Research Laboratory in Pinawa, Manitoba, Canada. Regular development rounds (3.5m long) were excavated in an elliptical shaped drift 4.4 metres wide and 3.5 metres high. Previous work by Martino and Chandler (2004) demonstrated that the damage to the surrounding rock mass is not uniform and there are inner and outer damage zones around the drift (Figure 14 Image A). Kuzyk and Martino (2008) quantified the distances in their work (Figure 14 Image B). It shows that when controlled blasting was used, the majority of the damage was within one metre of the drift wall. It also showed that 2.6 metres into the wall the rock mass was undisturbed.

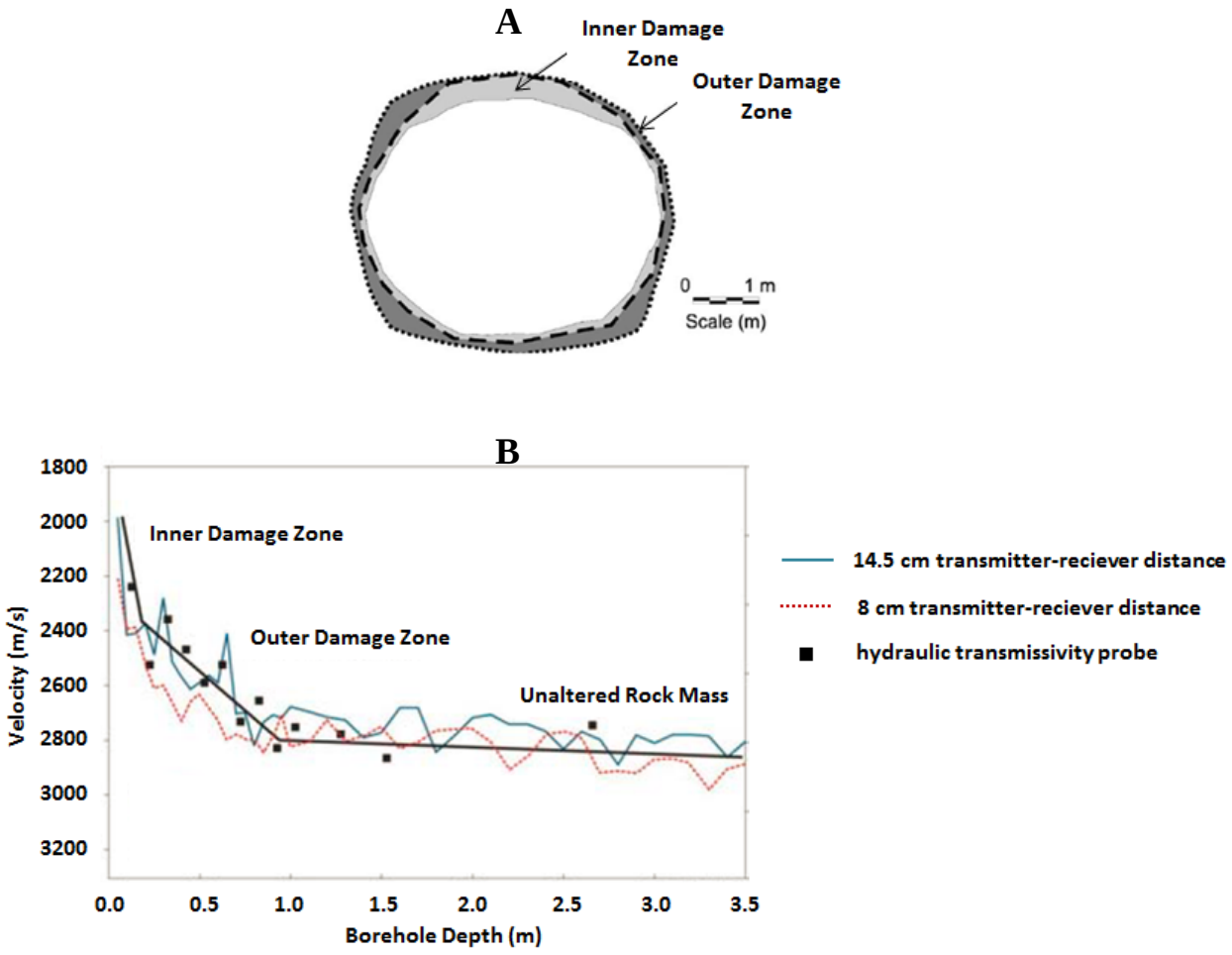

Figure 14: Image A - The damage zones are identified in Martino and Chandler (2004). Image B - Quantifying the excavation disturbed and damaged zones (after Kuzyk and Martino, 2008).

In a similar manner, a cave zone was theoretically described in Duplancic (2001) (Figure 15). A seismogenic zone was quantified (~200m) in Abolfazlzadeh and Hudyma (2016) (Figure 16).

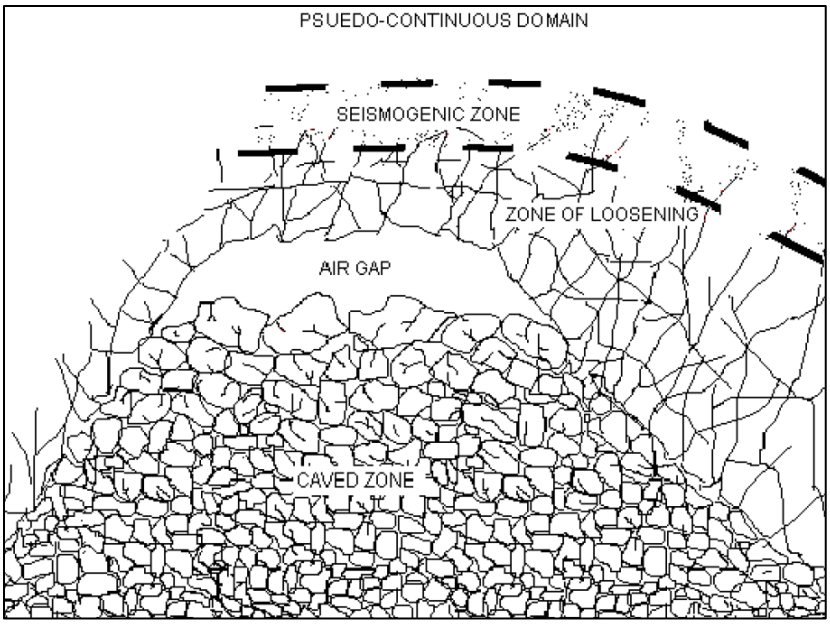

Figure 15: A conceptual model of a normal rock mass response to block caving (Duplancic, 2001)

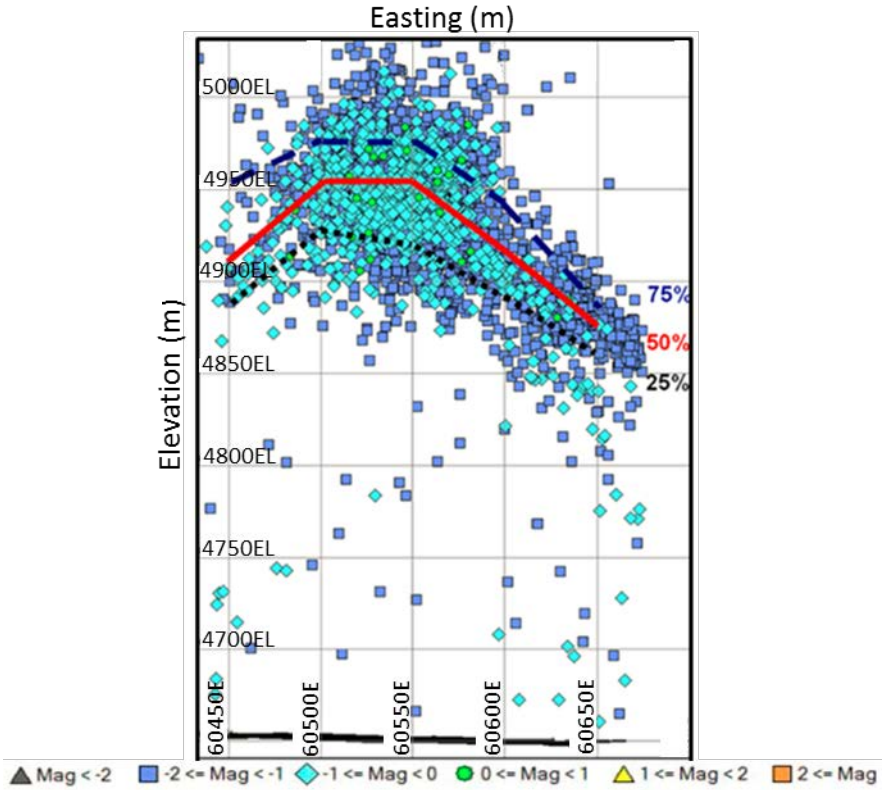

Figure 16: Seismogenic zone activity (December 2007) in a sublevel caving mine (after Abolfazlzadeh and Hudyma, 2016). The red 50% line shows the location in the seismogenic zone where the population of events is evenly split (50% of the events are above and below the red line).

These examples from the literature show that a normal response to mining at different excavation

sizes can be estimated from the seismicity that develops around the excavation (Figure 17). This thesis will continue to explore this concept in order to discern what distance seismicity can be expected to occur at different scales of mining – including mine scale. This will ensure that the proper populations of seismic events are studied.

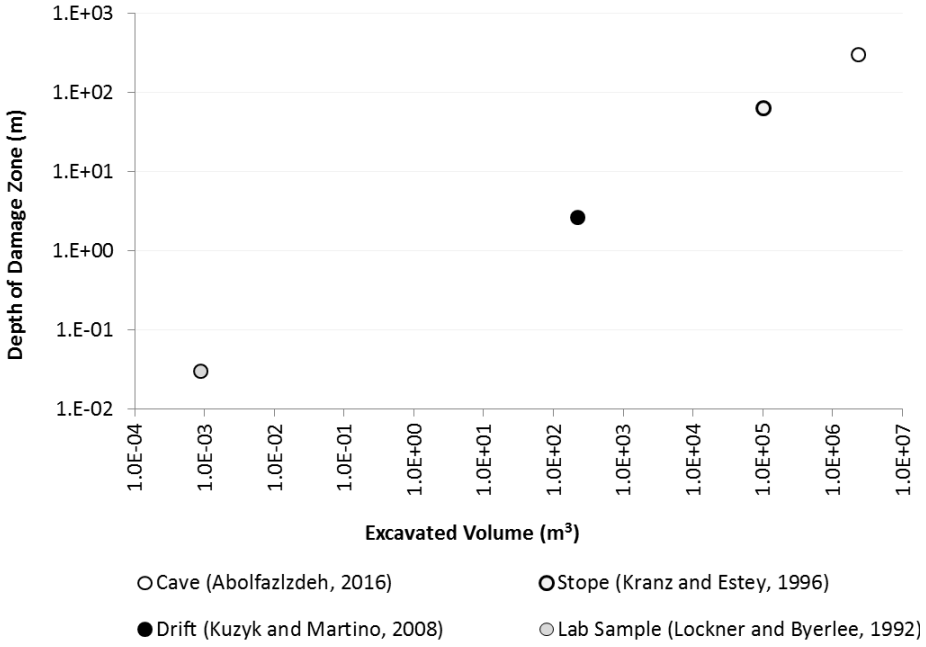

Figure 17: Examples of damage zones around excavations at various scales

2.1.5 Limitations and Opportunities

Despite years of research, two factors affecting seismicity in mines remain elusive: the temporal pattern for various seismic sources and a proactive method to determine if, when, and where a large event may happen.

The Eloise Copper Mine located in Queensland, Australia installed a microseismic system in 2011, primarily to monitor a cave zone and to mitigate an air blast hazard. Despite their efforts, an unexpected M_L 1.8 rockburst occurred on January 12, 2012. The event seriously injured a worker

and closed the mine for a month while back analysis of seismic events, modelling, and a review of ground support were conducted (Keily, 2013). The Westwood Mine in Quebec, Canada also experienced large seismic events that required back analysis (Kalenchuk *et al.*, 2017). In this case, a team of experts trained in advanced seismology examined and modelled the seismic events from the May 25, 2015 3:28AM – M_N 3.2 event, 3:38AM – M_N 2.7 event, and the May 27, 2015 8:11 PM -M_N 2.4 event. Despite these best efforts, the panel of experts concluded that events were unforeseen and did not have an obvious trigger such as blasting (production or development). It is clear that current analysis methods are insufficient to deal with the seismic events that are an abnormal response to mining.

Mining seismic analysis methods have traditionally been adopted from earthquake analysis. However the opportunity to apply a different approach to mine seismicity makes logical sense as there are multiple seismic sources in mines that are different than earthquakes. Mines provide the opportunity to see and measure more information in the walls, backs and floors of drifts and stopes. The scale in mining is also much smaller. For example, non-mining periods (absence of blasting and void creation) can be studied to determine if the seismically active time period of a seismic source is different than during a mining period. A number of articles listed in Table 2 make reference to seismicity that continued in mines during non-mining periods. These papers all show that seismic activity continues for different seismic sources during non-mining periods.

Table 2: Seismicity during non-mining periods

Mine	Seismic Period in Absence of Mining	Note	Reference
Beaconsfield Mine (Australia)	1 year 6 months	Temporary closure April 25, 2006 Reopened October 2007	Hills, 2012 Figure 10 Hills *et al.*, 2013
Big Bell Mine (Australia)	1 year 4 months	Temporary closure Sepember 2000 Reopened January 2002	Beneteau, 2012 Figure 18, Barrett and Player, 2002
Creighton Mine (Canada)	1 year 1 month 5 days	Temporary closure June 3, 2009 Reopened July 8, 2010	Morissette *et al.*, 2012
Falconbridge Mine (Canada)	7 years 5 months	Permanent closure June 20, 1984 (rockburst)	Wetmiller *et al.*, 1993
Galena Mine (U.S.)	3 months	Feb-April 1990	Swanson, 1992
Galena Mine (U.S.)	2.5 months	Temporary closure June 9, 1990 Reopened August 21, 1990	Boler and Swanson, 1992
Galena Mine (U.S.)	1 year 2 months 26 days	Permanent closure June 1992	Kranz and Estey, 1996
Kolar Gold Fields (India)	17 years	Permanent closure 1991 - deep levels only Permanent closure 2001 -whole mine	Srinivasan *et al.*, 2009 Figure 3 Figure 8 - seismicity until 2008
Long Shaft (Australia)	1 year 4 months	Temporary closure March 1999 Reopened June 2000	Mollison *et al.*, 2003 Figures 7-10
Strathcona Mine (Canada)	2 months	Temporary closure April 14, 1991 Reopened July 15, 1991	Trifu *et al.*, 1993 Figure 2

An opportunity not widely used is to follow seismic events sequentially. Along with the estimation of how far seismic events can normally be expected around an excavation of a certain size (Table 2), a test can be created to determine the location of an anomalous event. For example, the distance between nearest neighbour events can be statistically evaluated to determine which events are closest to each other on any given day. As events continue to occur one at a time, seismic events that have the anomalous event as a nearest neighbour can be analyzed to determine if the new location of seismic activity poses a hazard to other areas in the mine.

2.2 Clustering of Seismic Events in Mines

Seismic events have been noticed to group together spatially in mines (Trifu *et al.*, 1993; Basson and Ras, 2005; Tsirel *et al.*, 2011, Rebuli and Kohler, 2014). Jain and Dubes (1988) describe a cluster as “a number of similar objects collected or grouped together”. Clusters are useful to manage data and identify similarities between objects. As researchers work to increase the

understanding of seismicity in mines, there are significant benefits when applying clustering algorithms on seismic event populations. A seismic event in a mine is a dynamic stress wave that emits when a rock mass fails in a particular location. However, the failure of a rock mass is a process that takes place over a period of time (Hudyma and Potvin, 2010). In order to cluster seismic events from a mining environment, the similarities between the events must reflect the process of a failing rock mass. First, an understanding of clustering methods and techniques is needed.

2.2.1 Clustering Methods and Techniques

Parsha and Pacha (2013) and Ester *et al.*, (1996) provide good summaries of clustering methods. This section is largely based on these papers. There are two fundamental ways to breakdown a database.

Hierarchical algorithms use each object in the database in one of two ways. An agglomerative, hierarchical algorithm assigns like objects to a cluster. It then gradually merges smaller clusters into increasingly larger clusters until all the objects are in one cluster, or until some end point is specified before unity. Divisive hierarchical algorithms are the opposite of agglomerative hierarchical algorithms in that they start with all the objects in one cluster and then subdivide the clusters into smaller ones (Figure 18).

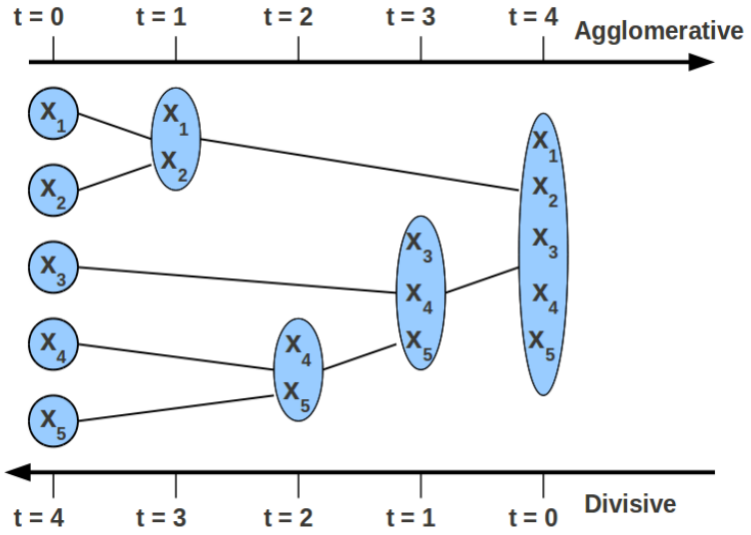

Figure 18: Divisive and agglomerative clustering techniques. Agglomerative cluster technique is shown on the scale above the image. The divisive approach can be followed using the bottom scale (Rai, 2011)

Both divisive and agglomerative hierarchical algorithms do not require an input parameter; however they do need a termination condition such as the distance between the objects. Garcia *et al.* (1995) used the divisive approach and were able to automatically derive a termination condition. The algorithm calculates the distance between each pair of points, making it computationally heavy. At the time of this work (early 1990's), computers were very limited in computational processing and the amount of data they could handle. This is much less of an issue today.

Partitioning algorithms break a database (*D*) with a number (*n*) of objects into a number (*k*) of cluster sets. Partitioning algorithms need an input parameter (*k)* to create an initial partition. A limitation of this method is that the number of objects in the data set cannot change during the clustering process. Should data be added to the data set, the updated data set would need to be clustered a second time.

Before deciding on what type of algorithm is needed, Jain and Dubes (1988) recommend making

sure that data being studied shows a tendency toward clustering. If data does not show a tendency toward clustering, they recommend using a different analysis method. They also recommend stating the goal of the cluster analysis to ensure the proper method is chosen.

2.2.2 Limitations in Clustering Applications

Kijko *et al.* (1993) were among the first to apply the concept of clustering seismic events in mines. An agglomerative, hierarchical algorithm was used to cluster seismic events in space and time. A time window of ten days was chosen and events were only linked to other events within that time window and only allowed a single link to form between two events in a cluster. The choice of the moving time window biased the results because if it were too short, clusters would end prematurely. If the window were too large, only one cluster would result. Basson and Ras, (2005) also tried to use a space-time clustering approach, however seismic events were studied in two dimensions (depth eliminated) and the conclusions were based on visual observation instead of a clustering algorithm.

Rebuli and Kohler (2014) also used an agglomerative, hierarchical algorithm based on the density of an event with other events in close proximity called DBSCAN (Ester *et al.*, 1996). The algorithm requires two parameters, a maximum search distance and the minimum number of neighbours required to form a cluster. The disadvantage of the method is that it cannot adequately deal with data sets that have large differences in densities. It also removes outliers which may become important over time. Rebuli and Kohler (2014) used the algorithm as part of a retrospective analysis and commented that it would need to be automated to be useful as a proactive tool.

This is a key short coming of many clustering algorithms – they require a significant size data set and give no additional consideration for the addition of events on an incremental basis (Table 3). The removal of outliers or single events is also problematic unless they are proven to statistically remain single events for the entire data set.

When seismic events are considered part of a local failure process, the timing and location of consecutive events are important to understand the failure process. The consideration of consecutive events within a cluster is valuable, crucial information needed to understand the failure process of a rock mass.

Table 3: Clustering Algorithms Requiring Reclustering With Additional Events

Algorithm	**Reference**
CURE (Clustering Using Representatives)	Guha *et al.,* 1998
C^2P (Closest Pairs)	Nanopoulos *et al.,* 2001
DENCLUE (DENsity based CLUstEring)	Hinneburg and Keim, 1998
K-means	MacQueen, 1967
CLARANS (Clustering Large Applications based on RANdomized Search)	Ng and Han, 1994

K-means and CLARANS are not designed to handle data with large variations in size or arbitrary shapes, making them unsuitable for seismic data on their own.

With respect to the study of time, a parameter may not necessarily be well suited to clustering and may need to be analyzed using other methods such as time between events (TBE) (Beneteau, 2012). This work demonstrated that different seismic sources exhibit different time frames. There also remains a portion of a seismic population that is not understood with respect to time, particularly those in or near geological structures and faults.

2.2.3 Considerations to Cluster Seismic Events in Mines

Existing clustering techniques were developed for data sets not related to mining. These techniques and cluster based on the results desired for a particular application. For example, the CHAMELEON algorithm (Figure 19) uses K-mean to create initial clusters; partitions them and then merges clusters based on clusters in close proximity that share the same intrinsic properties within the clusters (Karypis *et al.*, 1999).

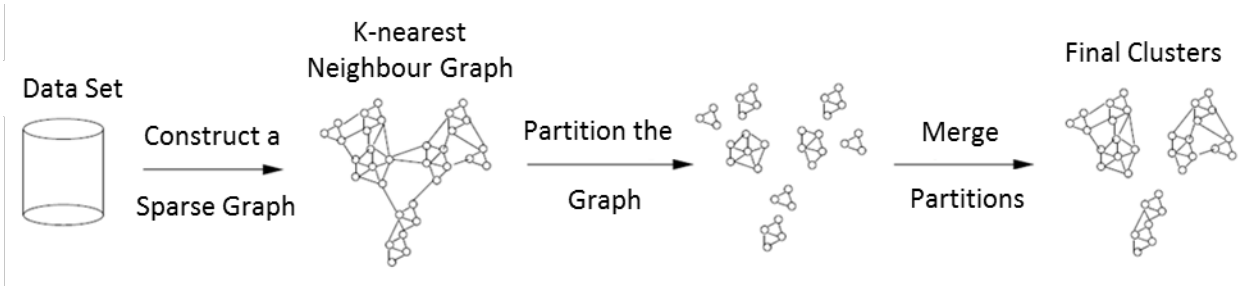

Figure 19: CHAMELEON framework (after Karypis *et al.*, 1999)

Another partitioning algorithm that may be modified to suit seismic clustering goals is MMD (Mean Minimum Distance, Peng-Yeng and Ling-Hwei, 1994). It is a two pass algorithm in which the mean distance from each event to its nearest neighbour is calculated in the first pass. Any event outside of the mean distance is an outlier and removed. Then a second pass is run and the nearest neighbour distances are computed for each event. Clusters are then created with events located closer than half the new mean distance. This method was applied in Lesniak and Isakowz (2009) which resulted in 40% of the data being eliminated. The advantage is that the data were able to be clustered sequentially. The algorithm also assumes a fifty percent split of the mean distance of nearest neighbours; however the data could be evaluated at different percentages to determine the best fit to the data.

2.3 Fractal Dimension

This thesis intends to use fractal dimensions to build on the concept of seismic clustering and seismic sources. Fractal dimension is a statistical method used to calculate non-linear geometry (non-Euclidian) specifically for scale invariant, complex systems (or physical processes), such as seismicity (Mandelbrot, 1982).

2.3.1 Mathematical Description of Fractal Dimension

Turcotte (1997), summarized fractal dimension by Equation 4:

$$N_i = \frac{C}{r_i^D} \qquad \text{(Equation 4)}$$

Where:

N_i = the number of objects (or fragments)

r_i = the characteristic linear dimension of the fragments (ie. ruler or yardstick)

C = constant of proportionality

D = fractal dimension

When D is a whole number such as 0, 1, 2 or 3, it is an Euclidian dimension. For example the Euclidian dimension of a point is D=0, a line segment D=1, a square D=2 (a plane), and a cube D=3 (solid volume) (Figure 20). However, if a line were broken into 3 pieces and one piece was removed, only a fraction of the line would remain. Thus when a dimension is a fraction, it is called a fractal dimension. The fraction is calculated using Equation 4. The same logic is applied to a partial plane or partial cube (Figure 20).

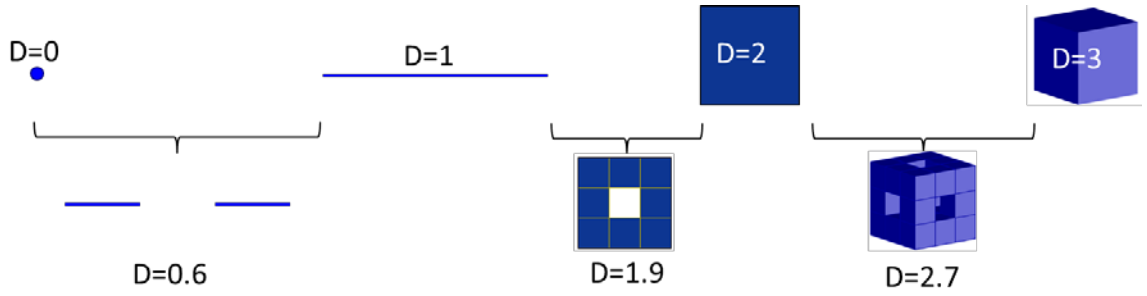

Figure 20: The difference between Euclidian dimension and fractal dimension

In terms of seismicity, when a fractal dimension is greater than 0 but less than 1 (0>D<1) it can be used to determine a point in time or a distance. An example of this application to seismicity is given in Kagan and Jackson (1991), where the fractal dimensions of the time-distance relation between seismic events in the HARVARD earthquake catalogue was determined using the correlation dimension method (Grassberger and Procaccia, 1983):

$$m(t) \propto t^{D} \qquad \textbf{(}\text{Equation 5}\textbf{)}$$

Where:

m = moment (Nm)
t = time (s)
D = fractal dimension

In Figure 21, when the fractal dimension has a value close to 0, it means the events are very closely clustered in time. As the fractal dimension value becomes closer to one, the clustering of events is more disperse. By determining the fractal dimension of varying depths in the catalogue, it was determined that shallower earthquakes are more densely clustered in time than deep earthquakes.

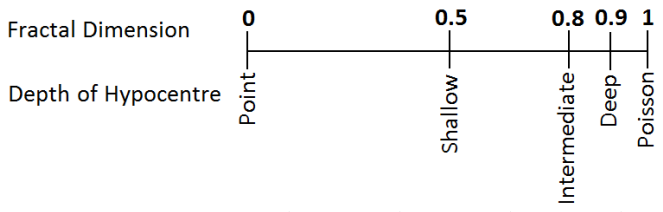

Figure 21: The relation between fractal dimension *(D)* and temporal behavior of earthquake seismicity

When a fractal dimension is greater than one and less than two, it represents a plane. Robertson *et al.*, (1995) applied this concept to the hypocenter of four fault structures in three dimensions (Table 4). Faults that are large in two dimensions and small in the third appear to be behaving as a plane with a high degree of complexity. The Big Bear fault, which has a fractal dimension slightly greater than 2, suggests it may have enough width for the fault to behave more as a three dimensional object.

Table 4: Fractal Dimension of Four Fault Zones

Fault Zone	**Fractal Dimension 3D**
Joshua Tree	D(3D) = 1.92 ± 0.02
Parkfield	D(3D) = 1.82
Big Bear	D(3D) = 2.01
Upland	D(3D) = 1.79

2.3.2 Fractal Dimension Calculation Methods

There are various ways to calculate fractal dimension (Klinkenberg, 1994). The most common methods applied to mining seismicity examples are the correlation dimension, number radius method, and the box counting method. The box counting and number radius methods both need input parameters that can affect the outcome of the results, particularly the size of the box or radius of the circle. Both these methods also require large amounts of data. The correlation dimension method does not require large amounts of data and does not introduce a bias based on an input parameter. The method uses a correlation integral (Hirata *et al.*, 1987) described by Equations 6 and 7.

$$C(R) = \frac{n(r<R)}{P} \qquad \text{(Equation 6)}$$

$$C(R) = \frac{2n(r<R)}{N(N-1)} \qquad \text{(Equation 7)}$$

Where:

$C(R)$ = correlation integral

$r < R$ = inter-event distances (metres)

P = pair ratio $P = N(N-1)$

$n(r < R)$ = # of pairs

N = number of events

R = maximum inter-event distance (metres)

If a plot of log $C(R)$ versus log R results is a straight line, it means $n(r < R)$ is proportional to the power function of R, and the relation is fractal.

Coughlin and Kranz (1991) applied the correlation integral to seismic events around a stope using inter-event distances during two different time periods. No rationale for the time periods chosen is given in the paper. The plot of the results (Figure 22) show the inter-event distances are fractal, and that the fractal dimension decreases as time increases.

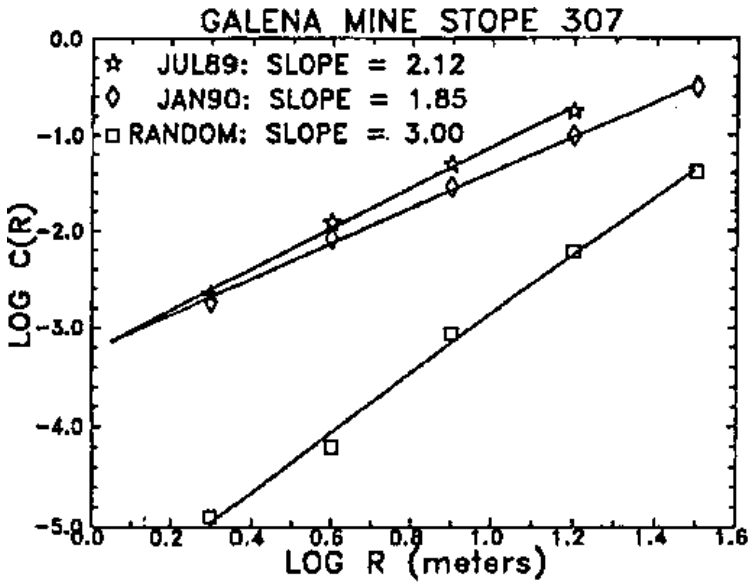

Figure 22: Plot of the inter-event distances around a stope during two different time periods

The data were compared to a synthetic data set with random inter-event distances. The events around the stope had a fractal dimension an order of magnitude lower than the random data set, which demonstrates the seismic event inter-event distances were not random.

In the same paper, the two point correlation method was used on the inter-event times after two rockbursts to see if the after shock event times were the same as or different than the precursory shock event times (Figure 23). It was found that the fractal dimensions were the same for both periods. Data set A and B are post-event events and Data set C is pre-rockburst events (redrawn from Coughlin and Kranz, 1991).

Both examples in this paper demonstrate the relative ease in which correlation integrals can be used on inter-event distances and time to gain information from seismic events about rock mass failure. The method is not limited to these two parameters but can be used on other seismic source parameters depending on the theory being tested.

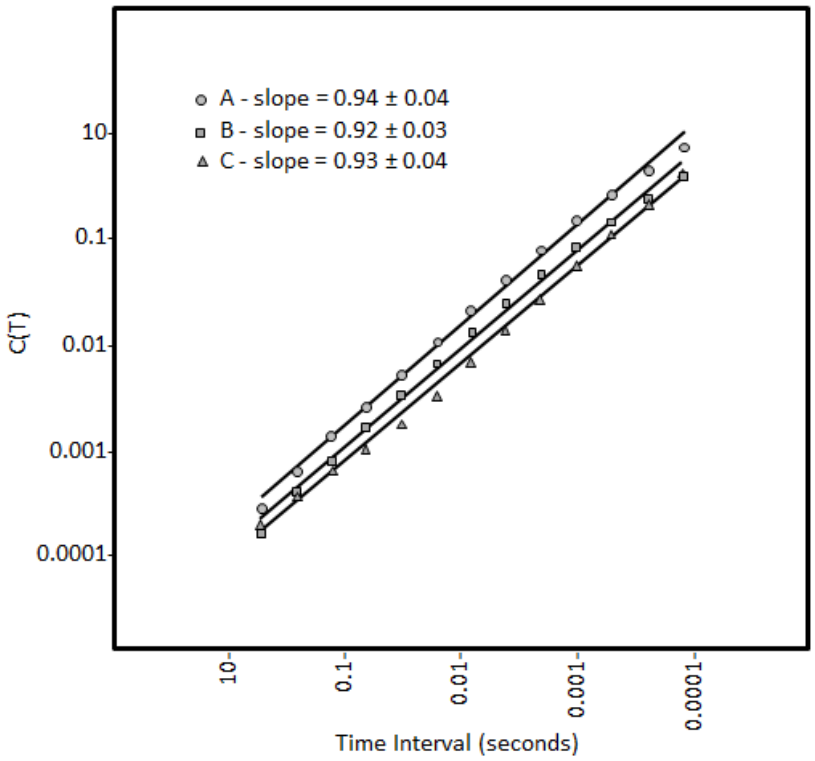

Figure 23: Comparison of the inter-event times before and after a rockburst

Other applications of fractal dimension to mining seismic data are reviewed comprehensively in Gibowicz and Lasocki (2001). The motivation for the research at that time was focused on using fractals to prove/disprove that seismicity (earthquake and mining) was self-similar and if a method could be found to predict earthquakes or rockbursts.

2.3.3 Fractal Dimension Applications to Seismicity in Underground Mines

The prediction goal was never realized, and fractal dimension methods were applied in different ways in underground mines (Table 5).

Table 5: Fractal Dimension Applications in Underground Mines

Mine	Country	Reference
Westwood	Canada	Kalenchuk *et al* ., 2017
Creighton	Canada	Eneva and Young, 1993 Eneva, 1994 Eneva and Villeneuve, 1997 Eneva and Ben-Zion, 1997 Eneva, 1998 Pasten *et al.* , 2015
Strathcona	Canada	Trifu *et al.* , 1993
Upper Silesia Coal Basin	Poland	Idziak and Teper, 1996
Katowice	Poland	Mortimer and Lasocki, 1996a Mortimer and Lasocki, 1996b Mortimer, 1997
Rudna	Poland	Lizurek and Lasocki, 2014 Weglarczyk and Lasocki, 2009
Champion Reef	India	Shivakumar, *et al* ., 1996
Western Deep Levels	S. Africa	Gibowicz, 1997
Galena	U.S.	Coughlin and Kranz, 1991 Xie and Pariseau, 1993 Lu, *et al.* , 2005

The difficulty with the research using fractal dimensions is that the basis for analysis behind each study is narrow and varies from research group to research group. For example, the number of events used differed from one researcher to another and limited data sets were used. Mortimer and Lasocki (1996a) stated that reliable estimates of fractal dimension were only achieved with greater than 1500 events; Shivakumar *et al.*, (1996) used three data sets of 125 events. The volume of area studied also varied (670 x 630 x 390 m^3 in Gibowicz (1997); 400 x 400 x 180 m^3 in Eneva and Young (1993)). Other parameters that varied widely were magnitude ranges and time periods. Despite the variability in approaches a few common themes did emerge. These themes will be discussed in the following section.

2.3.4 Change in Fractal Dimension with Changing Seismic Source

Along the same line as Mandal *et al.*, (2005) and Lizurek and Lasocki (2014), Wyss *et al.*, (2004)

found that the San Andreas fault had very different fractal dimensions for the locked portion of the fault (D = 0.96 - 1.14) than the creeping portion (D = 1.45 – 1.72). The fractal dimensions corresponded to frequency magnitude b-values (locked b = 0.5-0.7; creeping b = 1.1 – 1.6). The theory that fractal dimension is different for different mechanisms has merit worth exploring.

This brings to mind the question: Do seismic sources that have the same mechanism have the same size magnitude? It would appear not, as a fault-slip earthquake has a magnitude >2 while a fault-slip event in a mine is usually magnitude <2 (Bohnhoff *et al.*, 2010). In Figure 24, one would expect the larger volume of the high stress pillar between stopes to retain and then release more seismic energy than a smaller pillar between drawpoints. How would it then compare to a crown pillar or sill pillar?

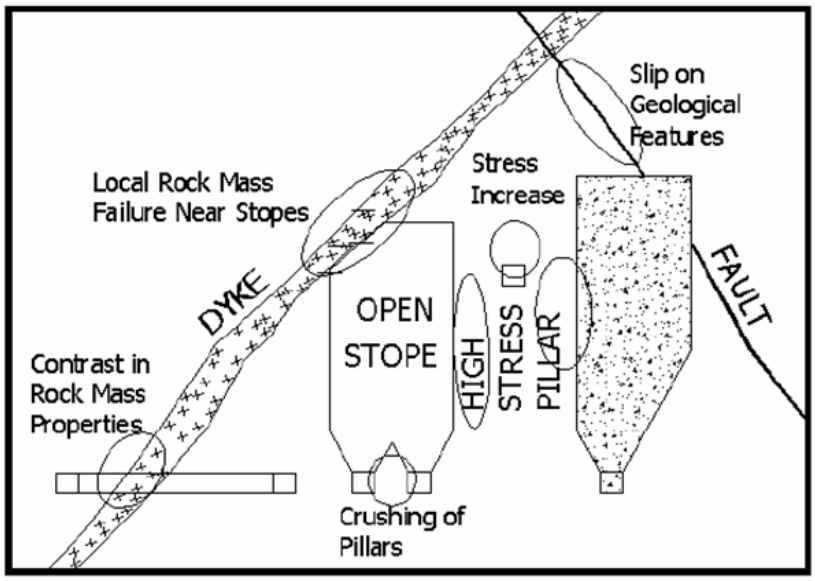

Figure 24: Common seismic sources in a mine (Hudyma *et al.*, 2003)

2.3.5 Drop in Fractal Dimension Prior to a Large Event

The first observation was made by Hirata (1987) in a study of fractal dimension and earthquakes. It was found that the fractal dimension decreased with increased rock fractures and the decreasing

fractal dimension was a precursor to an earthquake. At the Galena mine, Xie and Pariseau (1993) observed an increase in the quantity of clusters (increase in local cracks in the rock mass) before a rockburst with a corresponding decrease in the fractal dimension. Eneva and Young (1993) made a similar observation of increased number of clusters preceding some $M \geq 2$ events at Creighton and a decrease after. Recently Pasten *et al.*, (2015) revisited the theory at Creighton mine and used a multifractal method to confirm that the fractal dimension dropped prior to a seismic event of 3 sizes ($M > 1.0$, $M > 1.5$, and $M > 2$). It was recommended that more data sets needed to be examined. Not all researchers agreed. Mandal *et al.*, (2005) studied earthquake data from India and found that the fractal dimension could increase or decrease before a large event depending on which mechanism was active in the fault. Lizurek and Lasocki (2014) also found changes in fractal dimension prior to large events; however the patterns differed depending on the moment tensor solution. As Mandal *et al.*, (2005) found, this suggests that fractal dimension may also change with different seismic sources. This is the second common theme found.

2.4 Chapter Summary

Despite a large body of research into seismic events in mines, major seismic events are still occurring unexpectedly and with serious implications. As mines progress deeper, the need for additional research is required to understand seismic events that occur in unexpected places and at unexpected times. Seismic systems in underground mines are currently able to cover a range of moment magnitudes (M_W -3 to +3) using a combination of geophones and accelerometers with a range of sensitivities. These systems provide the record of thousands of seismic events every day for analysis. The location and time of each event are two seismic source parameters that are readily available for analysis. However, efforts to study time and space together may yield

inconclusive results as time periods to study are chosen by researchers which may or may not be correct for a data set. Another short coming of previous studies is the manner in which seismic data is clustered. The use of agglomerative clustering techniques has made interesting and important progress with respect to clustering seismic data up until the turn of the century. However, the techniques used can require large data sets, partial supervision and are unable to allow cluster formation to be studied over time. These techniques also have a tendency to remove events because outliers are considered to be of no importance. Surprisingly most if not all studies remove outliers without proving they have no effect on seismic analysis results.

The use of fractal dimension as a statistical method to study seismicity was also introduced in the 1990's. It is often used on complex system or processes – such as seismicity – that have non-Euclidian geometry and are scale invariant. While there are a number of ways to calculate fractal dimension, the correlation integral method is most often used as it does not require a large data set nor does it introduce a bias based on an input parameter. The application of fractal dimension to the study of seismicity in mines has met with mostly inconclusive results. Studies included different size data sets often containing multiple seismic sources, blasts or noise. Two themes did emerge that were recommended for further study. The first is that some researchers noticed that the fractal dimension dropped before a large event and second that the fractal dimension may change with a change in seismic source mechanism. There is an opportunity to learn more about rock mass failure through seismic events by creating a new clustering method that does not require large amounts of data that can be studied over time, and can identify different seismic sources. The clusters can then be studied statistically using the correlation integral method to determine if changes in fractal dimension reflect changes in a rock mass as it fails.

Chapter 3

3 Sequential Spatial Clustering

This thesis proposes a new clustering technique called sequential spatial clustering. This method is novel in that seismic clusters are formed one event at a time (in the order that they occur) to the events that precede it. In this way, the sequence of events that form a cluster is preserved. By replacing the sequence number with the actual date and time of the event, the cluster formation can be viewed over time without using time as an explicit metric in the clustering process.

3.1 Ramp Development - Base Case

A base case of the seismic response to the development of a ramp using current analysis methods will be shown as basis for which to evaluate the sequential clustering. In this case, the development of a down ramp from May 18th to August 1st, 2005 will be used. Figure 25 shows the ramp at the start of the study period (Image A) and the actual completed ramp (Image B).

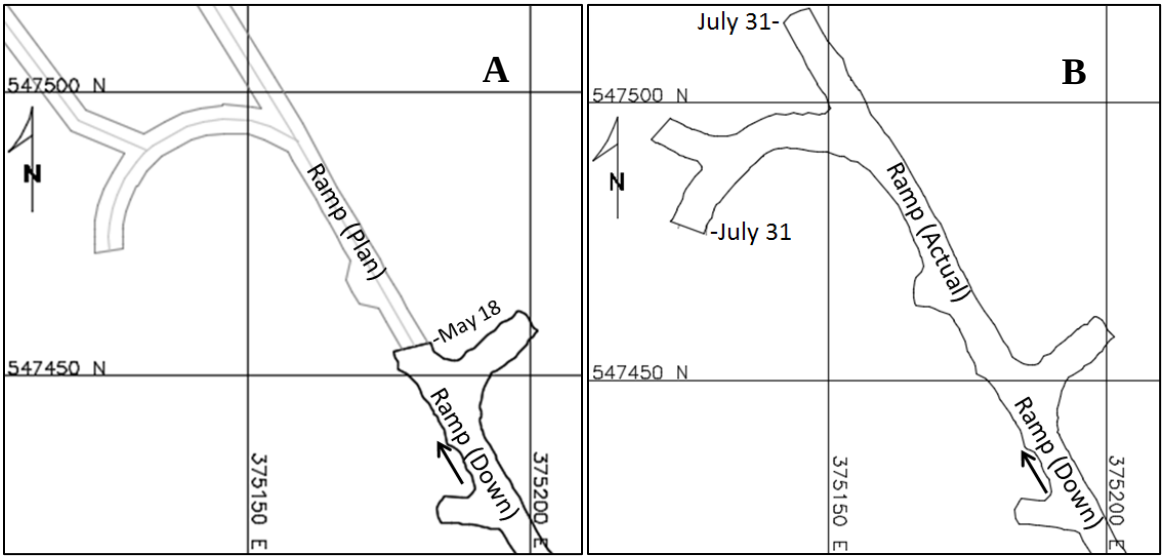

Figure 25: Down ramp developed between May 18th and July 31, 2005. Image A - The actual ramp already excavated is shown by the dark black line; the planned excavation is shown with a grey center line. Image B - The outline of the completed ramp on July 31, 2005.

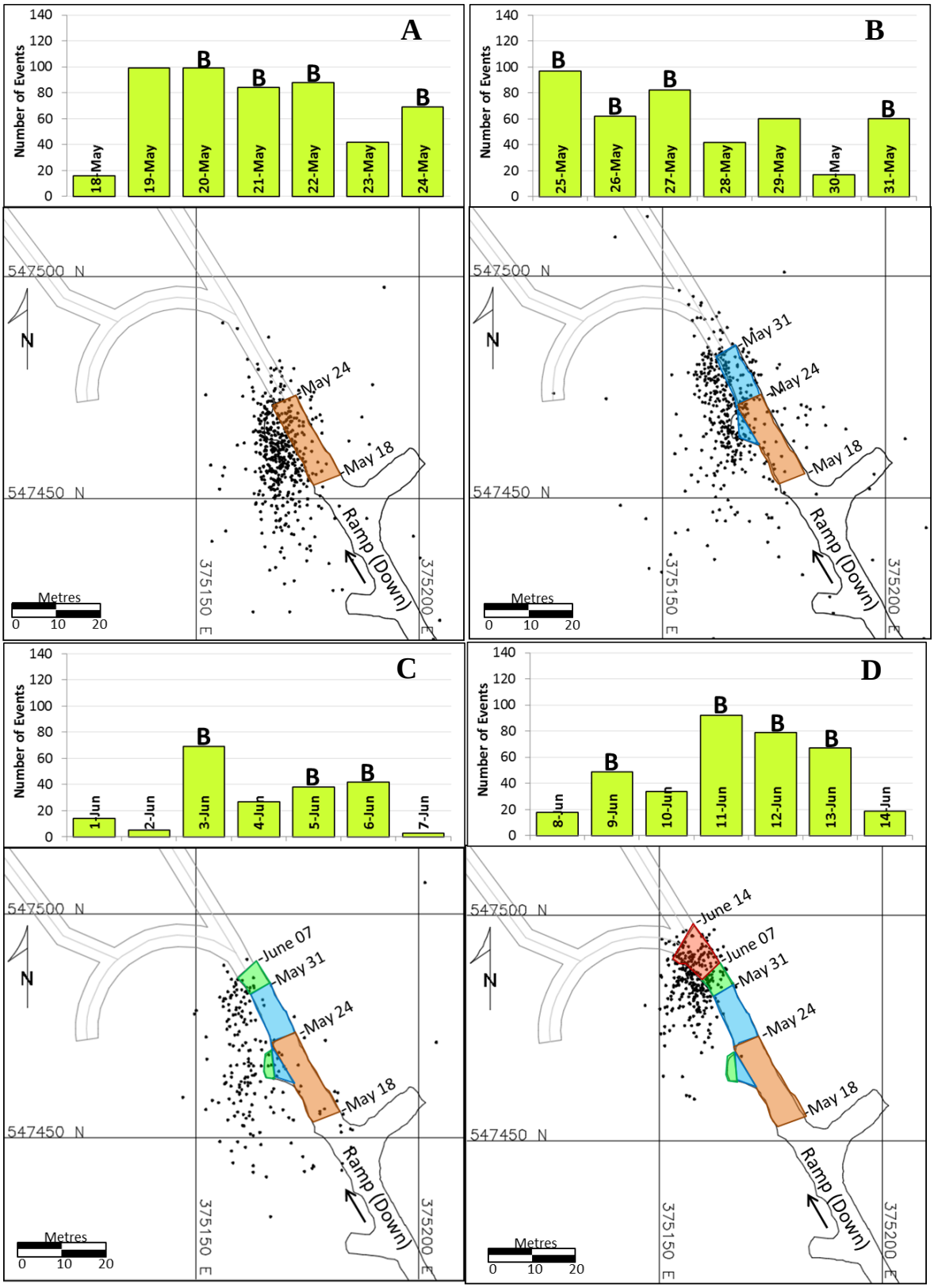
A
Number of Events
18-May
19-May
20-May
21-May
22-May
23-May
24-May
B
547500 N
547450 N
N
May 24
May 18
Ramp (Down)
375150 E
375200 E
Metres
0 10 20
B
25-May
26-May
27-May
28-May
29-May
30-May
31-May
May 31
May 24
May 18
Ramp (Down)
C
1-Jun
2-Jun
3-Jun
4-Jun
5-Jun
6-Jun
7-Jun
June 07
May 31
May 24
May 18
Ramp (Down)
D
8-Jun
9-Jun
10-Jun
11-Jun
12-Jun
13-Jun
14-Jun
June 14
June 07
May 31
May 24
May 18
Ramp (Down)

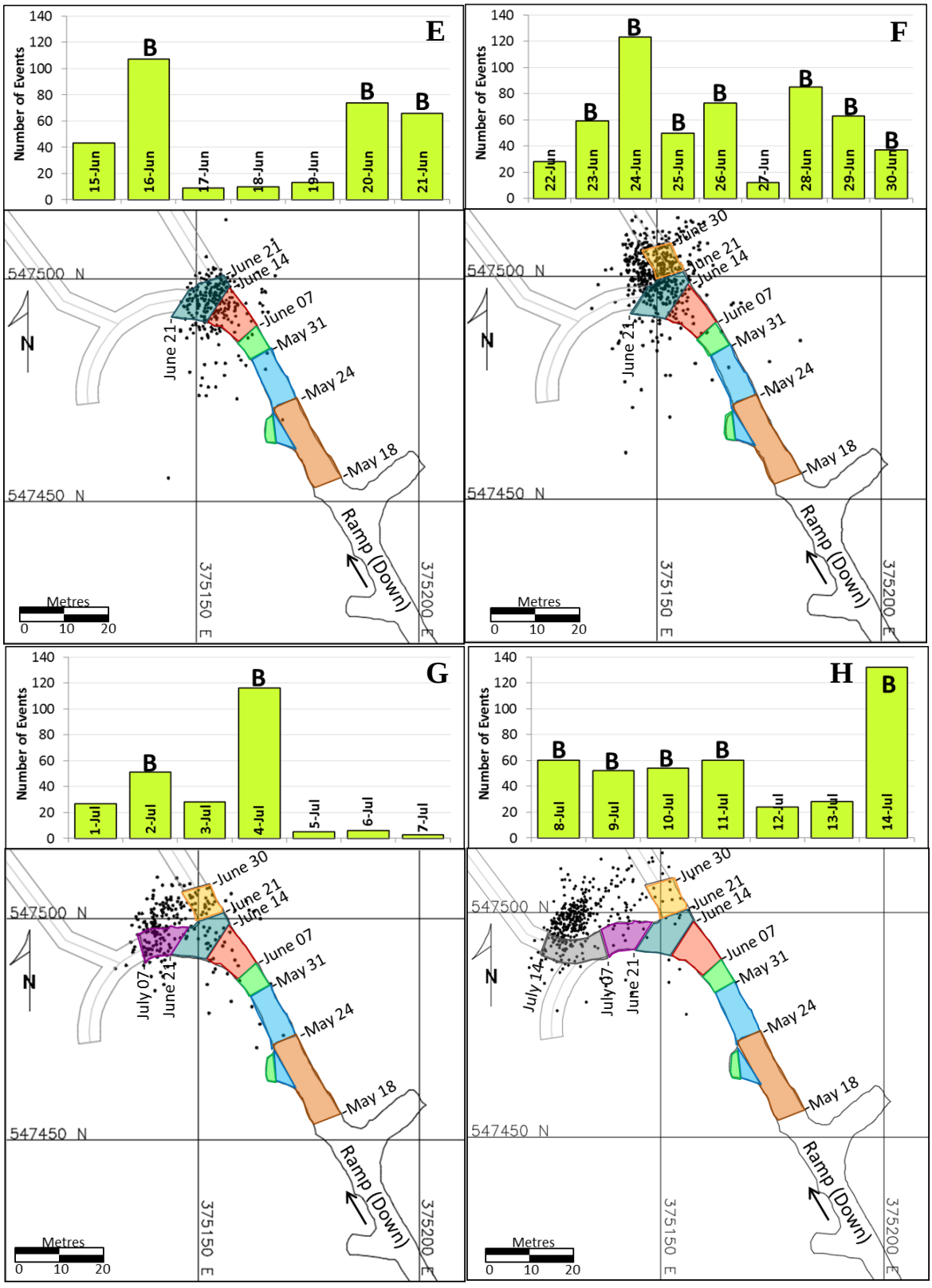
E
Number of Events
15-Jun
16-Jun
17-Jun
18-Jun
19-Jun
20-Jun
21-Jun
F
22-Jun
23-Jun
24-Jun
25-Jun
26-Jun
27-Jun
28-Jun
29-Jun
30-Jun
G
1-Jul
2-Jul
3-Jul
4-Jul
5-Jul
6-Jul
7-Jul
H
8-Jul
9-Jul
10-Jul
11-Jul
12-Jul
13-Jul
14-Jul
547500 N
547450 N
375150 E
375200 E
N
Metres
0 10 20
June 30
June 21
June 14
June 07
May 31
May 24
May 18
Ramp (Down)
July 14
July 07
June 21

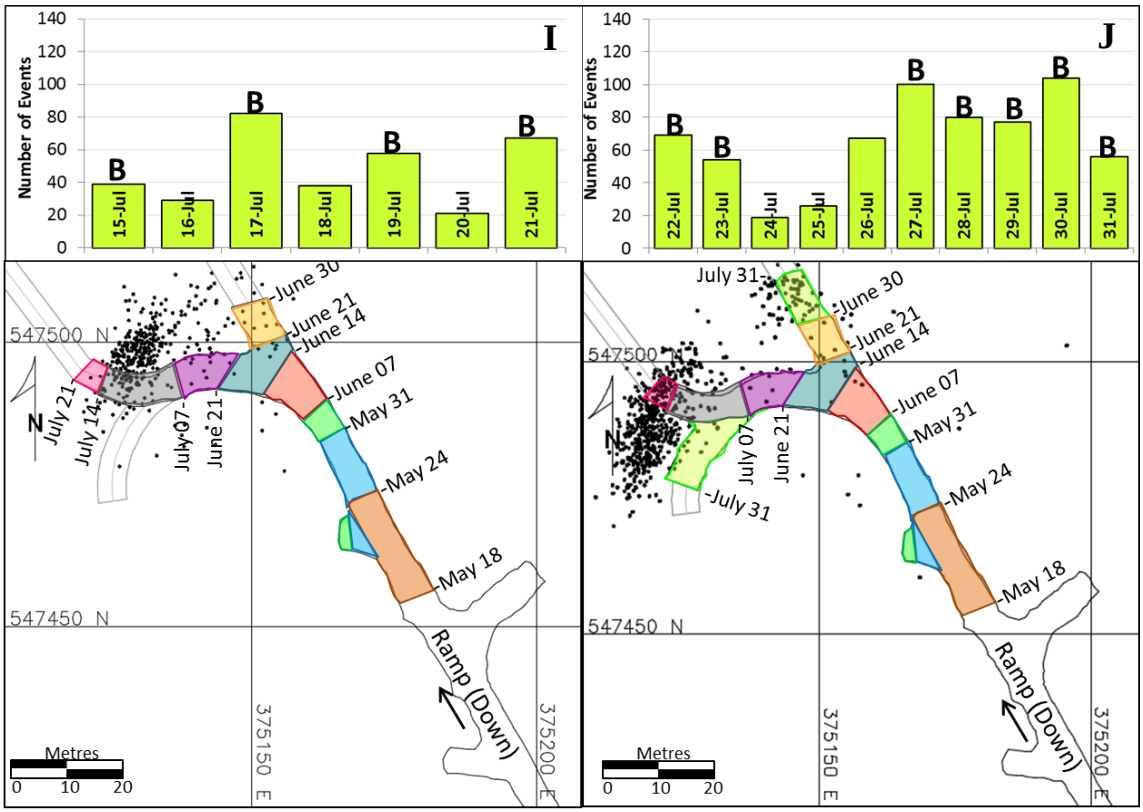

Figure 26: Images A through J show the seismic events around the ramp as it is being developed

In Figure 26 Image A, the ramp advances with a blast almost every day (blasts are noted by the letter B above the date in each figure). In a 24 hour period, the images show that a full three metre development round in the ramp usually has a response of fifty or more seismic events. Image B shows fewer metres of advance than image A with the same number of events despite having fewer metres of advance. The difference is that Image B shows a section of the ramp has been widened using a partial round (called a slash). Image C shows the completion of the slash and some further advance in the ramp. Images D to I show the ramp advancing through a curve. This is achieved by a combination of development rounds and slashes. This type of development is slow, has fewer metres of advance, has a larger number of blasts and the seismic activity is relatively close to the ramp. The final development is shown in Image J. This example shows development rounds advancing in a straight line or around a curve with seismicity in close proximity to the ramp.

Figure 27, shows the seismic events that occurred after a development round was blasted on May 31, 2005. The events colored in red are closest to the three metre round that was blasted (shown by the small grey box). The blue events indicate some rock fracturing ahead of the development round, and the black colored events indicate additional fracturing of the rock around the drift blasted prior to May 31st.

Figure 27: Seismic events occurring after a development round blast on May 31, 2005

The box outlined by dashed lines in Figure 27 shows the area seismic events can be expected according to McGarr (1976). The drift width and height are both five metres. The box lines have been drawn twice the drift width - ten metres away from the sides, ahead and behind the development round blasted. In this example all the seismic events are within the box which is common for a blast of this size. A normal seismic response to a development blast would typically have events with magnitude less than zero (Talebi and Young, 1993). The events of May 31, 2005 range from $M_{R=}$ -0.22 to $M_{R=}$ -3.01, meeting the criteria for a normal response.

When considering the time of these events, most of them occur in the first few hours following the blast at 4:30 am (Figure 28) and the event rate rapidly decreases to a few events per hour over the remaining twenty four hour period after the blast. It is considered a normal response to a development round blast based on the location of the events, the rate of post-blast seismicity, and the magnitude of the events.

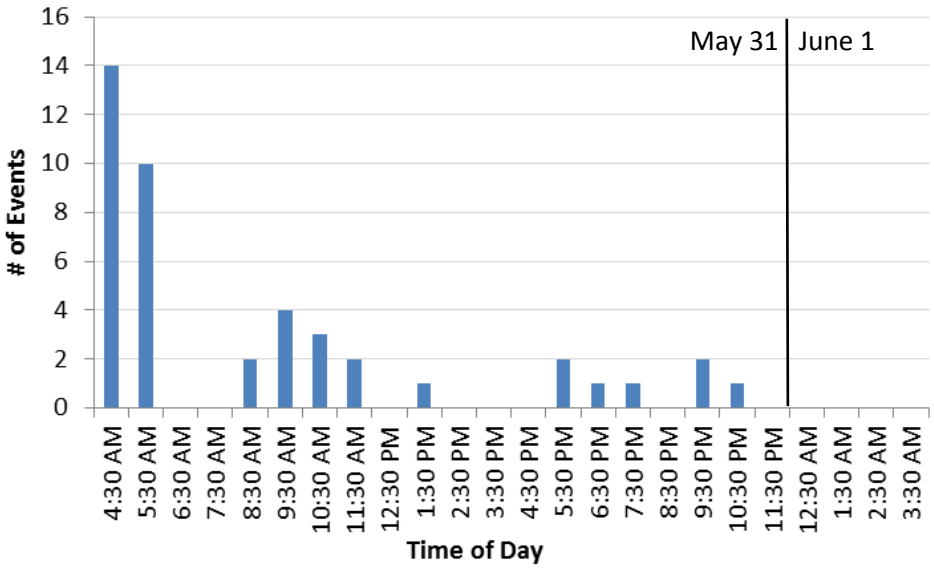

Figure 28: Seismic event frequency after a development round blast at 4:30am in the ramp on May 31, 2005

An abnormal seismic response is defined as seismic events that occur either in an unexpected location or at an unexpected time after mining (rock excavation) has taken place. An abnormal seismic response to development blasting can be seen in Figure 29. The events in this figure are from development in the down ramp during the week of July 22 to 31, 2005.

Figure 29: The seismic events from July 22nd to 31st are shown by the black dots. The light green areas are outlines of the areas that were excavated during this period. The dashed line boxes indicate the areas that are within ten metres of each excavation. The seismic events shown in the red circle are outside of the normal area.

The events within the boxes with dashed lines are within ten metres of the excavations. The red circle shows seven events that are abnormally located fifteen to fifty metres away from the blast locations. With respect to time, the events inside the red circle also occur at abnormal times (not following any particular blast). The event furthest south occurred four hours before the blast in the ramp on July 26, 2005. Also, the area where the event occurs was developed two months earlier in May, making it abnormal in two ways, there is no active mining within ten metres (closest mining is fifty metres away) and the event does not follow a development blast. The three events closest to each other in the middle of the red circle occur on different days (July 22, 26 and 28). They each occur at abnormal times relative to the blasting on their respective days. One event occurs before the blast and the other two occur six to seven hours after a blast. The location of the ramp these events are closest to was excavated at the end of May, almost two months prior. The timing of these events is also abnormal. While the magnitude of the events are all within the range of the

normal events (M_R ~-2 to -3), the time of the events and their locations are all abnormal.

When looking at the events on any given day, they would likely be dismissed as outliers because they are relatively close to the blasting area and they are small in number. Outliers are typically removed before analysis of the remaining seismic events (Richardson and Jordan, 2002; Julia *et al.*, 2009; Cranswick, 2011). The underlying assumption is that outliers are not relevant to the area of study. This may not be true and the opportunity to study outliers is lost when they are removed from a database. This thesis uses all events in a data set.

3.2 Sequential Spatial Clustering

Rock mass failure is a time dependent process. A rock mass' failure rate is fundamentally affected by the excavation process. Any increase or decrease in the excavation process strongly influences the location and rate of the rock mass failure. Seismic monitoring data can be used to quantify the location and rate of rock mass failure. There is significant importance associated with the sequential occurrence of the recorded seismic events as they show the evolution of the rock mass failure process. A novel method of clustering seismic events is proposed based on a seismic event's location and proximity to preceding seismic events.

3.2.1 Sequential Spatial Clustering Method

In this method, the inter-event distance that determines whether or not a seismic event joins a cluster is determined by examining the inter-event distances of previous events. This is accomplished by calculating the distance between each seismic event and every other prior seismic event. The event that is closest to the most recent event is the nearest neighbour and the distance between them is the nearest neighbour distance.

To demonstrate how clusters form, the progression of twenty six seismic events will be followed in Figure 30 (Images A to AB). Events are added one at a time, and they may form a cluster with one other event, join an existing cluster of more than two events or remain as a single event. One other note, the Images A to AB in Figure 30 are isometric views of the seismic event locations in three dimensions. As an isometric view, a scale cannot be put on the three dimensional images. To give the reader some perspective, a line is drawn between each event sequentially clustered to prior events if it is within 1.7 metres of a previous event. How the clustering distance of 1.7 metres is determined will be explained later in this section. If no line is drawn, the events are more than 1.7 metres apart. It should be noted that the images are a two dimensional representation of a three dimension isometric drawing. As such, events may have the appearance of being closer together in two dimensions than they are in three dimensions.

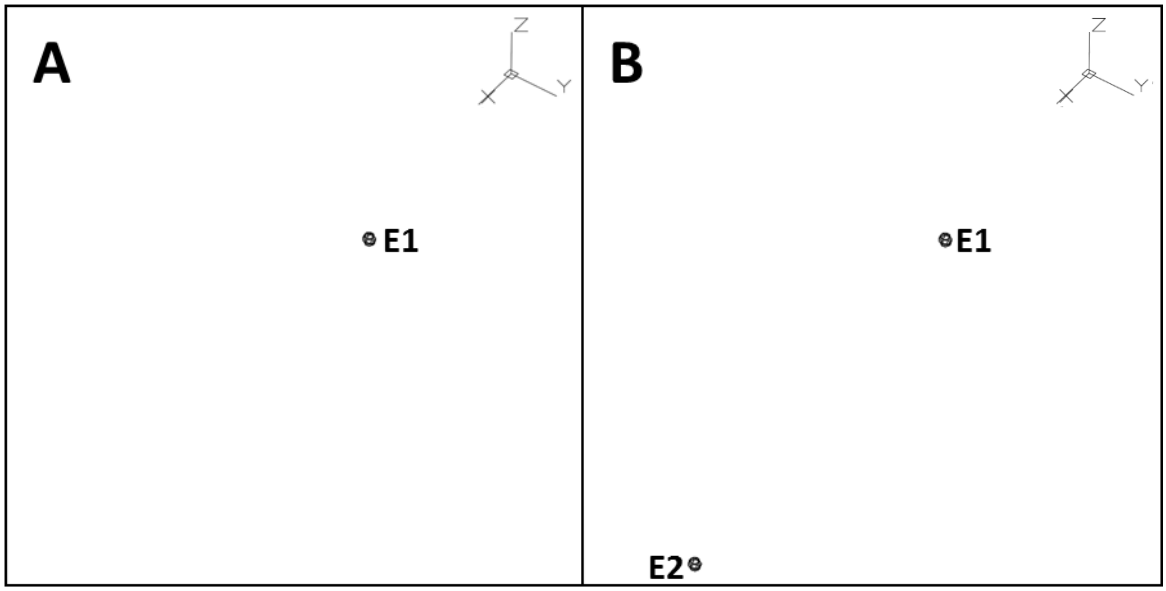

Figure 30: Image A - The location of the first seismic event in a 26 event sequence. It does not have a nearest neighbour so it remains a single event (E1). Image B - When the second event occurs, the distance between Event 1 and Event 2 is calculated. At 4.2 metres, it is well above 1.7 metres so Event 2 does not form a cluster with Event 1. Instead, the two events remain single events (E1 and E2).

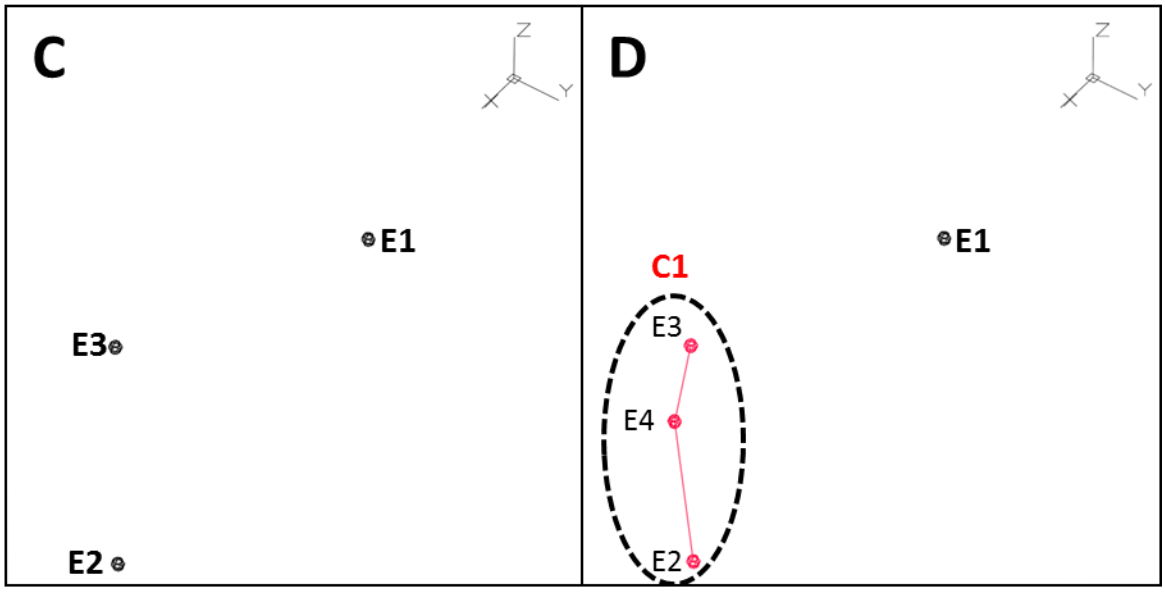

Figure 30: **Image C - Event 3 is also more than 1.7 metres from Events 1 and 2, so three single events (E1, E2, and E3) are present at this point. Image D - When Event 4 occurs, it is found to be within 1.7 metres of Events 2 and 3 and a cluster of three events is formed (C1 shown by dotted line). Event 1 remains as a single event (E1). Note that the sequential method allows for multiple links to form between events. Active clusters will be shown in color (for example C1 is pink), single events are colored black, and inactive clusters will appear in grey.**

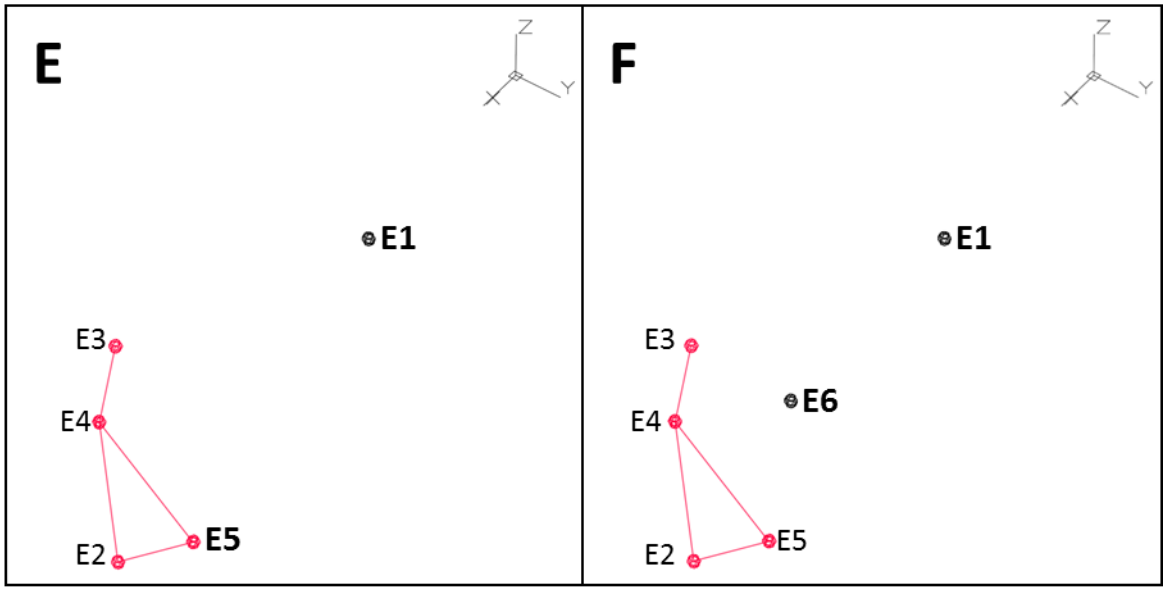

Figure 30: **Image E - Event 5 joins C1 as it is less than 1.7 metres from Events 2 and 4. C1 now contains four events and E1 remains a single event. Image F - Event 6 is not within 1.7 metres of any other event, so it remains a single event along with E1. C1 remains a cluster of four events.**

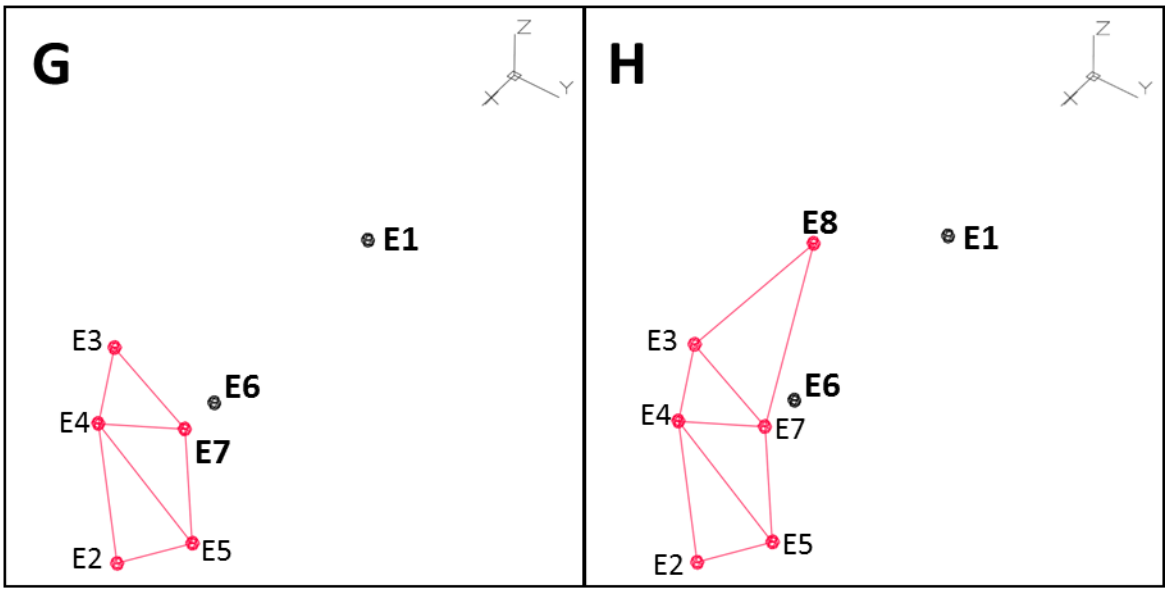

Figure 30: **Image G - Event 7 joins C1 as it is less than 1.7metres from Events 3, 4, and 5. Thus C1 is a cluster of five events, and E1 and E6 remain single events. Image H - Event 8 also joins C1 as it is within 1.7metres of Events 3 and 7. C1 is now a cluster of 6 events and E1 and E6 remain single events. Notice how the shape of C1 changes as events are added. This is significantly different than single link clustering as sequential clustering allows multiple links to form.**

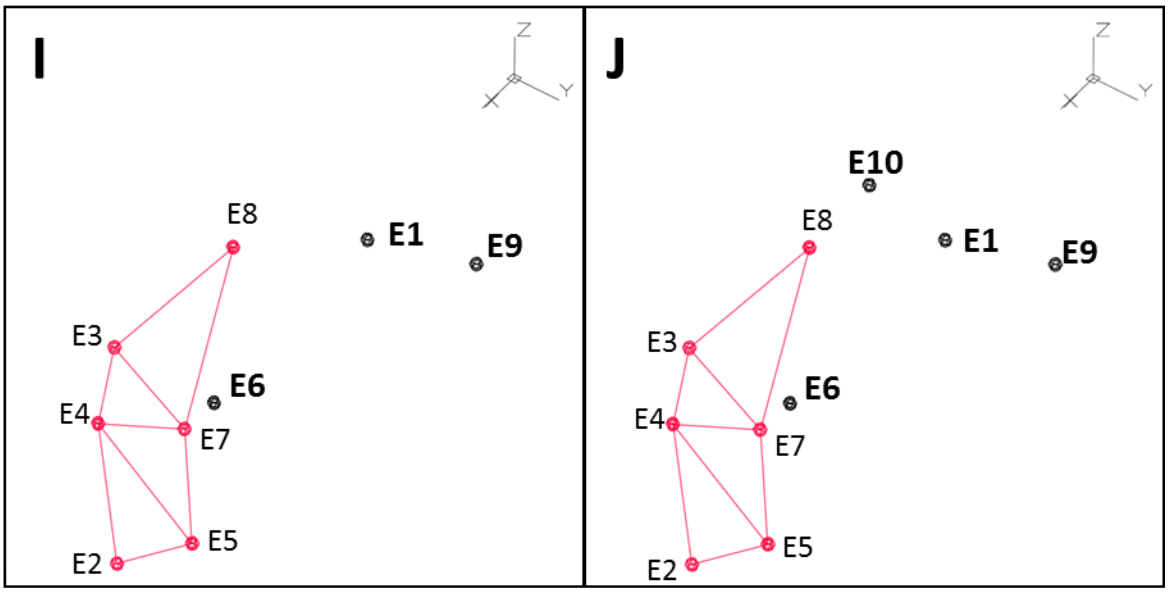

Figure 30: **Image I - Event 9 is not in close proximity to the other events and remains as a single event (E9) along with E1 and E6. Image J - Event 10 also remains a single event, along with E1, E6, and E9. C1 doesn't change at this stage and remains a cluster of 6 events.**

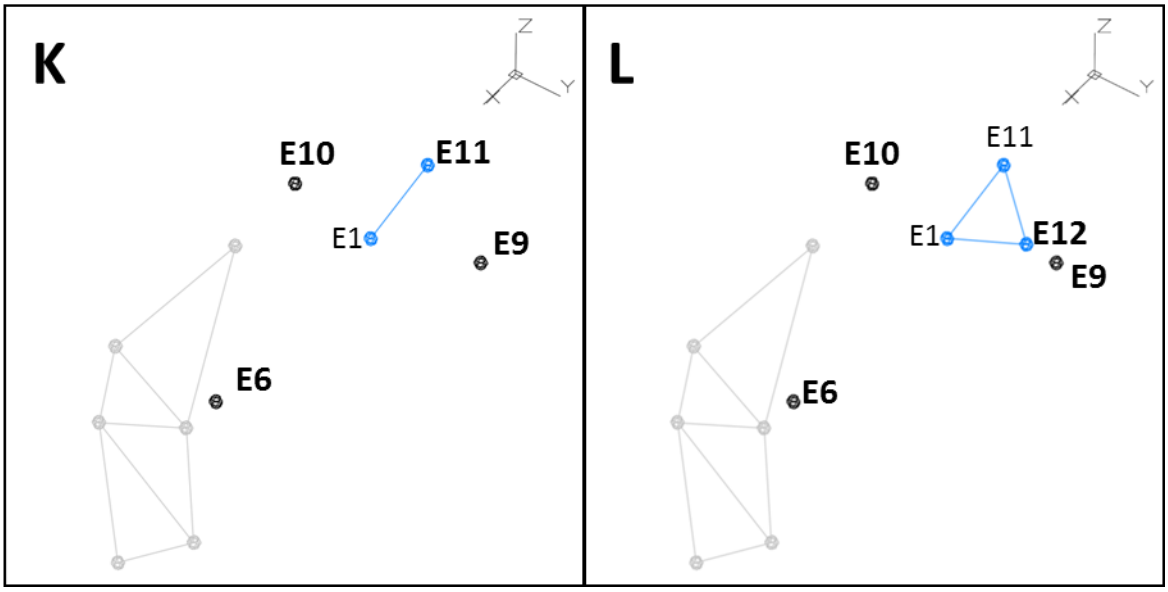

Figure 30: **Image K - A second cluster forms (C2-shown by blue lines and dots) when Event 11 occurs and becomes the nearest neighbour to Event 1. C1 remains the same with 6 events and E6, E9 and E10 remain single events. Image L - Event 12 adds to C2 increasing its size to three events (E1, E11 and E12) and there is no change to C1 (6 events) and the single events (E6, E9 and E10).**

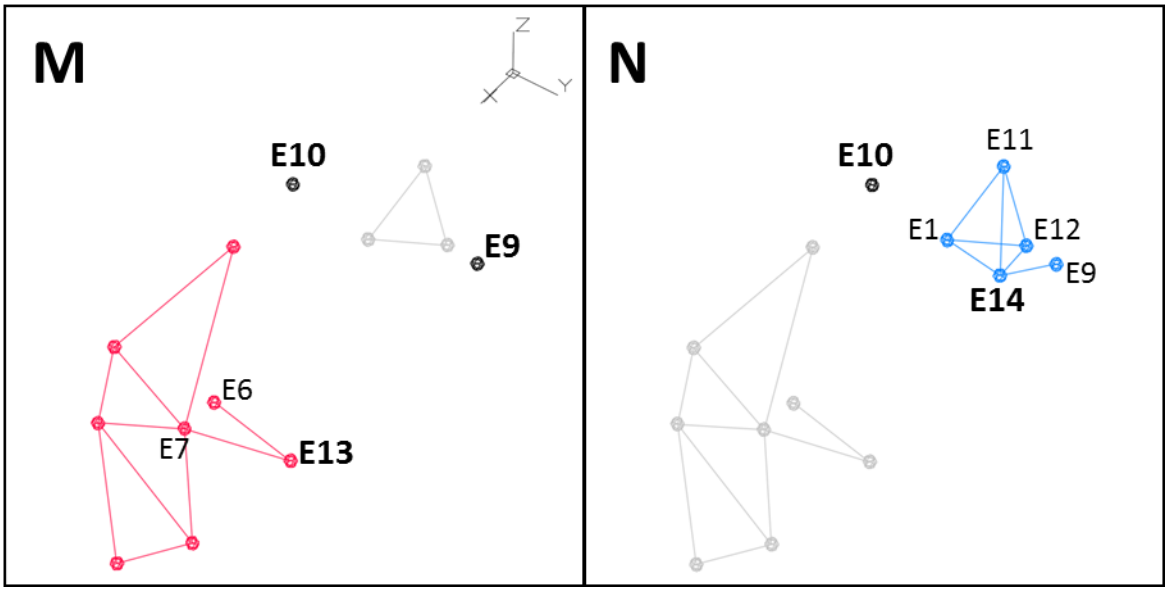

Figure 30: **Image M - Event 13 joins C1 and E6 to create a larger C1 (8 events). C2 remains unchanged with 3 events and there are now only two single events (E9 and E10). Image N - In the same manner Event 14 is within E1, E12, and E9 making C2 a larger cluster with 5 events. C1 remains unchanged with 8 events and E10 remains as the only single event.**

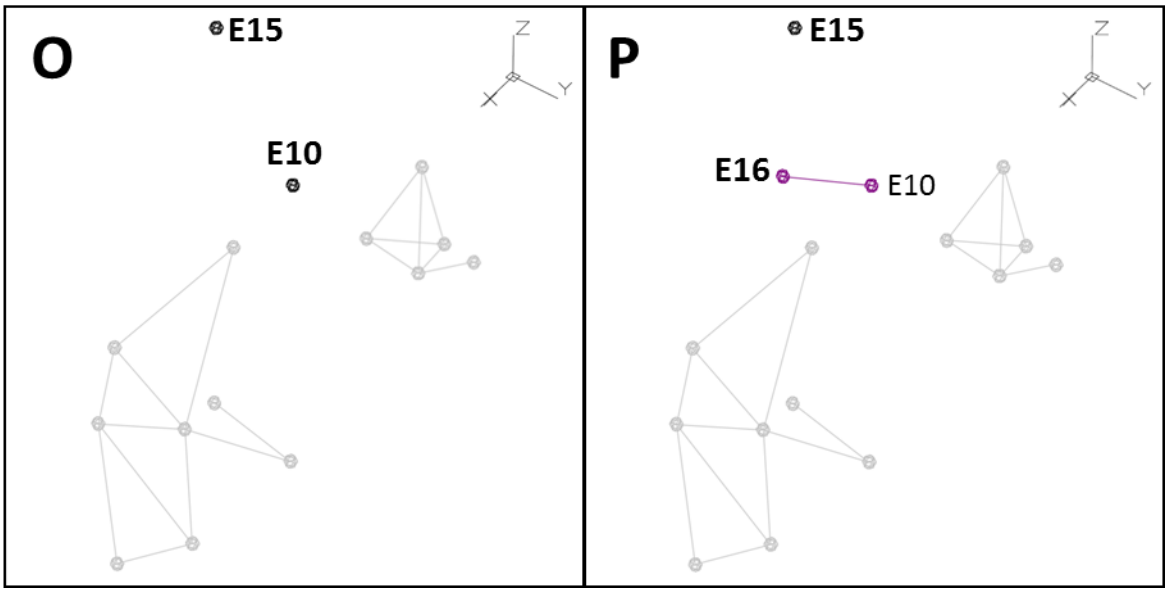

Figure 30: **Image O - Event 15 remains a single event (E15) along with E10, while C2 and C2 remains the same with 5 events and 8 events respectively. Image P - Event 16 joins Event 10 to form a new cluster (C3 - purple lines and dots). There are now three cluster sizes (C1-8 events, C2-5 events and C3-2 events) and one single event (E15).**

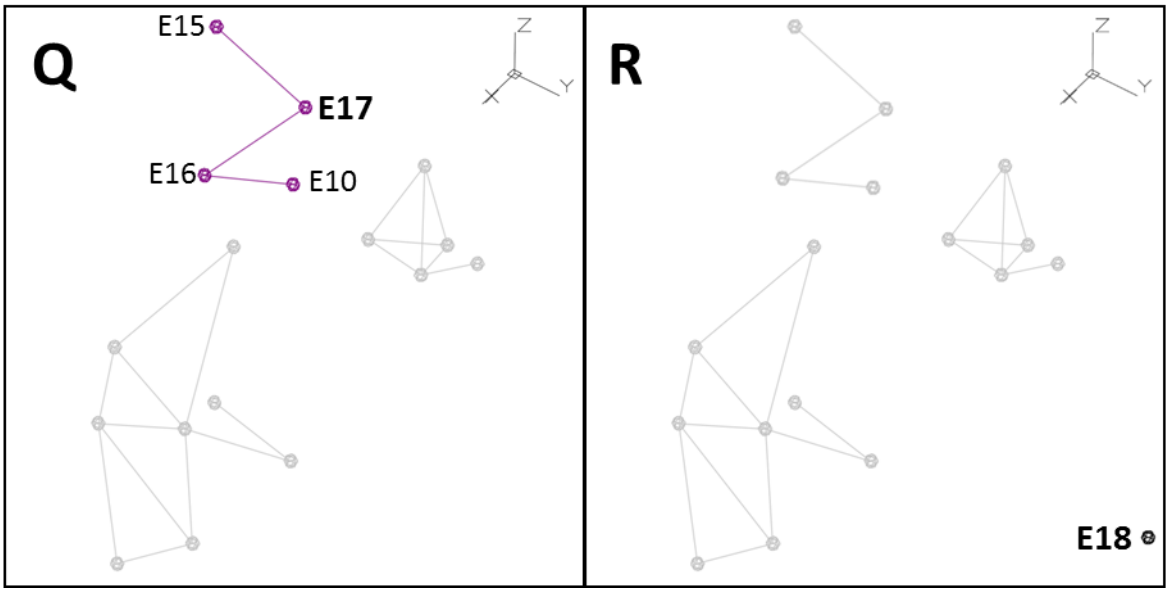

Figure 30 **Image Q - Event 17 joins E15 to C3 and increases the size of C3 to four events. There are no single events remaining and C1 and C2 are unchanged (C1-8 events, C2-5 events). Image R - Event 18 is not in close proximity to any other event so it remains a single event (E18). The clusters remain unchanged (C1-8 events, C2-5 events and C3-4 events).**

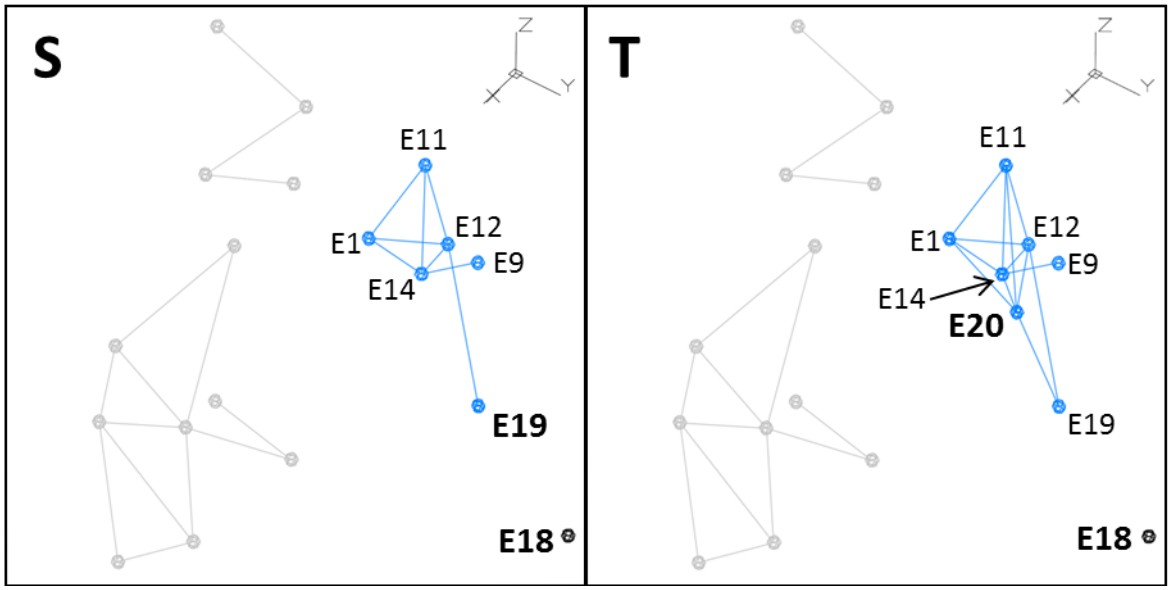

Figure 30: **Image S - C2 becomes active again and increases in size with the addition of Event 19 (C2-6 events). Clusters 1 and 3 remain unchanged (C1-8 events, C3-4events) and E19 remains a single event. Image T - The size of C2 increases again with the occurrence of E20 (C2-7 events). Clusters 1 and 3 do not change (C1-8 events, C3-4 events) and E18 remains a single event.**

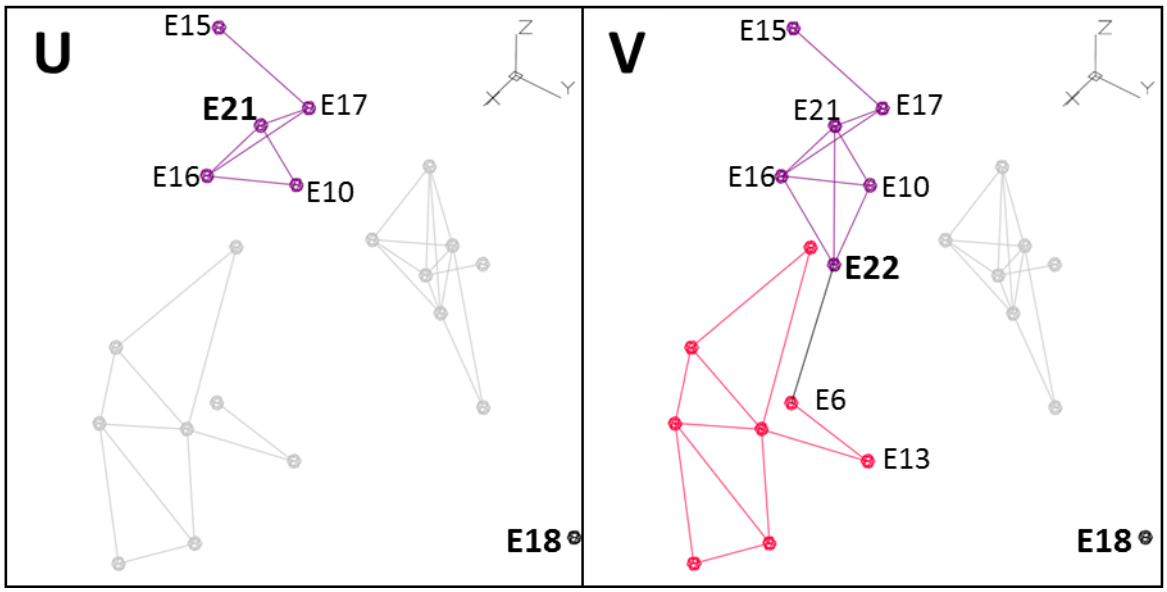

Figure 30: **Image U - Event 21 increases the size of C3 to 5 events. Clusters 1 and 2 do not change (C1-8 events, C2-7 events) and E18 remains a single event. Image V - In a similar manner to Event 13 joining E6 with C1 (Image M), Event 22 joins two clusters because of its proximity to Event 6 in C1 and three events (E10, E16, and E21) in C3. This is a significant change as now there are only two clusters (C1-14 events, C2-7 events) and one single event (E18). Cluster 3 ceases to exist as it now becomes part of Cluster 1. Also, note the original cluster color (C3-purple), has not changed to reflect the color of C1 (pink). This has been done to show the original history of C3 (now a sub-cluster within Cluster 1) is retained in sequential clustering.**

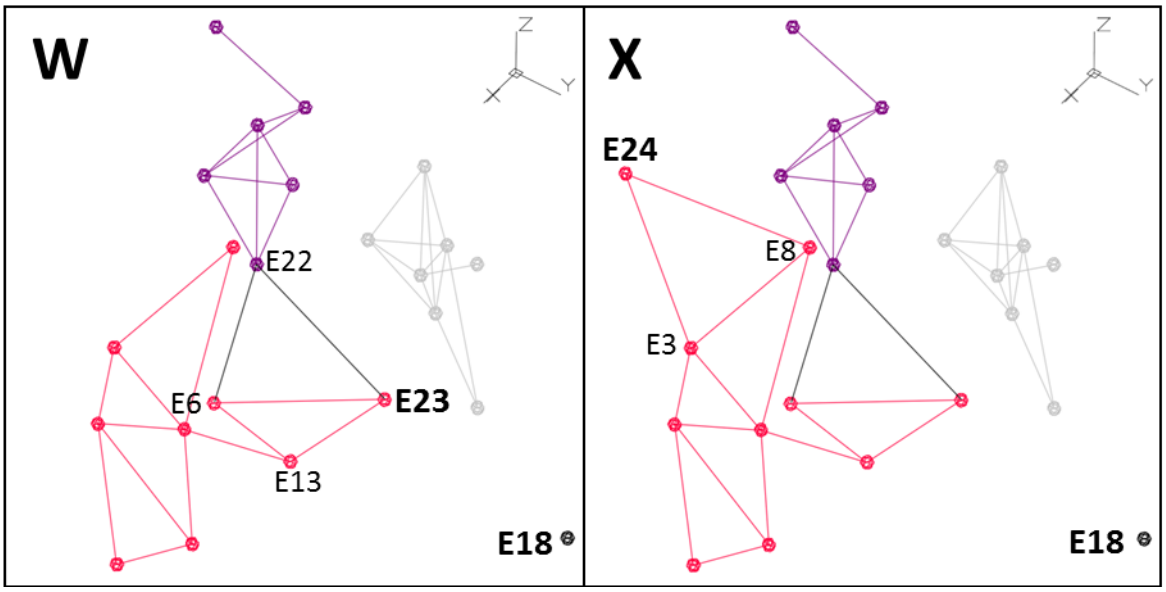

Figure 30: **Image W - Event 23 becomes part of C1 through its proximity to E6, E13, and E22. There are still two clusters (C1-15 events, C2-7 events) and one single event (E18). Image X - Event 24 also joins C1 because of its proximity to Events 3 and 8. There are now still two clusters (C1-16 events, C2-7 events) and one single event (E18).**

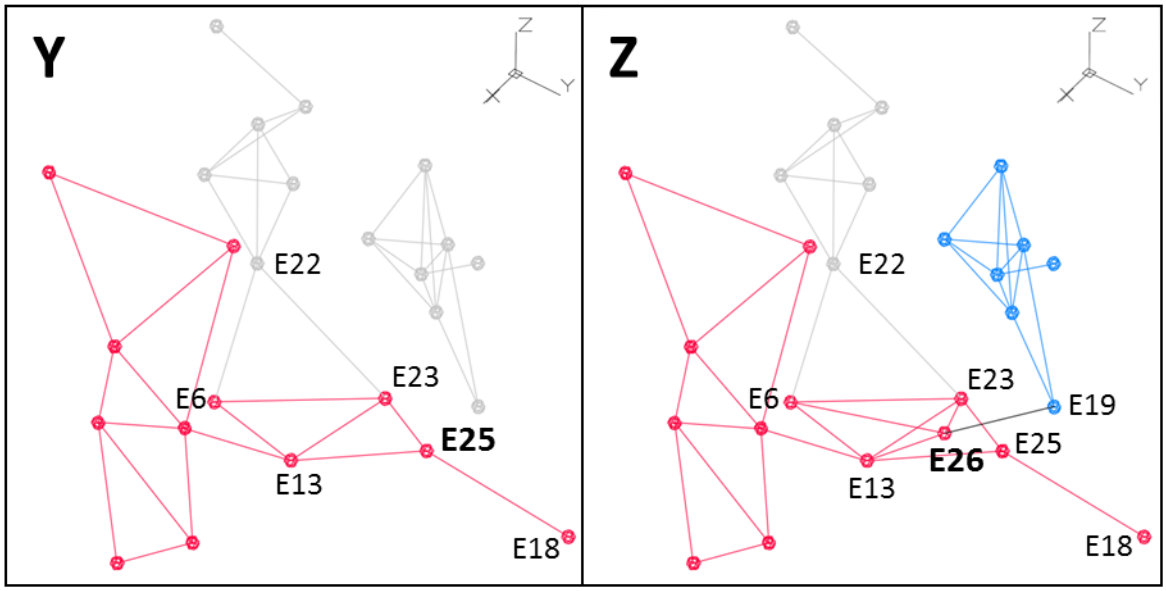

Figure 30: **Image Y - Event 25 joins Event 18 to C1 through Events 13 and 23. There are now only two clusters (C1-18 events, C2-7 events). Image Z - The last event in this example, Event 26 joins the final two clusters together (C1 and C2) through Events 6, 13 and 23 (C1) and Event 19 (C2). These 26 events are now one cluster (C1-26 events).**

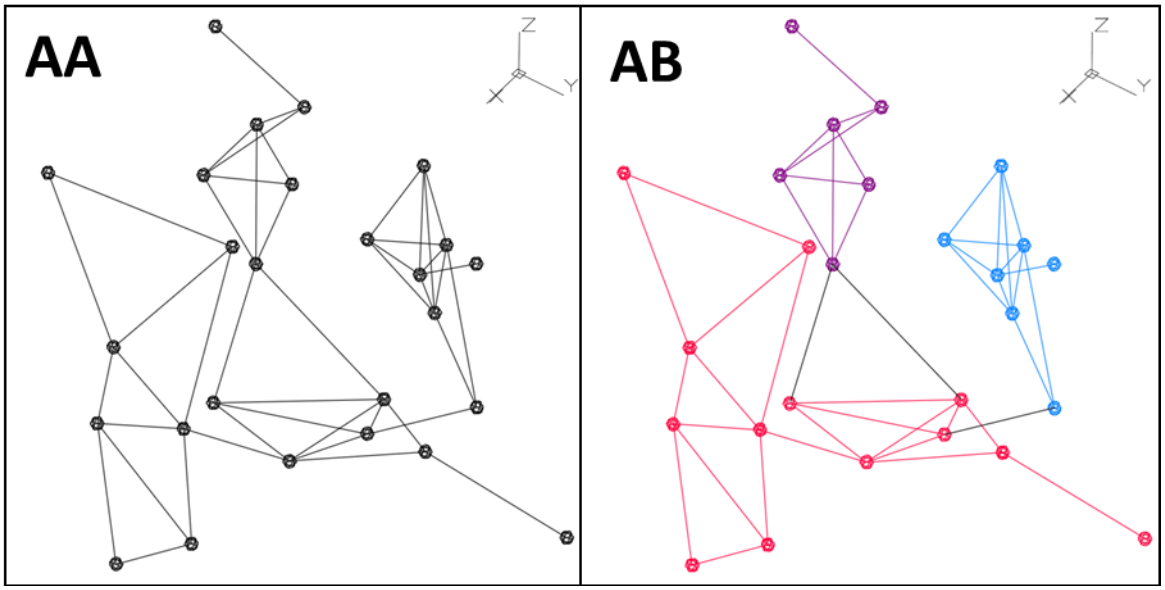

Figure 30: Image AA - C1 after 26 events; Image AB - C1 showing the progression of the events and clusters over time by color. The colors denote clusters with more than one event: C1 (pink), C2 (blue), and C3 (purple). The black lines in the image on the right hand side show the link between the events that join clusters.

Images A to AB in Figure 30 show how clusters form one event at a time using the distance between nearest neighbours. Links were established between events with a nearest neighbour distance of 1.7 metres or less with multiple links allowed to form. By clustering seismic events in this way, the history of an event that may initially be a single event and then part of a cluster, can be followed over time without stipulating a time period. For example, Event 1 starts as a single event (E1, Figure 30 Image A) and remains solitary and isolated until Events 11 occurs and a cluster is created (C2). When Event 12 occurs, C2 increases by one event (Figure 30 Images K and L). Event 14 joins C2 with Event 9 (Figure 30 Image N), such that C2 now contains 5 events (E1, E9, E11, E12, and E14). C2 increases to seven events with the addition of Events 19 and 20 (Figure 30 Images S and T). The cluster remains isolated until Event 26 joins Events 6, 13 and 23 (C1) to Event 19 (C21) (Figure 30 Image Z). C1 now contains 26 events (Figure 30 Image AA and AB). The sequence can be seen in Figure 31.

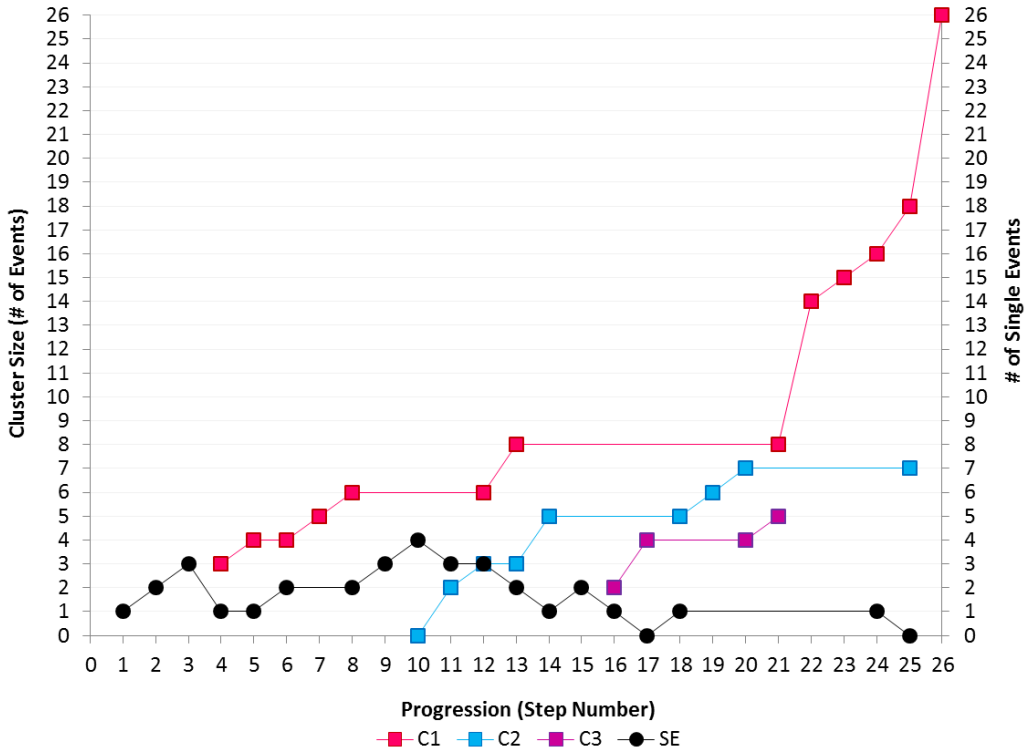

Figure 31: Sequence of twenty six seismic events that form a cluster. Clusters (denoted with a "C") form when an event is within 1.7 metres of a preceding event.

The advantage of sequential clustering is that the step number can be replaced with the date and time of the event that occurs at each step. The same clustering sequence is shown in Figure 32. The difference is that the step number on the x axis of Figure 31 has been replaced with the date of each event. The sequence is preserved but now the actual time that seismic activity takes place in these clusters is clear. In this case, the seismicity begins on January 4th, 2003 and the pillar remains seismically active between the 4th and 20th. During this time there are multiple events per day and the events become closer together indicating the rock mass failure is increasing. After the 20th there is a marked decrease in the activity rate, however the area remains seismically active for another month until the last event on February 22nd. This type of information is invaluable for studying rock mass degradation because the events nearest to each other remain associated by belonging to the same cluster and the cluster can be studied over time.

3.2.2 Time Periods of Sequential Spatial Clusters

A particular difficulty with previous spatial-temporal studies of seismicity is that a study time frame must be chosen (Kijko *et al.*, 1993; Eneva and Villeneuve, 1997; Lesniak and Isakow, 2009). The time frame chosen (a week, month, year, etc.) is imposed on the data and the results of space-time clustering can vary drastically based on the time frame chosen. These types of clustering methods are unable to preserve the sequence which inhibits temporal study of clusters.

By clustering spatially and sequentially the time period for a cluster can be studied without having to choose a study time frame. This is accomplished by plotting each cluster sequentially with respect to the date and time each event occurred. Table 6 shows the date and time of the twenty-six events previously shown in the sequential cluster formation (Images A to AB in Figure 30).

Table 6: Date and Time of Twenty-Six Sequential Events

Sequence Number	Date	Time	Time Between Events (hrs)
1	4-Jan-03	7:09 AM	0
2	5-Jan-03	8:45 AM	26
3	6-Jan-03	11:51 PM	39
4	7-Jan-03	5:12 AM	5
5	9-Jan-03	4:00 PM	59
6	10-Jan-03	8:46 PM	29
7		10:30 PM	2
8	11-Jan-03	10:54 PM	24
9	12-Jan-03	11:39 AM	13
10	14-Jan-03	4:24 PM	53
11	15-Jan-03	5:50 AM	13
12	18-Jan-03	3:37 AM	70
13		4:03 AM	0
14	18-Jan-03	10:51 AM	7
15		4:46 PM	6
16	19-Jan-03	1:08 AM	8
17		9:01 AM	8
18		11:47 AM	3
19		1:07 PM	1
20	20-Jan-03	7:28 AM	18
21		2:01 PM	7
22		7:01 PM	5
23	24-Jan-03	9:11 PM	98
24	26-Jan-03	12:28 AM	27
25	8-Feb-03	9:04 PM	333
26	22-Feb-03	7:48 AM	323

A sequential plot of this data can now be made using the date of each event instead of the sequence number. The sequence is still preserved but more meaningful information with respect to cluster activity periods can now be analyzed (Figure 32). Two significant items to notice in this figure are

that multiple events can occur on the same date (January 10, 18, 19 and 20) and longer periods between events can occur (pink lines - January 27 to February 7, and February 9 to 22nd).

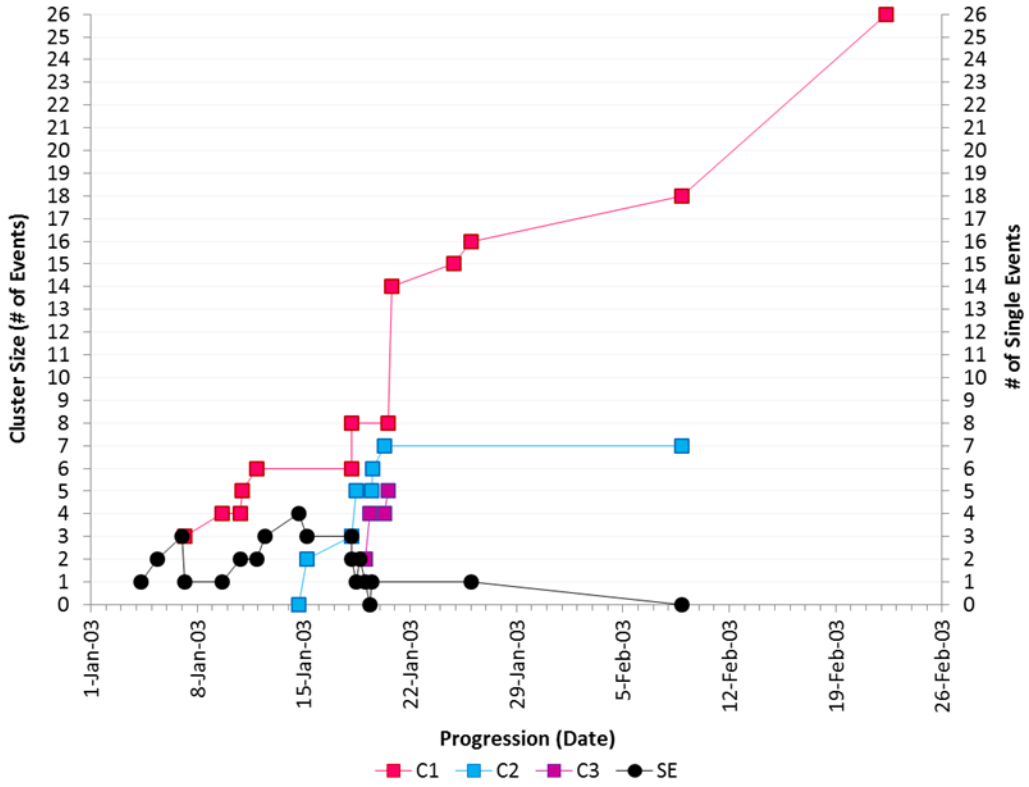

Figure 32: Time sequence of twenty six seismic events in a cluster

The graph also shows that Cluster 1 (pink squares in Figure 32) has two periods of inactivity (January 27-February 10th, February 11th to February 22nd), with little activity in between. The active periods January 15, 18 and 19 have seismic rates of 3, 5 and 7 events per day respectively. These short but active periods for Cluster 1 followed by periods of inactivity are more reflective of changes in the rock mass at the location of Cluster 1, than the average activity rate of 0.8 events/day implies. Following this cluster for a longer period of time may show that the cluster has this type of periodicity.

The seismic activity is from a failing pillar. The highest seismic activity takes place between January 4th and January 20th, 2003, but the pillar continues to fail and remains seismically active

for another month until February 22, 2003, albeit at a much lower rate. By February 22nd, all twenty six events belong to the same cluster. This example gives insight into where the pillar failed (each individual cluster location) and that the rock mass between the clusters also failed (all events close enough together to form one cluster).

This example has a very small population of seismic events, which is another important contribution to studying seismic events. Other seismic analysis methods require large data sets before meaningful results can be interpreted. The sequential spatial clustering method begins with one event and adds events one at a time, regardless of the number of events in a data set. This thesis will demonstrate that the method of sequential spatial clustering can give new insight into a variety of seismic event populations undergoing rock mass failure.

Another key contribution of the sequential clustering method is that single events are included and not removed from the clustering process. In current clustering analysis techniques, single events that happen in the past can often be removed, lost or forgotten. However, these single events represent a rock mass fracture in an area and need to be preserved. The area may not become seismically active again for a long period of time, but the fracture or weakness in the rock still exists. Thus while a single event may not seem important at the time it happens, it is record of a location of a previous fracture in a rock mass that should be included with later seismic events should the area become seismically active again. Including the previous fracture or fractures will give a more complete picture of the state of the rock mass than if they were not retained. Keep in mind that single seismic events that remain isolated events for the duration of the mine are true outliers and can then be identified as such.

The importance of retaining single event or clusters with a small number of events is also

demonstrated by E1. E1 (Figure 30 Image A) remains isolated as a single event while C1 starts to form (Figure 30 Images D, E, G, and H). This early activity and growth of C1 tends to shift the focus to it and away from E1. While this example is small it makes the point that single event (such as outliers or clusters with a small number of events) may appear to be unimportant at the time they occur, however they may be early indicators of a location that may become seismically active over time. As the sequential progression of E1 shows (Figure 31), the event remains isolated for ten events - a significant portion of a sequence with twenty-six events. By Event 26, E1 has become a large cluster (C2), relative to the number of events.

Sequential clustering is a unique method for studying seismicity because it can be used with a small number of events. It can also be used proactively as clusters form – which is more effective than retroactive analysis. To demonstrate this point, consider three glasses each containing a different colored liquid, one red, one yellow and one blue. If all three glasses were poured into one glass, the colors would blend together and create a black colored liquid. Now take the black colored liquid and try and separate out the three colored liquids back into their original glasses. It is not easy and may not be possible. This is analogous to collecting seismic events from different locations or with different mechanisms and putting them all together into the same data set and then trying to separate the events into clusters in the order they occurred. Like the eyedropper in Figure 33 which adds one drop of blue liquid at a time to the glass containing the same blue liquid, sequential clustering adds seismic events one at a time to the cluster that contains other seismic events that are closest to it.

Figure 33: Sequential clustering is analogous to adding one drop at a time of one colored liquid to a glass with the same colored liquid (photo GIPhotoStock / Getty Images).

By placing nearest neighbour seismic events in the same cluster as they occur, the cluster can be studied as it progressively gets larger. Most seismic analysis methods, particularly clustering methods, need large numbers of seismic events and generally take place retroactively. This new type of sequential spatial clustering preserves the order and association each event has with other events that are closest to it. With the order preserved and the relations between nearest neighbours known, clusters of a single seismic source can be studied over time. In this way, clusters created using the sequential clustering method can be used to help identify seismically active areas early and at any point in time and space, particularly as seismicity progresses. This ability to detect unexpected seismically active locations early is a key component to reducing seismic hazards in mines.

3.2.3 Determination of Nearest Neighbour Distance

Sequential clustering is dependent on the distance between seismic events because it defines which events join a cluster. The difficulty is choosing which distance to use. Fortunately, the location of the seismic events and the distances between each event gives good information on which distance

to use. In Figure 34, the nearest neighbour distances of 4225 seismic events are plotted. The distribution of this data was compared to a variety of distributions (Normal, Weibull, Student t, Exponential, Gamma, Max Extreme, Logistic) using EasyFit® software. The seismic nearest neighbour distances were found to have the closest fit to a lognormal distribution (Figure 34).

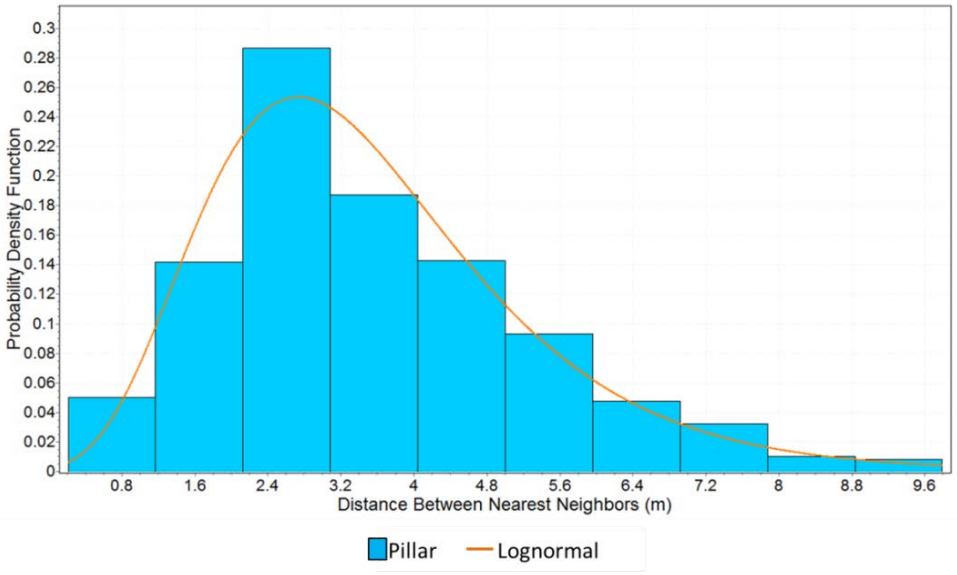

Figure 34: The nearest neighbour distances (in metres) of 4225 seismic events were plotted and compared to Normal, Lognormal, Gamma, Max Extreme, Weibull, Logistic, Exponential and Student t distributions. The best fit of the data is to a lognormal distribution.

A variable X has a lognormal distribution if Y has a normal distribution: Y = ln(X). The probability density function of a lognormal distribution can be calculated using Equation 8, (Niwitpong, 2013):

$$f(x,\mu,\sigma^2) = \begin{cases} \frac{1}{x\sigma\sqrt{2\pi}}\exp\left(-\frac{(ln(x)-\mu)^2}{2\sigma^2}\right) & ; \quad for\ x > 0 \\ 0 & ; \quad for\ x \leq 0. \end{cases} \qquad \text{Equation 8}$$

Where:

μ = mean
σ^2 = variance

In order to determine which events are closest to each other, a distance between the events needs to

be specified. If the distance chosen is too small, the events remain as single events. If the distance is too large, the events tend to form clusters with large numbers of events. These large clusters tend to have more than one seismic source. Rather than arbitrarily choose a distance, the probability distribution of the nearest neighbour distances is considered. A comparison of the number and size of clusters for the distance specified by the mode (4.5 metres), mean (8.0 metres) is shown in Figure 35 using the probability density function of a population of 1350 seismic events.

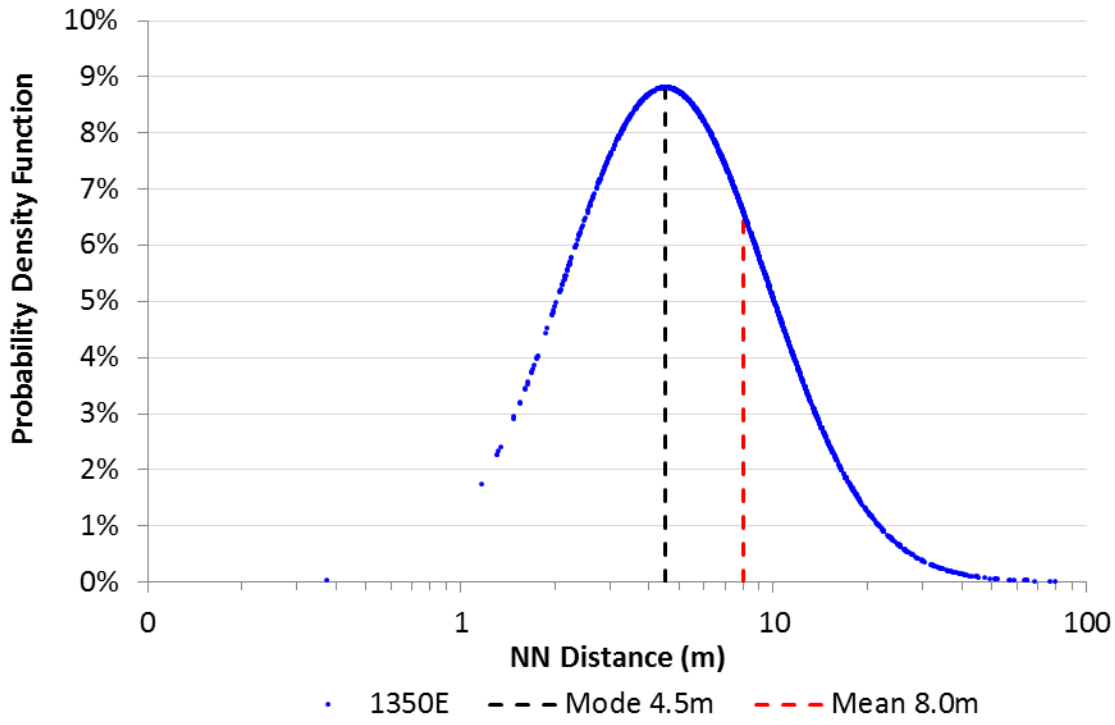

Figure 35: A plot of the frequency of the distances between seismic events and their nearest neighbour event for a population of 1350 seismic events has a log normal distribution.

The distance between each event and the events preceding it was determined. An event with no nearest neighbour at the specified distance is described as a single isolated event. Events with one nearest neighbour become a cluster of two events, an event with two nearest neighbours becomes a cluster of three and so on until all the events either belong to a cluster or remain as a single isolated

event. Using this method ensures that all events are included and no bias is introduced by the elimination of single events.

For the distances identified in Figure 35 for the 1350 events around an abutment, it was found that as the nearest neighbour distance increased, the number of clusters and single events decreased and size of the largest clusters increased (Figure 36).

NN Distance - 4.5m (Mode)		
Size # of Events	Frequency	Total # of Events
28	1	28
12	1	12
9	1	9
8	2	16
7	1	7
6	4	24
5	6	30
4	11	44
3	22	66
2	108	216
1	898	898
Total	1055	1350

NN Distance - 8.0m (Mean)		
Size # of Events	Frequency	Total # of Events
513	1	513
15	1	15
14	1	14
13	1	13
11	2	22
10	1	10
9	4	36
7	8	56
6	2	12
5	8	40
4	14	56
3	19	57
2	65	130
1	376	376
Total	503	1350

Figure 36: The size and quantity of clusters and single events at the mode (4.5 metres) and mean (8.0 metres) nearest neighbour of a seismically active abutment (1350 events).

For this population of 1350 seismic events, the largest number of clusters and single events (1055) occurs when the mode distance (4.5 metres) is used. There is a high percentage (93%) of the events in small clusters (between 2 and 5 events) or single events (898). The largest cluster is made of 28 events (C233). When the mean nearest neighbour distance is used (8.0 metres) there is a significant drop (50%) in the number of single events and the size of C233 increases by more than a factor of ten (from 28 to 513 events).

To understand the significance of how the larger nearest neighbour distance changes a cluster's size, a visual representation of C233 is shown in Figure 37. As the nearest neighbour distance

increases, cluster size (number of events) also increases through the addition of other smaller clusters or single events.

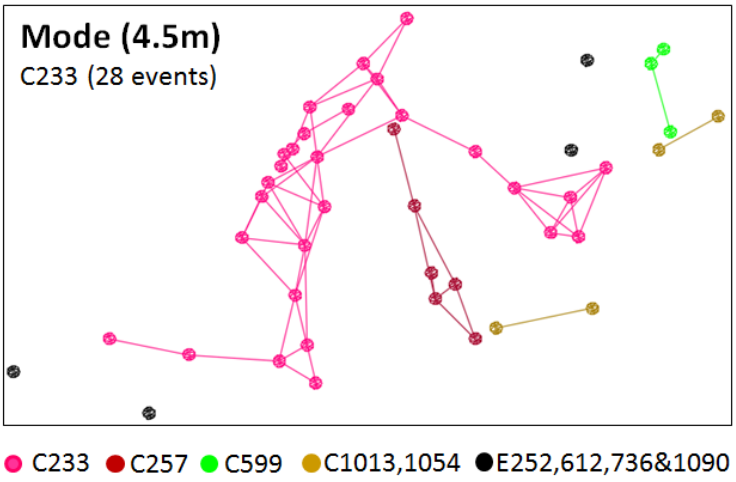

Figure 37: Size of Cluster 233 at the mode nearest neighbour distance (4.5 metres)

For example at a nearest neighbour distance of 4.5 metres, there are five clusters ranging in size from two to twenty eight events and four single events. Specifically, the four single events are (E252, E612, E736 and E1090); two clusters each containing two events (C1013 and C1054), one cluster of three events (C599); one cluster of six events (C257) and the largest cluster (C233) with twenty eight events. When the mean nearest neighbour distance of 8.0 metres is used, all forty five events are within 5.3 metres of another event in Cluster 233 (Figure 38). The smaller clusters may or may not belong to the same seismic source so as the nearest neighbour distance increases, the chance of having more than one seismic source in a cluster increases. It is more difficult to make meaningful and reproducible results from seismic populations with mixed or multiple seismic sources.

Figure 38: Cluster 233 contains 513 events when the nearest neighbour distance of 8.0 metres (mean) is used. All the clusters and single events in Figure 37 are shown so that they can be distinguished within the larger cluster formed using the mean distance.

Clustering at the mode and mean nearest neighbour distances reveal different insights into a seismic source. The mode distance shows the seismic source location, while the mean distance gives a good indication of the extent of the failing rock mass. Clusters at other distances can be created if more or different insight is needed or desired.

3.2.4 Seismic Event Population Selection

While it would be ideal to study seismic event clusters created from the first event in a database, it is not practical to try and create clusters for mines with years of data containing millions of events. Current practice is to select seismic data from an area of concern by defining the boundaries (in three dimensions) around the area of interest. Selecting a population of seismic events in this manner can be problematic as events that may appear to be close together when they may not be

close to each other at all. It is important to keep in mind that the seismic events recorded by a system are not the entire population of all the seismic events that have occurred. Locations of sensors, system downtime, and seismic system sensitivity are only a few factors that determine which seismic events are recorded. Therefore when selecting an area of interest for clustering, only a small portion of the entire population is actually chosen. It is assumed that the portion selected is representative of all the seismicity at this location.

As an example, two populations of seismic events around a mining block were chosen based on which events appeared to be associated with the block. In Figure 39, the seismic events closest to the stopes outlined in pink are the events requiring seismic analysis. Most of the events appear to be in the bottom left hand corner, while the events on the upper right hand side near the stopes outlined in black may be associated with either the pink or black colored stopes. One population of 710 events was chosen around the events that appear to be closer together in the bottom left hand corner (light blue dots in Figure 39). A second population of 1350 events was chosen and comprised all the events (light and dark blue).

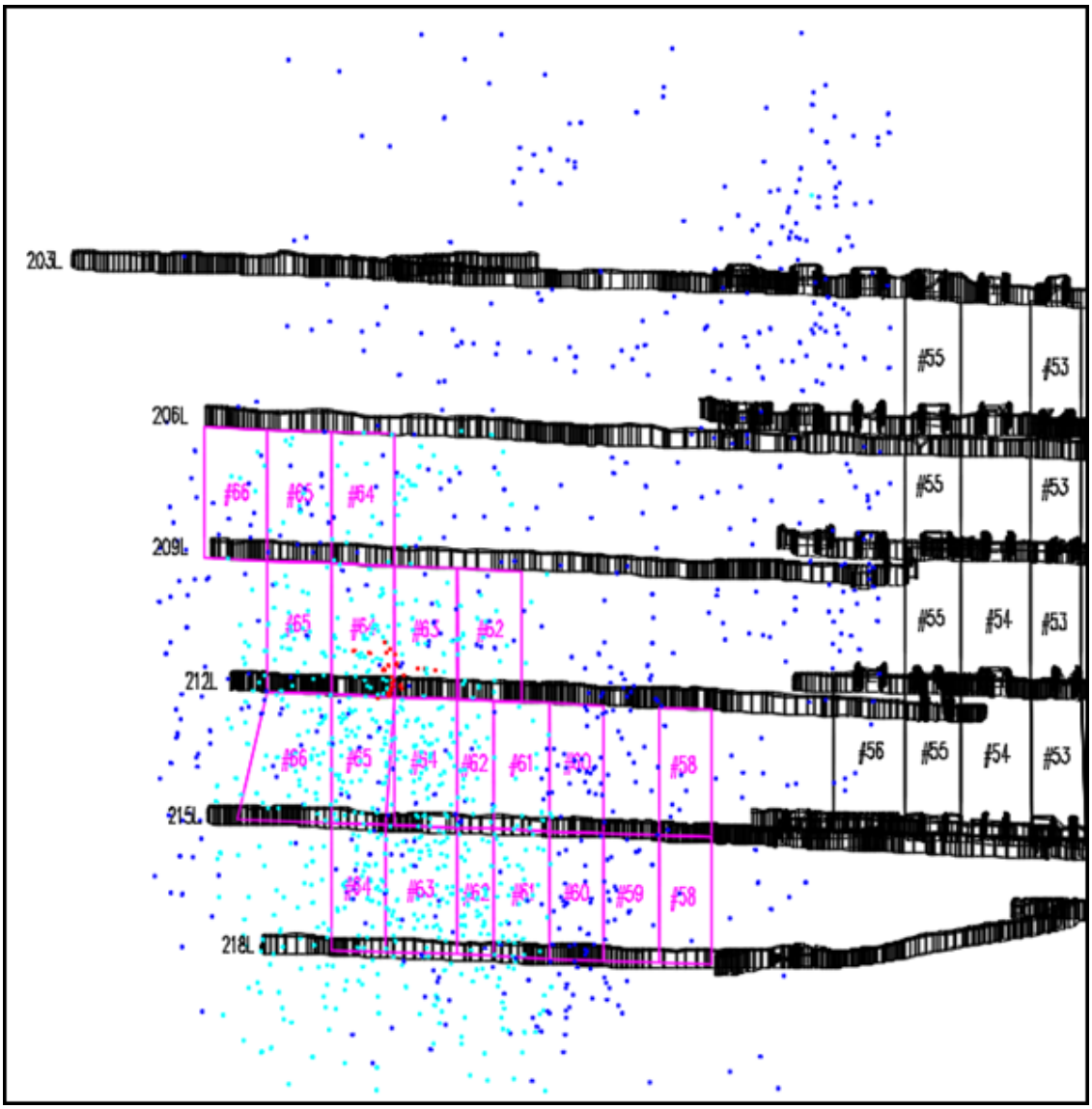

Figure 39: Selection of seismic event populations for analysis. The 710 events (light blue dots) in the bottom left hand corner are noted as Population 1, while all the events (light blue and dark blue dots – 1350 events) are noted as Population 2.

The distances between all nearest neighbours for each population was determined and plotted based on the probability density function for each population (Figure 40). Image A shows the distribution of nearest neighbour events for Population 1, and Image B for Population 2. While the mean nearest neighbour distance of the 1350 event population (8.0 metres) changed significantly from the smaller population of 710 events (6.8 metres), the value of the mode nearest neighbour distance of 4.5 metres is the same for both populations.

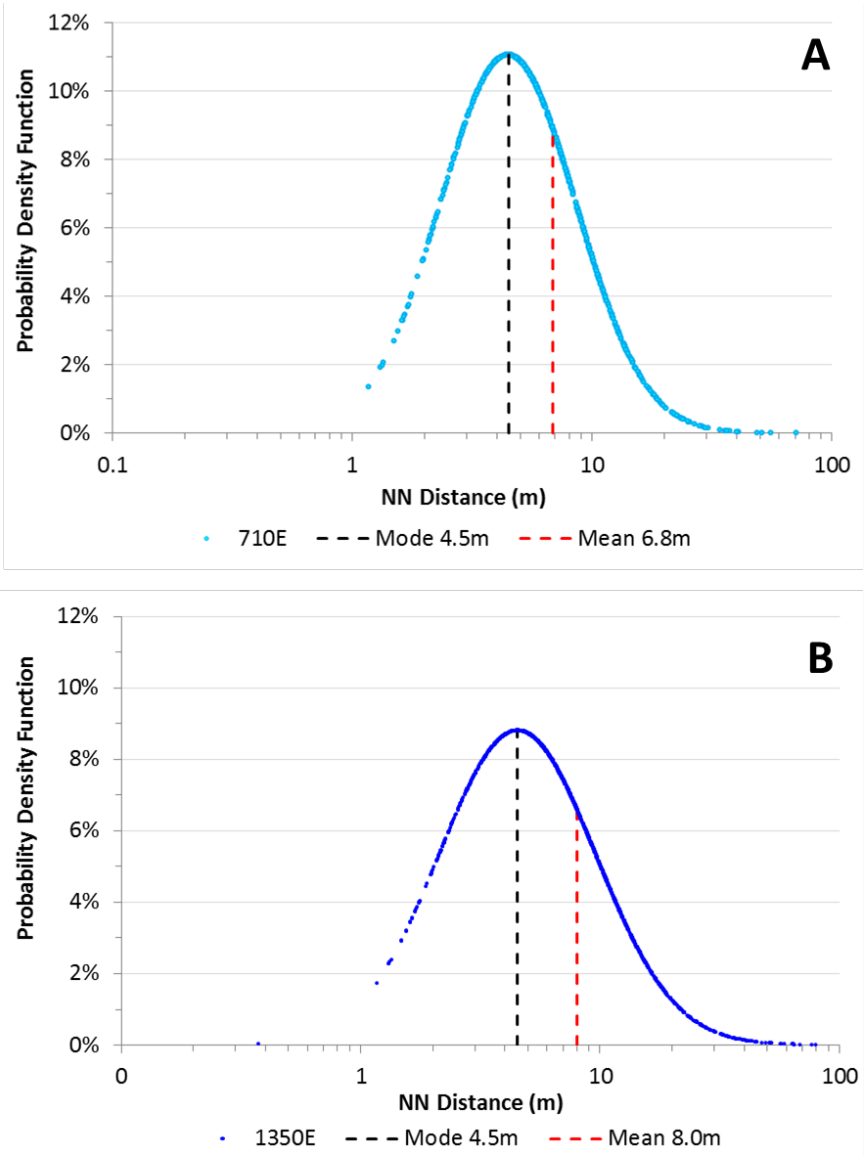

Figure 40: Lognormal distribution of Population 1 (Image A) and Population 2 (Image B)

This result makes intuitive sense as the population of 1350 events covers a much larger area with seismic events that are farther apart. The mode nearest neighbour distance does not change because the most nearest neighbour pairs occur at this distance in both populations. The size and total number of clusters and single events can be compared to confirm that this is true. In Figure 41, two tables summarizing the number and size of the clusters formed for each population is shown. The three largest clusters (red, light blue and green) in each population are very similar in

size (number of events) and are in the same locations.

Population #1Clustered at NN Distance of 4.5 metres (Mode)												
Size (# of E)	1	2	3	4	5	6	7	8	9	12	17	Total
Quantity	412	68	12	7	3	5	1	1	1	1	1	512
#E	412	136	36	28	15	30	7	8	9	12	17	710

Population #2 Clustered at NN Distance of 4.5 metres (Mode)												
Size (# of E)	1	2	3	4	5	6	7	8	9	12	28	Total
Quantity	898	108	22	11	6	4	1	2	1	1	1	1055
#E	898	216	66	44	30	24	7	16	9	12	28	1350

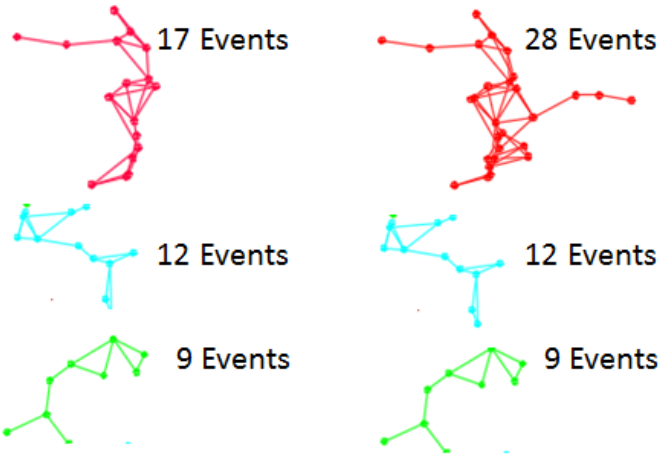

Figure 41: Comparison of clusters formed for Population 1 and 2 in abutments

The remainder of the population is also very similar. A graph of Population 1 and 2 clusters and single events are shown in Figure 42.

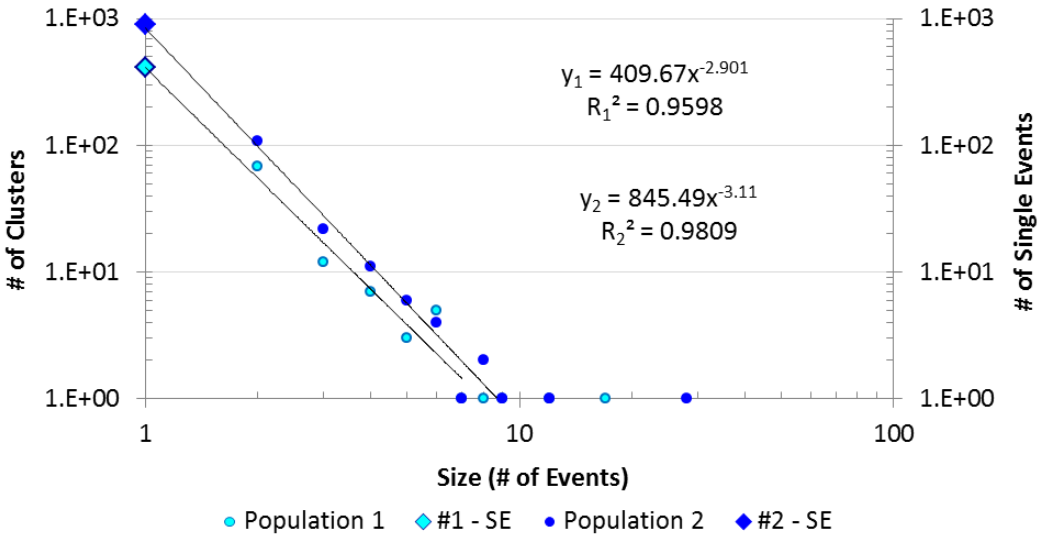

Figure 42: Cluster sizes for Population 1 (710 events) and Population 2 (1350 Events)

This comparison of the cluster and single event locations and cluster sizes for two different populations of seismic events chosen in an abutment area, demonstrates that the nearest neighbour distance mode value yields very similar results for both populations despite the very different sizes. The single events and smaller clusters (two to six events in size) follow a power law. The larger cluster sizes were also very similar in size and location. This example demonstrates that the practice of arbitrarily choosing seismic populations for study can be used, but requires validation. The sequential clustering method will be used in this thesis to show if the seismic populations chosen for study or analysis are nearest neighbours and belong together.

The mode and mean nearest neighbour distances were both used to create clusters for each of the four case studies. The mode distance shows the areas of the highest seismic activity while the mean distance provides a good representation of the size and shape of a seismically active area. The mean distance creates clusters that are an assemblage of single events and multi-sized clusters. This difference becomes obvious when the single events and clusters of the mode and mean nearest neighbour distances are compared for Population 1 (710 events - Figure 43). The three largest clusters that form when the nearest neighbour distance of 4.5 metres is used (17 events – red, 12 events – light blue, 9 events – green) become part of a much larger cluster (C233-337 events - grey) when the 6.8 metres is used to cluster nearest neighbours.

Cluster Distance - 4.5m		
Population 1 - 710 Events		
Size (# of E)	Frequency	#E
17	1	17
12	1	12
9	1	9
8	1	8
7	1	7
6	5	30
5	3	15
4	7	28
3	12	36
2	68	136
1	412	412
Total	512	710

Cluster Distance - 6.8m		
Population 1 - 710 Events		
Size (# of E)	Frequency	#E
337	1	337
10	1	10
8	2	16
5	1	5
4	6	24
3	13	39
2	35	70
1	209	209
Total	268	710

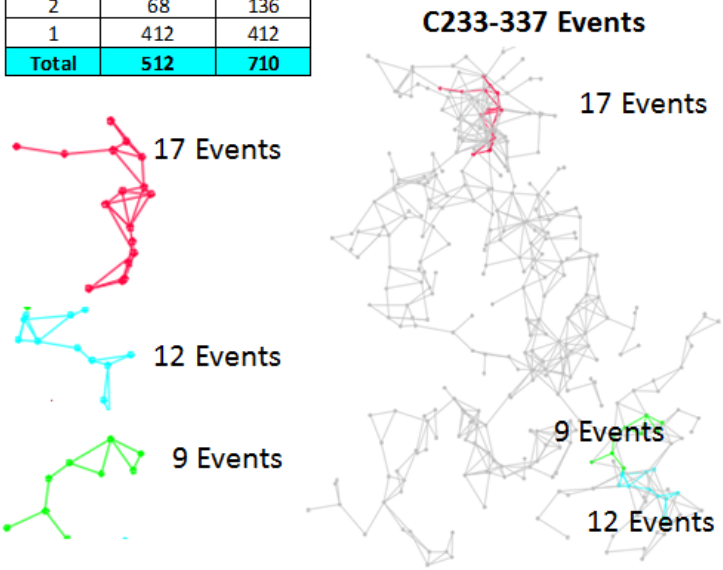

Figure 43: The difference in cluster size and number when the mode and mean nearest neighbour distance are used as the clustering distance for Population 1 (710 events)

The tables above the cluster images in Figure 43 also reflect the large change in the number and size of clusters at each distance. When the larger nearest neighbour distance is used (6.8 metres), there is almost a 50% decrease in the total number of clusters and single events (268 down from 512). The size of Cluster 233 is nearly twenty times larger at this distance having gone from 17 events to 337 events. Plots of the number of each cluster size and single events can also be used to show the effect different nearest neighbour distances have on cluster size (Figure 44).

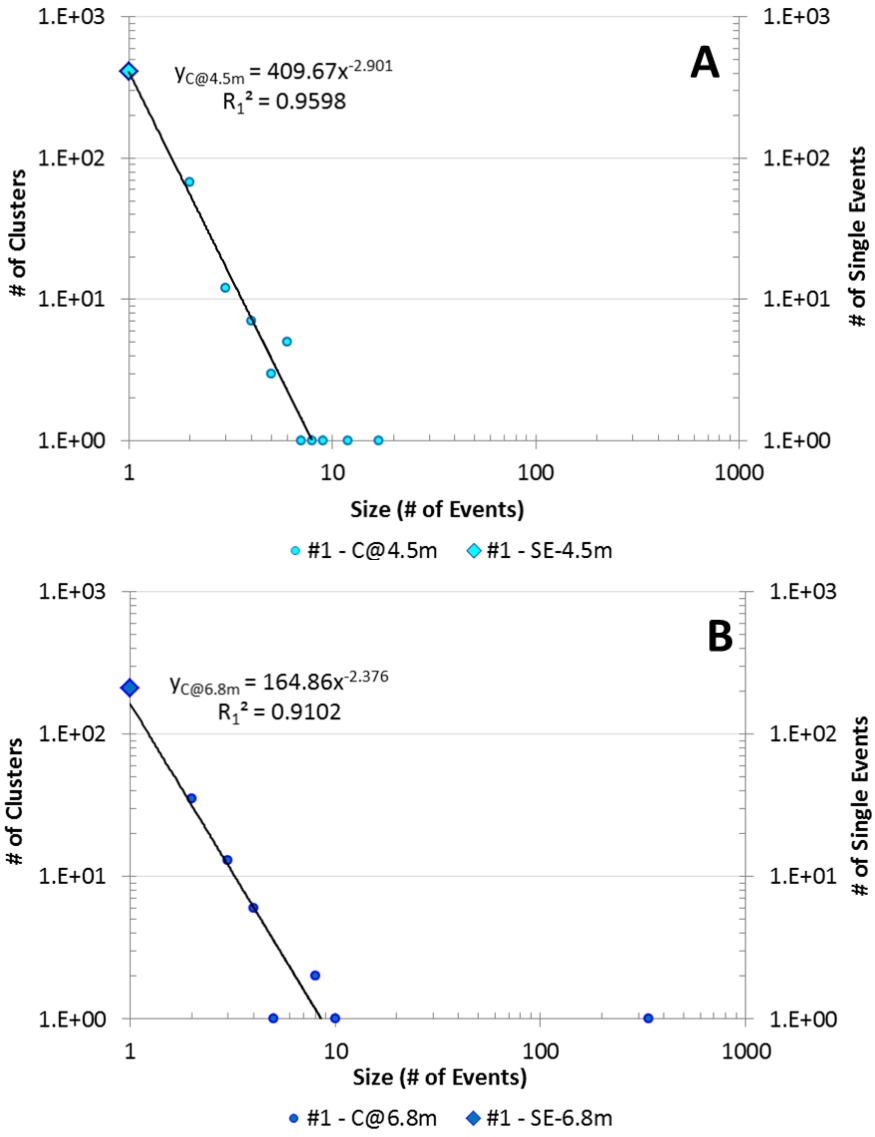

Figure 44: Graphical representation of cluster size and frequency for Population 1

Figure 44 provides insight into the smaller clusters which follow a power law. The slope of the line increases as the total number of clusters and single events decreases. The largest cluster (C233 – 337 events in this example) does not follow a power law; however the sequence of the cluster formation can be studied as shown previously in Figure 31 and the corresponding time frame in Figure 32. Both distances (mode at 4.5 metres and mean at 6.8 metres) are useful but serve different purposes. If a single source is desired to be studied, the mode distance identifies unique

locations better than the mean distance. However, the mean distance provides a better overall picture of the total rock mass failure because of its larger areal extent. Both of these distances provide new insight into rock mass failure.

3.3 The Application of Fractal Dimension to Sequential Clusters

This research proposes to calculate the fractal dimension for known seismic sources in four different hard rock mines. The hypothesis is that each seismic source will have a characteristic fractal dimension within a range of values. The identification of this characteristic fractal dimension could then be used, if the hypothesis is correct, to identify seismic event clusters in unexpected locations in order to complete a proactive hazard assessment.

3.3.1 The Correlation Integral

The correlation integral described in Hirata *et al.*, (1987) and previously shown in Equations 6 and 7, is used to determine the fractal dimension of nearest neighbour distance between events that have been clustered using the sequential spatial clustering method. The first twenty seismic events in Population 2 are used to demonstrate how the fractal dimension of the nearest neighbour distances are calculated using the correlation integral method. The relation between the two parameters statistically follows a power law if the correlation integral (y) varies as a power of the distance between nearest neighbours (x) (Equation 9).

$$y = cx^m \qquad \text{(Equation 9)}$$

Where:
y = correlation integral
x = distance between nearest neighbours (metres)
c = constant
m = slope (fractal dimension)

The correlation integral (CR) for each nearest neighbour distance is plotted on a log – log graph (Figure 45). The slope of a best fit line between the points is the fractal dimension of the nearest neighbour distances. In Figure 45, the relation between the correlation integral and the distance between nearest neighbours is described by the equation: $y = 0.0278x^{2.4161}$. The nearest neighbour fractal dimension (D_{NN}) equals 2.4161, which is the slope of the line. How well the data fits to the slope of the line is described by the Coefficient of Determination (R^2). It uses the method of least squares to determine how close the actual data fits to the calculated values and varies between 0 (no correlation) to 1 (perfect correlation). The value of $R^2 = 0.9805$ in Figure 45 is very close to 1, indicating a strong correlation. The higher the fractal dimension the more highly correlated the relation between the two parameters. It should also be noted that the relation is not infinite; it only exists between the minimum and maximum values of the nearest neighbour distances. In this example, the power law relation only exists when the nearest neighbour distance is between 1.4 metres (x_{min}) and 3.9 metres (x_{max}). The fractal dimension of the nearest neighbour pairs for this example is noted as**:** ***$D_{NN\ 1.4\text{-}3.9m}$ = 2.42.***

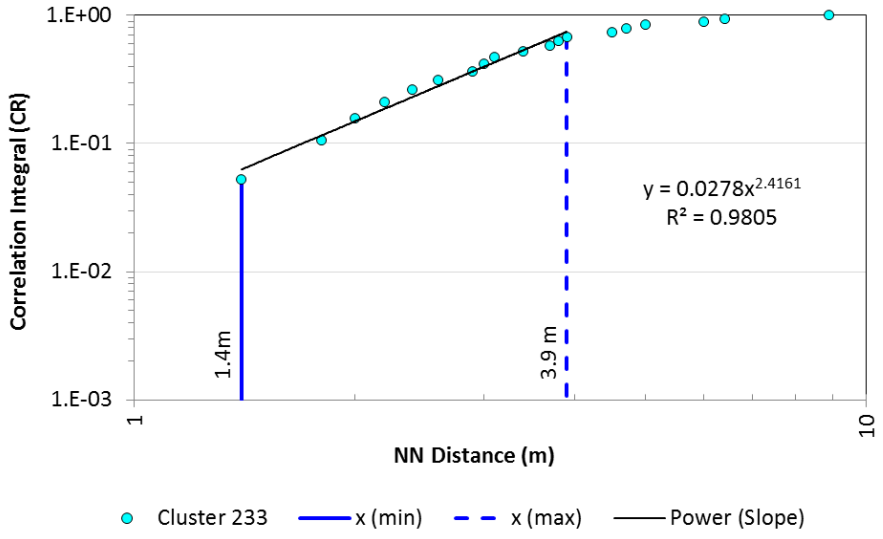

Figure 45: Determination of the fractal dimension of nearest neighbour distances using the correlation integral method for the seismic events in Cluster 233.

3.3.2 Combining Nearest Neighbour Fractal Dimension with the Probability Density Function

Nineteen events with a lognormal distribution (Figure 46) have a mean nearest neighbour distance of 3.32 metres. The mean and mode distances are used to cluster seismic events for all the case studies in this thesis. In this example, the mean distance is 3.32 metres, and the mode distance 2.70 metres.

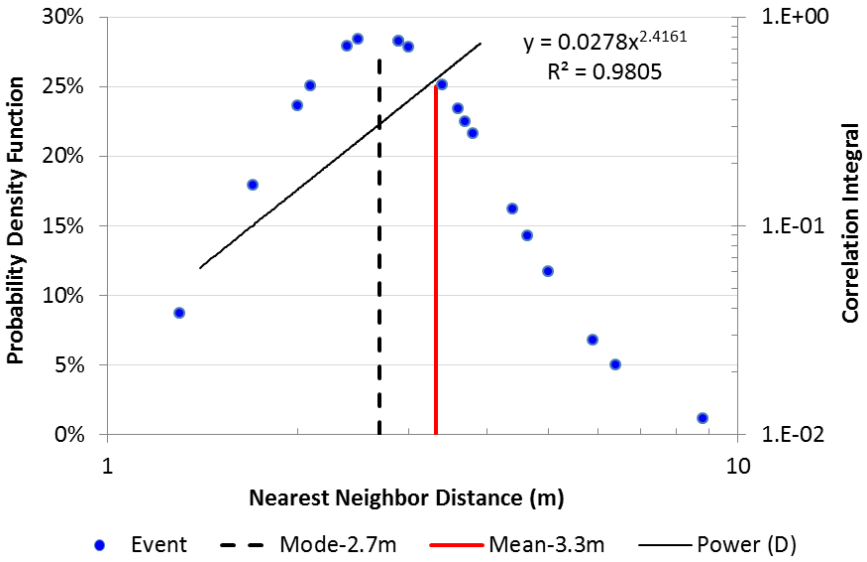

Figure 46: Lognormal distribution of 19 nearest neighbour events

Combining the probability density function and the fractal dimension of a seismic cluster shows that the seismic events with a nearest neighbour distance between 1.4 and 3.9 metres are associated with the high fractal dimension of 2.42 ($\boldsymbol{D_{NN\ 1.4\text{-}3.9} = 2.42}$) and have a higher probability of occurring. Nearest neighbours that are 4 to 10 metres apart are not fractal and are associated with the distances that occur less often.

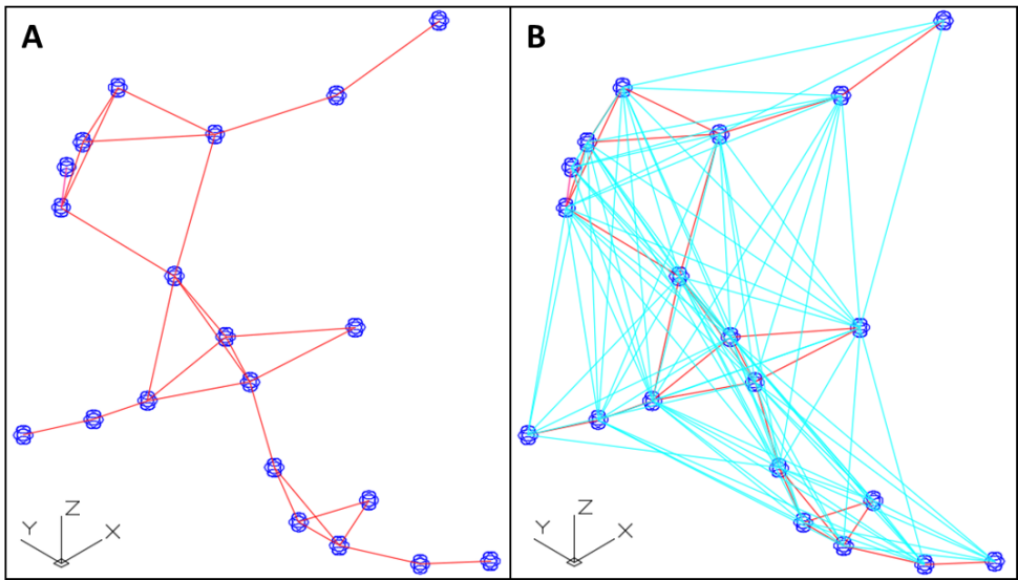

Figure 47: Comparison of seismic events with a fractal relation to a nearest neighbour (Image A-red lines) and seismic events that do not have a fractal relation (Image B-light blue lines).

Figure 47 Image A shows the seismic events that are fractal (nearest neighbours within 1.4 to 3.9 metres). Red lines are drawn between the events to show how close they are. Thus when comparing fractal dimensions of seismic event distances, a lower fractal dimension would indicate the seismic events are farther apart than those with a higher fractal dimension.

This method of combining the probability density function with the fractal dimension of a seismic event cluster will be applied to four different seismic sources to determine if they can be spatially described using the fractal dimension of nearest neighbour distances.

3.3.3 Application of Time Sequences to Seismic Source Parameters

Since the twenty events were clustered sequentially and spatially, each event in the cluster can be plotted in order of sequence and then have the sequence number replaced with the actual date and time of the event (Figure 48).

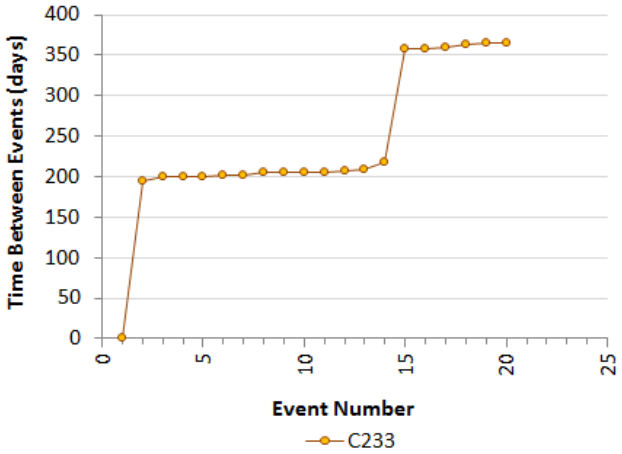

Figure 48: A plot of each event in order of the date and time of occurrence shows that the cluster is active three times over the course of a year

Cluster 233 shows that the cluster is not active all the time but at time intervals approximately 150 to 200 days apart. The first event, shown at time zero, remains a single isolated event until thirteen events occur over a twenty three day period (Day 195 to Day 218). The cluster becomes active again with six events over seven days (Day 358 to Day 365). This method is useful for investigating time sequences of seismic events without imposing a bias of a study time frame.

Since this method can be applied to small populations of seismic events, it may be possible that the combined methods of sequential space clustering, fractal dimension and the measure of change of certain seismic source parameters or inferred techniques (such as magnitude) may provide proactive and progressive information as a rock mass fails.

This novel approach to seismic analysis will be tested using data sets with different seismic sources. Similarities and differences will be noted in each case to determine if there is statistically a way to characterize each seismic source. The seismic data sets to be studied are of ramp development, a failing pillar, a failing abutment and a shear zone adjacent to an orebody.

3.4 Chapter Summary

This chapter presents a novel method of sequential spatial clustering and applies fractal dimension to these clusters in new ways. The development of a ramp is used as a base case to demonstrate that the excavation of rock can have a normal response and an abnormal response. The abnormal response results in seismic events that occur in locations or a time where and/or when they are not expected.

Sequential spatial clustering is a novel method proposed as a potential way to gain insight into the process of rock mass failure. Seismic events are clustered based on their proximity to their preceding nearest neighbours. The clustering distance is not arbitrarily chosen but derived from the data itself. All the nearest neighbour distances between the events are calculated and plotted using a probability density function. The nearest neighbour distance with the highest occurrence (mode) is used for cluster formation to locate a seismic source. Figure 43 demonstrates this point. When the mode distance is used three clusters form which identify three seismic sources. When the mean distance is used, one large cluster forms with the three mode clusters within it. The larger areal extent of the mean cluster shows where seismic events and rock mass degradation have occurred. Keep in mind that the example in Figure 43 is a very small number of events where the seismic sources are the same. As will be seen in the case study of the ramp Figure 51A and B, the six largest clusters resulting from the mode clustering distance remain independent of each other but become larger in size when the mean distance is used. This clustering method does not require a large number of seismic events to be used. The nearest neighbour distances can be calculated and re-evaluated with each new event if desired.

The method retains the sequence of the events as they are clustered. The method then allows for the sequence number of an event to be replaced with the event's actual date and time so that the seismic activity of a cluster can be viewed over time without introducing a bias. A plot of a cluster's seismic activity over time provides new insight into rock mass failure.

A brief discussion and example are also shown to explain how seismic events can be selected for analysis by defining an area to be studied. A population of a certain size can be sequential and spatially clustered to determine if multiple seismic sources are present. If that is the case, the same method can be used to isolate a single source before further analysis is performed.

Finally, the use of fractal dimension is reintroduced. Using the correlation dimension method, the fractal dimension of nearest neighbour distances, or any other seismic parameter, can be calculated to determine how a cluster of seismic events is changing. The correlation dimension has been chosen because it also requires a minimal amount of data and is widely used in a number of fields to study complex systems.

Clusters of seismic events resulting from different seismic sources can then be compared to determine if seismic events can be characterized by their fractal dimension of one or more seismic source parameters. The correlation dimension can be used to compare seismic event source parameters, to determine if they are fractal and if so what the fractal dimension is for a given parameter. Combining the sequential spatial clustering and fractal dimension methods provides a novel way to characterize and study seismic events. The methodologies presented in this Chapter will be used on four data sets with different seismic sources, the results of which are provided in the following Chapter.

Chapter 4

4 Application of Clustering and Fractal Dimension

Four data sets of seismic events are used as case studies to determine if seismic sources could be characterized using sequential spatial clustering and fractal dimension. The first data set is the development of a ramp (previously presented in Chapter 2); the second set pertains to abutments that are created as a block of stopes are mined; the third a rib pillar that is in the process of failing; and the fourth, a shear zone adjacent to an orebody. Each case offers a different seismic source and will be presented separately and then compared.

4.1 Case 1 - Ramp Development

The first case study is the development of a down ramp over an eighty day period (May 19th to August 1st, 2005). Figure 49 shows the ramp at the start of the study period (Image A) and the actual ramp that was excavated (Image B).

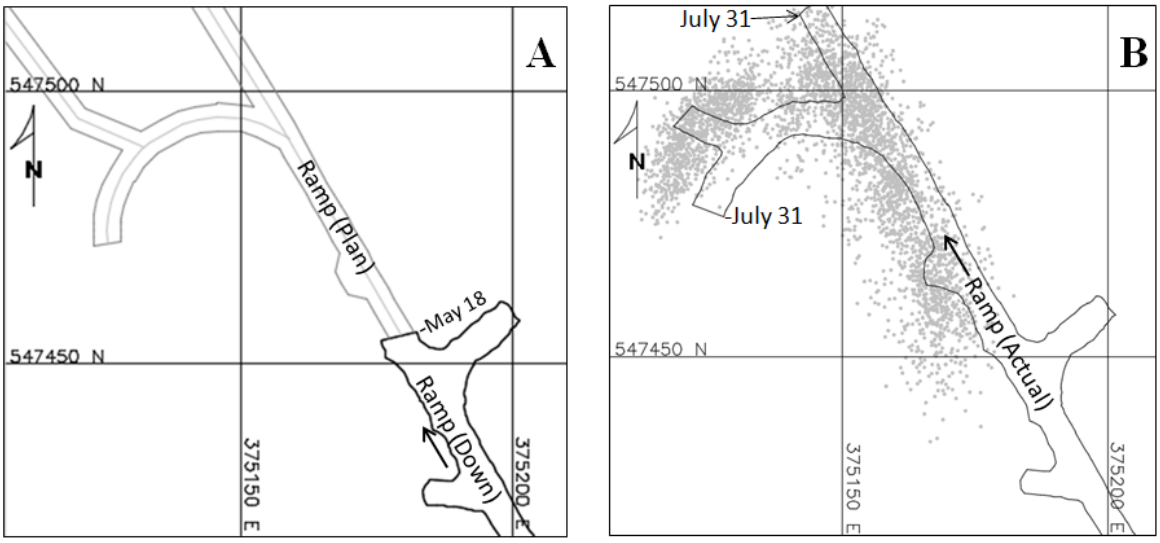

Figure 49: Down ramp developed between May 13th and July 31, 2005. Image A - The actual ramp excavated prior to May 18th is shown by the dark black line; the planned excavation is shown with a grey center line. Image B - The outline of the completed ramp on July 31, 2005. The grey dots are the locations of 3704 seismic events that occurred as the ramp was being developed.

The seismic response of the rock mass during the development period is shown by the grey dots which represent the 3704 seismic events. This particular data set contains the time, location and magnitude for each event. Typical analysis of this data would require studying all the events together or separated by an arbitrary time line or by a range of magnitudes. In this case study, the events will be clustered using sequential spatial clustering, however first the clustering distance needs to be determined.

4.1.1 Nearest Neighbour Distance and Resulting Clusters

A plot of the probability that each nearest neighbour distance occurred is used to determine which distance occurs most often (mode) and on average (mean). The mode distance is 1.11 metres and the mean distance is 1.65 metres. Both distances are shown in Figure 50.

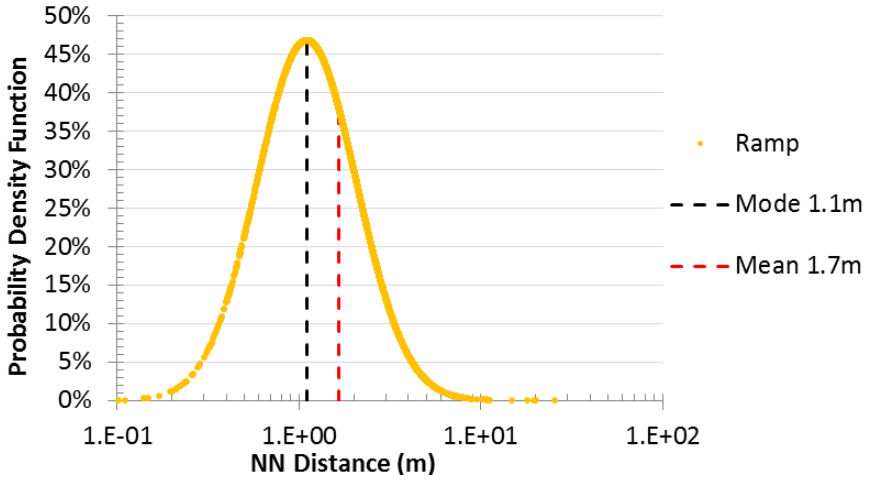

Figure 50: Plot of probability density function for nearest neighbour distances of 3704 seismic events around the development of a down ramp

Creating clusters using the mode distance of 1.11 metres resulted in small cluster sizes of fourteen events or less. Additionally, sixty percent of the events (2218 events) did not cluster and remained as single, isolated events (Table 7 and Figure 51 – Image A).

Table 7: Ramp cluster size and frequency using mode nearest neighbour distance (1.11m)

Clustered at NN Distance of 1.11 metres (Mode)														
Size (# of E)	1	2	3	4	5	6	7	8	9	11	12	13	14	Total
Quantity	2218	337	76	50	17	7	8	5	7	2	3	2	1	2733
#E	2218	674	228	200	85	42	56	40	63	22	36	26	14	3704

The attempt to cluster the events using the mean distance of 1.65 metres resulted in fewer single, isolated events (1038 events - 28%) (Table 8). Clustering at this distance provides insight into which sections of the ramp experienced the most seismicity; (Figure 51-Image B).

Table 8: Ramp cluster sizes using the mean nearest neighbour distance (1.65m)

Clustered at NN Distance of 1.65 metres (Mean)																								
Size (# of E)	1	2	3	4	5	6	7	8	9	10	11	12	13	14	15	21	23	27	46	164	195	228	284	378	Total
Quantity	1038	218	63	43	21	8	10	7	5	5	2	3	1	2	2	1	1	1	1	1	1	1	1	1	1437
#E	1038	436	189	172	105	48	70	56	45	50	22	36	13	28	30	21	23	27	46	164	195	228	284	378	3704

Since the development of the ramp was continuous during the period of study it was thought that one large cluster could result. A brief investigation was done to see what clustering distance was needed to achieve this. At a nearest neighbour distance of 2.07 metres, all of the medium size clusters (20~300 events) joined into one large cluster made up of 2364 events (Table 9).

Table 9: Ramp cluster sizes and frequency using 2.07m as the clustering distance

Clustered at NN Distance of 2.07 metres																	
Size (# of E)	1	2	3	4	5	6	7	8	9	10	11	12	14	20	30	2364	Total
Quantity	546	131	47	14	16	5	6	2	4	1	3	2	1	1	1	1	781
#E	546	262	141	56	80	30	42	16	36	10	33	24	14	20	30	2364	3704

The remaining clusters are less than 30 events in size and are evenly distributed around the main cluster (multi colored events in Figure 51-Image C).

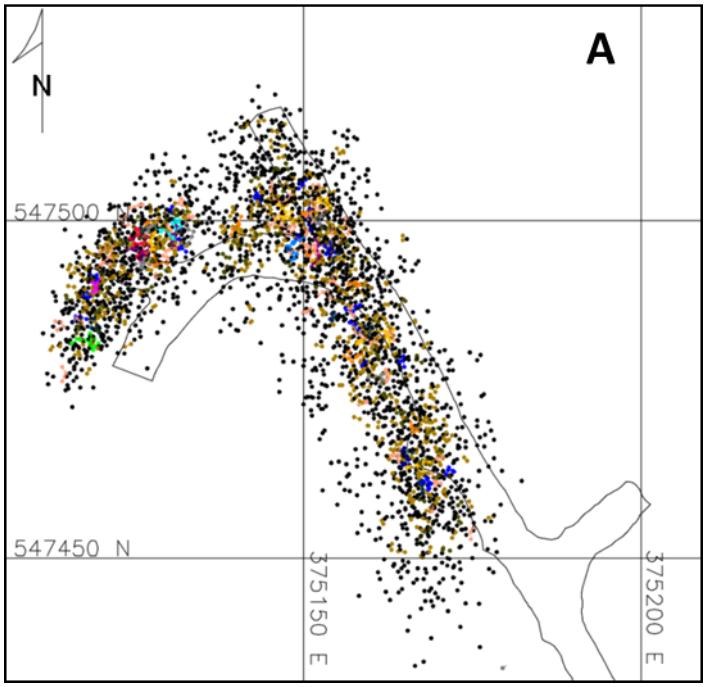

Figure 51: Image A - The 1038 clusters resulting from clustering using a nearest neighbour distance of 1.11 metres

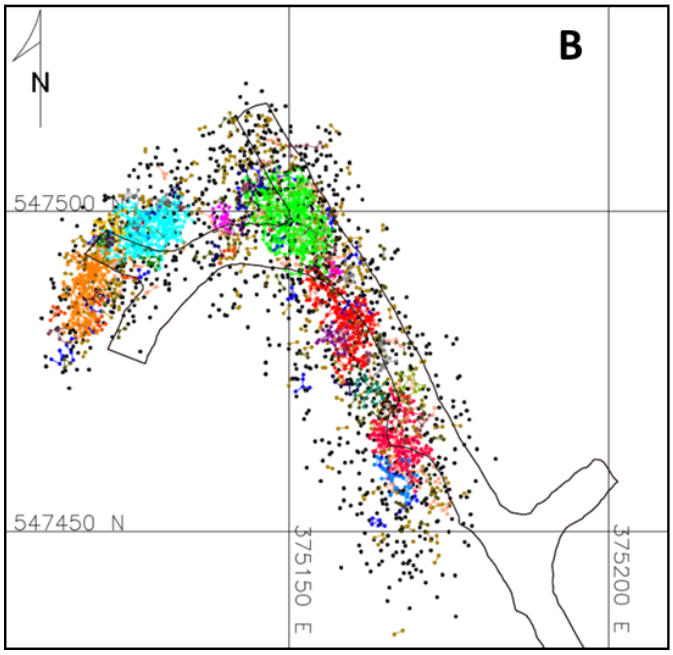

Figure 51: Image B - Clusters created using the mean nearest neighbour distance of 1.65 metres

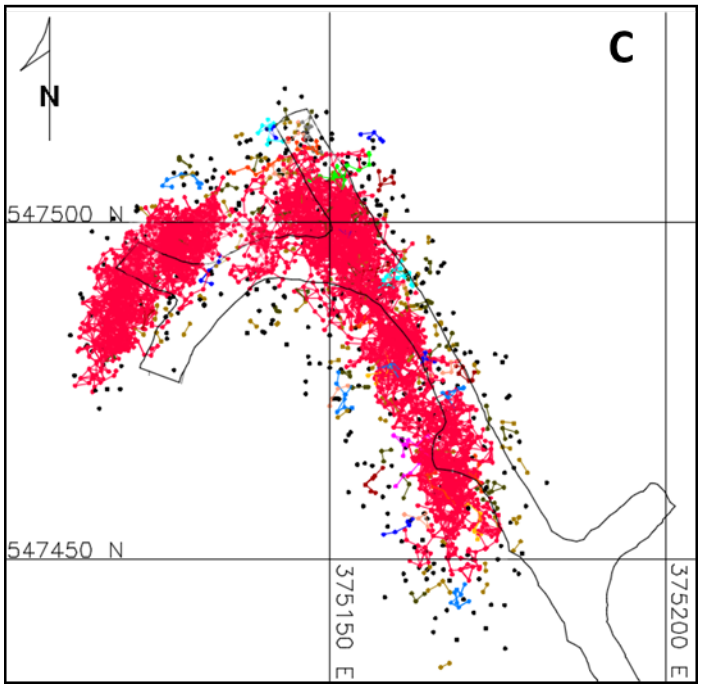

Figure 51: Image C - Clusters created using the nearest neighbour distance of 2.07 metres. The largest cluster (red dots and lines) contains 2364 events

Using the distance of 2.07 metres resulted in 235 clusters ranging in size from 2 to 30 events, one large cluster of 2364 events, and 546 events that do not cluster and remain as single isolated events. Events that are within 2.07 metres of any other event have a line drawn between the events. These lines give some perspective to the events that are closest to each other. If an event is more than 2.07 metres from all events, it remains a single isolated event. This exercise pointed out one area of the ramp that had few seismic events (just to the left of the ramp when it curves to the left). Examination of the data showed that the seismic system had been off for several days over a long weekend and was the reason for the lack of data in this area.

The seismic source parameters of these clusters can be studied to give insight into the rock mass failure process at the cluster location over time. For example, a cluster can be examined if there is a need to know if a seismic zone is static or moving in a particular direction over time. A moving seismic zone occurs as a mining front advances in one direction; a fault slips in one direction, the

progression of a cave front or chimney failure. The 2364 event cluster in the ramp seismic catalogue is a good example of how a seismic zone can move over time. The method used here is to quantify the movement by plotting the average x, y, and z coordinates of all the seismic events in successive twenty four hour periods. In this case, the time frame chosen is reflective of the blasting practice – one development round blasted per day. A line joining the average of the coordinates every day is created and compared to the actual development of the ramp (Figure 52).

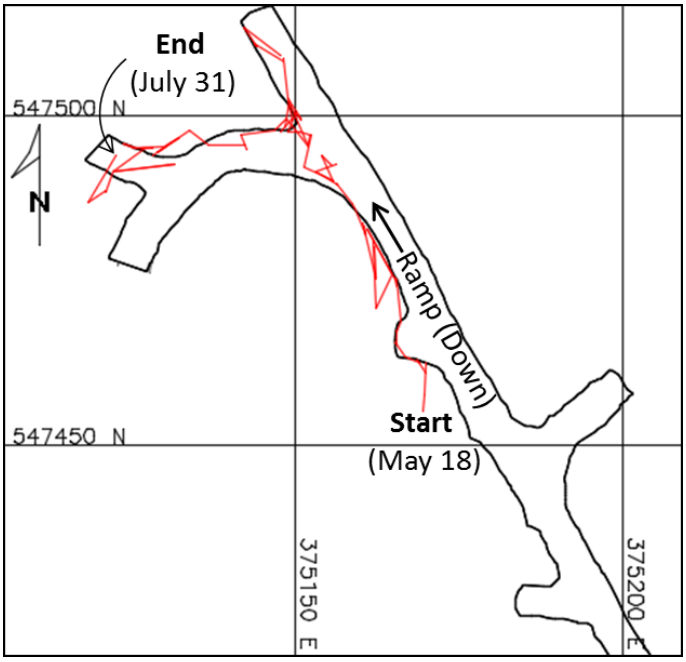

Figure 52: The direction and movement of seismic events between May 18th and July 31st, 2005 (red line)

The line is not perfectly straight as rock mass degradation is different on non-blasting days and by a number of abnormally located seismic events. However the line quantifies the direction and progression of the seismic events and is a relatively simple way to follow the failure path of a rock mass failing in a particular direction.

4.1.2 Fractal Dimension

Fractal dimension is a mathematical term used to describe data that follows a power law with an

exponent that is a fraction and not a whole number. The two quantities statistically follow a power law if a relative change in one quantity varies as a power of the other. In the case of the fractal dimension of nearest neighbour distances calculated using a correlation integral, a power law exists because the change in the nearest neighbour distance is by the power of 10 which corresponds to a change of the correlation integral also by a power of 10.

When calculating or referring to fractal dimension, it is imperative to state what is being characterized by a fractal dimension, such as the nearest neighbour distances. The fractal dimension of the time between nearest neighbour events has a different meaning. This is another piece of information that will provide further insight into which distances are fractal – that is which distances are highly correlated.

4.1.2.1 Fractal Dimension – Nearest Neighbour Distance

A plot of the correlation integral for all nearest neighbour distances is shown in Figure 53. The fractal dimension is the slope of the line of the nearest neighbour distances that follow the power law. In the case of the ramp, the distances between nearest neighbour events range from 0.1 to 25.6 metres, however only those that are within 0.1 to 1.1 metres of each other have a fractal dimension of 2.83. The nearest neighbour distances greater than 1.1 metres and up to 25.6 metres are not fractal – meaning they are not statistically related to one another.

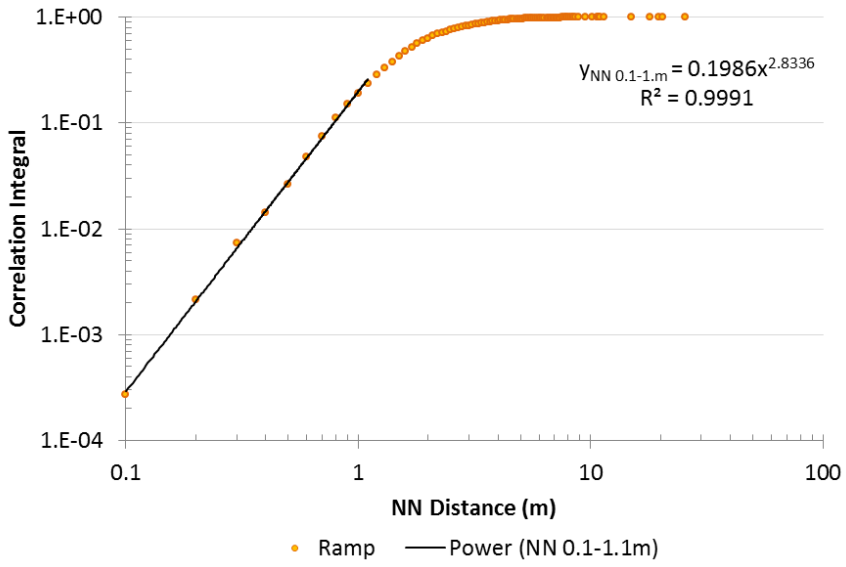

Figure 53: The fractal dimension of the nearest neighbour distances in a ramp

The fractal dimension value of 2.83 means that all nearest neighbour events up to the mode distance of 1.1 metres are very highly correlated. In this case, the nearest neighbour distance with the highest probability of occurring results in a large number of very small size clusters (Table 7 and Figure 51-Image A). The clusters created using the mode distance are important because they identify the locations with the highest seismic activity. This graph will be used to characterize development seismic events and will be compared to the other seismic sources presented later in this thesis.

4.1.2.2 Fractal Dimension of Time Between Nearest Neighbours (TBNN)

The time between nearest neighbour events is important because it gives good information on how much time can be expected between events closest to each other. In the case of the ramp nearest neighbour events two fractal periods exist (Figure 54).

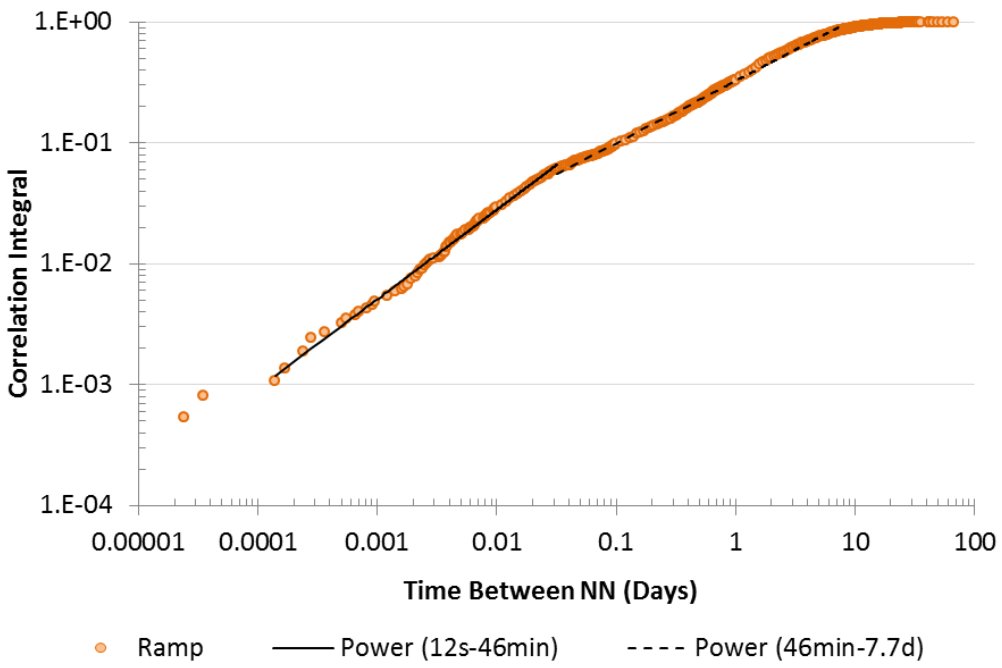

Time Period	FD	R^2
12s-46 min	0.74	99.6%
46 min-7.7 days	0.51	99.7%

Figure 54: The fractal dimension of the time between nearest neighbour events in a ramp

The first fractal dimension is 0.74 that ranges between one second and just under an hour (46 minutes) ($D^{Ramp}_{TBNN\ 1s-46min} = 0.74$). The second fractal dimension is lower (0.51) and ranges from 46 minutes to 7.7 days ($D^{Ramp}_{TBNN\ 46\ min-7.7d} = 0.51$). There are also nearest neighbour events that are not fractal and occur between 7.7 to 69 days apart. These pairs of events are a very small part of the population.

4.1.2.3 Fractal Dimension of Event Intensity (Magnitude) – Ramp

The fractal dimension of intensity using a scale such as the Richter scale includes negative values and cannot be directly calculated. Since it would be meaningful to know how far large events occur from other events, it was decided to calculate the fractal dimension of the nearest neighbour distance for each range of magnitudes. The seismic events around the ramp vary from

magnitude -3 to 0, with one event at 0.5.

4.1.2.4 The Fractal Dimension of Event Intensity and NN Distances

The fractal dimension of the seismic intensity with its corresponding range of nearest neighbour distances is shown in Figure 55. Individual graphs are included in Appendix IV.

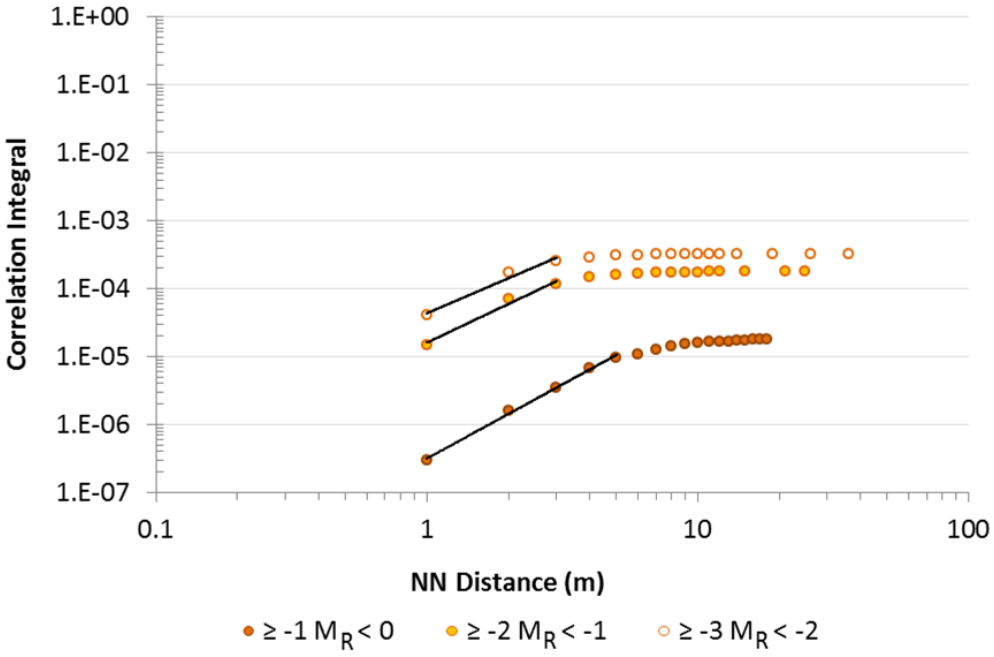

Mag R Range	FD	R^2	NN (m) Range		Max
-1 to 0	2.18	99.6%	1	5	18
-2 to -1	1.71	96.8%	1	3	25
-3 to -2	1.71	96.8%	1	3	36

Figure 55: Fractal dimensions of ramp nearest neighbour distances with magnitudes ranging from -3 to 0

The fractal dimension and corresponding range of nearest neighbour distances by magnitude range allows the quantification of a normal response to rock relaxation around a drift scale excavation. The largest events between magnitude 0 and -1 have a fractal dimension of 2.18 within one to five metres of the drift ($D_{NN\ 1-5m}^{M_R -1\ to\ 0} = 2.18$). The furthest nearest neighbour distance at this magnitude is eighteen metres. While not fractal, this distance is an indicator of how far away an event of this

size could be expected from another event. The maximum nearest neighbour distance increases with decreasing magnitude for this seismic source. The furthest distance is 36 metres (events with magnitudes between -2 and -3).

These distances and magnitude ranges can be used together to create magnitude isoclines on a development print. For example in Figure 56 Image A, the distance ranges for each magnitude range are measured from the seismic events that occur at the furthest extent of all the seismic events (worst case scenario). The isoclines show what the seismic response has been up to that point in time and what distances and magnitudes could be expected with the next development round if the conditions remain the same.

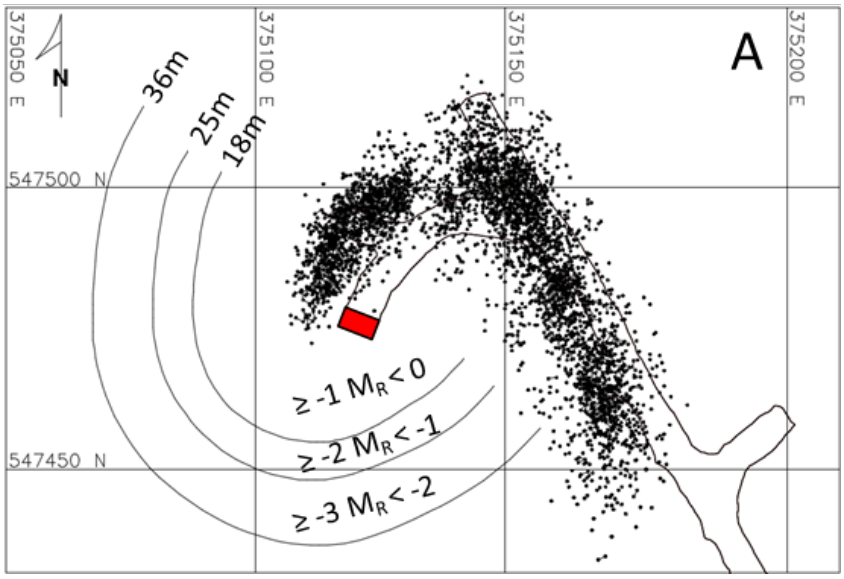

Figure 56: Image A - Magnitude isoclines developed from the maximum nearest neighbour distances

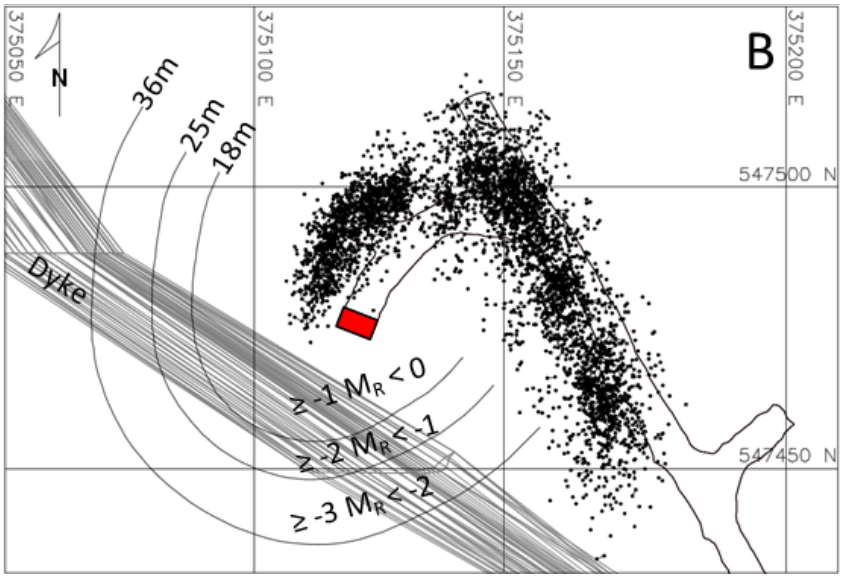

Figure 56: Image B – A dyke is present ahead of where the ramp development is planned

Calculating the isoclines based on the seismic response after every blast also provides an opportunity to anticipate when a geological structure may start to be influenced by blasting. Figure 56 Image B shows how close a dyke is to each magnitude isocline calculated after the last blast. Since the two already overlap (dyke and isoclines), it would be worthwhile to go back and check if the seismic response of the ramp development changed as the ramp curve turned toward the dyke. If it did, it would give the mine personnel the opportunity to proactively estimate what the seismic response might be as the ramp gets closer to the dyke.

This novel method of combining magnitude and nearest neighbour distances for a given seismic source contributes to the knowledge of approximately where and how large a subsequent seismic event could occur from existing events. Since the method uses only existing events in the calculations, the method can be used proactively instead of retroactively.

4.1.2.5 The Fractal Dimension of Event Intensity and Time Between NN Events

For each magnitude range, the fractal dimension of the time between nearest neighbour events

gives visibility to the time frames a seismic source is active. The ramp development data is shown in Figure 57. Detailed individual graphs are provided in Appendix V.

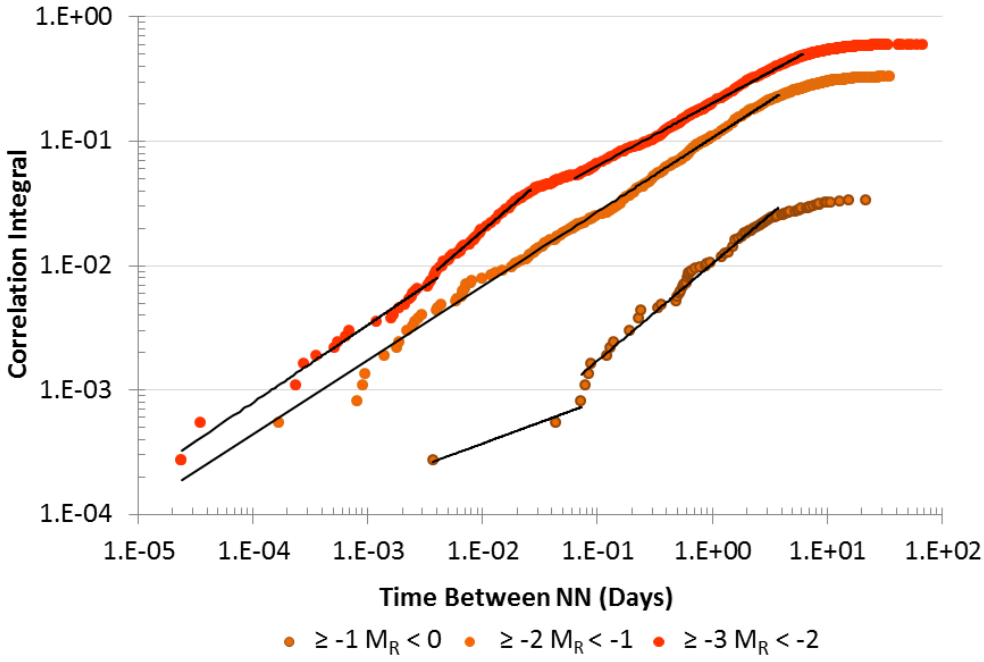

Magnitude Range	FD	R^2	Time Period	Max
0 to -1	0.34	95.32	5.3 min to 1.7 hrs	21.6 days
	0.78	98.26	1.7 hrs to 6.8 days	
-1 to -2	0.59	99.56	14.7sec to 3.8 days	35.4 days
-2 to -3	0.62	98.36	2 sec to 6.2 min	68.1 days
	0.79	99.72	6.2 to 37.4 min	
	0.50	99.80	1.5 hr to 6.7 days	

Figure 57: The fractal dimension of the time between nearest neighbours ramp events by magnitude range

The largest magnitude events (M_R= 0 to -1) tend to occur within one of two time periods after the nearest neighbour event. The first period is between 5 minutes to 1.5 hours ($D^{Ramp}_{M_R=0\ to\ -1)} = 0.59_{(TBNN\ 5.3min\ to\ 1.7\ hrs)}$). The second period has a higher fractal dimension of 0.78 with most events occurring within 1.7 hours to 6.8 days of their nearest neighbour ($D^{Ramp}_{M_R=0\ to\ -1} = 0.78_{(TBNN\ 1.7hrs\ to\ 6.8\ days)}$). This is somewhat contrary to conventional thinking that seismicity around development headings dies down within a day or two. The magnitude range of M_R -1 to -2 is well correlated over a shorter time period ($D^{Ramp}_{M_R=-1to-2} = 0.59_{(TBNN\ 14.7s\ to\ 3.8d)}$).

The lowest magnitude events are more variable however have fractal dimensions of the same size and over the same time periods as the other two magnitude ranges. It should be noticed that each magnitude range has non-fractal periods of which the maximum time frame is also shown in Figure 57. For example, the largest magnitude events have occurred in the non-fractal period of 6.8 days up to 21.6 days. What is important to remember is that the fractal time periods are the most likely periods to expect seismicity of this magnitude. The non-fractal time period is the least likely to experience a large magnitude event. It is suggested that the events that are fractal can be considered a normal response to development and those that are not fractal represent a possible but unlikely response.

4.1.3 Applying Nearest Neighbour Distances – Proximity Test

The combination of sequential clustering and fractal dimension provide a means to describe normal seismicity around a drift, it can also be used to describe abnormal seismicity. By applying the same methods to seismic events in a one day period, a test has been developed to identify what could be considered abnormal seismicity around a ramp sized excavation. The purpose of the proximity test is to identify seismically active locations that are not in close proximity to the other seismicity in the area. The test uses the nearest neighbour distance between seismic events that occur on the same day to discriminate between normal and abnormal locations. In the case of the ramp development, the nearest neighbour distance was calculated between the seismic events in each twenty four hour period. One day was chosen because blasting is usually conducted on a daily basis for development. The cumulative frequency of the furthest distance between events recorded each day is then plotted (Figure 58). The linear portion of the plot includes 80% of the nearest neighbour distances. For this ramp, the daily nearest neighbour distances are between eight

and twenty-one metres and can be considered a normal response for the ramp development. The remaining 20% of the distances are further than 21 metres and can be considered an abnormal response.

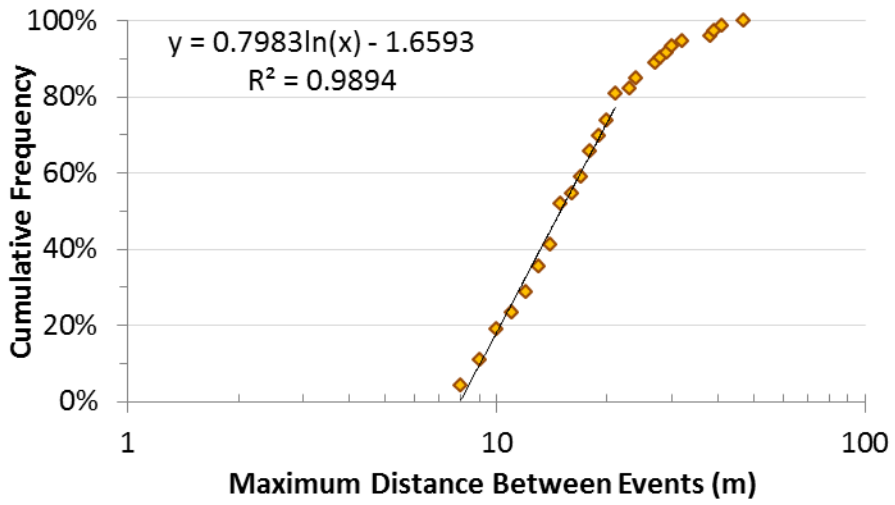

Figure 58: The cumulative frequency of the seismic events that are furthest from all other events for each day of a seventy five day development period

The seismic events furthest away from the majority of the other seismic events each day identify the abnormal locations. Of the 3704 events around the ramp, only fourteen events are more than twenty one metres away from the other events on the day they occurred (Table 10).

Table 10: Events identified using a Proximity Test

Date	Event	Single Event or Cluster #	Distance to NN (m)	NN	
				E	C
5-Jun-05	2659	Single	31.4	E1344	C1222
17-Jun-05	4112	C263	29.6	E2376	C263
18-Jun-05	4183	Single	40.3	E379	Single
19-Jun-05	4255	Single	26.2	E395	C395
21-Jun-05	4484	Single	37.4	E935	Single
23-Jun-05	4787	C1316	22.5	E1721	C1721
3-Jul-05	5812	C1239	23.2	E2761	C1239
9-Jul-05	6201	C263	28.2	E1716	C263
11-Jul-05	6348	C263	23.3	E3737	C3737
23-Jul-05	7455	Single	26.6	E6183	Single
23-Jul-05	7526	C263	24.1	E4327	C263
26-Jul-05	7693	C263	46.4	E371	C263
27-Jul-05	7799	C263	27.5	E2264	C263
28-Jul-05	8113	C263	26.8	E1731	C263

The day an event is identified as being in an abnormal location, the location and source parameters can be examined initially and then followed over time. Event 1359 is a particularly interesting event because it occurs one month before the ramp is excavated at this location (Figure 59).

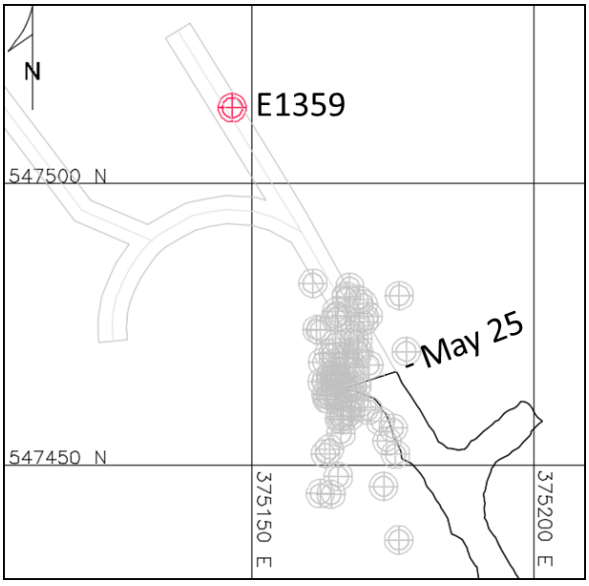

Figure 59: Event 1359 occurs on May 25th in an area of the ramp that won't be developed for another month

The event's nearest neighbour is 38 metres away and 50 metres away from the location of the blast. E1359 is a M_R = -3.1 event. Given its low magnitude, the event would likely be dismissed as

insignificant. However, it is a very significant event because it indicates the location of a new seismic source. As the ramp development progressed toward the location of E1359, other seismic events occurred at this location. Further investigation found the events were located on the underside of a dyke located above the drift (Figure 60).

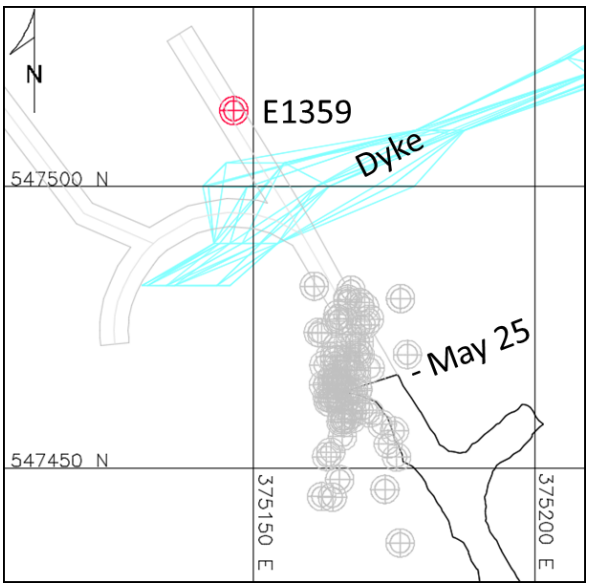

Figure 60: Dyke above and ahead of the developing ramp. Event 1359 is located very close to the dyke.

The advantage of the proximity test is that once an anomalous location is identified, measures can be taken before the development reaches this point to determine if the dyke poses a hazard and if so how to mitigate it.

The proximity test can also be used after an area is developed to identify locations that remain seismically active long after the area has been developed. Event 4787 occurs in the west wall of the ramp, has a nearest neighbour 22.5 metres away (E1721) and occurs three weeks after the ramp was blasted in this location (Figure 61). The location continues to remain active after Event 4787 (Events 6201 and 7799). Often when one seismic event occurs far away from the current development activity it is disregarded as important because it is only one event. However, if all the

events within 2.42 metres of E4787 are identified, it becomes evident that there are other events that precede E4787 (E4146 and E4262) and two events that follow it (E6201 and E7799).

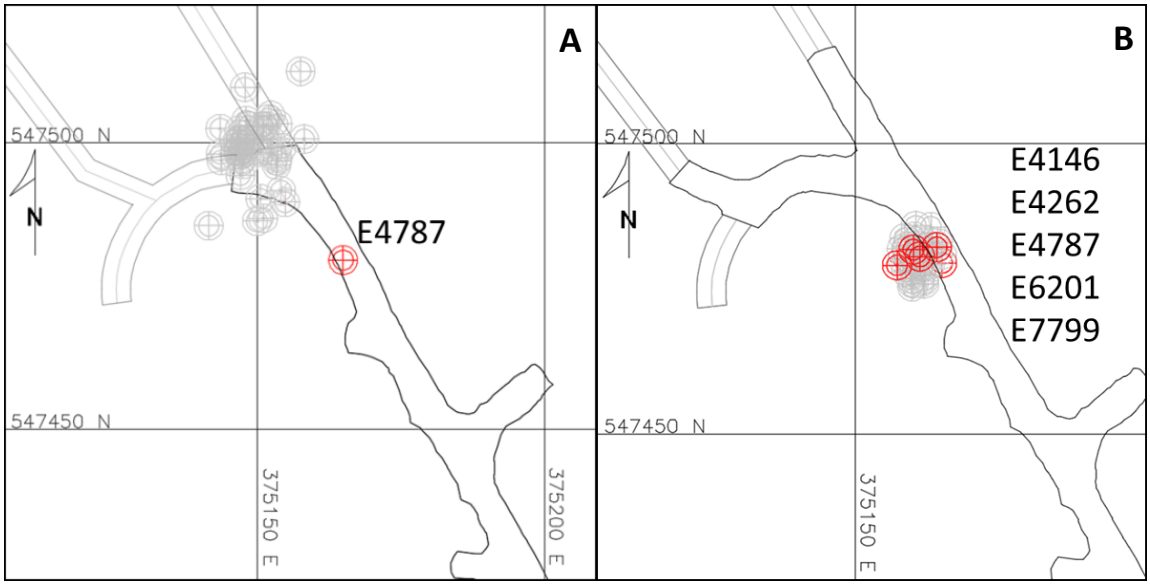

Figure 61: Image A - The proximity test identified Event 4787 which occurs just above the ramp on June 23rd, three weeks after the area was developed. Image B - The grey circles show the seismicity that occurred when the ramp was blasted on May 31st and June 2nd at this location

Once an anomalous location has been identified, the location can be studied. For example a plot of the time and magnitude (called a magnitude time history graph) of the events at this location can also be created and analyzed (Figure 62).

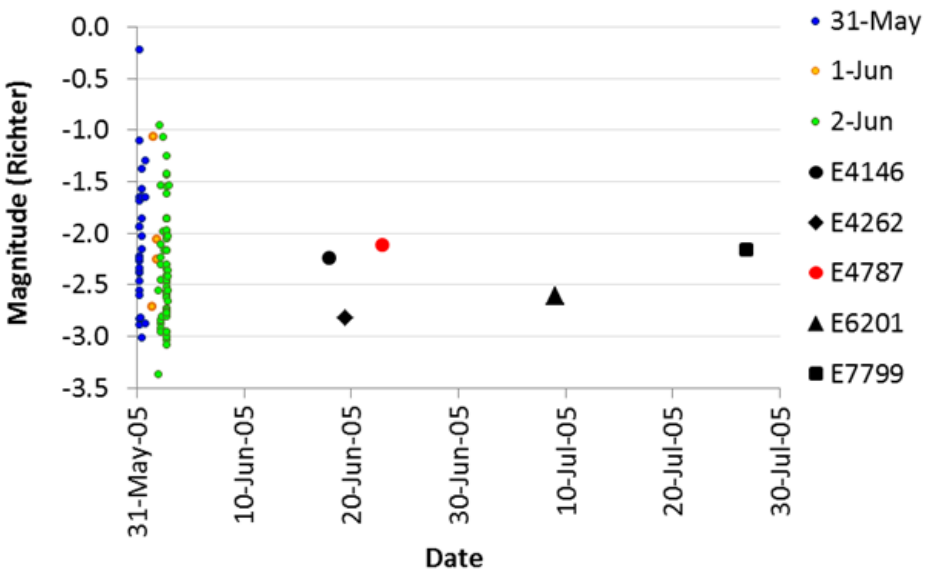

Figure 62: A magnitude time history of the seismic events located by the proximity test after the blasts on May 31 and June 1st

Studying the time between events in cases like this is complicated because of the size, frequency and changing location of each blast. The use of the maximum nearest neighbour distance graph (previously shown in Figure 58) removes the need to quantify each blast parameter. It shows there is a linear relation between the cumulative number of events and the furthest nearest neighbour distance each day. In terms of rock mass behavior, the rock mass around the ramp will be in different stages of failure at any point in time. Some events will occur ahead of the development face, most around the most recently blasted walls and back and some behind as the stresses redistribute around the newly excavated opening. Therefore, it may be too simple to describe the estimated damage zone around an excavation as twice the drift height or width as suggested by McGarr (1976). Instead, the proximity test could be applied to a number of case studies such as this ramp example to create an empirical plot of the deformation zones around various scale excavations much like that previously presented in Figure 17.

When an event occurs in an area already excavated, a visual inspection of the area can be

conducted to determine if the area is deteriorating, if a structure is present, a change in rock type or some other reason for the seismic event.

Some locations identified by the proximity test occur once with no further activity (Figure 63 Image A). E4183 is in an area that was developed a month earlier. There is another location - the safety bay - that is approximately twenty metres away from E4183. The four events around the safety bay (E4112, E4255, E5812, and E7693) were also identified by the proximity test (Figure 63 Image B).

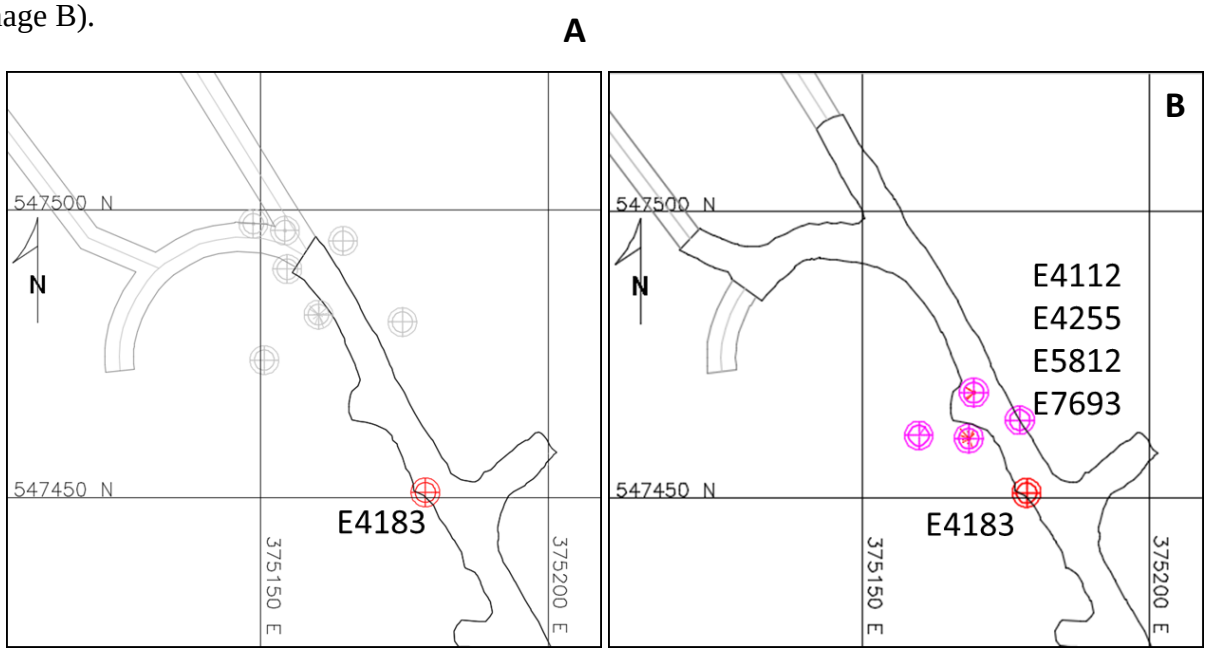

Figure 63: Image A - Event 4183 occurs over forty eight metres away from its nearest neighbour (Image B)

It may be that E4183 is at the end of a structure associated with the safety bay or it may be an isolated event. In either case, the proximity test is providing good information about unexpected seismically active locations that are not detected by current seismic analysis methods. The details of each event identified in the proximity test are included in Appendix I. Additional analysis using other seismic source parameters such as energy or moment can also be conducted to further describe the area. In this case no further study using energy or moment can be done as the data set only includes seismic event location, time and magnitude.

4.1.4 Summary of Case 1 - Ramp

The 3704 seismic events that occur during 75 days of ramp development have been clustered using sequential spatial clustering and characterized by the fractal dimension of the distance, time and magnitude of the events.

Since daily blasting was used to develop the ramp, the mode and mean distances between the nearest neighbour events are very small (1.1 metres – mode, 1.65 metres – mean). Clustering at these distances resulted in a large number of small clusters. Investigating the distance between the clusters created using 1.65 metres found that at 2.07 metres the clusters ranging in size from 20~300 events) coalesce into one large cluster of 2364 events.

This particular case study lead to the creation of several applications that 1) help identify when a seismic source is moving, 2) identify when a seismic event is in an abnormal location (proximity test); and 3) use past history to create isoclines that show how far and approximately how large a new event may occur adjacent to a current seismic zone if the rock mass remains the same.

Moving seismic sources such as a chimney failure or a caving front are hard to detect unless they happen rapidly. Using sequential spatial clustering and the centerline technique provides a mathematical approach to identifying unknown seismic sources moving in a particular direction. The proximity test developed also mathematically determines if a seismic location is significantly further away than all other seismic events occurring in a development heading. These anomalous locations indicate that there may be a change in the rock mass ahead of a ramp. This indicator provides the opportunity to investigate the rock mass ahead of the development to determine if the seismic response may change. The creation and use of isoclines is an extension of the proximity

test that incorporates seismic intensity. If changes in the rock mass are expected ahead of a developing ramp or drift - such as a new geologic structure or change in rock type, then the seismic response would be expected to change. If no change is expected and one still occurs the isoclines will change to reflect the new seismic response. A complete summary of the characteristics of the ramp development are included in Table 11.

Table 11: Summary of Ramp Development Seismic Characteristics

Seismic Source	NN Distance		Fractal Dimensions			
			NN		Time Between NN	
	Mode (m)	Mean (m)	D_{NN}	Range (m)	D_{TBNN}	Range
Ramp	1.1	1.7	2.83	0.1-1.0	0.74	12s- 46min
					0.51	46min-7.7d

Seismic Source	Fractal Dimension (metres)		
	Distance between NN (m) by Magnitude Range		
	≥-1 and <0	≥-2 and <-1	≥-3 and <-2
Ramp	2.18 (1-5m)	1.71 (1-3m)	1.71 (1-3m)

Seismic Source	Fractal Dimension (days)		
	Time between NN (Days) by Magnitude Range		
	≥-1 and <0	≥-2 and <-1	≥-3 and <-2
Ramp	0.34 (53min-1.7h)	0.59 (14.7s-3.8d)	0.62 (2s-6.2min)
	0.78 (1.7hr-6.8d)		0.79 (6.2-37.4min)
			0.50 (1.5h-6.7d)

4.2 Case 2 – Abutment

The seismic events around an abutment of a stoping block occurred in just over two years (760 days) from April 1st, 2004 until April 30th, 2006. Prior to analyzing the seismic events, a decision needs to be made which events to study. Since this is an arbitrary decision, it was decided to choose two populations and compare the results. This approach will give insight into the similarities and differences of the different populations and the impact this may have on interpretation of the seismic events present in the failing rock mass around the stopes being mined.

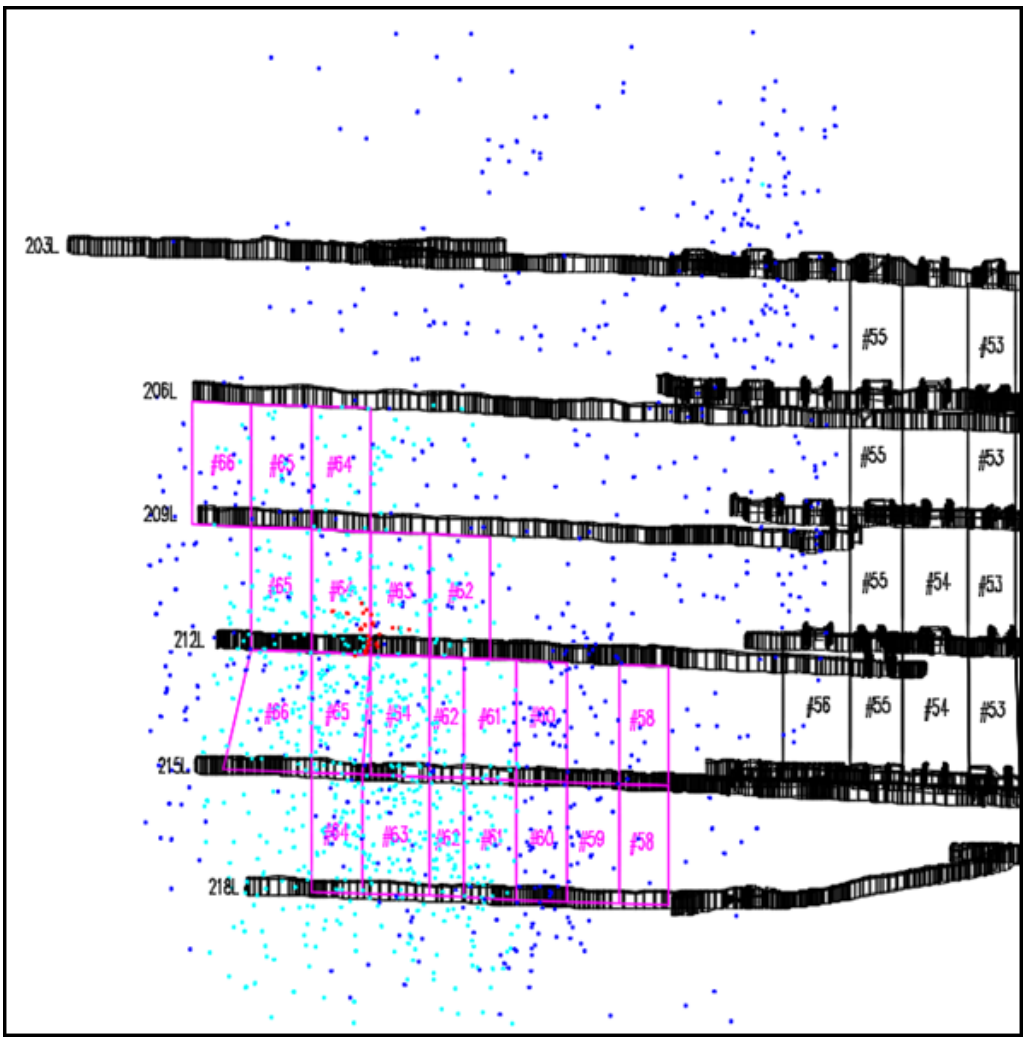

Figure 64: Seismic events around stope abutments. Population 1 (light blue dots - 710 events) and Population 2 (both dark blue and light blue dots – 1350 events)

The two populations of seismic events chosen are; Population 1 which contains 710 events that appear to be located more closely to each other (light blue dots in Figure 64) than Population 2, this contains all 1350 events (both light and dark blue dots). Both populations occur over the same time period - 759 days (two years, 1 month).

4.2.1 Nearest Neighbour Distance and Resulting Clusters - Abutment

The distance between each event to every other event that occurred prior to it was calculated for each population. The probability density function, based on each event's nearest neighbour distance, is shown in Figure 65 for both Population 1 and 2. The events in Population 1 are closer together than Population 2 because Population 1 has a higher probability of nearest neighbours that are 4.5 metres apart.

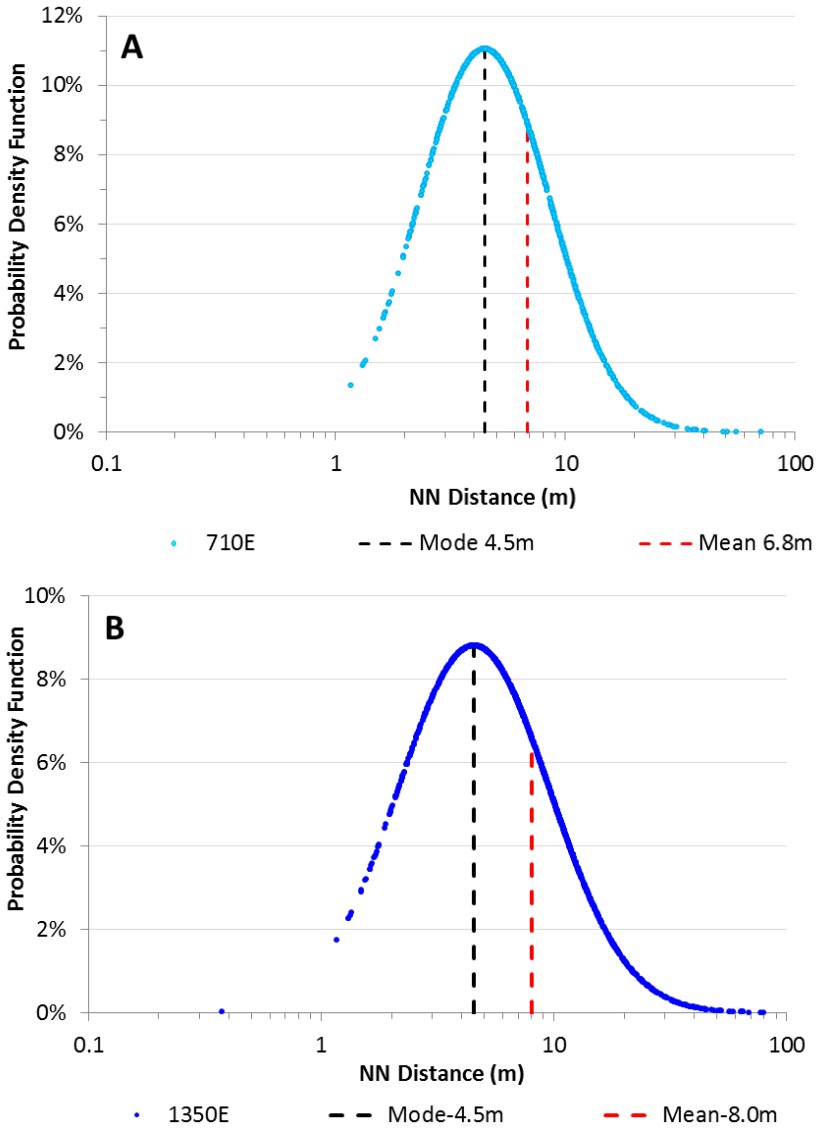

Figure 65: Probability of nearest neighbour distances for seismic events in an abutment (Image A Population 1- light blue, Image B Population 2 – dark blue)

Since the both populations have the highest probability of nearest neighbours occurring at 4.5 metres, this distance will be used to cluster events for each population. The results of the size and number of clusters and single isolated events are shown in Figure 66.

Population #1Clustered at NN Distance of 4.5 metres (Mode)												
Size (# of E)	1	2	3	4	5	6	7	8	9	12	17	Total
Quantity	412	68	12	7	3	5	1	1	1	1	1	512
#E	412	136	36	28	15	30	7	8	9	12	17	710

Population #2 Clustered at NN Distance of 4.5 metres (Mode)												
Size (# of E)	1	2	3	4	5	6	7	8	9	12	28	Total
Quantity	898	108	22	11	6	4	1	2	1	1	1	1055
#E	898	216	66	44	30	24	7	16	9	12	28	1350

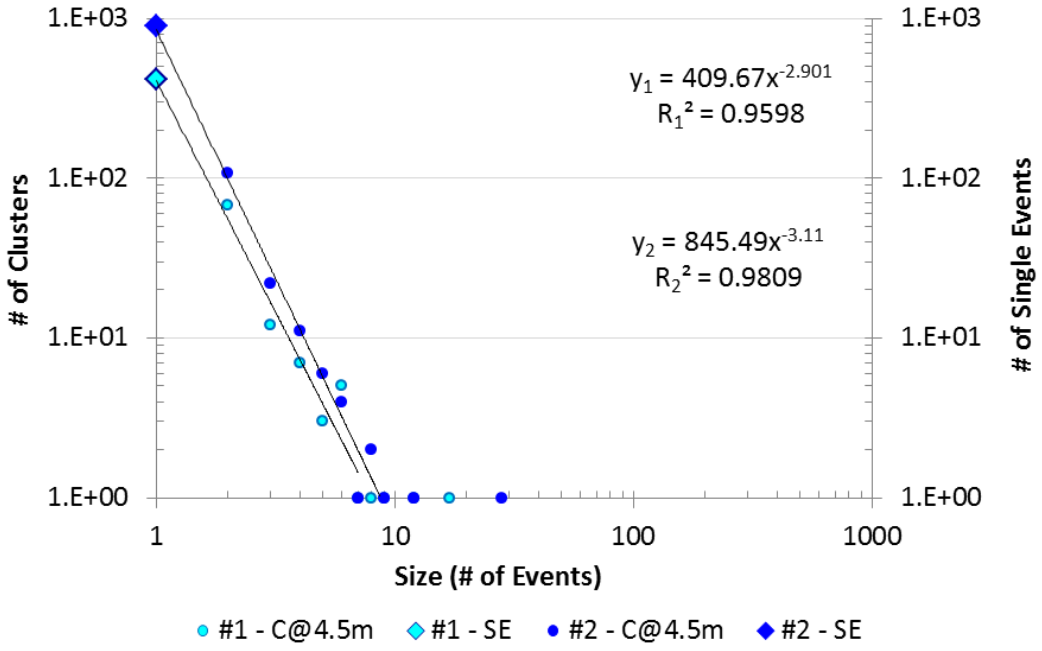

Figure 66: Cluster summary for Population 1 and 2 seismic events in an abutment

The clusters created using the nearest neighbour distance of 4.5 metres for both populations in Figure 66 show some striking similarities. Most notably, the cluster populations are both follow a power law for clusters with two to six events as well as the single events that do not join any cluster. The larger clusters (seven events or more) tend to only form one cluster. The clusters created using a nearest neighbour distance of 4.5 metres for each population have been shown to be located in the same physical location (previously shown in Figure 41). The events in each cluster from Population 1 are the same events that form the clusters in Population 2, with Population 2 having more events in the largest cluster.

The effect of using a larger nearest neighbour distance, such as 6.48 metres instead of 4.5 metres to cluster Population 1, is investigated. The results (shown previously in Figure 43), demonstrate that using the larger distance increases the size of the largest cluster (C233 in this case) and reduces the size of the smaller clusters. The previous clusters shown in Figure 41 are now part of the largest cluster in Figure 43. In order to determine if the seismic data provides any further insight into how the choice of nearest neighbour distance affects the outcome of clusters, the fractal dimension of the nearest neighbour distances was investigated.

4.2.2 Fractal Dimension of Nearest Neighbour Distances - Abutment

The seismic events in Population 1 with a nearest neighbour event 1.4 to 2.8 metres away have a fractal dimension of 4.1 ($D_{NN\ 1.4-2.8m}^{710E}$ = 4.1) (Figure 67 Image A). The nearest neighbour fractal dimension for Population 2 is 4.3. Events that are within 1.4 to 2.4 metres of its nearest neighbour have a fractal dimension of 4.3 ($D_{NN\ 1.4-2.4}^{1350E} = 4.3$) (Figure 67 Image B). Despite the difference in the number of events between the two populations, the fractal dimension for the nearest neighbour distances are very nearly the same and over very similar ranges. Thus at this point choosing one population or the other for analysis would appear to yield similar results.

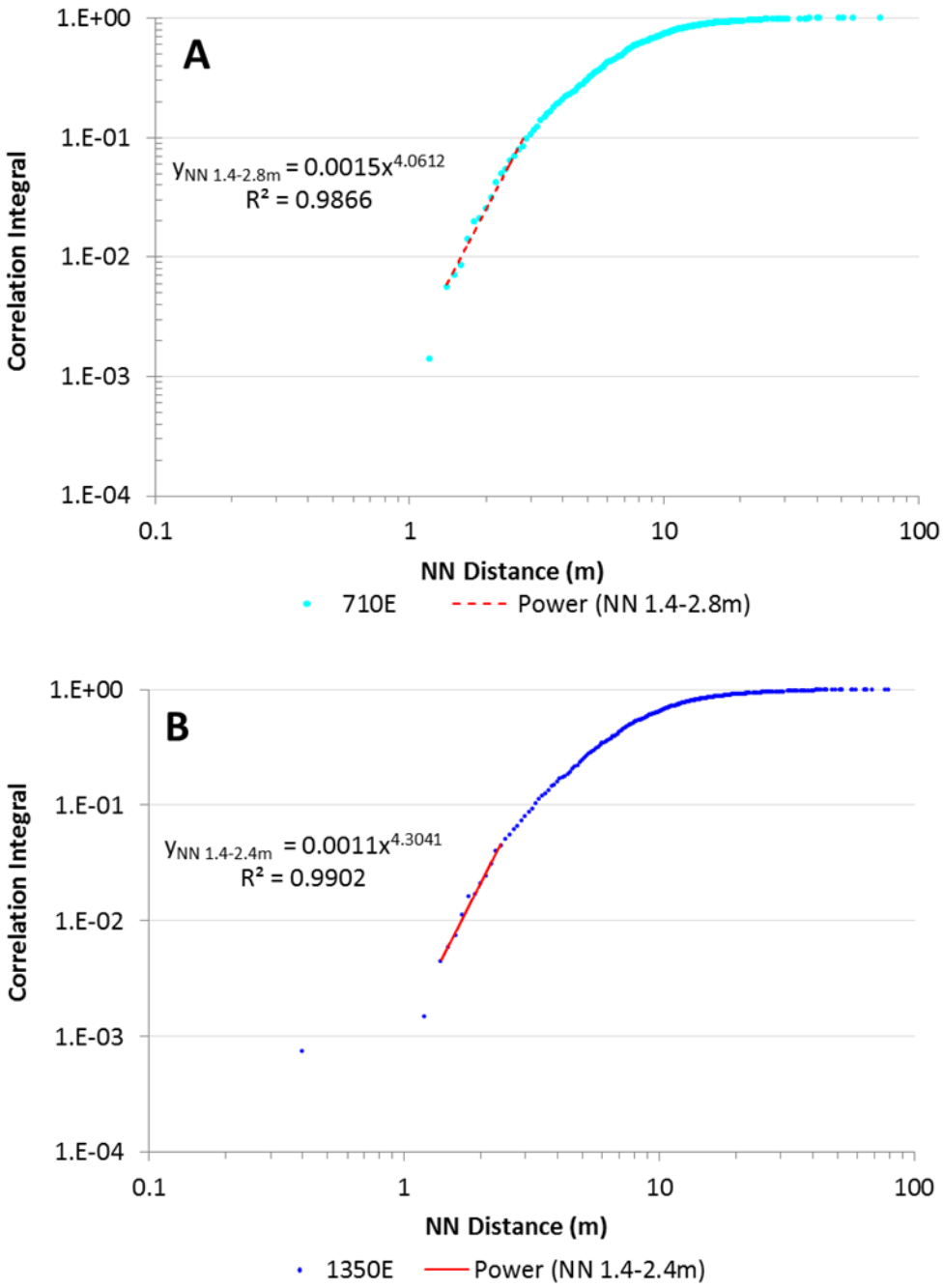

Figure 67: Fractal dimensions of nearest neighbour distances for Populations 1 (Image A) and Population 2 (Image B) in an abutment.

Since there is a range of distances that can be used to cluster seismic events, combining the probability density function with the fractal dimension for the same population will give additional insight into the number and size of clusters that characterize a population. In Figure 68, the fractal

dimension and probability density function for each population are combined and it is observed that the nearest neighbour distances used to cluster the seismic events (mode at 4.5 metres and mean at 6.84 metres) are not within the limits of the fractal dimension.

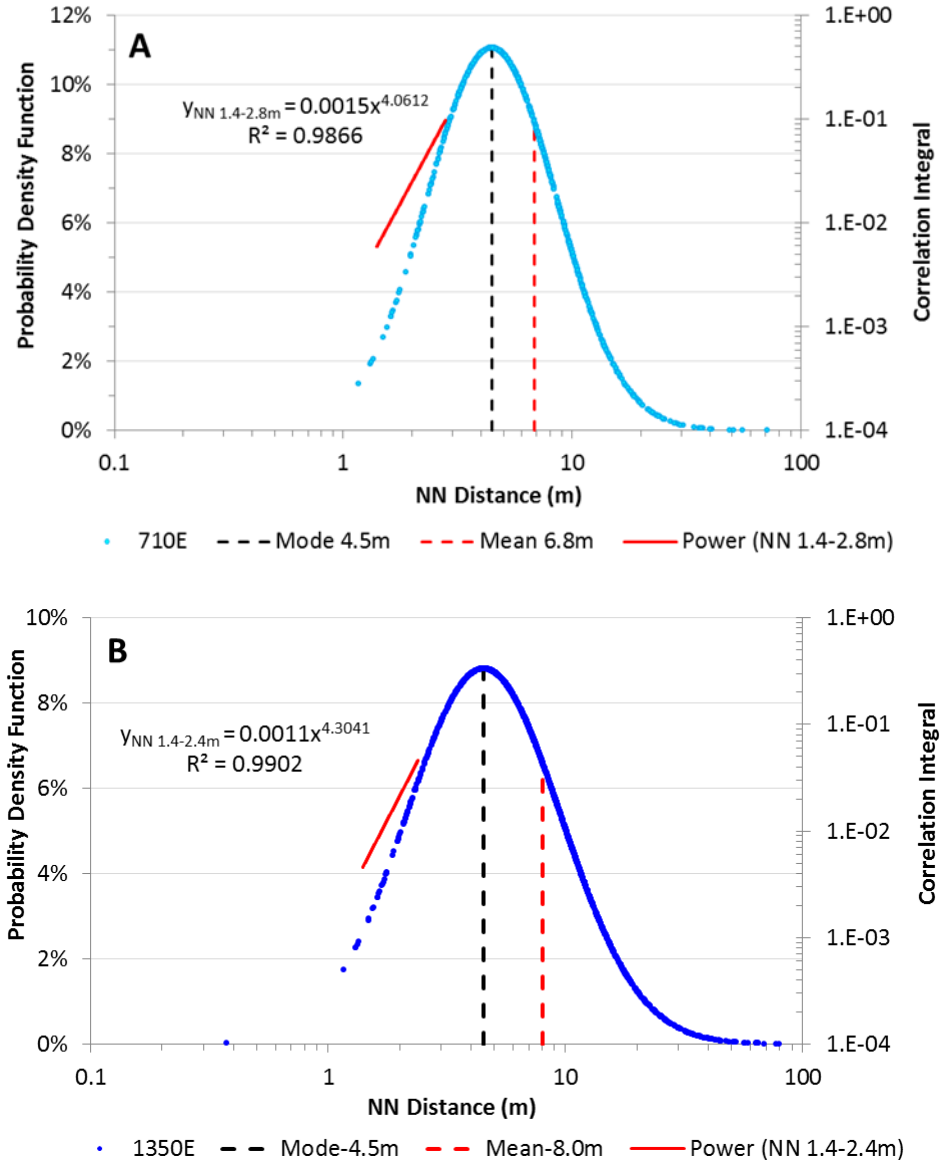

Figure 68: Combining the fractal dimension and probability density function for the nearest neighbour distances for Population 1 (Image A) and Population 2 (Image B).

In order to determine the cause of the high fractal dimension at the shortest distance between events, clusters were created using the fractal range for Population 1 (Figure 69).

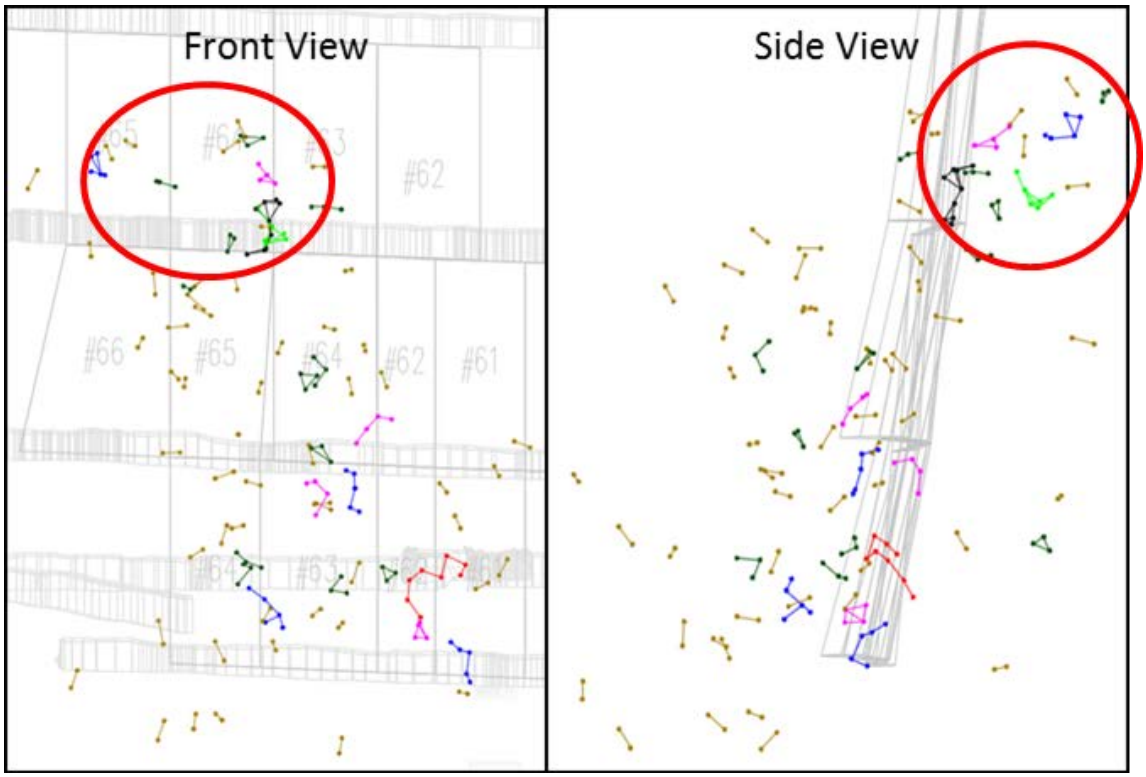

Figure 69: Population 1 clusters with events 4 metres or less apart (shown by a line between the events) have single links between events. The location shown by the red circle contains clusters that have multiple links between the events.

Most of the clusters created in the fractal region have single links between the nearest neighbours. There is one area (shown by the red circles in Figure 69) where the nearest neighbours form multiple links with events within 4 metres of each other.

This case demonstrates two points with respect to fractal dimension and seismic events. The first point is that the fractal dimension of nearest neighbour distances can be used to compare seismic event populations that have been selected arbitrarily. The second point is that if a population shows a very short fractal range, there may be more than one seismic source within the data set. The fractal dimension of the nearest neighbour distance in the abutment will be used to

characterize the failing rock mass so that it can be compared to the other case studies.

4.2.3 Fractal Dimension of Time

The time between nearest neighbours is examined for both Population 1 and #2. In this case study, there is a significant difference that is evident between the two populations and important information about multiple seismic sources when the time between nearest neighbours is used.

Fractal analysis of each population looking at the time between nearest neighbours shows a sharp contrast between Populations #1 and #2 (Figure 70-Images A and B).

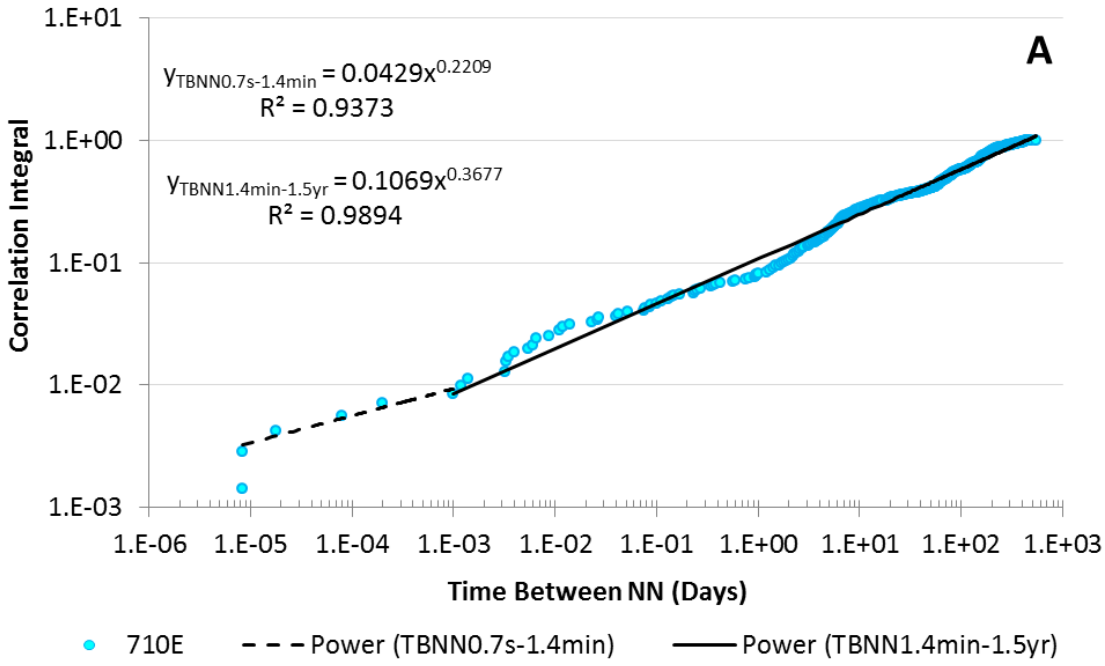

Figure 70: Image A – The fractal dimension of time between nearest neighbours for Population 1 (710E)

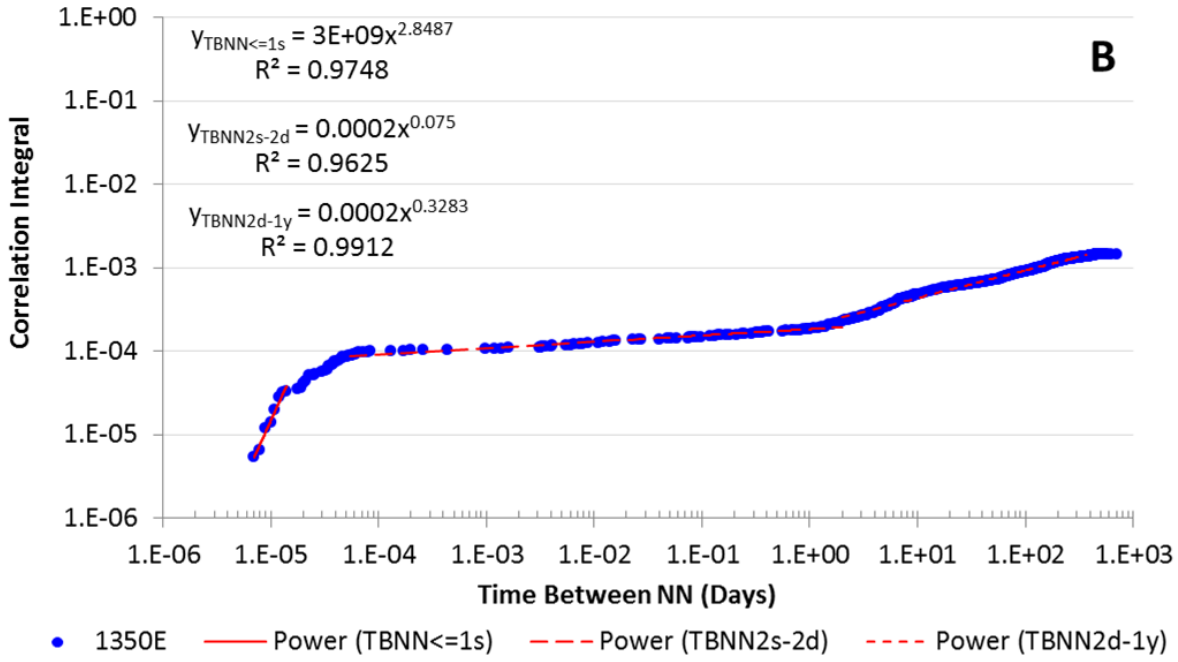

Figure 70: Image B - The fractal dimension of time between nearest neighbours for Population 2 (1350E)

In Figure 70 – Image A the fractal dimension of the time between nearest neighbour events for Population 1 is 0.22 for the pairs occurring very close together in time ($D^{710E}_{TBNN\ 0.7s-1.4\ min}$ = 0.22).

There is a second much longer period where the nearest neighbours are further apart in time and have a similar low fractal dimension of 0.37 ($D^{710E}_{TBNN\ 1.4min-1.5\ yrs}$ = 0.37). Both these periods are not well correlated and have low fractal dimension. It suggests that Population 1 may also have some events that are from a second seismic source. Where more than one seismic source is suspected in a data set, the time between nearest neighbour analysis could be used to distinguish between them.

In Figure 70 Image B, Population 2 has three time periods that are fractal. The first period has a fractal dimension of 2.85 meaning all nearest neighbour pairs that are less than or equal to one second are well correlated ($D^{1350E}_{TBNN \leq 1\ s}$ = 2.85). The second period, while fractal (D=0.08), has a very low fractal dimension which means the nearest neighbour pairs are very poorly correlated ($D^{1350E}_{TBNN\ 2s-2days}$ = 2.85). The third period has a low fractal dimension of 0.33 between 2 days and one year ($D^{1350E}_{TBNN\ 2d-1yr}$=0.33). This third fractal period for Population 2 is very similar to the second fractal period of Population 1. Population 2 and 1 both appear to have more than one seismic source, with Population 2 possibly having three.

Further insight into the differences between the two populations can be seen by the correlations of event intensity to both the distance and time between nearest neighbour events.

4.2.4 Fractal Dimension of Event Intensity (Magnitude) – Abutment

Event intensity described by magnitude does not lend itself directly to fractal analysis. The addition of the magnitude range of a dataset to the fractal dimension, of either time or distance, will be more useful to characterize the different seismic sources present in the data sets, particularly Population 2.

4.2.4.1 Fractal Dimension of Nearest Neighbour Distance by Magnitude Range

The combination of magnitude with nearest neighbour distances showed one very important difference between the two Populations. Population 1 does not have any seismic events with a magnitude larger than one (Figure 71 Image A). The details for Figure 71 Image A can be found in Appendix VII and Image B can be found in Appendix VI.

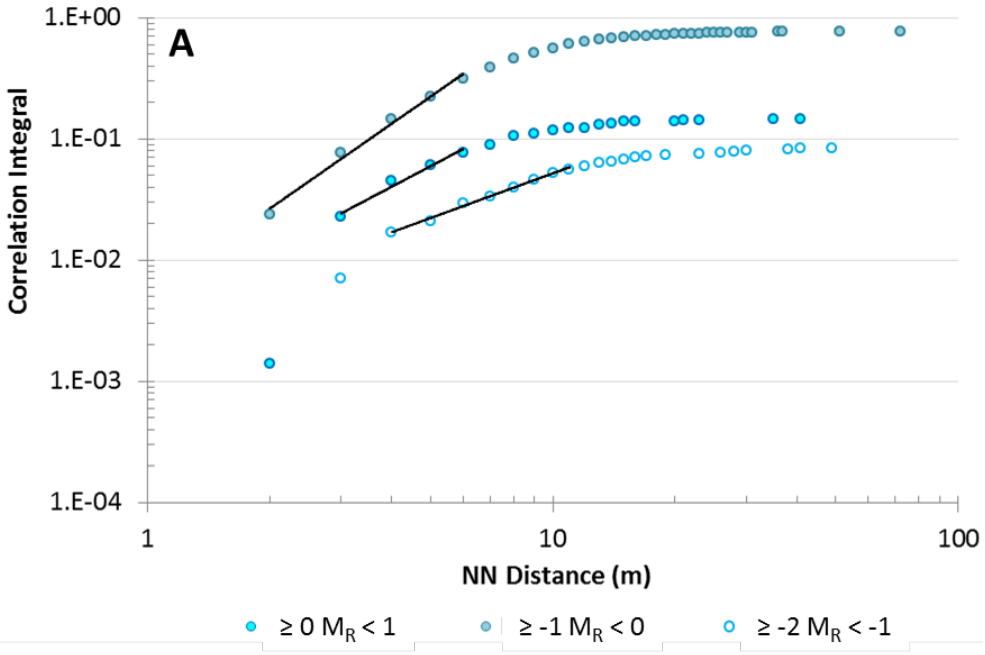

710 Events						
Mag R Range	FD	R^2	NN (m) Range		Max	# NN
>1	-	-	-	-	-	-
0 to 1	1.76	97.4%	3	6	29	104
-1 to 0	2.33	99.0%	2	6	72	544
-2 to -1	1.22	99.4%	4	11	49	60

Figure 71: Image A - Fractal dimension of Population 1 nearest neighbour distances by magnitude range

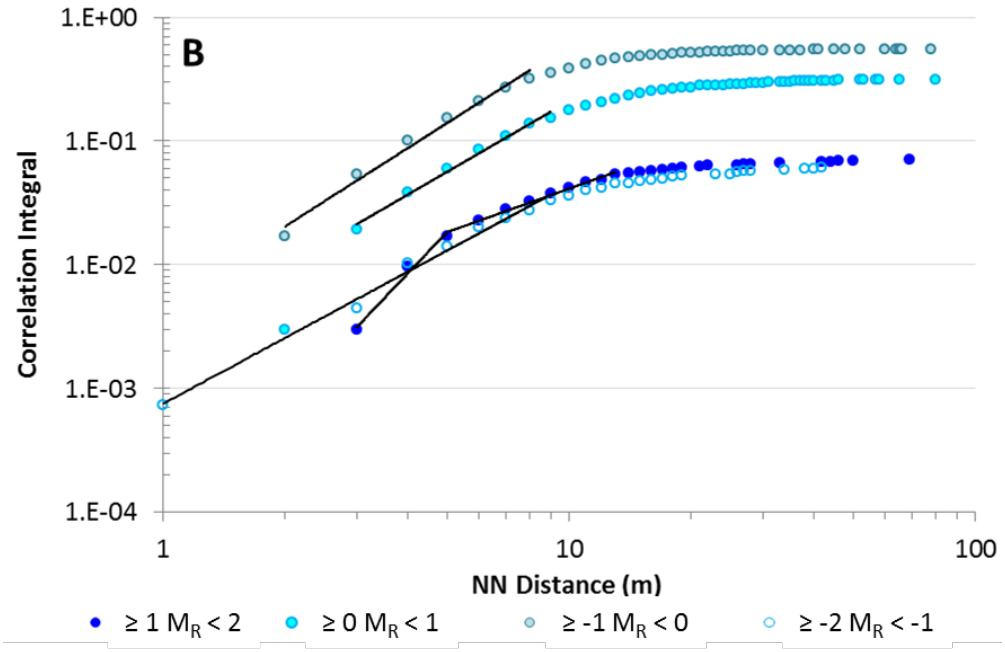

1350 Events						
Mag R Range	FD	R^2	NN (m) Range		Max	# NN
1 to 2	3.46	98.4%	3	5	69	95
	1.17	98.8%	5	13	69	95
0 to 1	1.90	99.0%	3	9	119	427
-1 to 0	2.09	98.4%	2	8	125	745
-2 to -1	1.77	99.2%	1	9	42	82

Figure 71: Image B - Fractal dimension of Population 2 nearest neighbour distances by magnitude range

These large events in Population 2 are located almost exclusively in the footwall (Figure 72) and may be indicative of a structure or change in material properties.

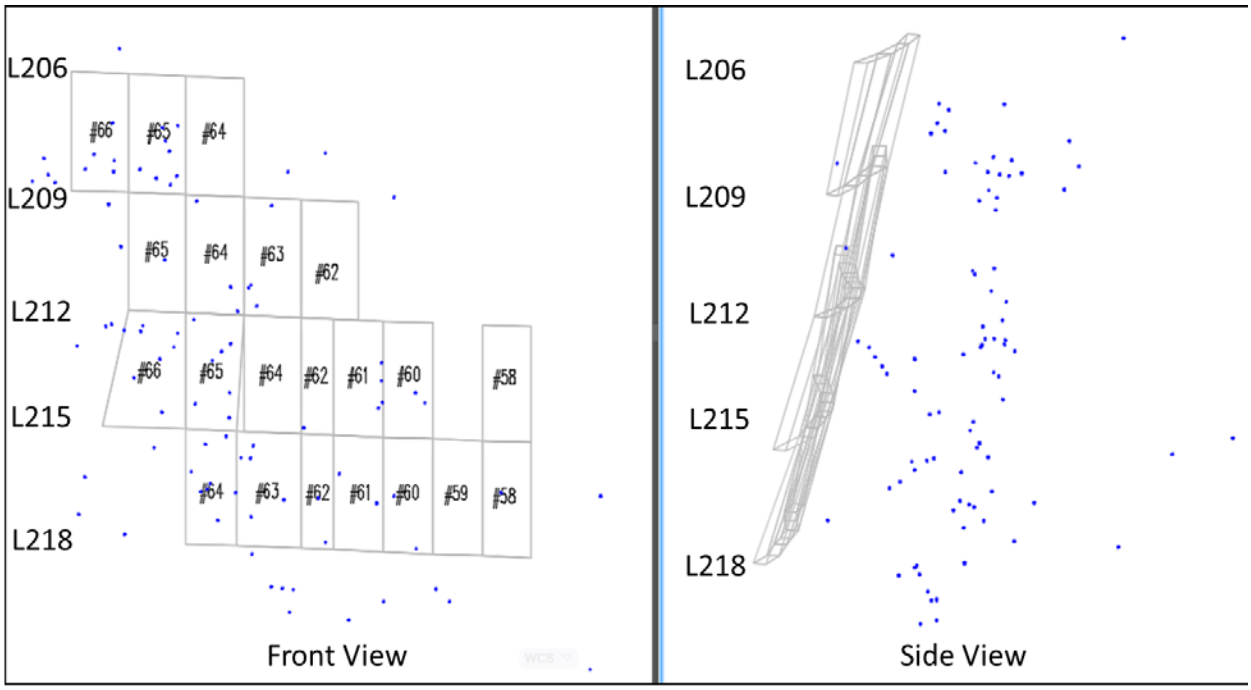

Figure 72: Location of 104 events with magnitude of greater than or equal to 1. All the events belong to Population 2 (1350 events) and are predominantly located in the footwall.

4.2.4.2 Fractal Dimension of Time Between Nearest Neighbours by Magnitude Range

The fractal dimension of the time between nearest neighbours demonstrates that there are clearly two seismic sources within the 1350 events. In Figure 73, the time between the events that are greater than magnitude one occur in two distinct time periods – the first within a fraction of a second with a high fractal dimension ($D_{MR\geq1}^{1350E} = 2.03_{0.6-0.8s}$). The second period has a very low fractal dimension over a much longer period of time ($D_{MR\geq1}^{1350E} = 0.19_{1.3-63.5d}$). Neither of these two periods is similar to the time between nearest neighbours for the events that are less than magnitude one. These events have fractal dimensions ranging from approximately 2 to 6 and occur from a few days to about a week of their nearest neighbour. Since it is clear that 1350 events in Population 2 come from different seismic sources, it is recommended not to study the events together but rather separate the seismic sources before carrying out further analysis. Using the

fractal dimension of the time between nearest neighbours can provide a very useful tool for separating seismic sources.

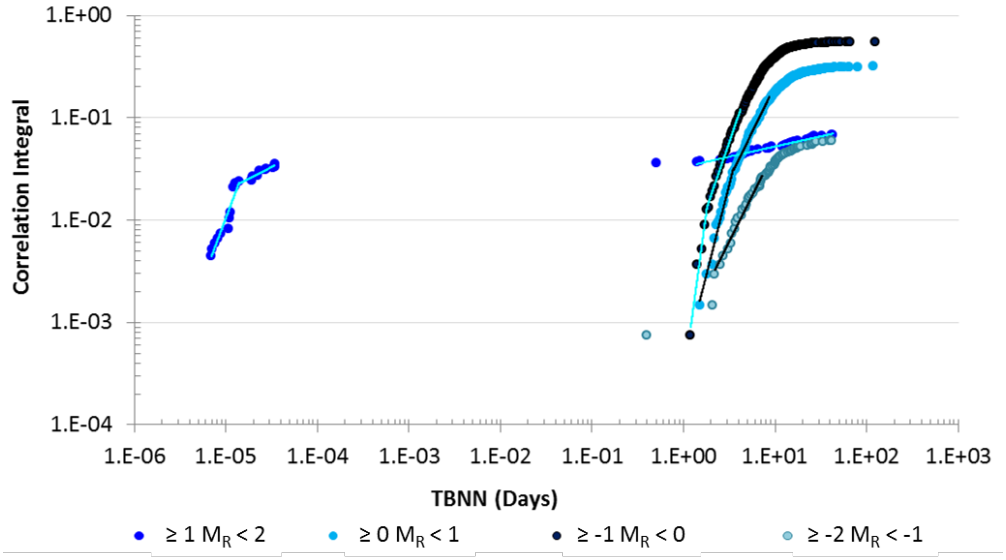

Magnitude Range	FD	R^2	TBNN Range	TBNN Max(d)
1 to 2	2.03	99.9%	0.6-0.8s	64
	0.19	97.9%	1.3-63.5d	
0 to 1	3.52	97.5%	1.5-3.5d	119
	1.83	99.4%	3.5-8.7d	
-1 to 0	6.59	95.5%	1.2-1.8d	125
	2.60	99.3%	1.8-4.2d	
-2 to -1	1.79	97.8%	2.2-7.2d	41

Figure 73: The fractal dimension of time between nearest neighbours by magnitude range in an abutment with 1350 events

The individual graphs supporting Figure 73 can be found in Appendix VIII. The time between the nearest neighbour events with $M_R \geq 1$ shows that the events have two distinct time characteristics – those that occur very quickly (less than five seconds) after their nearest neighbour event and those that occur over a day and up to a year later (Figure 73).

This type of analysis confirms that large magnitude events can have two different time characteristics and also shows that there are time periods when large events do not occur for this

particular seismic source. Figure 74 shows the location of the large events for each time period. The events from both periods occur in the same places – mostly in the footwall.

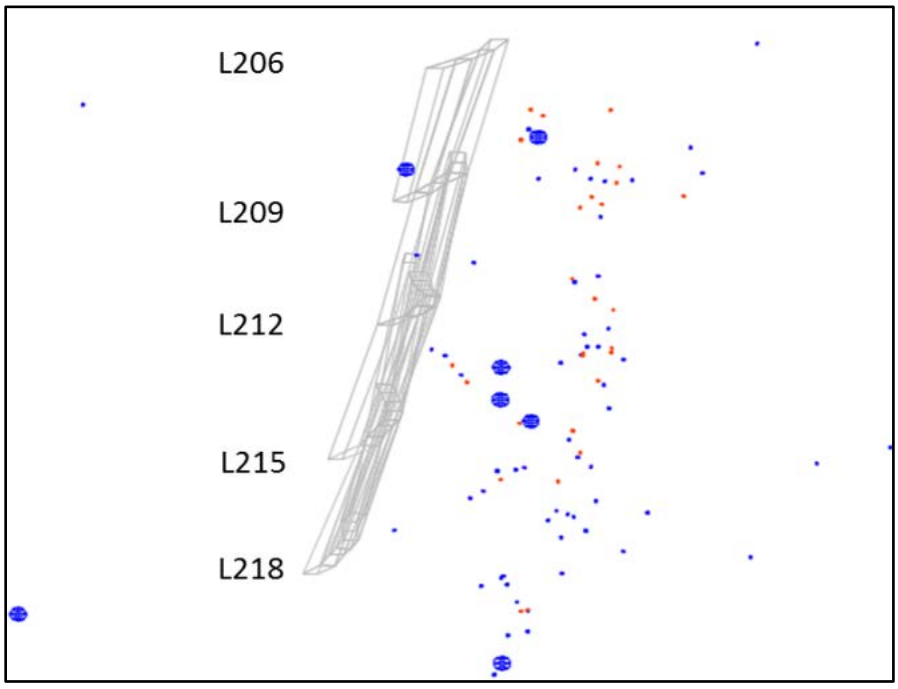

Figure 74: Side view of Population 2 events that are $M_R \geq 1$. The blue dots represent the events that occur more than a day and up to a year after its nearest neighbour event. The orange dots are those events that occur in quick succession (fractions of a second) after their nearest neighbour event. The large diameter blue dots are the locations of the seven largest events M_R = 1.5 to 1.6

Since the large events occur mostly in the footwall, it suggests that there may be a different seismic source, such as a structure of stiff rock. A stiffer rock mass could respond initially to a large stope blast then respond again later to a stress field that changes over time.

The large events ($M_R \geq 1$) have nearest neighbours that are between 5 and 13 metres away whereas events with smaller magnitude events (≥ 0 M_R <1) are closer to their nearest neighbours varying between 3 to 9 metres away.

The same method is applied to Population 1 which is also believed to have one seismic source (Figure 75). Individual graphs supporting Figure 75 are provided in Appendix IX.

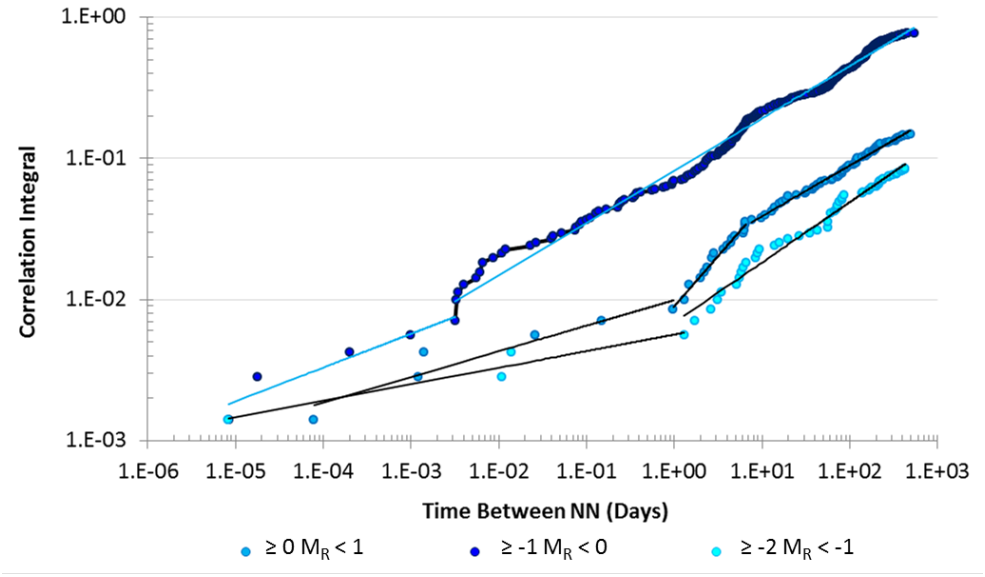

Magnitude Range	FD	R^2	TBNN Range	TBNN Max
>= 0 < 1	0.18	90.6%	6.8s-23.5h	489d (1.3y)
	0.71	98.2%	23.5h-6.5d	
	0.36	99.2%	7.6d-1.3y	
>= -1 < 0	0.24	91.2%	0.7s-4.6min	542d (1.5y)
	0.37	99.1%	4.6min-1.5y	
>= -2 < -1	0.12	93.2%	0.7s-1.3d	426d (1.2y)
	0.43	97.8%	1.3d-1.2y	

Figure 75: Time between nearest neighbours by magnitude range for the 710 events in Population 1

Population 1 also appears to have two distinct time periods and may have two seismic sources as well. However, there are a couple of distinct differences between Populations 1 and 2. Population 1 does not have any events that have a magnitude greater than one, whereas Population 2 has many. The short time period of Population 1 is seconds to days, not fractions of a second like Population 2. Population 2 also did not have nearest neighbours that are between seconds and days the way Population 1 has.

Figure 76 shows the location of events in the range of ≥ 0 M_R <1. In this range both populations are present with Population 1 located predominantly around the stopes while Population 2 is around and above the stopes and also in the footwall.

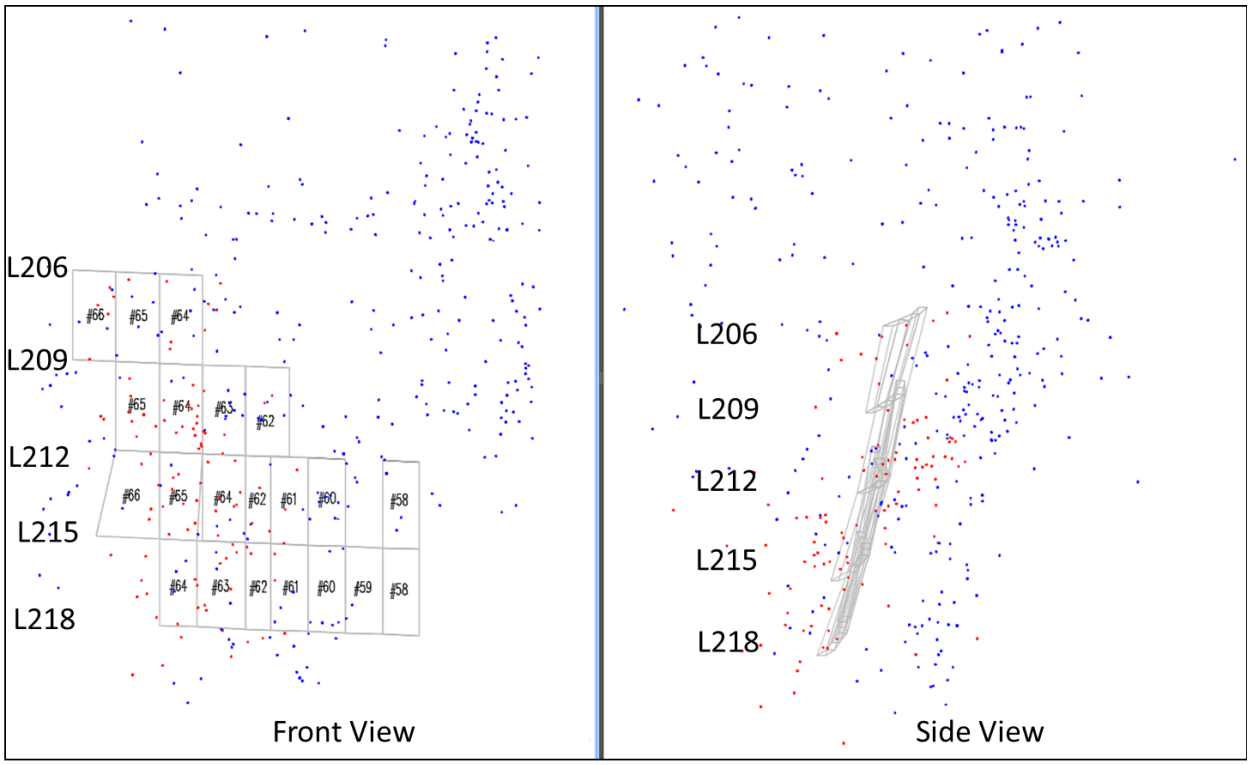

Figure 76: Location of events in the ≥ 0 M_R < 1 for Population 1 (red) Population 2 (red and blue)

This study of the fractal dimension of nearest neighbour distances by magnitude ranges and particularly the fractal dimension of the time between nearest neighbours has shown that at least two and possibly three seismic sources are present in Population 2. It is also very likely Population 1 contains two seismic sources as well. Both populations have distinct variations in the fractal dimension of location, magnitude and time. Further analysis of both populations in the abutment data set should be conducted after the seismic sources are separated.

4.2.5 Summary of Case 2 - Abutment

This case studied two seismic populations to determine how similar/dissimilar they are when used to describe the seismic events around stope abutments. Initially the Population 1 and 2 appeared to have many similarities – perhaps because Population 1 is a subset of Population 2. They had the same mode distance, sequential spatial clustering resulted in similar clusters with Population 2

clusters having more events but the same locations, and the fractal dimension of nearest neighbour distances were very similar over the same distance intervals.

However, very distinct differences became apparent when the fractal dimension analysis of the distance between nearest neighbours and the time between nearest neighbours over their various fractal ranges was completed. Population 2 showed a group of seismic events in a distinct area in the footwall with events of $M_R \geq 1$. Population 1 does not contain any events with this magnitude and only a few events in this location. The large magnitude events ($M_R \geq 1$) showed that they occurred in two distinct time periods as well. They occurred either very quickly after their nearest neighbour event or after 1.8 days and up to a year later. The longer time period associated with these large events is often described as an abnormal seismic response. The analysis methods used in this study are able to quantify and confirm that these events are representative of this seismic source by their fractal dimension and fractal range. A summary of the characteristics of the seismicity around the stope abutments for both populations is given in Table 12.

.

Table 12: Summary of Abutment Seismic Characteristics

Seismic Source	NN Distance		Fractal Dimensions			
			NN		Time Between NN	
	Mode (m)	Mean (m)	D_{NN}	Range (m)	D_{TBNN}	Range
Abutment (710E)	4.5	6.8	4.06	1.4-2.8	0.22	0.7s-1.4min
					0.37	1.4min-1.5y
Abutment (1350E)	4.5	8.0	4.68	1.2-2.4	2.85	≤1 s
					0.08	2s-2d
					0.33	2d-1y

Seismic Source	Fractal Dimension (metres)			
	Distance between NN (m) by Magnitude Range			
	≥1 and <2	≥0 and <1	≥-1 and <0	≥-2 and <-1
Abutment (710E)	-	1.76 (3-6m)	2.33 (2-6m)	1.22 (4-11m)
Abutment (1350E)	3.46 (3- 5m)	1.90 (3-9m)	2.09 (2-8m)	1.77 (1-9m)
	1.17 (5-13m)			

Seismic Source	Fractal Dimension			
	Time between NN (days) by Magnitude Range			
	≥1 and <2	≥0 and <1	≥-1 and <0	≥-2 and <-1
Abutment (710E)	-	0.18 (6.8s-23.5h)	0.24 (0.7s-4.6min)	0.12 (0.7s-1.3d)
		0.71 (23.5h-6.5d)	0.37 (4.6min-1.5y)	0.43 (1.3d-1.2y)
		0.36 (7.6d-1.3y)		
Abutment (1350E)	2.03 (0.6-0.8s)	3.52 (1.5-3.5d)	6.59 (1.2-1.8d)	1.79 (2.2-7.2d)
	0.19 (1.3-63.5d)	1.83 (3.5-8.7d)	2.60 (1.8-4.2d)	

Studying the fractal dimension of the distance between nearest neighbour events and the time between nearest neighbours gives insight into the use of these two different methods. When multiple seismic sources are suspected, the new methods were able to identify the different seismic sources. In order to compare the single seismic source of rock mass failure around stopes and their abutments, Population 2 will be used. However since it contains more than one seismic source, it is not advised to use this as a benchmark case until the seismic sources are separated and analyzed further which is beyond the scope of this thesis.

To summarize, Population 2 has a mode nearest neighbour distance of 4.5 metres and a mean distance of 8.0 metres. The fractal dimension of the nearest neighbour distances is 4.30 for nearest

neighbours 1.4 to 2.4 metres apart. Events that are within the magnitude range of ≥1 M_R < 2 has two fractal dimensions and ranges, $D_{\geq 1\ M_R<2}^{1350E} = 3.46_{(NN\ 3-5m)}$, and $D_{\geq 1\ M_R<2}^{1350E} = 1.17_{NN\ 5-13m}$. The fractal dimension of events with ≥ 0 M_R < 1 is 1.90 for events with a nearest neighbour 3 to 9 metres apart ($D_{\geq 0\ M_R<1}^{1350E} = 1.90_{NN\ 3-9m}$). Events in the range of ≥ -1 M_R < 0 have a fractal dimension of 2.09 and occur within 2 to 8 metres of their nearest neighbour ($D_{\geq -1\ M_R<0}^{1350E} = 2.09_{NN\ 2-8m}$). Lastly, Population 2 is still well correlated with a fractal dimension of 1.77 for nearest neighbour events that in the range of ≥ -2 M_R < -1 with nearest neighbour events within 1 to 9 metres ($D_{\geq -2\ and\ M_R<-1}^{1350E} = 1.77_{NN\ 1-9m}$). The fractal dimension and ranges for the events below magnitude 0 are very close. These values will be used for comparison to the other seismic source case studies.

4.3 Case 3 – Failing Pillar

The third case study is a remnant pillar located at a depth of approximately 600 metres. Over a period of just under two years, 1368 seismic events were recorded inside the pillar. Only the events inside the pillar will be studied in Case 3 (Figure 77). Level 300 is approximately 600 metres below surface.

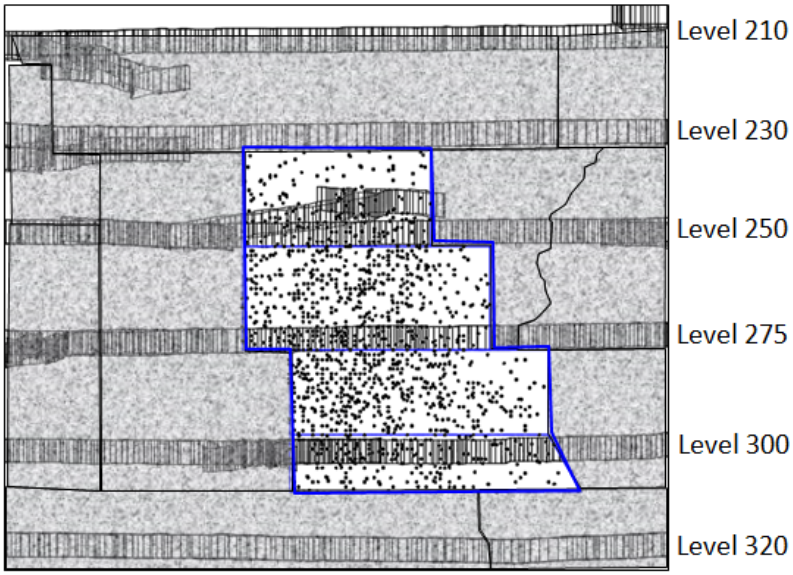

Figure 77: Front view of seismic events inside a remnant rib pillar. The 1368 seismic events (black dots) occurred inside a remnant pillar over a period of 23.5 months, (~ two years). The pillar is outlined in blue. The grey areas around the pillar represent the stopes that have been previously mined and backfilled.

4.3.1 Nearest Neighbour Distances and Resulting Clusters

The distance between each event and every other prior event is calculated for the population of seismic events. The probability density function is based on each event's nearest neighbour distance (Figure 78).

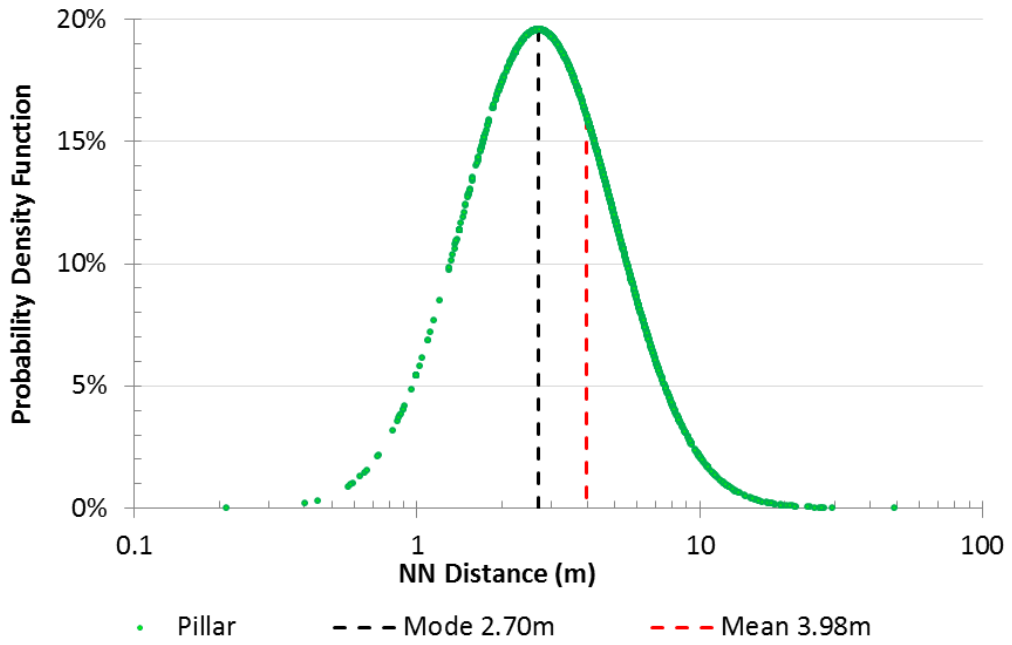

Figure 78: The mode (2.70 metres) and mean (3.98 metres) distances for the seismic events in a failing pillar

Both the mode and mean distances will be used, along with the range of the nearest neighbour fractal dimension to cluster the seismic events in the pillar.

The fractal dimension calculated is the distance between each event and its nearest neighbour event (1368 pairs). This number describes the shortest distances between events and identifies the areas with the highest amount of seismic activity. The fractal dimension of the nearest neighbour events in the pillar is 2.7 with the population being strongly correlated between 0.3 and 3.4 metres (noted as $D_{0.3-3.4m}^{1368DNN} = 2.7$). The fractal dimension describing the nearest neighbour distances between the seismic events in the failing pillar are shown in Figure 79.

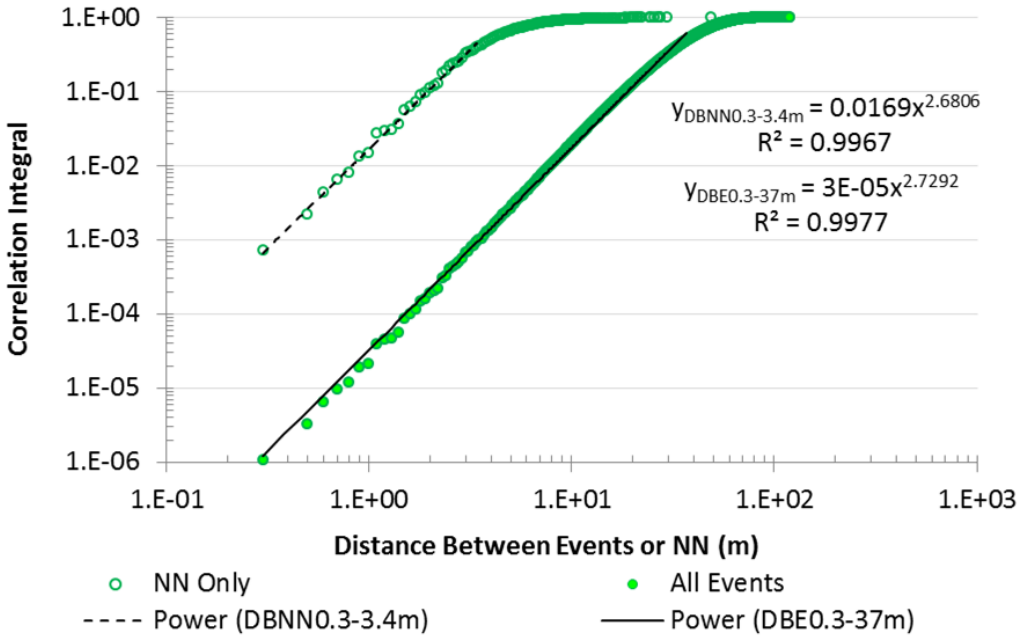

Figure 79: Fractal dimensions that describe the distance between nearest neighbours and between seismic events in a pillar

In Figure 79 the fractal dimension is calculated in two ways to describe the pillar seismic events. The fractal dimension of the nearest neighbours is shown at the top and is compared to the fractal dimension of the distance between each event and every other event (1,635,336 pairs) which describes the whole population. The fractal dimension is also 2.7 with the population being strongly correlated between 0.3 to 37 metres (noted as $D_{0.3-37m}^{1368DBE} = 2.7$). The fractal dimension of nearest neighbour distances compared to the fractal dimension of the distances between all events is found to be the same (2.7 metres) inside the failing pillar. The only difference is that the range of distances between all events is higher (0.3 to 37 metres compared to 0.3-3.4 metres) (Figure 79). If the distance between all events is used, it is important to understand that an assumption has been made that all the events are from the same seismic source. This may or may not not be true. In the case of this failing pillar, the assumption is valid, and the extent of pillar failure (37 metres) is useful information.

Since both the nearest neighbour fractal dimension and that of the whole population are the same, it suggests that the rock failure for the seismic events in the pillar is predominantly from one seismic source within the respective ranges. It does not however mean the same assumption will be valid in every failing pillar scenario. Therefore the fractal dimension of the nearest neighbour distances is best used to characterize rock mass failure.

Since the fractal dimension provides a range of distances between seismic events that are strongly correlated, nearest neighbour distances can also be used to cluster the events. To get a better understanding of the range of nearest neighbour distances that are fractal, a probability density curve is used (Figure 80).

4.3.2 Fractal Dimension Characteristic

Superimposing the fractal dimension of nearest neighbours distances over its probability curve (Figure 80) shows that the mode distance of 2.7 metres is within the fractal range while the mean distance of 4.0 metres is not fractal.

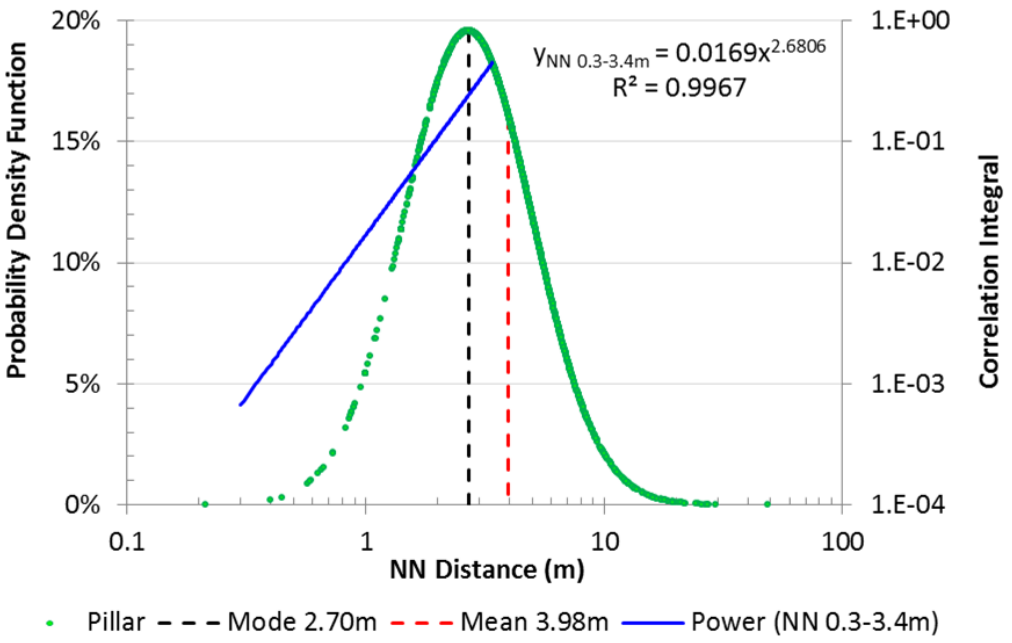

Figure 80: Probability density function and fractal dimension of the nearest neighbour distances for 1368 seismic events inside a failing pillar

Since the fractal dimensions of the nearest neighbour distances and the inter-event distances are the same, it suggests that only one failure mechanism is present inside the pillar. The events that have the very shortest nearest neighbour distances are indicative of locations with the highest amount of rock mass failure. The fractal dimension and the distances between nearest neighbours will be used to characterize the seismic source inside a failing pillar. The significance of this will become apparent when the case studies are compared.

The data were clustered at both the mode and mean nearest neighbour distances (2.7 metres and 4.0 metres respectively). When 2.7 metres was used, the cluster sizes were small (eleven events or less) and the number of single isolated events is 57% of the whole population. When 4.0 metres was used the clusters were larger (247 events or less) which results in fewer single isolated events (336 SE - 25% of the whole population). The cluster summary charts are shown in Table 13.

Table 13: Cluster sizes, quantities and residual single events resulting from clustering seismic events inside a failing pillar using the mode and mean nearest neighbour distances

Clustered at NN Distance of 2.7 metres (Mode)												
Size (# of E)	1	2	3	4	5	6	7	8	9	10	11	Total
Quantity	778	135	48	12	6	6	3	-	1	1	2	992
#E	778	270	144	48	30	36	21	-	9	10	22	1368

Clustered at NN Distance of 4.0 metres (Mean)																						
Size (# of E)	1	2	3	4	5	6	7	8	9	10	11	13	14	16	17	20	23	25	31	33	62	247	Total
Quantity	336	71	39	12	12	10	7	2	2	1	1	1	1	1	1	1	1	1	1	1	1	1	504
#E	336	142	117	48	60	60	49	16	18	10	11	13	14	16	17	20	23	25	31	33	62	247	1368

It was noticed that both the mean and mode clustering distances resulted in multiple clusters of approximately the same size for cluster sizes of two to eleven events and unique cluster sizes above eleven events. A plot of the cluster sizes and quantity in which they occur is shown in Figure 81. A linear relation exists between the smaller size clusters (less than 11 events) and single isolated events for both clustering distances. The slope of the line decreases in Image B as the number of smaller sized clusters and single isolated events decreases. As previously described in Figure 30 (Images A to Z), the smaller clusters and single isolated events join to form larger clusters. Image B is a graphical representation of the clustering results.

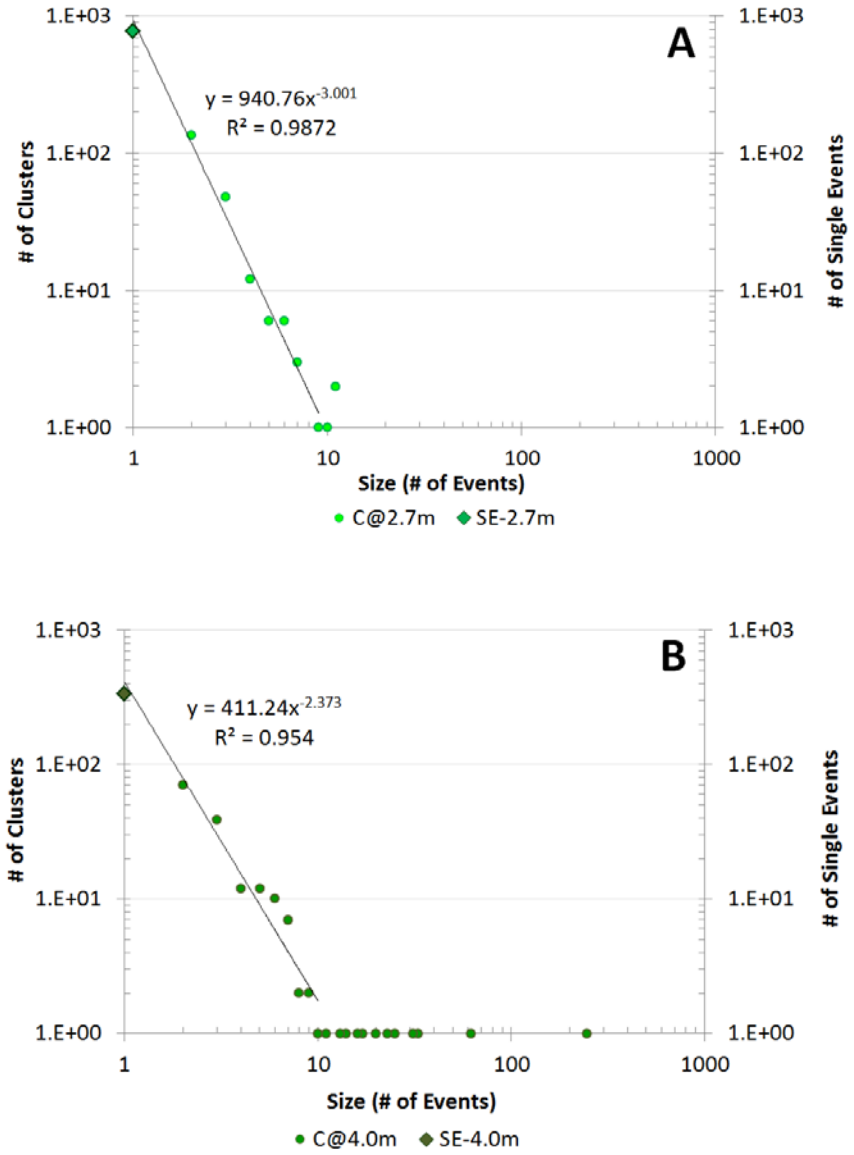

Figure 81: Cluster size and quantity results when the mode (2.7 metres - Image A) and mean (4.0 metres - Image B) nearest neighbour clustering distances are used for seismic events in a failing pillar

The size of clusters (number of events) created using the mode nearest neighbour distance of 2.7m is relatively small with the largest cluster containing only eleven events. Clusters this small are useful for identifying the areas that have seismic events that are closest together. Figure 82 shows the four largest clusters (two eleven event clusters, one ten event cluster, and one nine event cluster) all of which are located close to each other.

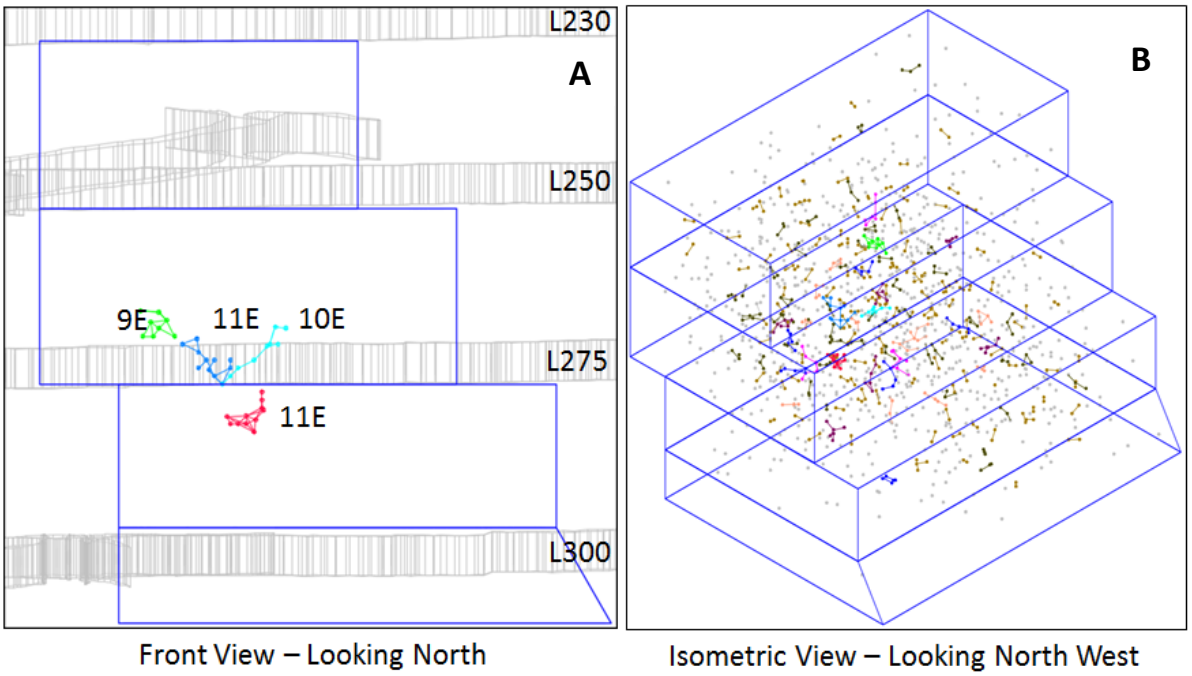

Figure 82: Image A - The four largest clusters created after the seismic events in the pillar clustered using the mode nearest neighbour distance of 2.7 metres. Image B - This isometric view shows all the clusters and single events as well as the four largest clusters.

The clusters created using the mean distance of 4.0 metres give more information about the areas within the pillar that are most active. A unique characteristic of the failing pillar is the occurrence of 45 events that were recorded simultaneously with at least one other event (Figure 83).

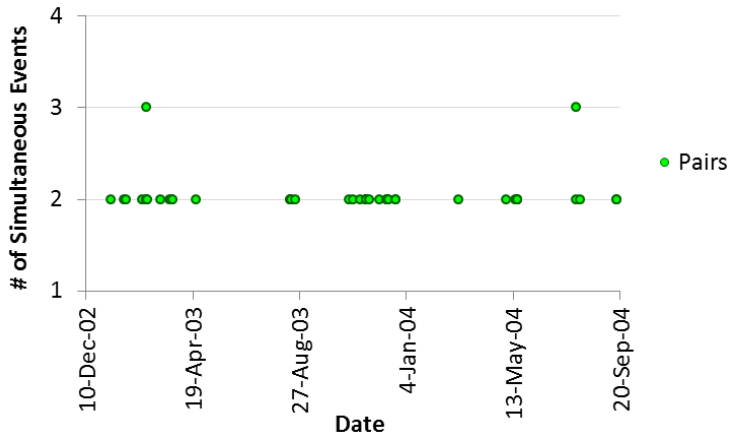

Figure 83: Simultaneous event occurrences.

This is a unique characteristic of the pillar failure, as the other cases have one or two occurrences,

but none with the regularity shown in the pillar. It is possible that the sensitivity of the seismic system of the pillar case is different from the other case studies. Since it cannot be known for sure, these events will be considered simultaneous.

4.3.3 Fractal Dimension of Time Between Nearest Neighbour Events – Pillar

The time between nearest neighbour events in the pillar is shown in Figure 84.

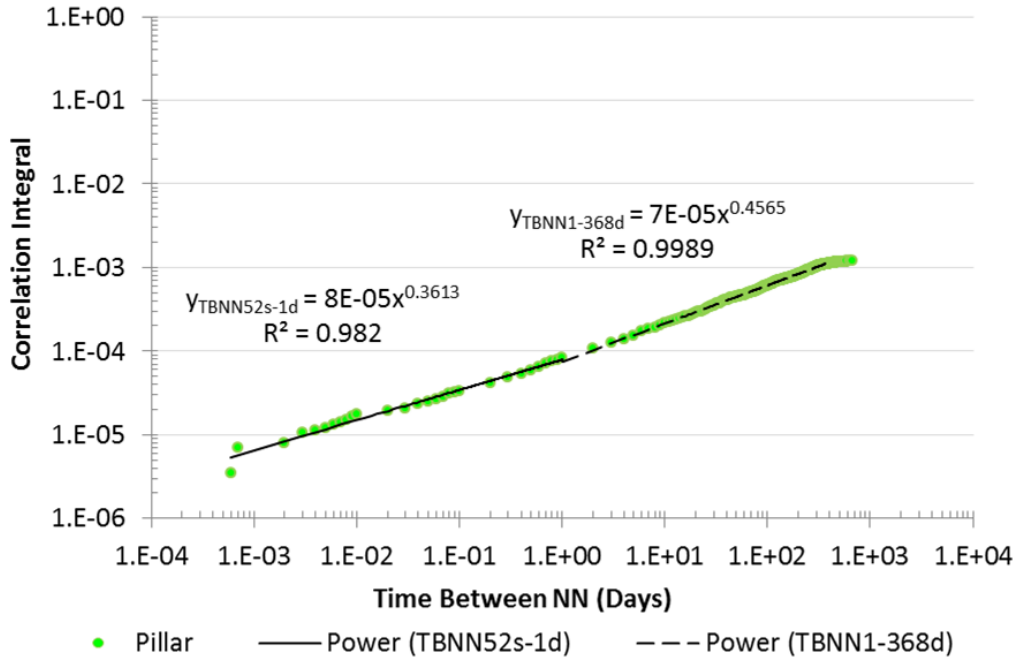

Figure 84: Time between nearest neighbour events in a failing pillar

In this case, the nearest neighbour events have two fractal periods - slightly less than one minute to a day ($D^{Pillar}_{TBNN\ 52s-1d} = 0.36$) and then a day to just over a year ($D^{Pillar}_{TBNN\ 1-368d} = 0.46$). The unique part that characterizes the pillar failure is the fractal dimension increases after one day. The fractal dimension is the opposite (decreases over time) in the other case study seismic sources. Since the fractal dimension increases after one day, it means that the longer nearest neighbour time is more highly correlated than the shorter time period. This information is useful when trying to understand the time frame in which the seismic source will be most active and may be an indicator

of the role of short term stress changes after a blast or a large magnitude event occurrence.

4.3.4 Fractal Dimension of Event Intensity in a Failing Pillar

Since nearest neighbour events occur in a very similar location, the fractal dimension of each magnitude range was determined to characterize the seismic source. It can be seen in Figure 85 that the fractal dimension ranges from 2.26 to 2.49 for nearest neighbour events that are between magnitudes 2 to -1, suggesting a similar source for these events. Appendix X contains complete detail for each magnitude range in Figure 85.

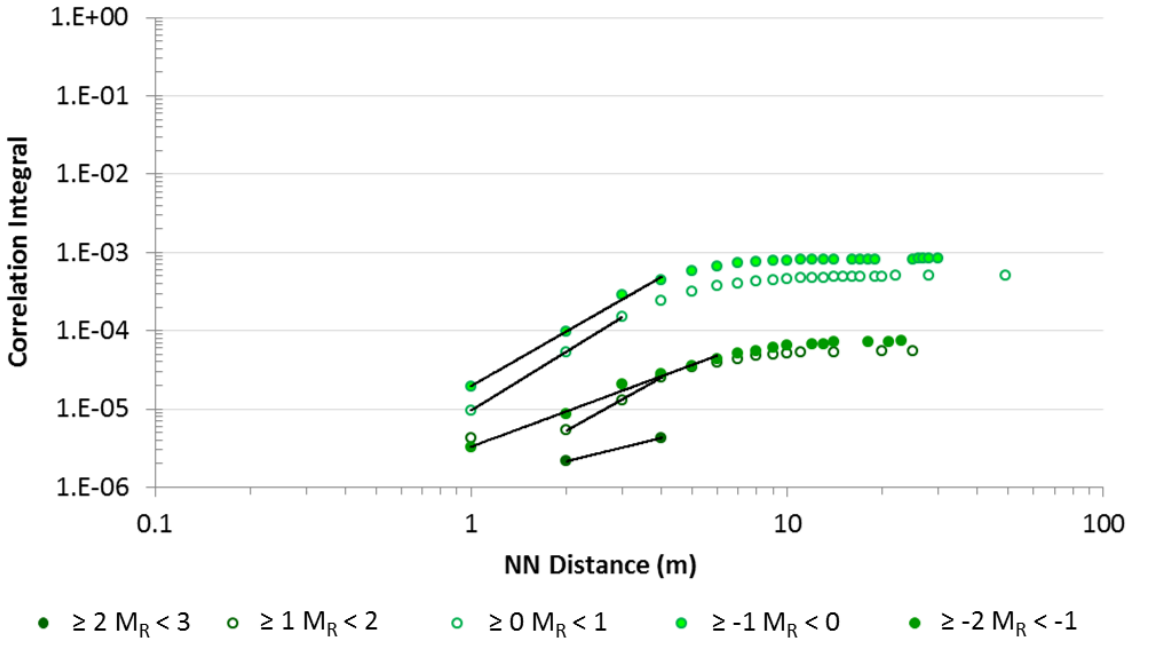

Mag R Range	FD	R^2	NN Distance (m) Range		Max
>2	1.00	100.0%	2	4	4
1 to 2	2.26	99.9%	2	4	25
0 to 1	2.49	100.0%	1	3	49
-1 to 0	2.31	99.4%	1	4	30
-2 to -1	1.49	99.0%	1	6	23

Figure 85: Fractal dimension of the intensity (magnitude) of nearest neighbour events inside a failing pillar

The events below magnitude -1 and above 2 have lower fractal dimensions, meaning they are less

well correlated. What is interesting to note is that each fractal range has a corresponding nearest neighbour distance range and a maximum distance. The range of distances in the fractal range for each magnitude is very small – 1 to 6 metres. However the maximum distance for each range is greater than 20 for all ranges except for the largest magnitude range of 2. In this case ($M_R \geq 2$), the maximum nearest neighbour distance is within four metres and in the fractal distance range of 2 to 4 metres. The next largest events (magnitudes 1-2) have a much larger maximum nearest neighbour distance of up to 25 metres. This provides good information on how far large seismic events could occur from existing seismic events within the pillar.

The fractal dimension of the time between nearest neighbours is more complicated (Figure 86). While the fractal dimensions are very close to one another (0.25 to 0.53), the range of time frames by magnitude range is very different. The smaller magnitude events are fractal from milliseconds to a day, whereas the larger events (above magnitude 0) are fractal from seconds to hundreds of days. For individual graphs for all magnitude ranges see Appendix XI.

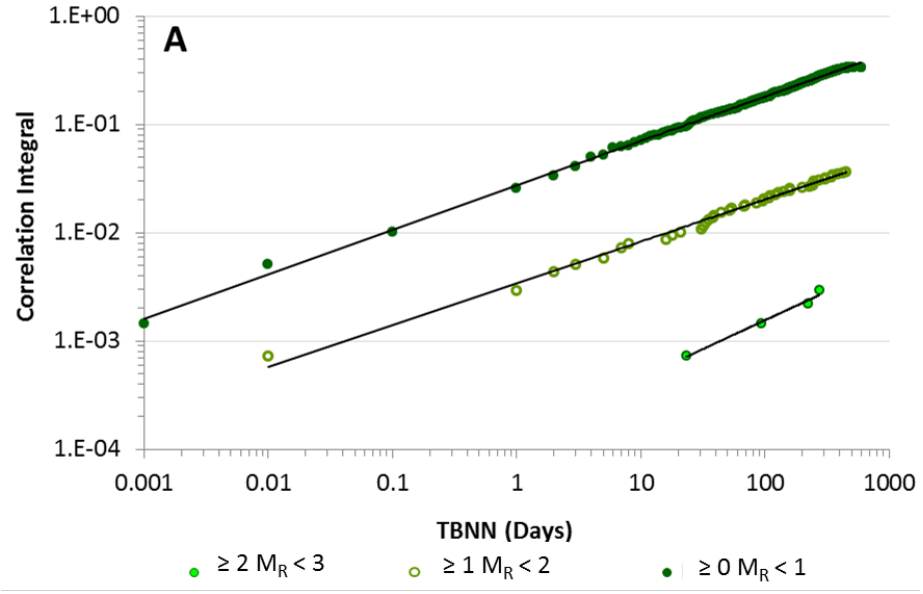

Figure 86: Image A - The fractal dimension of time between nearest neighbours within magnitude range M_R=0 to M_R>2inside a failing pillar

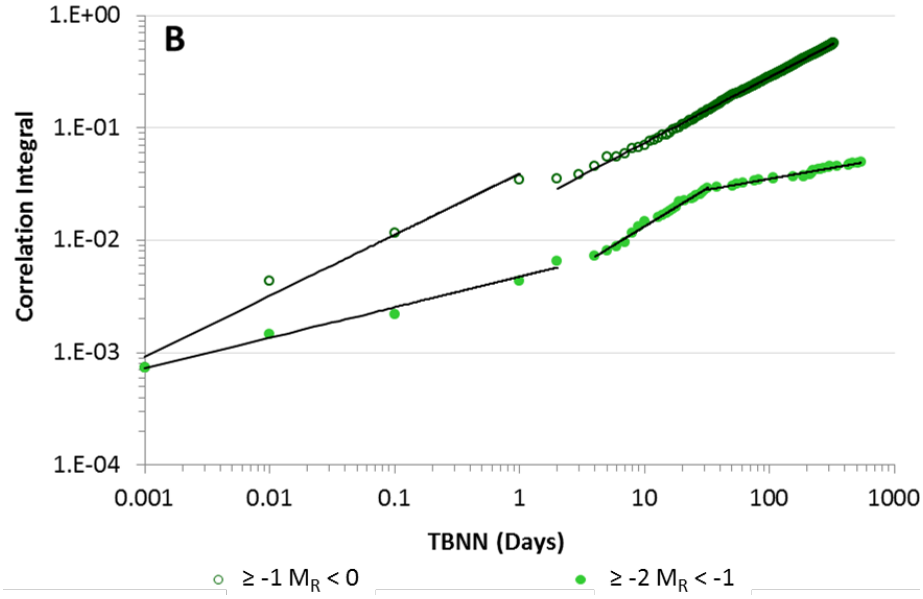

Mag R Range	FD	R^2	TBNN Range	TBNN Max
>2	0.53	98.5%	23-276d	276
1 to 2	0.39	99.3%	14min-451d	451
0 to 1	0.41	99.8%	1.4min-594d	594
-1 to 0	0.54	97.9%	1.4min-327d	327
	0.58	99.9%	2-327d	
-2 to -1	0.25	99.0%	1.4min-2d	539
	0.68	99.0%	4-32d	
	0.19	97.2%	32-539d	

Figure 86: Image B - The fractal dimensions of the nearest neighbour events within a failing pillar with M_R >0

Of particular note in this example is the time frame of the largest magnitude events (M_R>2). These events are showing that they occur between 23 and 276 days after their nearest neighbour event (that is, they are poorly correlated to the smaller magnitude events). Therefore, while it may seem that large events such as these come out of nowhere, this method shows that this time frame is normal for the rock mass failing inside this pillar. The preservation of the sequence of the seismic events and how they relate to the event closest to them allows actual time frames to be seen.

4.3.5 Determination of Static or Directional Moving Seismicity

The same method applied to the ramp development seismic event locations (previously shown in Figure 52 and used for comparison in Figure 87-Image A) were applied to the failing pillar data. In this case the direction of the seismic events did not take on any one direction over time but rather changed directions repeatedly as different parts of the pillar failed over time. This pillar provides a good example and benchmark for a static seismic source (Figure 87-Image B).

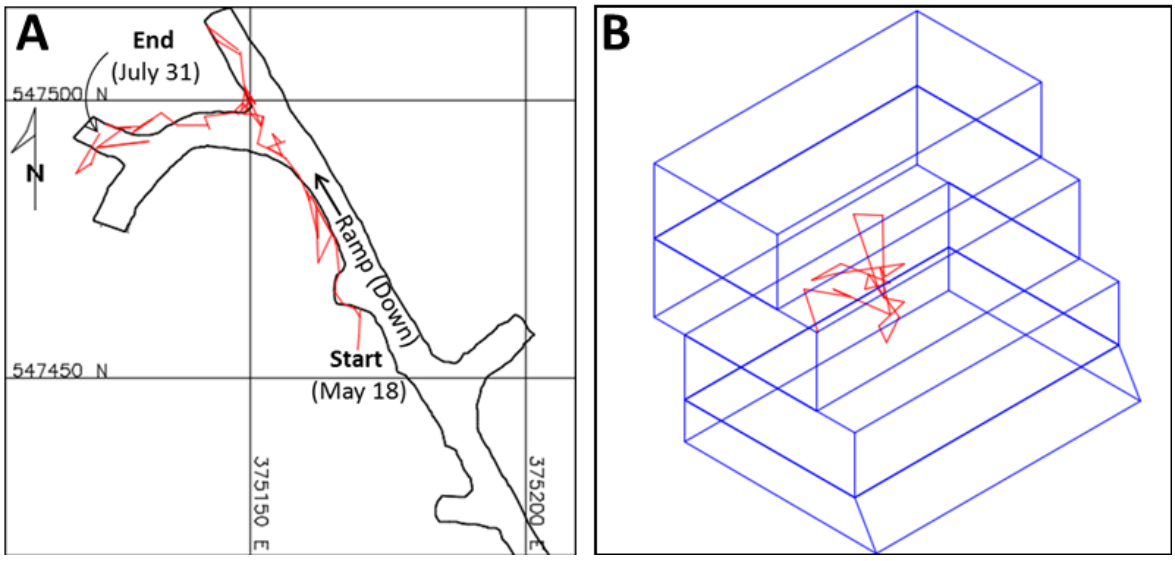

Figure 87: Comparison of moving and static seismicity

The line within the pillar was created using the average of all the coordinates each month for

approximately two years in this example. The number of days being averaged can change depending on the desired level of detail. In the case of the pillar, a plot of the line on a daily basis, for example, would not change the fact that the seismicity within the pillar is static.

4.3.6 Summary of Case 3 – Pillar

The 1368 seismic events inside a failing pillar have a mode nearest neighbour distance of 2.7 metres and mean distance of 4.0 metres. Both distances were used to cluster the events. When the mode distance was used the largest cluster size was only eleven events or less. Analysis of the clusters created using the mode distance showed that the clusters were relatively evenly dispersed throughout the pillar (Appendix II).

Additionally, the seismic events were used to characterize the failing pillar by calculating the fractal dimension and its relevant ranges for the distance between nearest neighbours ($DBNN^{Pillar}_{0.3-3.4m} = 2.7$), and the time between nearest neighbour events ($TBNN^{Pillar}_{52s-1d} = 0.36$, $TBNN^{Pillar}_{1-368d} = 0.46$). The pillar also contained 45 events that occur at the same time as at least one other event and in a few cases more than one event. The events did not occur all at once but spread out over two years. This is a unique characteristic of the pillar failure.

The fractal dimension of the different magnitude ranges was also determined for the nearest neighbour distances and time between them. Nearest neighbour events between one and four metres have a fractal dimension of between 2.26 and 2.49 between magnitudes -1 to 2. The largest magnitude events (>2) have a lower fractal dimension of 1 between 2 and 4 metres and the lowest magnitude events (<-1) also have a low fractal dimension of 1.36 between 1 and 6 metres. One significant difference is that all the events with magnitude below 2 have a non-fractal range as

well. The non-fractal range varies from twenty to fifty metres for the various magnitude ranges except for the largest, which does not have a non-fractal range. This is significant because it means the largest events are only occurring very close (within 4 metres) of a previous event. The next largest events (M_R=1 to M_R=2) occur further away at a maximum of 23 metres. Using this technique as a pillar fails can give mine personnel important information about where the largest events typically occur, which could be extrapolated to estimate future large magnitude events.

The fractal dimension of time between nearest neighbours by magnitude range was also determined. Each magnitude range has a fractal dimension of 0.25 to 0.5. What differs between the ranges is the lower magnitude events (< 0) are fractal over very short periods of time (seconds to a day); and events with magnitude greater than zero but less than two, are fractal from seconds to hundreds of days. The largest events (greater than 2) only occur 23 days after their nearest neighbour and up to two years. This means that these events do not occur immediately after a seismic source is active but rather occur only after three weeks and up to two years. The results are summarized in Table 14.

Table 14: Summary of Pillar Seismic Characteristics

Seismic Source	NN Distance		Fractal Dimensions			
			NN		Time Between NN	
	Mode (m)	Mean (m)	D_{NN}	Range (m)	D_{TBNN}	Range
Pillar	2.7	4.0	2.68	0.3-3.4	0.36	52s to 1 day
					0.46	1-368 days

Seismic Source	Fractal Dimension (DBNN)					
	Distance between Nearest Neighbours (m) by Magnitude Range					
	≥2	≥1 and <2	≥0 and <1	≥-1 and <0	≥-2 and <-1	≥-3 and <-2
Pillar	1.00 (2- 4m)	2.26 (2- 4m)	2.49 (1-3m)	2.31 (1-4m)	1.49 (1-6m)	-

Seismic Source	Fractal Dimension (TBNN)				
	Time between Nearest Neighbours by Magnitude Range				
	≥2	≥1 and <2	≥0 and <1	≥-1 and <0	≥-2 and <-1
Pillar	0.53 (23-276days)	0.39 (14 min-1.2y)	0.41 (1min-1.6y)	0.54 (1.4min-327days)	0.25 (1.4min-2days)
				0.58 (2-327days)	0.68 (4-32 days)
					0.19 (32-1.5y)

These results will be compared at the end of this chapter to the other seismic sources.

4.4 Case 4 – Shear

Case 4 will examine the 4548 seismic events associated with a shear. It is a major, mine-wide structure that is situated approximately 150 metres from the footwall/orebody contact and runs parallel to the orebody. The orebody and shear strike 30° from magnetic north and dip approximately 72° to the east. The shear is visible in drifts at a few locations in the mine. Where exposed, the thickness of the shear is only a few millimetres to several centimetres wide (Reimnitz, 2004). Over a period of three years, and four and a half months, 4548 seismic events occurred in the shear and are shown in Figure 88.

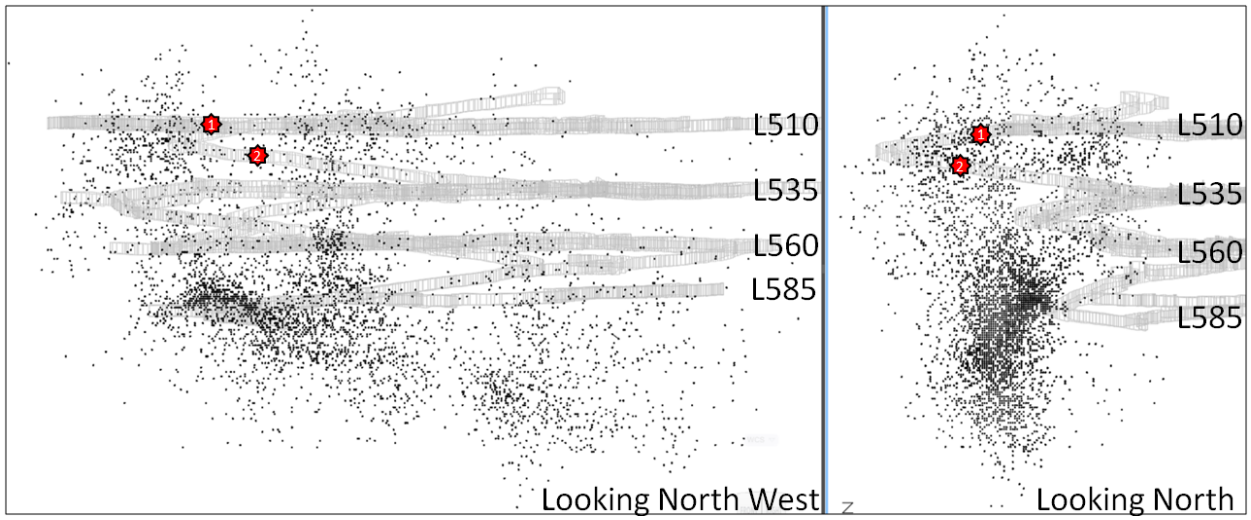

Figure 88: The shear was seismically active over a period of three years and four and a half months. The red stars (#1and #2) indicate two locations between the 510 and 535 Levels where the shear is visible in the ramp walls.

The events seen in Figure 88 will be correlated using the fractal dimension and probability density function methods to determine the clusters within the shear (Figure 89).

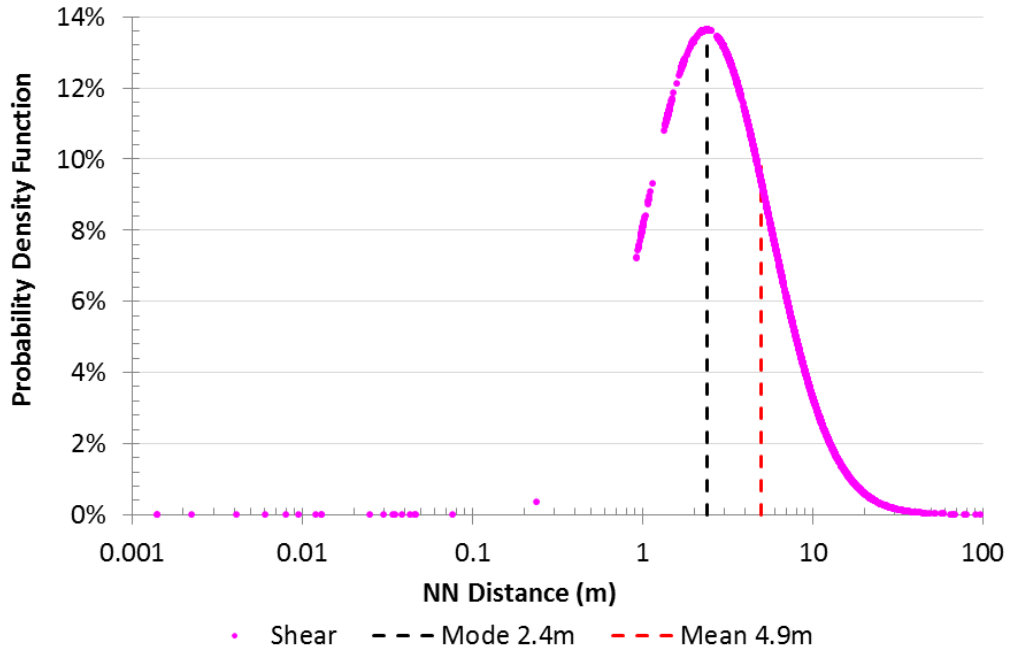

Figure 89: The distribution of nearest neighbour distances of seismic events in the shear

The mode nearest neighbour distance in the shear is 2.4 metres and the mean 4.9 metres. In this case there are a large number of nearest neighbour pairs that are very close together (centimetres to

less than a metre) which is unique for this seismic source.

4.4.1 Fractal Dimension of Nearest Neighbour Distances - Shear

The shear seismic events are fairly evenly distributed except on the western end of the 585 Level where the events are located closer together. This difference in seismic density within the shear can be described by the fractal dimension of the nearest neighbour distances. For example, events that have an inter event distance over 7.6 metres between 0.3 and 7.9 metres have a fractal dimension of 2.6 ($DBE_{0.3-7.9m}^{Shear}$ =2.6). The events between 7.9 and 33.7 metres are further apart and range over a larger distance (25.8 metres). In this case the fractal dimension drops to 2.1 ($DBE_{7.9-33.7m}^{Shear} = 2.1$). The events furthest apart (33.7 to 140 metres) have the lowest fractal dimension of 1.5 ($DBE_{33.7-140m}^{Shear}$ = 1.5) (Figure 90). The fractal dimension of the nearest neighbour distances (hollow magenta circles in Figure 90) is notably lower ($D_{NN\ 0.3\text{-}4.6m} = 1.9$) than the fractal dimension of the inter event distance over the same distance ($DBE_{0.3\text{-}7.9m} = 2.6$). This is unique to the shear and reflects the two very different densities of seismic events in different parts of the shear.

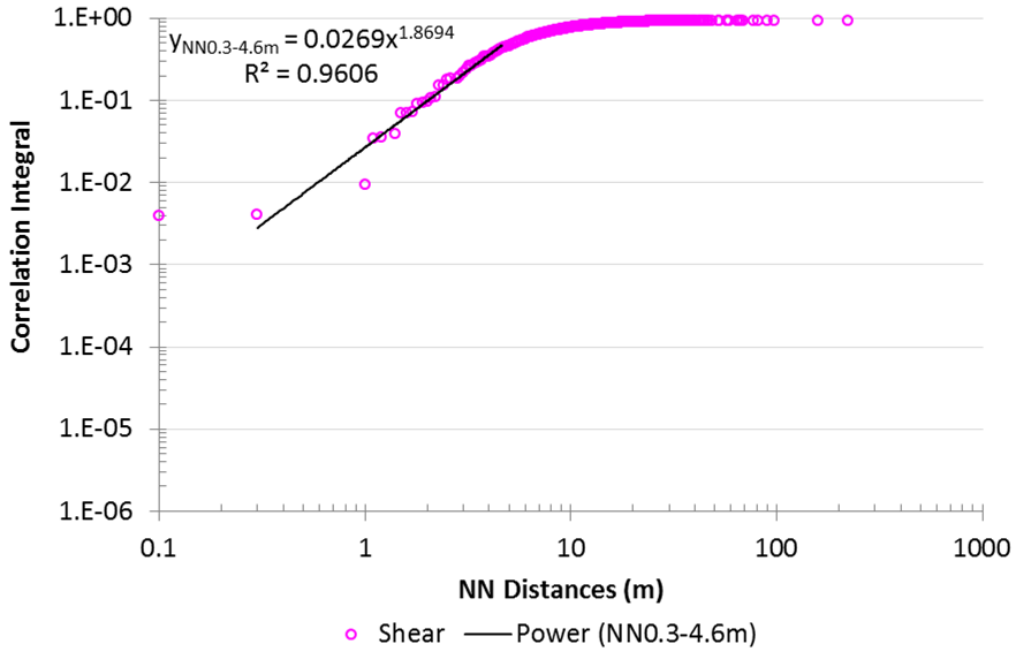

Figure 90: Fractal dimensions of the nearest neighbour distances for 4548 seismic events in a shear

These distances are important to consider when determining a clustering distance along with the mode and mean distances of the whole population.

4.4.2 Nearest Neighbour Distance and Resulting Clusters - Shear

The fact that the seismic events are closer together in one part of the shear influences which nearest neighbour distance to use (mode or mean) to cluster the events. In this case the nearest neighbour distance that has the highest probability of occurring is 2.4 metres. It will be used as the cluster distance so that the events that are closest together will not be buried within a larger cluster. Figure 91 shows the probability density function for the nearest neighbour events in the shear as well as the nearest neighbour fractal dimension range of distances between 0.3 and 4.6 metres.

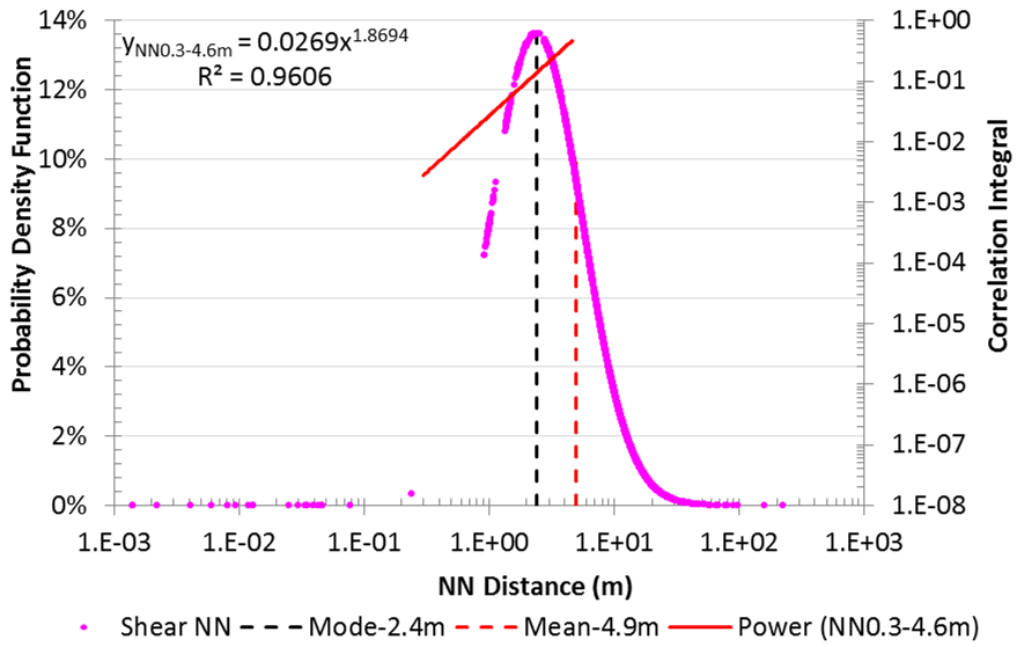

Figure 91: Probability density function and fractal dimension of the nearest neighbour seismic events in a shear

In the other case studies of seismic sources (failing pillar, development and abutment) clustering with the mode distance resulted in many small size clusters. The shear clustered differently using the mode distance which resulted in a wide range of cluster sizes. Single clusters of 292, 40, 25, 15, 13, and 11 to 1 events were created. Most importantly, the locations of all the clusters with more than 8 events were to the East of the 585 Level. A summary of the quantity, size of clusters and residual single events is shown in Table 15. The locations of the clusters are shown in Figure 92. Of the twelve largest clusters forms, ten are located close to the 585 level, another close to the 585 level but further north than the group of ten clusters, and one cluster located just above the ramp where the shear is visible.

Table 15: Quantity, size of clusters and number of residual single events when 4548 events in a shear were clustered using the mode NN distance (2.4 metres).

Clustered at NN Distance of 2.4 metres																	
Size (# of E)	1	2	3	4	5	6	7	8	9	10	11	13	15	25	40	292	Total
Quantity	3344	240	38	23	7	6	1	2	2	1	1	1	1	1	1	1	3670
#E	3344	480	114	92	35	36	7	16	18	10	11	13	15	25	40	292	4548

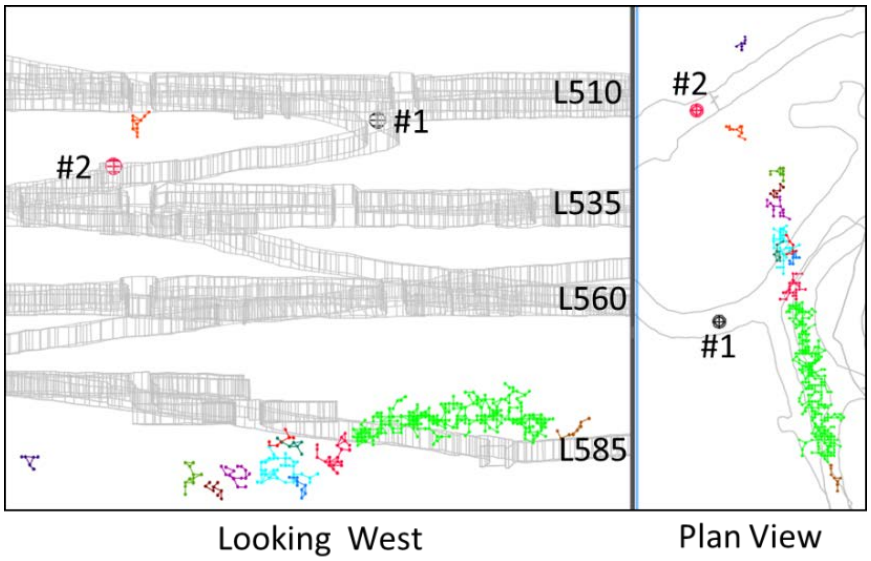

Figure 92: Location of clusters in a shear created using the NN distance of 2.4 metres

In this case, clustering with the most probable nearest neighbour distance of 2.4 metres shows a band of densely located seismic events that is associated with the lower fractal dimension of 1.9 previously shown in Figure 90 ($D^{Shear}_{NN\ 0.3-4.6m} = 1.9$).

4.4.3 Fractal Dimension of the Time Between Nearest Neighbours - Shear

The nearest neighbours in the shear are fractal between two frames – seconds to one day and then one to sixty days (Figure 93). Events that occur more than sixty days after their nearest neighbour are not fractal.

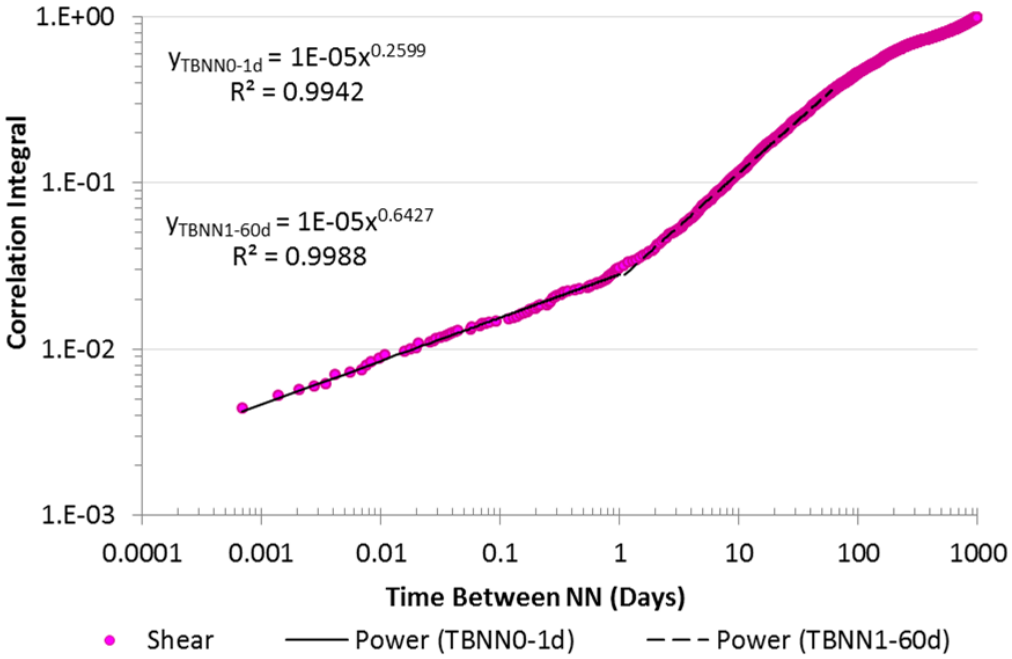

Figure 93: The fractal dimensions of time between nearest neighbour events in a shear

The two time frames that are fractal may be a reflection of the different density of seismic events. What is clear is that like the pillar events, shear events may also occur well after its nearest neighbour. These longer time frames help understand why events that occur a long time after they are expected are likely a normal response for this particular seismic source.

The shear seismic data also contains three events that occur simultaneously with one other event. Unlike the pillar, these events occur only on three separate days and not evenly throughout the shear seismic activity. Instead, these instances occur in specific locations identified as seismic areas in the clustering process. In the first case E63 and E64 occur four minutes after E62 which is 19.7 metres away. A minute later another pair of simultaneous events occurs (E65 and E66) on opposite sides of the shear (where it is visible in the ramp between the 510 and 535 levels) (Figure 94). One last event E67 ends the sequence of events in this area.

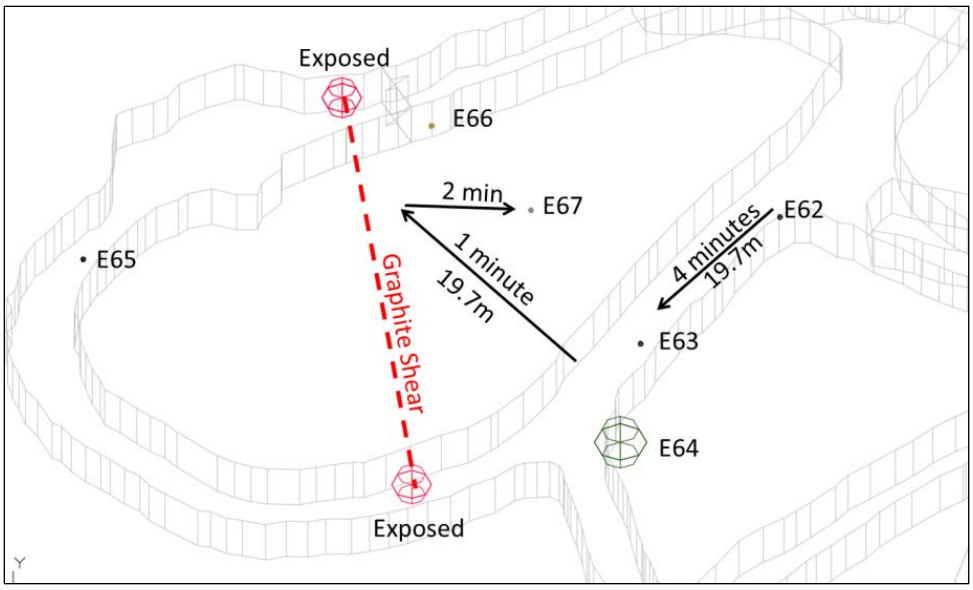

Figure 94: Two pairs of events occurring simultaneously adjacent to the shear

The other simultaneously occurring pair is events 410 and 411 which occur in another group of clusters near the 585 level. These two areas are the only occurrences of simultaneous events and the events in the shear are close together as well as being simultaneous. The pillar events did not occur in the same locations.

4.4.4 Fractal Dimension of Event Intensity - Shear

The intensity of nearest neighbour events gives additional insight into the seismic source or sources present in the shear. For example, the fractal dimension and corresponding nearest neighbour range varies widely in the shear (Figure 95 – details in Appendix XII). The lowest fractal dimension of 0.89 is associated with the largest events of magnitude greater than 2 within a range between 2 and 16 metres ($D^{Shear}_{DBNN\ M_R \geq 2} = 0.89_{2-16m}$). The maximum distance that an event of this magnitude could occur is 35 metres. However, since the fractal range is 2 to 16 metres, large events that occur between 16 and 35 metres are not fractal and are less likely to occur. The other three magnitude ranges have fractal dimension from 1.38 to 1.97 and have nearest neighbour

fractal ranges of approximately 2 to 8 metres. Their non-fractal regions vary from 35 metres to 222 metres for the smallest magnitude events, which is a much larger non-fractal region than the $M_R \geq 2$ non-fractal region (16-35 metres).

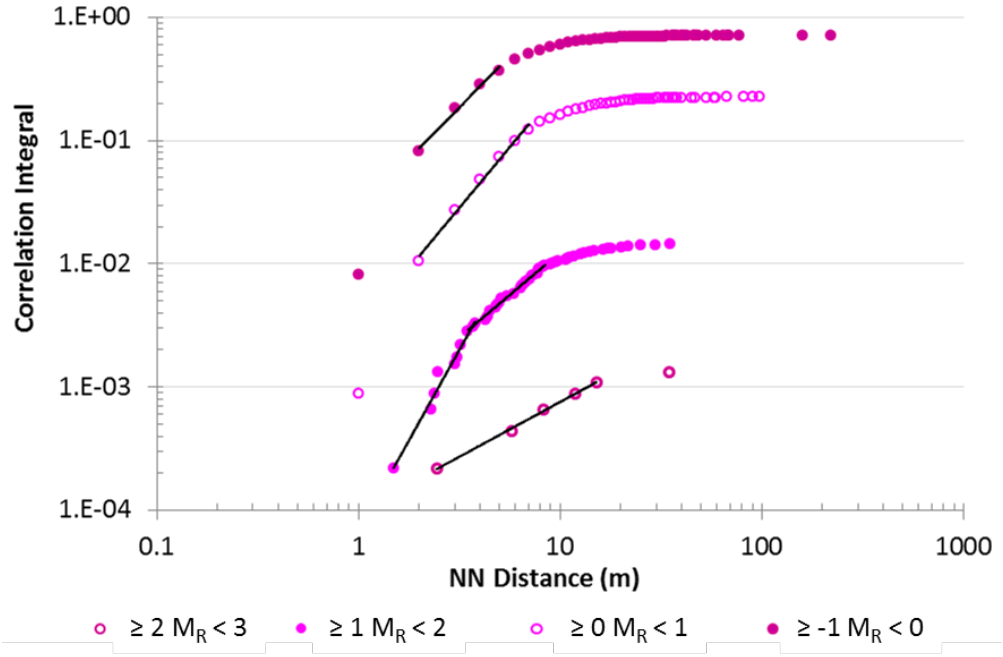

Magnitude Range	FD	R^2	NN (m) Range		NN (m) Max
>2	0.89	99.7%	2	16	35
1 to 2	2.94	97.9%	1	4	35
	1.38	99.3%	4	9	
0 to 1	1.97	99.3%	2	7	98
-1 to 0	1.67	98.8%	2	5	222

Figure 95: Fractal dimension of nearest neighbour distance by seismic event magnitude range inside a shear

The other large magnitude events (≥ 1 $M_R<2$) have a very high probability of occurring with the highest fractal dimension of 2.94 and is in very close proximity to the nearest neighbours (1-4 metres) ($D^{Shear}_{\geq 1 \; and \; M_R<2} = 2.94_{1-4m}$). This range has a second fractal dimension of 1.38 for nearest neighbours within 4 to 9 metres of each other. The shorter distance has a higher probability of occurring but it would not be unreasonable to expect this magnitude range within 9 metres of another event.

4.4.5 Fractal Dimension of Event Intensity and Time Between NN - Shear

The time between nearest neighbours for each magnitude range are fractal for almost all time periods (Figure 96). Details for each magnitude range are included in Appendix XIII. Within each magnitude range there are three fractal dimensions with the fractal dimension increasing and then decreasing. It is also interesting to note that the fractal regions for each magnitude range are very similar and exhibit the same character.

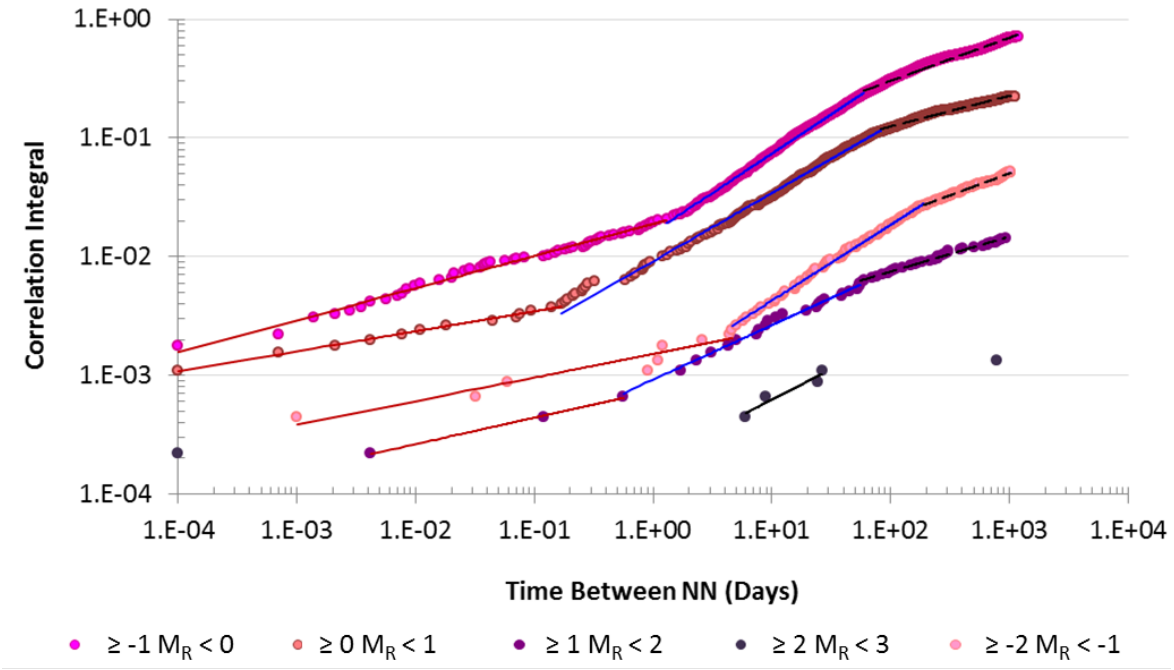

Magnitude Range	FD	R^2	TBNN Range
>2	0.51	91.7%	6-26 d
1 to 2	0.22	99.6%	6min-13.4h
	0.46	99.0%	13.4hr-55d
	0.30	98.9%	55d-2.6y
0 to 1	0.17	99.3%	8.6s-4.1h
	0.57	99.5%	4.1h-82d
	0.26	98.2%	82d-3y
-1 to 0	0.27	99.0%	8.6s-1.3d
	0.66	99.8%	1.3-59d
	0.36	98.9%	59d-3.1y
-2 to -1	0.20	92.4%	8.6min-4.6d
	0.64	99.8%	4.6-189d
	0.37	99.3%	189d-2.8y

Figure 96: Magnitude ranges for time between nearest neighbours in a shear

Each magnitude region has three time periods that are fractal with the exception of nearest neighbours with magnitude greater than 2. The other ranges show a short period of low fractal dimension (seconds to just over a day), a longer period of a day up to a couple of months and the longest period of months to years. The middle period of a day up to a few months has the highest fractal dimension for each magnitude range (≥ 1 M_R <2 $=0.46$, ≥ 0 M_R <1 $=0.57$, ≥ -1 M_R <0 $=0.66$, ≥ -2 M_R < -1 $=0.64$). The shear is a very large structure – it is possible and likely that the shear

contains more than one seismic source that may behave differently within different areas of the shear. This is based on the various widths of the shear that are exposed on different levels.

To help determine if different seismic sources are present, a frequency magnitude plot for the events in each time period was created. The b-values for each period and the entire population were then compared (Figure 97).

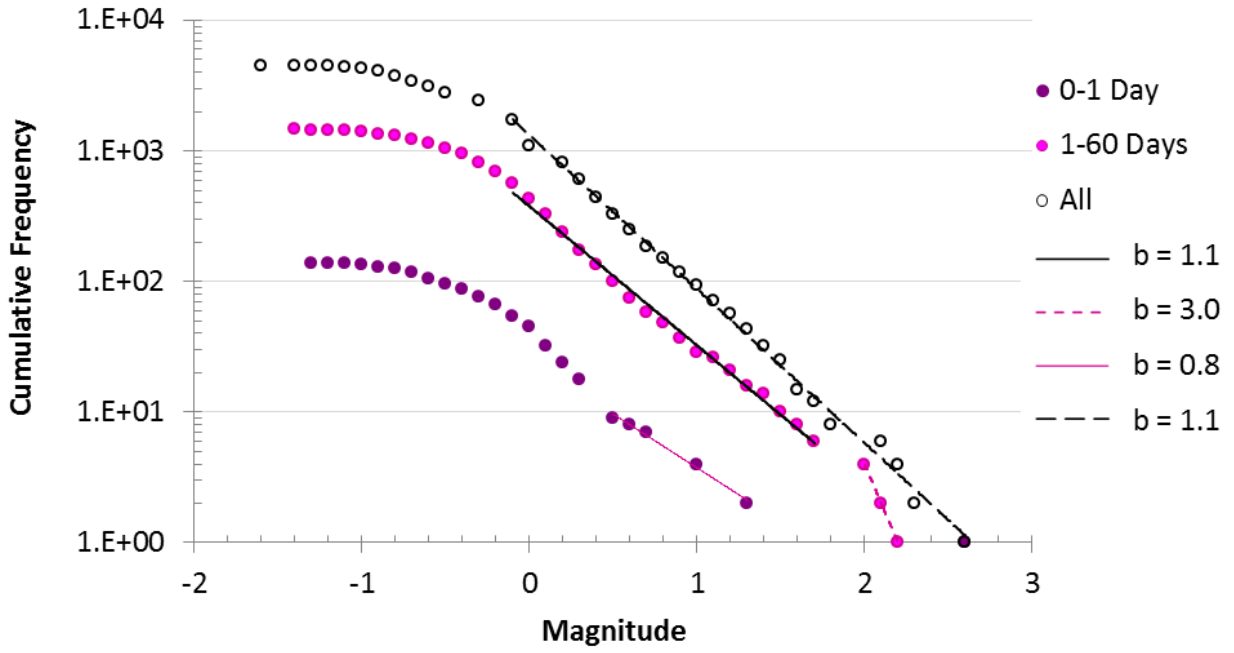

Figure 97: Comparison of frequency magnitude b-values for 4550 shear events

The events that occur with a day of their nearest neighbour have the lowest b-value of 0.8 and the highest magnitude event of 2.6. The events that occur within 1 to 60 days have a dominant b-value of 1.1 between magnitude zero and 1.8. The events above magnitude 2 during this time period have a very large b-value of 3; however there are very few events in this range. Since each of these time periods has very different b-values from the other it suggests that there are two seismic sources in the shear. Interestingly when the b-value of the whole population is determined, it is also 1.1 but ranges over two and a half magnitudes (0 to 2.6). The largest event is 2.6. This novel

method of using the frequency magnitude graph may prove to be useful to help separate seismic sources in a seismic data set.

This example also provides the opportunity to comment on previous work by Aki (1981) which states that the fractal dimension of distance between events is twice the b-value. While the theoretical calculation provided in Aki (1981) is not being disputed, it is suggested however that it may be more of a general description than a mathematical rule. In this case study, the fractal dimension of the distance between events is 2.63 for events within 0.3 to 7.9 metres of each other and 2.14 for events 7.9 to 33.7 metres of each other. If the distance between nearest neighbours is considered, the fractal dimension is 1.87 for events that are within 0.3 to 4.6 metres of their nearest neighbour. Given the new application of these methods, the approximation of fractal dimension and b-value can be further verified for different seismic sources in future work.

4.4.6 Summary Case 4 - Shear

While the shear was first thought to contain one seismic source, the sequential spatial clustering and fractal methods suggest that two are present. Since the nearest neighbour distance range was a lot smaller than the distance between all events, the mode distance of 2.4 metres was chosen to cluster the data so that the small clusters would not be lost inside a larger one. The results from clustering at this distance showed that ten of the twelve largest clusters are located near the 585 Level. One cluster is at a similar elevation to the ten clusters but is further to the North. One cluster remains just above the ramp between levels 510 and 535 – the location where the shear is visible in the ramp. These clusters show the areas with the highest amount of seismic activity. The shear also contains three occurrences of events that happen simultaneously. However these event pairs occur in areas identified as seismically active are isolated examples that only occur on a

couple of very specific dates whereas the pillar simultaneous events occur more frequently and not always in the same locations.

The calculation of the fractal dimensions and their ranges for the distance between nearest neighbours is ($D_{NN\ 0.3\text{-}4.6m} = 1.9$), and time between nearest neighbours ($TBNN_{1-60d}^{Shear} = 0.64$, and $TBNN_{0-1d}^{Shear} = 0.26$). These examples indicate two seismic sources may be present in the shear event population.

The fractal dimension for each magnitude range for nearest neighbour events also suggested more than one seismic source. The largest magnitude events (M_R>2) have a fractal dimension of 0.89 over the largest range of nearest neighbour distances (2 to 16 metres). The next largest magnitude ranges have similar fractal dimensions (1.38 to 1.97) with a shorter nearest neighbour distance range of approximately 2 to 8 metres. The time between nearest neighbour events shows three distinct time periods, a short range (seconds to a few days), a middle range (days to months) and a long range (months to years). All of the nearest neighbour distances are fractal with no non-fractal time periods. Finally the b-values of 0.8 and 1.1 for each of the two fractal time periods for the time between the nearest neighbours also support the concept of two seismic sources within the shear. A summary of the data results for this seismic source are shown in Table 16.

Table 16: Characteristic Summary for a Shear

Seismic Source	NN Distance		Fractal Dimensions			
			NN		Time Between NN	
	Mode (m)	Mean (m)	D_{NN}	Range (m)	D_{TBNN}	Range
Shear	2.4	4.9	1.89	0.3-4.5	0.86	4 sec - 2 yrs

Seismic Source	Fractal Dimension (DBNN - metres)			
	Distance between NN (m) by Magnitude Range			
	≥2	≥1 and <2	≥0 and <1	≥-1 and <0
Shear	0.89 (3-15m)	3.85 (2- 4m)	3.59 (1-2m) 1.97 (2-7m)	2.89 (1-3m)

Seismic Source	Fractal Dimension (TBNN)				
	Time between Nearest Neighbours (Days) by Magnitude Range				
	≥2	≥1 and <2	≥0 and <1	≥-1 and <0	≥-2 and <-1
Shear	0.51 (6-26d)	0.22 (6min-13.4hr)	0.17 (8.6s-4.1hr)	0.27 (8.6s-1.3d)	0.20 (8.6min-4.6d)
		0.46 (13.4hr-55d)	0.57 (4.1h-82d)	0.66 (1.3-59d)	0.64 (4.6-189d)
		0.30 (55-2.6y)	0.26 (82d-3y)	0.36 (59d-3.1y)	0.37 (189d-2.8y)

4.5 Summary of Seismic Source Characteristics

The seismic sources chosen for analysis in this thesis have different rock mass failure mechanisms. Case 1 is predominantly rock mass relaxation around a newly excavated void; Case 2 rock failure from high stress acting on stope abutments (Andrieux and Simser, 2001); Case 3 is crushing and volumetric fracturing of rock in a pillar (Hedley, 1992); and Case 4 is shear movement (Hedley, 1992). Each seismic source will be characterized using nearest neighbour distances, the fractal dimensions of the nearest neighbour distance (D_{NN}), distance between events (DBE), time between nearest neighbours (TBNN), and time between events (TBE), the size and number of clusters.

4.5.1 Characteristic Nearest Neighbour Distances

The nearest neighbour distances for each seismic source is shown in Figure 98. Individual graphs for each seismic source is included in Appendix III. The ramp events are the closest together ranging mostly between 0.1 to 10 metres apart with a mode distance of 1.1 metres and a mean

distance of 1.7 metres. The pillar events are further apart than the ramp events with most ranging between 0.8 to 8 metres apart.

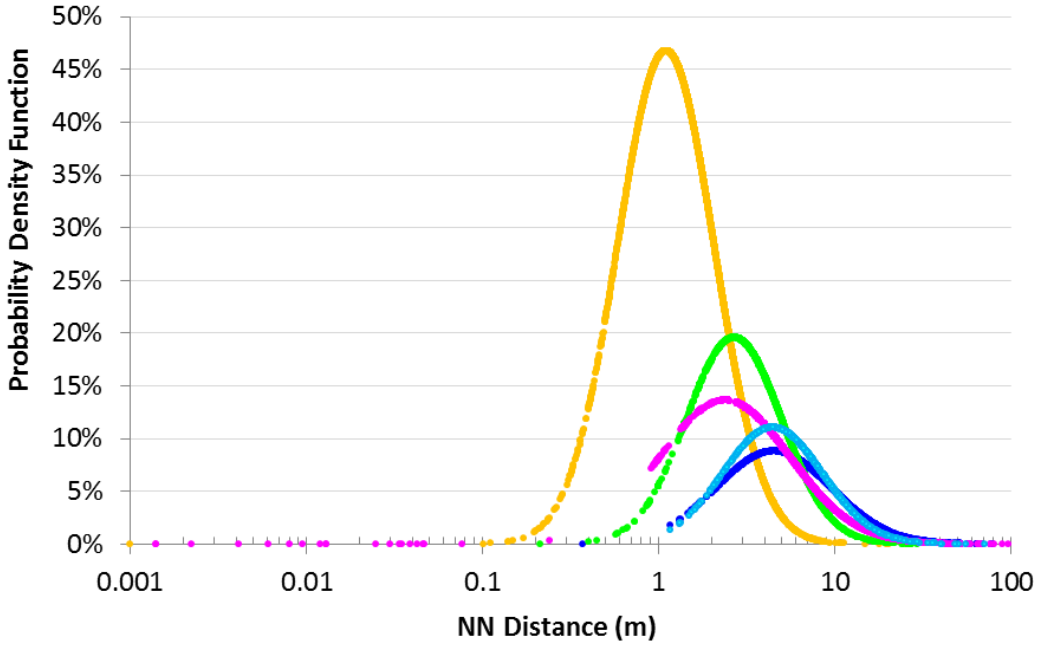

Case	# Events	NN Distance (m)	
		Mode	Mean
Ramp	3704	1.1	1.7
Abutment	710	4.5	6.8
Abutment	1350	4.5	8.0
Pillar	1368	2.7	4.0
Shear	4548	2.4	4.9

Figure 98: Probability of nearest neighbour distances by seismic source

The pillar events have a higher mode distance of 2.7 metres and a mean distance of 4.0 metres. The ramp also has a higher probability of 47% for the ramp mode distance of 1.1 metres compared to a 7% probability for the pillar nearest neighbour events at the same distance. The nearest neighbour events in the shear are more dispersed than both the pillar and ramp events. The mode distance in the shear is 2.4 metres which has a low probability (14%) compared to the mode probabilities for the ramp and pillar. While most of the nearest neighbour distances are further apart in the shear, there are 17 event pairs and 2 three event pairs that occur in almost identical

locations (0.001 to 0.1 metres apart). This characteristic is absent in the other three seismic sources. The abutment Population 2 (1350 events) has a nearest neighbour distance ranging from 1 to 20 metres. The mode distance at 4.5 metres is the furthest distance of all the seismic sources and also has the lowest probability at 9%. The mean distance is 8.0 metres which is the largest of all the seismic sources. The smaller abutment Population 1 has a similar range to Population 2 but a much higher probability of 11% at the mode distance of 4.5 metres. The mean distance is 6.8 metres, which is also lower than Population 2 but larger than the other mean distances.

The fractal dimension of the nearest neighbour distances is summarized for each seismic source in Figure 99. Not all nearest neighbour distances are fractal, so it is important to consider not only the fractal dimension but also range of distances in which the fractal correlation is valid. For example the fractal dimension of the ramp (2.83) and the pillar (2.68) are similar but the nearest neighbour distance ranges are different (ramp 0.1 to 1.1m and pillar 0.3 to 3.4m). The lowest fractal dimension at 1.89 is associated with the shear between 0.3-4.5 metres. The highest fractal dimension of 4.68 belongs to the abutment over a range of 1.2 to 2.4 metres.

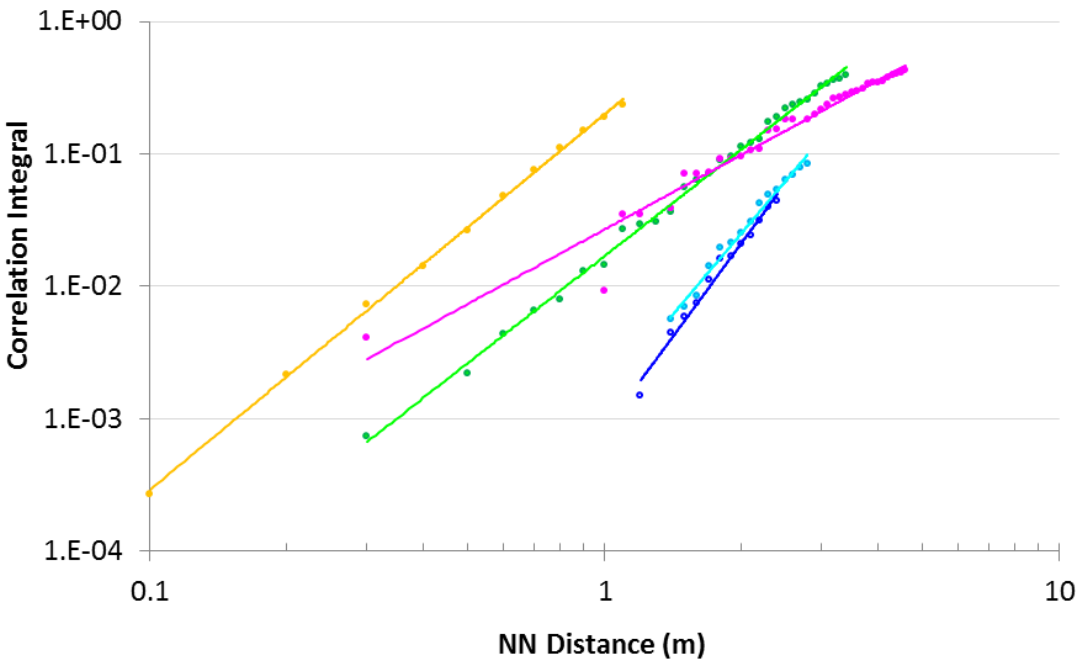

Case	# Events	FD	R^2	Range (m)	
Ramp	3704	2.83	99.9%	0.1	1.1
Abutment	710	4.06	98.7%	1.4	2.8
Abutment	1350	4.68	98.4%	1.2	2.4
Pillar	1368	2.68	99.7%	0.3	3.4
Shear	4548	1.87	96.1%	0.3	4.6

Figure 99: Fractal dimensions of the nearest neighbour distances for each seismic source

The lower the fractal dimension, the less correlated the nearest neighbour distances are. The abutment is highly correlated ($D_{NN\ 1.2-2.4m}^{Abutment} = 4.68$) for the closest nearest neighbour pairs (1.2-2.4 metres) but less well correlated for the nearest neighbour pairs that are further apart (2.4-8.0 metres) ($D_{NN\ 2.4-8.0m}^{Abutment} = 1.97$). The shear nearest neighbour distance is also not well correlated with a fractal dimension of 1.87 between 0.3 and 4.6 metres ($D_{NN\ 0.3-4.6m}^{Shear} = 1.87$). The shear can also be characterized by the nearest neighbour pairs that are not fractal and occur within 0.001 to 0.1 metres of each other (see the series of pink circles on the far left side of the x axis in Figure 98). Each pair (or triplet) of events occur in the same location – 19 different locations in the case of the shear. The ramp has nearest neighbours as low as 0.1 metres but they are within a fractal

region. The ramp does have one occurrence of two events occurring in the same location; however it is difficult to ascertain whether or not this is a characteristic of seismicity associated with development or indicative of something else. More examples of fractal dimensions of development nearest neighbour distances are needed to determine if it is a meaningful characteristic or not. The other two seismic sources (pillar and the abutment) do not have any occurrences of events in the same location.

The size of clusters created for each seismic source is summarized in Table 17. The goal to develop a method of clustering seismic events using a characteristic of the data itself (nearest neighbour distance) was successful in all cases. The method of clustering seismic events using the nearest neighbour distances is robust and can be refined as more case studies are completed. The main advantage of this new method is that the data itself determines the clustering distance and removes a bias imposed by arbitrarily choosing a clustering distance.

Table 17: Summary of clusters using NN mean and mode distances

Seismic Source	# Events	Mode				Mean				1m		
		(m)	#SE	#C	#E in LC	(m)	#SE	#C	#E in LC	#SE	#C	#E in LC
Ramp	3704	1.1	81.2%	18.8%	14	1.7	72.2%	27.8%	378	79.0%	21.0%	14
Abutment #1	710	4.5	80.5%	19.5%	17	6.8	78.0%	22.0%	337	100.0%	0	0
Abutment #2	1350	4.5	85.1%	14.9%	28	8.0	74.8%	25.2%	513	99.9%	0.1%	2
Pillar	1368	2.7	78.4%	21.6%	11	4.0	66.7%	33.3%	247	97.4%	2.6%	3
Shear	4548	2.4	91.1%	8.9%	292	4.9	78.6%	21.4%	1466	99.0%	1.0%	3

SE – Single Events C – Clusters E – Events LC – Largest Cluster

Using the clustering data to characterize a seismic source does not separate the sources clearly. When the mode distance was used all the seismic sources left approximately 80% of the clusters as single isolated events. The only exception was the shear which left a higher percentage (91%) as single isolated events. This is a characteristic of the shear in that it had a high percentage of single events. It also contained the largest cluster (292 events), while all the other largest cluster sizes were 28 or less events. When the mean nearest neighbour distance was used to cluster events, the

seismic sources were all relatively the same with approximately 75% of the clusters remaining as single isolated events with the exception of the pillar. In the case of the pillar, fewer single isolated events remained (66.7%) and it had the smallest cluster sizes. The shear did have the largest cluster size (1499 events). Finally, each seismic source was clustered at the same distance to create an equal comparison. One metre was chosen arbitrarily – any distance could be used as long as the same distance was used in each case. The ramp data resulted in the most and largest cluster and the least single isolated events. This indicates that the seismic events are closer together overall than for the other seismic sources. Population 1 in the abutment did not form any clusters when one metre was used. Population 2 formed one cluster of two events, meaning the seismic events in both abutment clusters are similar to each other and further apart than the ramp events. The pillar and the shear also formed a few very small clusters (cluster size less than or equal to 3 events), but did differ in the number of remaining single isolated events. The pillar data left 97.4% single isolated events while the shear left 99%. This means that the pillar created more clusters with events close to each other than the shear. These results do provide some characterization for each of the seismic sources; however it appears that cluster sizes alone could not be used. The clusters created do show areas of high seismic activity and could be used in future work to try and separate multiple seismic sources in a data set.

4.5.2 Time Between Nearest Neighbours Characteristic

The time between nearest neighbour characteristic gives a description of the behavior of a seismic source. Since the entire time spectrum is covered, no bias is introduced by imposing a specific time frame of study. Table 18 is a summary of the fractal dimension of the time between the nearest neighbour events for each case study.

Table 18: Summary of the Fractal Dimensions of the Time between Nearest Neighbours

Seismic Source	Time Between Nearest Neighbours		
	FD	R^2	Range
Ramp	0.74	99.6%	12 seconds to 46 minutes
	0.51	99.7%	46 minutes to 8 days
Abutment 710E	0.36	98.9%	1 second - 1.5 years
Abutment 1350E	1.10	92.6%	0 to 5 seconds
	0.20	98.14%	1 day to 1 year
Pillar	0.36	98.2%	52 seconds to 1 day
	0.46	99.9%	1 day to 1 year
Shear	0.26	99.9%	1s to 1 day
	0.64	99.9%	1 to 60 days

What is most noticeable is that each seismic source has two fractal dimensions. The first is of a short duration and the second a longer period. Two cases, the pillar and the shear have a higher second fractal dimension than the first. This means the nearest neighbour events that happen closest together are not as well correlated as those that occur over a longer time period. The other two cases – the ramp and abutment – have very strongly correlated short times between nearest neighbour events than their longer time frames. The difference between the long and short period fractal dimensions for the abutment is very large (Δ0.9) while the difference between the ramp fractal dimensions is smaller (Δ0.2). There is also a very large difference between the pillar and shear fractal dimensions. The difference between the short and long period fractal dimensions for the shear is moderately large (Δ0.4) while the difference for the pillar is much smaller (Δ0.1). The difference between fractal dimensions may very well be a good indicator of multiple seismic sources. For example, where the difference between the first and second fractal dimension is small (pillar) a single seismic source likely exists. Where the difference is very large (abutment) more than one seismic source likely exists. Overall, the fractal dimensions of the time between nearest neighbours are distinctly characteristic in all cases and are a good characterization for each seismic source.

4.5.3 Event Intensity Characteristic of NN Events – Magnitude

Characterizing nearest neighbour distances by calculating the fractal dimension of each magnitude range provides good information about each seismic source. The magnitude ranges for the fractal dimensions of the distance between nearest neighbours (DBNN) and the time between nearest neighbours are shown (TBNN).

4.5.3.1 Magnitude Range of Distance Between Nearest Neighbours

The range of magnitudes differs for each seismic source (Figure 100). The ramp events have the smallest range of magnitudes (-3 to 0), while the pillar has the largest range from magnitude -2 to 2. The shear and the abutment both have events over four magnitudes, however the shear events occur at higher magnitudes (range -1 to 2) than the abutment (-2 to 1).

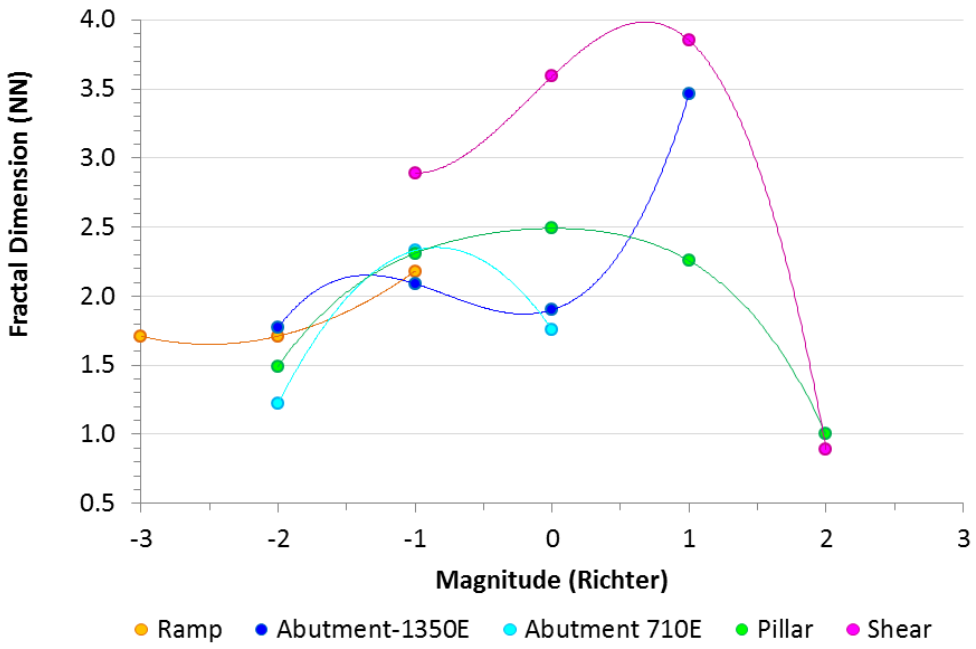

Magnitude Range	Fractal Dimension (NN)				
	Ramp	710E	1350E	Pillar	Shear
>2				1.00	0.89
1 to 2			3.46	2.26	3.85
0 to 1		1.76	1.90	2.49	3.59
-1 to 0	2.18	2.33	2.09	2.31	2.89
-2 to -1	1.71	1.22	1.77	1.49	
-3 to -2	1.71				

Figure 100: Comparison of the fractal dimensions of the distances between nearest neighbour by magnitude range for each seismic source

Of even more interest is the manner in which the fractal dimension changes (increase/decrease) over each magnitude range. Initially all the seismic sources increase in fractal dimension and then decrease with the exception of the ramp which only increases. The abutment fractal dimension starts to decrease for events greater than magnitude -1 and both the pillar and shear events decrease steadily for events with magnitude 0 and higher.

4.5.3.2 Magnitude Range of Time Between Nearest Neighbours

The magnitude ranges for the time between nearest neighbours is shown in Figure 101. Individual

graphs of each seismic source can be found in Appendix XII. The change in fractal dimension with respect to time of the abutment populations shows a distinct difference from the other three seismic sources. The reason is the abutment has multiple seismic sources within both Populations 1 and 2. The change in fractal dimension between of the time between nearest neighbour distances appears to provide a method to identify when a seismic data set has more than one seismic source. The advantage of calculating the TBNN first is that the seismic sources can be separated using the sequential spatial clustering method before time is spent on further analysis. In this way the results the analysis for each seismic source are more reflective of each seismic source.

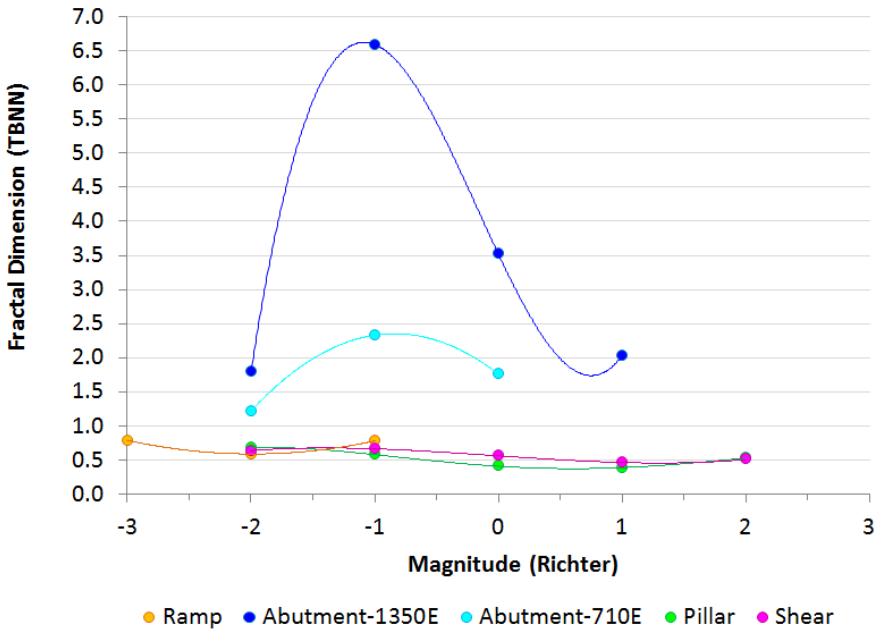

Magnitude Range	Magnitude Range	Fractal Dimension (TBNN)				
		Ramp	710E	1350E	Pillar	Shear
>2	2				0.53	0.51
1 to 2	1			2.03	0.39	0.46
0 to 1	0		1.76	3.52	0.41	0.57
-1 to 0	-1	0.78	2.33	6.59	0.58	0.66
-2 to -1	-2	0.59	1.22	1.79	0.68	0.64
-3 to -2	-3	0.79				

Figure 101: Comparison of fractal dimensions of the time between nearest neighbours by magnitude range for each seismic source

The goal of this research is to be able to study rock mass failure of one seismic source one step at a

time instead of all sources and all steps together.

4.5.4 Benchmark Summary of Seismic Sources

A summary of the characteristics of each seismic source provides a benchmark for comparison for other seismic data sets with known or unknown sources. Table 19 summarizes the characteristics of each seismic source's nearest neighbour population, fractal dimensions, and fractal ranges for both the distance between nearest neighbour seismic events and the time between the nearest neighbour events.

Table 19: Summary of Seismic Source Characteristics

Seismic Source	NN Distance		Fractal Dimensions			
			NN		Time Between NN	
	Mode (m)	Mean (m)	D_{NN}	Range (m)	D_{TBNN}	Range
Ramp	1.1	1.7	2.83	0.1-1.0	0.74	12s-46 min
					0.51	46min-7.7d
Abutment (710E)	4.5	6.8	4.06	1.4-2.8	0.22	0.7s-1.4min
					0.37	1.4min-1.5y
Abutment (1350E)	4.5	8.0	4.68	1.2-2.4	2.85	≤1 s
					0.08	2s-2d
					0.33	2d-1y
Pillar	2.7	4.0	2.68	0.3-3.4	0.36	52s-1d
					0.46	1-368d
Shear	2.4	4.9	1.89	0.3-4.5	0.86	4s-2y

The mode and mean nearest neighbour distances are a measure of how far apart seismic events occur from each other. The larger abutment population has the widest distribution of nearest neighbours with the mode at 4.5 metres and the mean at 8.0m. The ramp has the smallest range (1.1 to 1.7 metres) which means all the events are very close together. The pillar and the shear have very similar nearest neighbour distances so these seismic sources cannot be separated on nearest neighbour distance alone. If you compare the fractal dimension of the nearest neighbour distances the pillar has a higher correlation than the shear because it has a higher fractal dimension. They also differ in their fractal dimension of the time between the nearest neighbours. The pillar

has two fractal periods and is not as well correlated as the shear. The shear has only one fractal period and has a higher fractal dimension than the pillar. Each seismic source can be characterized by one or many categories depending on how different (ramp and abutment) or similar (pillar and shear) the seismic sources are. In Table 20, each seismic source is characterized by the range of magnitudes – the ramp has only magnitudes below 0; the shear only above 0. Each magnitude range is further described by the fractal dimension and range of the nearest neighbour distances.

Table 20: Summary of Seismic Source NN Fractal Dimension by Magnitude Range

Seismic Source	Fractal Dimension (DBNN) Distance between Nearest Neighbours (m) by Magnitude Range					
	≥2	≥1 and <2	≥0 and <1	≥-1 and <0	≥-2 and <-1	≥-3 and <-2
Ramp	-	-	-	2.18 (1-5m)	1.71 (1-3m)	1.71 (1-3m)
Abutment (710E)	-	-	1.76 (3-6m)	2.33 (2-6m)	1.22 (4-11m)	-
Abutment (1350E)	-	3.46 (3- 5m) 1.17 (5-13m)	1.90 (3-9m)	2.09 (2-8m)	1.77 (1-9m)	-
Pillar	1.00 (2- 4m)	2.26 (2- 4m)	2.49 (1-3m)	2.31 (1-4m)	1.49 (1-6m)	-
Shear	0.89 (3-15m)	3.85 (2- 4m)	3.59 (1-2m) 1.97 (2-7m)	2.89 (1-3m)	-	-

The largest magnitude events are interesting. For example the shear and the pillar are similar in that they both have seismic events greater than magnitude 2 with very nearly the same fractal dimension of ~1. Where they differ is that the largest magnitude events in the shear can be further apart (3 to 15 metres) from their nearest neighbours while the largest events in the pillar are much closer (2 to 4 metres) from their near neighbour event. The largest magnitude events in the shear will affect much a greater volume of the rock mass than the pillar will. Another noticeable difference is between the two abutment populations. Below magnitude 1, the fractal dimension and ranges of the populations are very similar. However, only the Population 2 (1350 events) has events with magnitudes greater than 2. The events are well correlated and can influence the rock mass from 3 to 13 metres. There is clearly a different seismic source within Population 2 that is not present in Population 1.

Characterizing seismic sources by the time between nearest neighbours over the largest magnitude range ($M_R \geq 2$) also shows the difference between the pillar and shear seismic sources Table 21.

Table 21: Fractal Dimension for TBNN by Magnitude Range

Seismic Source	Fractal Dimension (TBNN) Time between Nearest Neighbours (days) by Magnitude Range					
	≥2	≥1 and <2	≥0 and <1	≥-1 and <0	≥-2 and <-1	≥-3 and <-2
Ramp	-	-	-	0.34 (53min-1.7h) 0.78 (1.7hr-6.8d)	0.59 (14.7s-3.8d)	0.62 (2s-6.2min) 0.79 (6.2-37.4min) 0.50 (1.5hr-6.7d)
Abutment (710E)	-	-	0.18 (6.8s-23.5h) 0.71 (23.5h-6.5d) 0.36 (7.6d-1.3y)	0.24 (0.7s-4.6min) 0.37 (4.6min-1.5y)	0.12 (0.7s-1.3d) 0.43 (1.3d-1.2y)	-
Abutment (1350E)	-	2.03 (0.6-0.8s) 0.19 (1.3-63.5d)	3.52 (1.5-3.5d) 1.83 (3.5-8.7d)	6.59 (1.2-1.8d) 2.60 (1.8-4.2d)	1.79 (2.2-7.2d)	-
Pillar	0.53 (23-276d)	0.39 (14 min-1.2y)	0.41 (1min-1.6y)	0.54 (1.4min-327d) 0.58 (2-327d)	0.25 (1.4min-2d) 0.68 (4-32 d) 0.19 (32-1.5y)	-
Shear	0.51 (6-26d)	0.22 (6min-13.4h) 0.46 (13.4hr-55d) 0.30 (55-2.6y)	0.17 (8.6s-4.1h) 0.57 (4.1h-82d) 0.26 (82d-3y)	0.27 (8.6s-1.3d) 0.66 (1.3-59d) 0.36 (59d-3.1y)	0.20 (8.6min-4.6d) 0.64 (4.6-189d) 0.37 (189d-2.8y)	-

Both seismic sources have nearly the same fractal dimension (0.53 and 0.51) but the shear is only fractal from a week to a month (6-26 days) whereas the pillar is fractal from a month to almost 10 months (23-276 days). The largest events in the shear are more likely to occur during a short time period whereas the pillar is likely to have large events over a much longer time. The larger abutment population once again shows a much higher fractal dimension than the smaller population for all magnitude ranges making it very clear that the seismic source present in the large population does not exist in the smaller.

These charts shows how the character of each seismic source can be quantified using the distribution of the seismic events and the fractal dimension and range of the parameters of time, distance and intensity (magnitude). The multiple seismic sources in the abutment population can also be distinguished using the characteristics. Moreover the seismic sources within the abutment population can also be separated by the different fractal dimension ranges for time between the

nearest neighbour events. Separation of the multiple seismic sources should be done and the individual seismic sources re-characterized using the fractal methods established in this thesis.

Characterizing seismic sources using the nearest neighbour distance and time between nearest neighbour events and fractal dimension/ranges are meaningful and useful because it reflects the change in the rock mass between subsequent events over time. It also allows for seismic sources to be separated and studied individually giving better insight into each seismic source.

Chapter 5

5 Discussion

The creation of sequential spatial clustering and the novel application of fractal dimensions using the seismic source parameters of time, distance and intensity have shown to provide new insight into what seismic data can reveal about rock mass failure. Each method, how it can be used and the meaning derived from the results will be discussed. It should be noted that the data used in this thesis does not have waveforms. Therefore a discussion of system sensitivity, moment tensor or seismic source mechanism is not possible. The seismic arrays are also provided in Appendix XVI.

5.1 Sequential Spatial Clustering

The unique method of clustering seismic events developed in this thesis preserves the order in which the events join a cluster. The key to this method is that each event is associated with the event that occurs before it and is closest to it. The clustering process requires a distance between events to be established. Rather than arbitrarily choosing a distance or clustering on a range of distances, this method uses the seismic events themselves to determine which distance to use.

5.1.1 Clustering Distance - Mean, Mode or Other?

An initial examination of the frequency of the distance between each event and its preceding nearest neighbour event shows the seismic data for a seismic source has a lognormal distribution. The mode distance and mean distance were chosen as clustering distances because they represent the highest frequency (mode) and overall average distance. For every seismic source it was observed that clustering using the mode distance resulted in large numbers of very small clusters

(often less than 10 events per cluster) and a very high percentage (~ >80%) of the events not joining a cluster. While the mode distance is the nearest neighbour distance that occurs most often, there are many other nearest neighbour distances in the data set. The clusters resulting from the mode distance serve one very important purpose – they identify the areas of the highest amount of seismic activity. These areas can be used to reveal different seismic sources such as in the shear data set where one large cluster formed near the 585 level that was distinctly different from the other shear clusters.

In cases where no major cluster forms using the mode distance, it may be difficult to distinguish meaning from too many clusters. In these instances the use of the mean distance to cluster is more useful as the cluster size increases and the number of clusters decreases. The pillar clustered with the mean distance showed that the clusters sizes and locations were relatively evenly distributed around the main cluster (Images in Appendix II). This supports the hypothesis that the pillar failed by one seismic source.

The addition of the fractal dimension of the events' nearest neighbour distances show that the nearest neighbour distances that are fractal are up to and including the mode distance. In some cases the mean distance was also fractal but not always. The nearest neighbour distances in the abutment populations were not fractal for either the mode or mean distances. When the fractal range does not include the mode distance it is providing an indication that the data set may contain multiple seismic sources.

In the case of Population 2 in the abutment, the events were all within 32 metres of another event. If an event occurs 100 metres away for all the other events it is likely not associated with the cluster. It may belong to another cluster or is an outlier. This method provides a way to quantify

expected distances versus unexpected distances for a seismic event at a seismic source. Since the fractal description of nearest neighbour distances is a measure of probability, it may make more sense to refer to fractal distances (instead of expected) and non-fractal distances (instead of unexpected) particularly if this method is used for seismic hazard estimation.

5.1.2 Fractal Dimension Applications

Calculating the fractal dimension of a mathematical data set using the correlation integral is not difficult and can be applied in a wide range of ways. In this thesis, the data sets chosen for study are three seismic source parameters of distance, time and intensity. The first applications were to calculate the fractal dimension of each parameter for a given data set and then to combine the parameters in a meaningful way. The goal was to use each application of the fractal dimension to characterize what were believed to be four different seismic sources – ramp development, abutment, failing pillar, and a shear.

5.1.2.1 Distance

The fractal dimension of the distance between nearest neighbours provides a good characterization of a seismic source and identifies if multiple seismic source exist in a data set. The pillar case study is a very good example of a single seismic source. In this case, the fractal dimension of the distance between nearest neighbour events and the fractal dimension of the distance between events are the same and highly correlated. The abutment case study is a very good example of a data set with more than one seismic source. In this case the fractal range of the distance between nearest neighbours was not well correlated and a large portion of the data set was not fractal. The original intent of the research was to use fractal dimensions to characterize a seismic source using

nearest neighbour distances and the time between nearest neighbours and the method has shown to be useful in this regard.

5.1.2.2 Time

The use of fractal dimension of time between nearest neighbours is an important contribution from this research because it does not make any assumption about the length of time to study a seismic population. When plotting the fractal dimension of a seismic data set, it becomes apparent which time periods of time have the highest probability of occurring, what the longest time period between nearest neighbours can occur, and if multiple seismic sources are present. As a comparison, the fractal dimension of the time between all events was also calculated in the case of the pillar. The two methods (TBNN and TBE) provide similar information if there is only one seismic source in the data set. However, the TBE method makes the assumption that all the events are related to one another, which may not necessarily be true. The TBNN method statistically shows that the nearest neighbours are related and no assumption is needed. Thus the TBNN method provides better information and can aid in identifying multiple seismic sources. Since there is no need to calculate using two methods, using the TBNN is preferred as it provides more information than TBE. The resulting fractal dimension and the time ranges between nearest neighbours are therefore a good means of characterizing a seismic source.

The time between nearest neighbours gives a more specific description of the events that occur closest together. Each seismic source in this study contained two time periods that were fractal. Each had one time period that was short - usually less than a day or hour, and one long period that varied from days to weeks to months depending on the seismic source. One of the two fractal dimensions is more highly correlated than the other. In the case of the pillar and the shear, the

longer time period was more highly correlated than the short period. The abutment was the opposite with the shorter time period being more strongly correlated than the longer. The ramp data did not exhibit a long time period, likely because the excavations and blasts were relatively small and took place on a frequent daily/twice daily pattern.

Equally important are the time frames that are not fractal such as events that occur at the same time. The pillar and the shear are the only seismic sources that contained simultaneous events. The pillar had multiple occurrences of simultaneous events in different locations, while the shear had a few occurrences of simultaneous events in a specific location. The abutment and ramp cases did not have any simultaneous events.

The maximum time between nearest neighbours is also every important because it describes the longest time frame that has occurred between nearest neighbours. While the longest time frame may not be well correlated (fractal), one could consider the fractal time frame to be a normal response and the non-fractal portion possible but much less likely. This concept could help explain the events that are currently unexpected in time and shift the perception that all seismic events occur in short time frames to some seismic events will occur at long time frames.

Since all time frames are included in the fractal dimension calculation, the shortest time between nearest neighbour events provide interesting insight. The case of the abutment populations demonstrates this rather well. The larger Population 2 has two very distinct fractal dimensions – one for the events that occur within seconds or fraction of seconds from each other and those that occur after a day. In between these two time frames, the nearest neighbours are not correlated at all. This case is particularly interesting because there are no blast events in the data set, so the short time between events is likely due to a different seismic source. Further research could use

this response as a benchmark for a seismic source and compare it with events tagged as blasts. This could potentially lead to a mathematical method that could identify blast events that appear as real seismic events from a data set. This would help improve the quality of a data set prior to seismic analysis. A natural extension would be to compare these benchmark studies to other false events such as ore pass, drill or fan noise which can also lower the quality of a data set and skew analysis results.

5.1.2.3 Intensity and Distance

The fractal dimension of intensity, magnitude in these cases, cannot be directly calculated using the integral method. While this characterization may have been useful, it was decided to combine magnitude with the distance between nearest neighbours and the time between nearest neighbours. All of the nearest neighbour distances and times are used and sorted by magnitude range. The events in a given range are then compared to the other events in that same range to determine how far apart they are. The correlation integral is then calculated for the nearest neighbour distances and time between nearest neighbours. This method gives insight into where and when the largest magnitude events are occurring relative to the other seismic events. Not only does it identify the range of magnitudes possible for a seismic source, it also shows how the fractal dimension changes with increasing intensity. In this study, the fractal dimension of nearest neighbour distances all increased or remained the same for magnitudes below zero. Above zero magnitude, the fractal dimensions decreased. Surprisingly, the largest magnitude events all have nearest neighbour distances within fifteen metres. This means the largest magnitude and potentially most hazardous seismic events are highly correlated are fairly close together. The non-fractal distances were also reasonably short for the maximum distance the large events occurred from their nearest neighbour,

and significantly closer than the maximum distances for the smaller magnitude events. The combination of intensity with nearest neighbour distances is particularly useful in understanding how far large events are occurring from existing events.

5.1.2.4 Intensity and Time

In addition to the need to identify where large magnitude events may occur, is the need to understand the time periods a large magnitude may occur. For each seismic source, the change in fractal dimension of the time between nearest neighbours by magnitude range also provided new insight. The most obvious was the large variability in the time periods within both abutment populations. This is indicative of more than one seismic source present in the data set. In sharp contrast, the failing pillar has one seismic source which is characterized by very little variability in the fractal dimension of the time between nearest neighbour events. The ramp development and shear seismic populations also show small variations in the TBNN fractal dimension but do have a small non-fractal region whereas the pillar does not.

5.1.3 Analysis Tools using Fractal Dimension

While initially fractal dimension was intended to be used to characterize seismic sources, several applications emerged as useful analysis tools. The proximity test uses the nearest neighbour distance calculation on a daily basis. The fractal dimension range of nearest neighbour distances for each day is considered the normal response to a development blast such as those in the ramp example. Events that are further away (in the non-fractal range) are considered an abnormal response. Once identified, these abnormally located events can be followed and investigated to determine if a new, different seismic source is becoming active. This allows for proactive

identification of seismic sources before mining advances into a new seismically active area.

The ramp development also provided a unique example to create a method to identify moving seismic activity. This method takes the average of all the location coordinates of the normal nearest neighbour events in a day (as was shown previously in Figure 52). A day is chosen for the development case because it matches the blasting sequence. As the development progresses the daily center points are connected. If the line created by joining the daily coordinate points has a distinct direction, the seismicity is deemed to be moving. If the direction of the line does not have a distinct direction the seismic activity is deemed to be static. This method applied to development is straight forward. It would be particularly interesting to investigate if the proximity test could identify directions in other seismic sources such as a fault, a caving rock mass, or a rock mass chimney failure.

Another application that is an extension of the proximity test is the creation of isoclines. The isoclines developed in this thesis are created by separating the ramp seismic events by their magnitude ranges and then using the non-fractal maximum nearest neighbour distance to determine the furthest distance seismic events have occurred from a blast site by magnitude range. The isoclines are calculated once in this thesis but the application would be most useful in a mine by calculating the isoclines after every blast. As the isoclines move, the areas within the isoclines can be assessed for new hazards such as a geologic structure – a dyke was shown in the ramp example (previously described in Figure 56 Images A and B). The isoclines are an indicator of past behavior and may be used as an indicator of future seismic activity if the rock mass within the isoclines is the same. However, the magnitude isoclines may underestimate the intensity of future seismic events if there is a change in the rock mass within the isoclines. Therefore, the isoclines

need to be used along with all geologic information in the areas identified by the isoclines.

The changing fractal dimension of nearest neighbour distances by magnitude range also provides for the opportunity to compare the fractal dimension to a frequency magnitude graph shown in the ramp case study. The fractal dimension and ranges of the time between nearest neighbour events was determined and then a frequency magnitude plot created from the event magnitudes that fall within each range. The ramp provides a good example of how this information can be used to assess seismic hazard. In this case, each range had a different b-value. The shortest events of less than a second had a b-value of 1.2, the events that occurred between one second and 8 days after their nearest neighbour had a b-value of 1.0 and the lowest b-value of 0.8 was associated with the events that occurred more than 8 days after their nearest neighbour. It is this last group of events that poses the greatest seismic hazard and in a time frame that one would not normally associate with blasting. One other comment can be made about the relation between the fractal dimension of each time frame and the b-values. In this case the fractal dimensions of the time periods are not double the b-value as previously theorized by others. The ramp fractal dimensions are 1.07, 0.74, and 0.51 which correspond to b-values of 1.2, 1.0, and 0.8. Given the changing nature of fractal dimension and ranges in which data is fractal, it would appear that the estimation of a fractal dimension being twice a b-value is more of a generalization rather than a mathematical rule. Given that fractal dimension range was not considered in the original research of the b-value, the fractal dimension - b-value relation may need to be revisited.

5.2 Benchmarks for Comparison

This thesis studied four seismic sources that will serve as benchmarks. The first case was the

development of a ramp which included blasting on a daily basis. The characterization of this seismic source is summarized in the previous chapter. The case study does provide a good example of a normal seismic response to blasting along with some events that occur in abnormal locations and times.

The second case study of the abutments around stopes was studied using two different population sizes to determine if a grab sample of seismic events was an appropriate method of event selection. The larger population clearly contained two distinct seismic sources – one around the stopes and the second in the footwall. The smaller Population 1 was predominantly one seismic source but showed some of the same characteristics of the larger Population 2. This case provided a good example of how the new methods of sequential spatial clustering and the use of fractal dimension applied to seismic parameters can be used to identify multiple seismic sources.

The third case study of a failing pillar was perhaps the most straight forward single seismic source of all four case studies. The clusters created, their locations, the range of magnitudes and distance between nearest neighbours of the seismic events in this data set all support a single source inside the failing pillar. This case could be used as a benchmark with the results presented in the previous chapter with no additional work. There is the opportunity to further characterize the seismic source by applying the fractal dimension to other seismic source parameters if it were deemed useful or necessary.

The last case study of a shear near an orebody provided another good example of how the new methods can be used to identify multiple seismic sources. In the case of the shear, the sequential spatial clustering identified the area in the shear near the 585 level that was more seismically active than the other areas in the shear. The analysis of the whole data set with multiple fractal

dimensions and ranges also supports the identification of multiple seismic sources.

Chapter 6

6 Summation

6.1 Motivation and Originality of the Research

The research was motivated by the number of serious and dangerous seismic occurrences in mines that have resulted in fatalities or serious injury to workers, extensive damage to the physical assets in a mine or the loss of ore reserves, particularly in the last five years. In the literature and in practice, a comment often quoted is that the seismic event came without warning. These seismic events were unexpected either in terms of where they were located, what time they occurred or that they were the largest event ever experienced. Often described as random events, a quote by the Dutch philosopher Baruch Spinoza (1632-1677) motivated this work:

> *"Nothing in nature is random … A thing appears random only through the incompleteness of our knowledge."*

The approach to seismic analysis in mines evolved from earthquake seismology – a logical place to start. However, there are important differences such as scale, seismic source mechanisms from void creation, the ability to observe geologic structures underground, and blasting to name a few. Therefore it was felt that a different approach was needed to fill the incompleteness of knowledge with respect to rock mass failure.

The originality of this research comes from previous application of fractal mathematics to the study of seismicity in mines that produced inconclusive and conflicting results. The work carried out approximately twenty years ago was hampered by heavy computation requirements at a time when computers were in their infancy. The analysis using fractal dimension was carried out retroactively

on data sets that contained multiple seismic source. The analysis was often skewed by assumptions such as time frame of the study, the seismic events chosen in the analysis, the inclusion of blast events or other false events such as noise. However, fractal dimension has successfully become a new scientific discipline since the research of Benoit Mandelbrot in the 1950's on fractal geometry in nature. Despite the lack of success and ultimate dismissal of the use of fractal dimension by previous researchers in seismic research, it seemed the problem lay not in the method but the application. It needed to be revisited with careful consideration into how to use it with respect to seismic data in mines.

There are two main original themes in this thesis. The first is the way in which data is clustered to create a proactive analysis method. In most cases the entire data set was used – all the events inside a pillar, all events around ramp development and all the events in a shear. The exception is the abutment where it is not clear where the seismicity around mined stopes started and stopped. A comparison of two population sizes showed that it did indeed make a difference. The novel method of sequential spatial clustering, only clusters seismic events to only those predate and are closest to it. This approach preserves the sequence of the cluster as it develops over time. The significance of this is that the method can be used as a proactive tool.

The second theme is to apply fractal dimension calculations to four data sets originally thought to contain a single seismic source. The fractal dimensions of seismic source parameters of location, time and intensity are used to characterize each seismic source. What is original to the application of the fractal dimension on seismic data is the identification of the range in which a fractal dimension is valid. For example the distance between seismic events may range from one to one hundred metres but may only be fractal between one to twenty five metres. Interestingly, the

fractal dimension application in this research successfully demonstrated that multiple sources exist in the abutment and shear data sets which were previously thought to contain only a single source.

Other original work stemming from the two main themes was also created. The proximity test mathematically identifies when a new seismically active location commences. This is a particularly important tool because it identifies areas proactively and with very few seismic events.

Another original tool created in this research is a mathematical means to determine if the location of a seismic source is moving in a particular direction or not. In this research the seismic events in the ramp development were used to provide an example of directional seismicity. The failing pillar case study demonstrated the opposite - seismicity within the pillar that did not move continually in the same direction (static within the pillar).

6.2 Accomplishments and Contributions

One of the most important contributions of this thesis is the development of a new clustering method called sequential spatial clustering. This method clusters events one at a time which permits seismic data to be analyzed as it occurs. All other seismic clustering methods can only cluster events retroactively. This means that a large magnitude event has to occur before it can be studied. Sequential spatial clustering identifies anomalous seismic events as they occur which allows time to evaluate if a potential new seismic area is developing. Sequential spatial clustering does not require large amounts of data and uses every event in the dataset. Thus the method does not introduce a bias by selecting which events to study or the time frame in which to study them. This method can cluster seismic events in both space and time and without introducing a bias.

Another contribution is the creation of two new tools that use the principles of sequential spatial

clustering to aid in identification of new seismic locations. The first tool was a proximity test which identifies anomalous seismic sources after a blast occurs. The test was created using the development of a ramp because of the regular pattern of blasting (daily) and rock mass failure within 10 metres of a development heading. Expanding the tool for use in other blasting scenarios (such as stope blasting) is possible.

The second tool created combines the largest nearest neighbour distances after each blast with the magnitude of the events to create isoclines around an advancing development heading. The isoclines empirically show how far away the largest magnitude events have occurred from the heading. The isoclines give an indication of how far away from the development heading that the rock mass is being affected by the blasting. The known geology of the area within the isoclines can be added to determine if there is any reason to expect a change in the seismic response of the rock mass such as a change in rock mass properties or a geologic structure.

Calculating the fractal dimension of the distance between near neighbour seismic events is a novel approach that statistically correlates seismic events and identifies seismic source locations. This is a second large contribution made in this thesis. Knowing where every seismic source is located is essential to know if new areas are becoming seismically active. In addition, it was found that seismic sources are not infinitely fractal and require the context of the fractal limits to aid in understanding a seismic source. This means that if the nearest neighbour distances are between 10 and 50 metres, only a portion may be fractal (for example 10 to 20 metres). The nearest neighbour events that are 20 to 50 metres apart can still occur but because they are not in the fractal range they are less likely to occur and may not be correlated to the seismic source. This is important information when assessing where to expect seismicity. Development of a technique to identify

the bounds of fractal behavior is an important contribution that will play a role in the question of what the fractal limits in mine seismicity are.

The second part of the application of fractal dimension to seismic events is with respect to time between nearest neighbour events. Since nearest neighbours are already statistically correlated by distance, the time between the nearest neighbours provides the information about the amount of time it takes for a rock mass to fail for each seismic source. Like the fractal range of distance, there is also a range of times that are fractal (highly probable) and those that are not fractal and less likely to happen. This gives insight into how long a seismic source stays active. The results of the four case studies have shown that rock mass failure can continue much longer (days/months) than previously thought.

The last contribution of applying fractal dimension to seismic events was to calculate the fractal dimension of the distance between nearest neighbours by magnitude range as well as the fractal dimension of the relation of the time between nearest neighbours and magnitude range. When the TBNN and the DBNN are combined with the magnitude ranges and used to characterize a seismic source, it was found that if multiple seismic sources were in the data set, the fractal dimension and ranges were significantly different. This means that there is a way to mathematically identify if multiple seismic sources are present in a data set previously thought to contain only one. A seismic source can be extracted from a dataset by extracting all the events with the same nearest neighbour time.

6.3 Limitations and Future Work

6.3.1 Limitations

The depth and reproducibility of the fractal dimension and clustering results are encouraging, however more examples of each seismic source are needed to determine how robust it is and how it can be practically applied.

The determination of the nearest neighbour distance that provides a meaningful clustering distance is subject to debate. The use of the probability density function to ascertain a population's mode and mean distance between nearest neighbours provides a way to quantify the data's character without introducing a bias. If two populations are being compared they can be clustered using the same distance. This research found that in most cases using the mean nearest neighbour distances provided a reasonable group of clusters. It is recommended to cluster at both mode and mean distances as a starting point to gain insight into a seismic population. Additional distances can be used for clustering depending on what the initial clusters reveal. This provides a reproducible and meaningful approach to clustering data.

Another limitation is the error inherent in seismic data parameters. The time of each event is finite and has very little error. The only consideration would be the sensitivity of the seismic system and what the lower limit time interval the system is set to record. The number of events recorded by a system is a representative sample of all the events that take place. There is no way to know how many seismic events really take place. The location, sensitivity and number of working seismic sensors all contribute to how accurately a seismic event and intensity are recorded. Seismic system algorithms that process the data use multiple sensors – usually a minimum of five – to reach a best

estimate of the parameters recorded, such as location. A seismic system uses a velocity for both the p and s wave to determine arrival times. Which velocity to use is determined by calibrating the seismic system to a known blast size at a known location. However the *p* and *s* wave velocities change over time as voids, backfill and changes in the rock mass composition occur. Unless the *p* and *s* wave velocities are regularly re-calibrated to reflect changing rock mass conditions, the error in the seismic source parameters will increase over time and cannot be quantified. It is not known if the *s* and *p* wave velocities were regularly recalibrated in the seismic systems that provided the data used in this thesis.

Another limitation, which is an opportunity for further research, is the factors that influence the time of seismic events. For example, blast practices can have a large impact on the time between seismic events. The location, size and time between blasts will impact the seismic response of a rock mass. In the case of development whether a full round is blasted every day or twice a day will impact the time between seismic events. The period of ramp development chosen for this research was fairly regular in terms of the size, location and time between blasts. When stope blasting is a factor such as in the abutment case, the effect of blasting on the seismic response is harder to quantify as stope blasts can vary in size and frequency depending on whether a blast is a slot raise, an undercut or a large/small number of rings being blasted at any one time. Until the effects of blasting and the seismic response can be studied quantified using fractal dimension in a variety of blast scenarios, the impact blasting has on the fractal dimension of time between events and nearest neighbour events will remain unknown. This research does not specify time frames but covers all time frames. The benchmarks created for each seismic source in this research are firsts and will be refined when multiple examples of each seismic source are completed in future research.

6.3.2 Future Work

Throughout the results and discussion chapters of this thesis reference has been made to areas of future research that could be carried out. A summary is contained here.

- Investigate the how different blast sizes, locations and frequencies affect the time between nearest neighbour or time between event fractal dimensions.

- Use the nearest neighbour and time between event methodologies to identify and remove blast events from a seismic catalogue. The same could be done for known rockburst data, noise from ore passes, drilling or fans with each application becoming a new benchmark.

- Develop a way to use fractal dimension, nearest neighbour or sequential spatial clustering to separate multiple seismic sources within a data set.

- Create additional examples for each seismic source to determine ranges for nearest neighbour distances and its fractal dimension.

- Apply the proximity test to larger scale blasts.

- Incorporate the proximity test and isoclines together.

- Investigate the use of isoclines at a stope blasting scale

- Create more benchmark case studies for other seismic sources and mining methods not covered in this thesis such as contrasting rock property contacts (dyke beside weaker rocks) or a block caving mining method.

- Extend the method to investigate how one seismic source changes depending on the type of rock mass.

- Explore how the method could be used to assess and rate seismic hazard.

- Use the nearest neighbour distances to create a mesh in a numerical model.

- Continue to develop the use of fractal dimension with other seismic source parameters such as energy, corner frequency and moment. Particularly the use of energy to characterize the intensity of a seismic source.

- Compare the data where the seismic source is unknown to the benchmark cases to determine if seismic source can be inferred for the unknown data. This application would be particularly useful to assess anomalous seismic events identified by the proximity test or other new areas of seismic activity where access does not exist.

These suggestions for further research are all interesting extensions of the work completed in this thesis and are recommended as future work.

References

ABERCROMBIE, R.E., 1995. Earthquake source scaling relationships from -1 to 5 ML using seismograms recorded at 2.5-km depth. *Journal of Geophysical Research.* **100**(B12), p. 24,015-24,036.

ABOLFAZLZADEH, Y., 2013. *Application of seismic monitoring in caving mines – case study of Telfer Gold Mine*. Thesis (MASc), Laurentian University.

ABOLFAZLZADEH, Y., and HUDYMA, M., 2016. Identifying and describing a seismogenic zone in a sublevel caving mine. *Rock Mechanics and Rock Engineering.* **49**(9), p. 3735-3751.

AKI, I., 1981. A probabilistic synthesis of precursory phenomena, In: SIMPSON, D.W., and RICHARDS, P.G., eds. *Earthquake Prediction*. Washington: American Geophysical Union, p. 566-574.

ANDREWS, D.J., 1986. Objective determination of source parameters and similarity of earthquakes of different size. In: DAS, S., BOATWRIGHT, J., and SCHOLZ, C.H., eds, *Earthquake Source Mechanics*. Washington: American Geophysics Union. p. 259-267.

ANDRIEUX, P.P., and SIMSER, B., 2001. Ground stability based mine design guidelines at the Brunswick Mine. *Underground Mining Methods – Engineering Fundamentals and Case Studies*. Littleton: Society for Mining Metallurgy and Exploration, p. 207-214.

ARJANG, B., and HERGET, G., 1997. *In situ* ground stresses in the Canadian hardrock mines: an update. *International Journal of Rock Mechanics and Mining Sciences.* **34**(3-4), Paper 15.

BAIG, A., URBANCIC, T., VIEGAS, G., and KARIMI, S., 2012. Can small events (M<0) observed during hydraulic fracture stimulations initiate large event (M>0)? *The Leading Edge*. **31**(12), p. 1310-1314.

BARRETT, D., and PLAYER, J., 2002. Big Bell, high stress at shallow depth. In: *1st International Seminar on Deep and High Stress Mining, Perth, November 2002.* Perth: Australian Centre for Geomechanics, Section 28.

BASSON, F.R.R., and RAS, D.J.R.M., 2005. A method to examine the time-space relationship between seismic events. In: POTVIN, Y., and HUDYMA, M.R., eds. *Proceedings of the Sixth International Symposium on Rockburst and Seismicity in Mines, Perth, March 2005.* Perth: Australian Centre for Geomechanics, p. 347-351.

BENETEAU, D.L., 2012. *A Study in Relating Time-Between-Events to Seismic Source Mechanisms in Hardrock Mining.* Thesis (MASc), Laurentian University.

BHP Billiton, 2014. Annual Report 2014. [online] Available at: http://www.bhpbilliton.com/home/investors/annualreporting2014/Pages/default.aspx [Accessed 21

October 2014].

BLAKE, W., and HEDLEY, D.G.F., 2001. *Rockburst Case Histories for North American Hardrock Mines*. Sudbury: CAMIRO.

BOATWRIGHT, J., 1980. A spectral theory for circular seismic sources; simple estimates of source dimension, dynamic stress drop, and radiated seismic energy. *Bulletin of the Seismological Society of America*. **70**(1), p. 1-27.

BOHNHOFF, M., DRESEN, G., ELLSWORTH, W.L., and ITO, H., 2010. Passive seismic monitoring of natural and induced earthquakes: case studies, future directions and socio-economic relevance. In: CLOETINGH, S., and NEGENDANK, J., eds. *New Frontiers in Integrated Solid Earth Sciences, International Year of Planet Earth*. Springer Science, p. 261-285.

BOLER, F.M., and SWANSON, P.L., 1992. Observations of heterogeneous stope convergence behavior and implications for induced seismicity. *Pure and Applied Geophysics.* **139**(3/4), p. 639-656.

BOLT, B.A., 1993. *Earthquakes*. New York: W.H. Freeman and Company. p. 1-331.

BRUNE, J.N., 1970. Tectonic stress and the spectra of seismic shear waves from earthquakes. *Journal of Geophysical Research*. **75**(26), p. 4997-5009.

CARMICHAEL, H., 2009. Xstrata down to single mine. *The Sudbury Star, February 11, p.* [online] Available at: http://www.thesudburystar.com/ [Viewed 14 October 2014].

COLLINS, D., 2012. Seismic source parameters and successful use of re-entry protocol tools. *Short Course June 10th, 2012, Sudbury, Canada.* ESG Mining Solutions, unpublished.

COLLINS, D.S., TOYA, Y., PINNOCK, I., SHUMILA, V., and HASSEINI, Z., 2014. 3D velocity model with complex geology and voids for microseismic location and mechanism. In: HUDYMA, M. and POTVIN, Y., eds. *Proceedings of the 7th International Seminar on Challenges in Deep and High Stress Mining, Sudbury, October, 2014.* Nedlands: Australian Centre for Geomechanics, p. 681-688.

COLLINS, D.S., and YOUNG, R.P., 2000. Lithological controls on seismicity in granitic rocks. *Bulletin of the Seismological Society of America*. **90**(3), p. 709-723.

COUGHLIN, J., and KRANZ, R., 1991. New approaches to studying rock burst-associated seismicity in mines. In: ROEGIERS, J-C., ed. *Proceedings of the 32nd U.S. Symposium Rock Mechanics as a Multidisciplinary Science, Norman, Oklahoma, July 1991*. Rotterdam: A.A. Balkema, *p. 491-500.*

CRANSWICK, E., 2011. Coincidence of mines and earthquakes in Australia. *In: Proceedings of the Australian Earthquake Engineering Society Conference, Barossa Valley, November, 2011.*

Retrieved: June 3, 2017, http://www.aees.org.au/downloads/conference-papers/2011-2/

DUAN, W., WESSELOO, J., and POTVIN, Y., 2015. Evaluation of the adjusted rockburst damage potential method for dynamic ground support selection in extreme rockburst conditions. In: POTVIN, Y., ed. *Proceedings of the International Seminar on Design Methods in Underground Mining, Perth, November, 2015.* Perth: Australian Centre for Geomechanics, p. 399-418.

DUPLANCIC, P., 2001. *Characterisation of caving mechanisms through analysis of stress and seismicity.* Thesis (PhD), University of Western Australia.

ENEVA, M., 1994. Monofractal or multifractal; a case study of spatial distribution of mining induced seismic activity. *Nonlinear Processes in Geophysics.* **1**(2-3), p. 182-190.

ENEVA, M., 1998. In search for a relationship between induced microseismicity and larger events in mines. *Tectonophysics.* **289**(1-3), 91-104.

ENEVA, M., and BEN-ZION, Y., 1997. Techniques and parameters to analyze seismicity patterns associated with large earthquakes. *Journal of Geophysical Research.* **102**(B8), p. 17,785-17,795.

ENEVA, M., and VILLENEUVE, T., 1997. Retrospective pattern recognition applied to mining-induced seismicity. In: GIBOWICZ, S.J., and LASOCKI, S., eds. *Rockbursts and Seismicity in Mines, Krakow, August 1997.* Rotterdam: Balkema, p. 299-303.

ENEVA, M., and YOUNG, R.P., 1993. Evaluation of spatial patterns in the distribution of seismic activity in mines: a case study of Creighton Mine, northern Ontario (Canada). In: YOUNG, R.P., ed. *Rockbursts and Seismicity in Mines 93: Proceedings of the 3rd International Symposium on Rockbursts and Seismicity in Mines, Kingston, Canada, August 1993*. Rotterdam: A.A. Balkema, p. 175-180.

ESTER, M., KRIEGEL, H-P., SANDER, J., and XU, X., 1996. A density-based algorithm for discovering clusters in large spatial databases with noise. *Kdd.* **96**(34), p. 226-231.

EVERNDEN, J.F., 1967. Magnitude determinations at regional and near-regional distances in the United States. *Bulletin of the Seismological Society of America*. **57**(4), p. 591-639.

GARCIA, J.A., FDEZ-VALDIVIA, J., CORTIJO, F.J., and MOLINA, R., 1995. A dynamic approach for clustering data. *Signal Processing*. **44**, p. 181-196.

GE, M., and KAISER, P.K., 1990. An innovating micro-seismic source location technique. In: Hustrulid, W.A., JOHNSON, G.A., eds, *Proceedings of the 31st U.S. Symposium, Rock Mechanics Contributions and Challenges*. Rotterdam, A.A. Balkema, pp. 43–50.

GIBOWICZ, S.J., and KIJKO, A., 1994. *An Introduction to Mine Seismology,* San Diego: Academic Press, 396 p.

GIBOWICZ, S.J., 1997. Scaling relations for seismic events at Polish copper mines. *Acta Geophysica Polonica.* **45**(3), p. 69-181.

GIBOWICZ, S.J. and LASOCKI, S., 2001. Seismicity induced by mining; ten years later. *Advances in Geophysics.* **44**, p. 39-181.

GIBOWICZ, S.J., YOUNG, R.P., TALEBI, S., and RAWLENCE, D.J., 1991. Source parameters of seismic events at the underground research laboratory in Manitoba, Canada: scaling relations for events with moment magnitude smaller than -2. *Bulletin of the Seismological Society of America*, **81**(4), p. 1157-1182.

GOODFELLOW, S.D., and YOUNG, R.P., 2014. A laboratory acoustic emission experiment under *in situ* conditions. *Geophysical Research Letters*. **41**, p.3422-3430.

GRASSBERGER, P., and PROCACCIA, I., 1983. Measuring the strangeness of strange attractors. *Physica*. **9**(D), p. 189-208.

GUHA, S., RASTOGI, R., and SHIM, K., 1998. CURE: An Efficient Clustering Algorithm for Large Databases. In: HAAS, .L.M., and TIWARY, A., eds, *Proceedings of the ACM SIGMOD International Conference on Management of Data, Seattle, June 1998.* Seattle: ACM Press. p. 73-84.

GUTENBERG, B., and RICHTER, C.F., 1956. Earthquake magnitude, intensity, energy and acceleration. *Bulletin of the Seismological Society of America.* **46**(2), p. 105-145.

HANKS, T.C., and KANAMORI, H., 1979. A moment magnitude scale. *Journal of Geophysical Research.* **84**(B5), p. 2348-2350.

HEDLEY, D.G.F., 1992. *Rockburst Handbook for Ontario Hardrock Mines*. CANMET Special Report SP92-1E. 305 p.

HILLS, P.B., 2012. Keynote Address: Managing Seismicity at the Tasmania Mine. In: POTVIN, Y., ed. *Proceedings of the 6th International Seminar on Deep and High Stress Mining, Perth, March 2012.* Nedlands: Australian Centre for Geomechanics, p. 129-148.

HILLS, P.B., REBULI, D.B., and LYNCH, R.A., 2013. Micro-seismic monitoring at the Tasmania Mine, Beaconsfield, Tasmania. In: MALOVICHKO, A., and MALOVICHKO, D., eds. *Proceedings of the 8th International Symposium on Rockbursts and Seismicity in Mines, Russia, September 2013.* Perm: Geophysical Survey of Russian Academy of Sciences and Mining Institute of Ural Branch of Russian Academy of Sciences, p. 485-494.

HINNEBURG, A., and KEIM, D.A., 1998. An efficient approach to clustering in large multimedia databases with noise. In: AGRAWAL, R., and STOLORZ, P., eds. *Proceedings of the 4th International Conference on Knowledge Discovery and Data Mining, New York, August 1998.* New York: AAAI press. p. 58-65.

HIRATA, T., SATOH, T., and ITO, K., 1987. Fracture structure of spatial distribution of microfracturing in rock. *Geophysical Journal of the Royal Astronomical Society.* **90**, p. 369-374.

HIRATA, T., 1987. Omori's power law aftershock sequences of microfracturing in rock fracture experiment. *Journal of Geophysical Research.* **92**(B7), p. 6215-6221.

HUDYMA, M.R., HEAL, D., and MIKULA, P., 2003. Seismic monitoring in mines – old technology – new applications. In: HEBBLEWHITE, B.K., ed. *Proceedings 1st Australasian Ground Control in Mining Conference, Sydney, November, 2003*. Sydney: UNSW Publishing and Printing Services, p. 209-226.

HUDYMA, M., and POTVIN, Y.H., 2010. An engineering approach to seismic risk management in hardrock mines. *Rock Mechanics and Rock Engineering*. **43**, p. 891-906.

HUDYMA, M., BROWN, L., and CORTOLEZZIS, D., 2016. Seismic risk in Canadian mines. In: *Maintenance Engineering-Mine Operators Conference, Sudbury, October, 2016*. Sudbury: Canadian Institute of Mining and Metallurgy, p. 1-15.

IDE, S., BEROZA, G.C., PREJEAN, S.G., and ELLSWORTH, W.L., 2003. Apparent break in earthquake scaling due to path and site effects on deep borehole recordings. *Journal of Geophysical Research*, **108**(B5), p. 16.1-16.13.

IDZIAK, A., and TEPER, L., 1996. Fractality of spatial distribution of both faults and seismic events within Bytom syncline, Upper Silesia. *Acta Montana Series A.* **9(**100), p. 65-72.

JAGER, J.A., and RYDER, A.J., 1999. *A Handbook on Rock Engineering Practice for Tabular Hard Rock Mines*. South Africa: The Safety in Mines Research Advisory Committee (SIMRAC).

JAIN, A.K., and DUBES, R.C., 1988. *Algorithms for Clustering Data*. New Jersey: Prentice Hall. 334 p.

JULIA, J., NYBLADE, A.A., DURRHEIM, R., LINZER, L., GOK, R., DIRKS, P., and WALTER, W., 2009. Source mechanisms of mine-related seismicity, Savuka Mine, South Africa. *Bulletin of the Seismological Society of America*. **99**(5), p. 2801-2814.

KAGAN, Y.Y., and JACKSON, D.D., 1991. Long-term earthquake clustering. *Geophysical Journal International.* **104**(1), p. 117-133.

KALENCHUK, K.S., MERCER, R.A., and WILLIAMS, E., 2017. Large-magnitude seismicity at the Westwood mine, Quebec, Canada. In: WESSELOO, J., ed. *Proceedings of the 8th International Conference on Deep and High Stress Mining, Perth, March, 2017.* Nedlands: Australian Centre for Geomechanics, p. 89-102.

KANAMORI, H., 1977. The energy release in great earthquakes. *Journal of Geophysical*

Research. **82**(20), p. 2981-2987.

KANAMORI, H., MORI, J., HAUKSSON, E., HEATON, T.H., HUTTON, L.K., and JONES, L.M., 1993. Determination of earthquake energy release and M_L using terrascope. *Bulletin of the Seismological Society of America*. **83**(2), p. 330-346.

KARYPIS, G., SAN, E-H., and KUMAR, V., 1999. CHAMELEON: a hierarchical clustering algorithm using dynamic modeling. *Computer*. **32**, p. 68-75.

KEILY, J., 2013. Seismicity and pre-shift seismic data analysis at Eloise Copper Mine. In: *23rd Seminar on Monitoring & Modelling the Seismic Rock mass Response to Mining, Tasmania, Australia, March 2013*. Tasmania: Institute of Mine Seismology, p 1-41.

KIJKO, A., FUNK, C.W., and BRINK, A.V.Z., 1993. Identification of anomalous patterns in time-dependent mine seismicity. In: YOUNG, P., ed. *Rockbursts and Seismicity in Mines 93: Proceedings of the 3rd International Symposium on Rockbursts and Seismicity in Mines, Kingston, Canada, August 1993*. Rotterdam: A.A. Balkema, p. 205-210.

KLINKENBERG, B., 1994. A review of methods used to determine the fractal dimension of linear features. *Mathematical Geology*. **26**(1), p. 23-46.

KRANZ, R.L., and ESTEY, L.H., 1996. Listening to a mine relax for over a year at 10 to 1000 meter scale. *Rock Mechanics*. Rotterdam: Balkema, p. 491-498.

KUZYK, G.W., and MARTINO, J.B., 2008. Development of excavation technologies at the Canadian Underground Research Laboratory. In: *Proceedings of the International Technical Conference on the Practical Aspects of Deep Geological Disposal of Radioactive Waste, Prague, Czech Republic, June 2008*. Prague: Czech Technical University. Section 22, p. 1-13.

KWIATEK, G., PLENKERS, K., NAKATANI, M., YABE, Y., DRESEN, G., and JAGUARS GROUP, 2010. Frequency-magnitude characteristics down to magnitude -4.4 for induced seismicity recorded at Mponeng Gold Mine, South Africa. *Bulletin of Seismological Society of America.* **100**(3), p. 1165-1173.

KWIATEK, G., PLENKERS, K., DRESEN, G., and JAGUARS GROUP, 2011. Source parameters of picoseismicity recorded at Mponeng Deep Gold Mine, South Africa: implications for scaling relations. *Bulletin of the Seismological Society of America.* **101**(6), p. 2592-2608.

LESNIAK, A.J., and ISAKOW Z., 2009. Space-time clustering of seismic events and hazard assessment in the Zabrze-Bielszowice coal mine, Poland. *International Journal of Rock Mechanics & Mining Sciences.* **46**, p. 918-928.

LIZUREK, G., and LASOCKI, S., 2014. Clustering of mining-induced seismic events in equivalent dimension spaces. *Journal of Seismology*. **18**, p. 543-563.

LOCKNER, D.A., and BYERLEE, J.D., 1992. Fault growth and acoustic emissions in confined granite. *Applied Mechanics Reviews.* **45** (3/2), p. S165-175.

LU, C., MAI, Y-W., and XIE, H., 2005. A sudden drop of fractal dimension: a likely precursor of catastrophic failure in disordered media. *Philosophical Magazine Letters*. **85**(1), p. 33-40.

LU, C., 2013. Revisit on the fractal dimension in damage and fracture. In: YU, S., ed. *Proceedings of the 13th International Conference on Fracture, Beijing, June 2013,* Beijing: The Chinese Society of Theoretical and Applied Mechanics. p. S47-004-1 to S47-004-5.

MACQUEEN, J., 1967. Some methods for classification and analysis of multivariate observations. In: CAM, L.M., and NEYMAN, J., eds, *Proceedings of the 5th Berkeley Symposium on Math, Statistics and Probability, Berkeley.* Berkeley: University of California. p. 281–297.

MADARIAGA, R., 1976. Dynamics of an expanding circular fault. *Bulletin of the Seismological Society of America*. **66**(3), p. 639-666.

MALONEY, S.M., KAISER, P.K., and VORAUER, A., 2006. A re-assessment of *in situ* stresses in the Canadian Shield. In: *Golden Rocks 2006, The 41st U.S. Symposium on Rock Mechanics (USRM): "50 Years of Rock Mechanics – Landmarks and Future Challenges, Golden, June 2006*. Virginia: American Rock Mechanics Association (ARMA).

MANDAL, P., MABAWONKU, A.O., and DIMRI, V.P., 2005. Self-organized fractal seismicity of reservoir triggered earthquakes in the Koyna-Warnia seismic zone, Western India. *Pure and Applied Geophysics*. **162**, p. 73-90.

MANDELBROT, B.B., 1982. *The fractal geometry of nature*. New York: W.H. Freeman and Company.

MARTINO, J.B., and CHANDLER, N.A., 2004. Excavation-induced damage studies at the Underground Research Laboratory. *International Journal of Rock Mechanics & Mining Sciences.* **41**, p. 1413-1426.

MCGARR, A., 1976. Seismic moments and volume changes. *Journal of Geophysical Research.* **81**(8), p. 1487-1494.

MCLASKEY, G., KILGORE, B.D., LOCKNER, D.A., and BEELER, N.M., 2014. Laboratory generated M -6 earthquakes. *Pure and Applied Geophysics*. **171**, p. 2601-2615.

MENDECKI, A.J., 1997. *Seismic Monitoring in Mines*. UK: Chapman& Hall. 262 p.

MENDECKI, A.J., and LOTTER, E.C., 2011. Modelling seismic hazard for mines. In: ANDERSON, S., ed. *AEES Conference 2011, Barossa Valley, November 2011*, Australia: Australia Earthquake Engineering Society, Paper 38.

MICHALEK, J., and FISCHER, T., 2013. Source parameters of the swarm earthquakes in West

Bohemia/Vogtland. *Geophysical Journal International*. **195**, p.1196-1210.

MINISTRY OF LABOUR, 2015. Final Report: Mining Health, Safety and Prevention Review. https://www.labour.gov.on.ca/english/hs/pubs/miningfinal/, June 2017.

MOLLISON, L., SWEBY, G., and POTVIN, Y., 2003. Changes in mine seismicity following a mine shutdown. In: HEBBLEWHITE, B.K., ed. *Proceedings 1st Australasian Ground Control in Mining Conference, Sydney, November, 2003*. Sydney: UNSW Publishing and Printing Services, p. 187-197.

MORISSETTE, P., HADJIGEORGIOU, J., and THIBODEAU, D., 2012. Validating a support performance database based on passive monitoring data. In: POTVIN, Y., ed. *Proceedings of the 6th International Seminar on Deep and High Stress Mining, Perth, March 2012*. Nedlands: Australian Centre for Geomechanics, p. 27-39.

MORTIMER, Z., and LASOCKI, S., 1996a. Studies of fractality of epicenter distribution geometry in mining induced seismicity. *Acta Montana A*. **10**(102), p. 31-37.

MORTIMER, Z., and LASOCKI, S., 1996b. Variations of the fractal dimension of epicenter distribution in the mining-induced seismicity. *Acta Montana Series A.* **9**(100), p. 73-81.

MORTIMER, Z., 1997. Fractal statistics for the local induced seismicity in some Polish coal mines. In: GIBOWICZ, S.J., and LASOCKI, S., eds. *Rockbursts and Seismicity in Mines, Krakow, August 1997.* Rotterdam: Balkema, p. 49-53.

NANOPOULOS, A., THEODORIDIS, Y., and MANOLOPOULO, Y., 2001. C^2P: Clustering based on closest pairs. In: APERS, P.M.G., ATZENI, P., CERI, S., PARABOSCHI, S., RAMAMOHANARAO, K., and SNODGRASS, R.T., eds, *Proceedings of the 27th International Conference on Very Large Data Base, Rome, September 2001*.San Francisco: Morgan Kaufmann Publishers Inc. p. 331–340.

NG, R. and HAN, J., 1994. Efficient and effective clustering methods for spatial data mining. In: BOCCO, J.B., JARKE, M., and ZANIOLO, C., eds, *Proceedings of the 20th International Conference on Very Large Data Base, Santiago, September 1994.* San Francisco: Morgan Kaufmann Publishers Inc. p. 144–155.

NIWITPONG, S-A., 2013. Confidence intervals for the mean of lognormal distribution with restricted parameter space. *Applied Mathematical Sciences*. **7**(4), p. 161-166.

NUTTLI, O.W., 1973. Seismic wave attenuation and magnitude relations for Eastern North America. *The Journal of Geophysical Research*. **78**(5), p. 876-885.

OYE, V., BUNGUM, H., and ROTH, M., 2005. Source parameters and scaling relations for mining-related seismicity within the Pyhasalmi Ore Mine, Finland. *Bulletin of the Seismological Society of America*. **95**(3). p. 1011-1026.

PARSHA, M.K., and PACHA, S., 2013. Recent advances in clustering algorithms: a review. *International Journal of Conceptions on Computing and Information Technology*. **1**(1), p. 1-4.

PASTEN, D., ESTAY, R., COMTE, D., and VALLEJOS, J., 2015. Multifractal analysis in mining microseismicity and its application to seismic hazard in mine. *International Journal of Rock Mechanics and Mining Sciences*. **78**, p. 74-78.

PENG-YENG, Y., and LING-HWEI, C. 1994. A new iterative approach for clustering. *Pattern Recognition Letters*. **15**(2), p.125–133.

RAI, P., 2011. *Data clustering: K-means and hierarchical clustering*. Lecture – The University of Utah, p. 1-24. Retrieved from: http://www.cs.utah.edu/~piyush/teaching/cs5350.html, June 3, 2017.

REBULI, D.B., and KOHLER, S.J., 2014. Using clustering algorithms to assist short-term seismic hazard analysis in deep South African mines. In: HUDYMA, M., and POTVIN, Y., eds. *Proceedings of the 7th International Seminar on Challenges in Deep and High Stress Mining, Sudbury, October, 2014.* Nedlands: Australian Centre for Geomechanics, p. 699-708.

REIMNITZ, M., 2004. *Shear-slip induced seismic activity in underground mines: a case study in Western Australia*. Thesis (Masters), University of Western Australia.

RICHARDSON, E., and JORDAN, T.H., 2002. Seismicity in deep gold mines of South Africa: Implications for tectonic earthquakes. *Bulletin of the Seismological Society of America*. **92**(5), p. 1766-1782.

RICHTER, C.F., 1935. An instrumental earthquake magnitude scale. *Bulletin of the Seismological Society of America.* **25**(1), p. 1-32.

ROBERTSON, M.C., SAMMIS, C.G., SAHIMI, M., and MARTIN, A.J., 1995. Fractal analysis of three-dimensional spatial distributions of earthquakes with a percolation interpretation. *Journal of Geophysical Research.* **100**(B1), p. 609-620.

SHIVAKUMAR, K., RAO, M.V.M.S., SRINIVASAN, C., and KUSUNOSE, K., 1996. Multifractal analysis of the spatial distribution of area rockbursts at Kolar Gold mines. *International Journal of Rock Mechanics and Mining Sciences Geomechanical Abstracts*. **33**(2), p. 167-172.

SRINIVASAN, C., AHNOCH WILLY, Y., and NAWANI, P.C., 2009. Post-closure seismicity in the mines of Kolar Gold Fields. In: TANG, C.A., ed., *Controlling Seismic Hazard and Sustainable Development of Deep Mines - Seventh International Symposium on Rockbursts and Seismicity in Mines, Dalian, August 2009*. New York, New Jersey: Rinton Press, p. 1325-1336.

SWAN, G., KAZAKIDIS, V., BRUMMER, R.K., and GRAHAM, C., 2005. Deep mining research: Implementing technology to manage risk. In: *Maintenance Engineering-Mine Operators*

Conference, Sudbury, February, 2005. Montreal: Canadian Institute of Mining and Metallurgy, Paper 11.

SWANSON, P.L., 1992. Mining-induced seismicity in faulted geologic structures: an analysis of seismicity-induced slip potential. *Pure and Applied Geophysics.* **139**(3/4), p. 657-675.

TALEBI, S., and YOUNG, R.P., 1993. Design of a microseismic monitoring system for the investigation of tunnel excavation damage. In: YOUNG, P., ed. *Rockbursts and Seismicity in Mines 93: Proceedings of the 3rd International Symposium on Rockbursts and Seismicity in Mines, Kingston, Canada, August 1993*. Rotterdam: A.A. Balkema, p. 423-428.

TRIFU, C.I., URBANCIC, T.I., and YOUNG, R.P., 1993. Non-similar frequency-magnitude distribution for M<1 seismicity. *Geophysical Research Letters.* **20**(6), p. 427-430.

TSIREL, S.V., TARATINSKII, G.M., and MULEV, S.N., 2011. Cluster location procedure for technogeneous seismic events in deep mines. *Journal of Mining Science.* 47(3), p. 297-306.

TURCOTTE, D.L., 1997. *Fractals and chaos in geology and geophysics-second edition*. Cambridge University Press: New York.

WEGLARCZYK, S., and LASOCKI, S., 2009. Studies of short and long memory in mining-induced seismic processes. *Acta Geophysica.* **57**(3), p. 696-715.

WETMILLER, R.J., GALLEY, C.A., and PLOUFFE, M., 1993. Post-closure seismicity at a hard-rock mine. In: YOUNG, P., ed. *Rockbursts and Seismicity in Mines 93: Proceedings of the 3rd International Symposium on Rockbursts and Seismicity in Mines, Kingston, Canada, August 1993*. Rotterdam: A.A. Balkema, p. 445-448.

WYSS, M., SAMMIS, C.G., NADEAU, R.M., and WIEMER, S., 2004. Fractal dimension and *b*-value on creeping and locked patches of the San Andreas Fault near Parkfield, California. *Bulletin of the Seismological Society of America.* **94**(2), p. 410-421.

XIE, H., and PARISEAU, W.G., 1993. Fractal character and mechanism of rock bursts. *International Journal of Rock Mechanics and Mining Sciences*. **30**, p. 343-350.

Appendix I
Seismic Events Identified by the Proximity Test

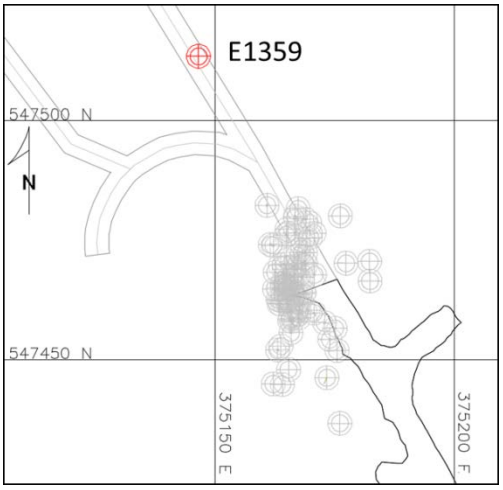

Event 1359
May 25, 2005
Magnitude = -3.1
NN Distance = 38.2m
Events on May 25: 88
Average NN Distance May 25: 3.2m

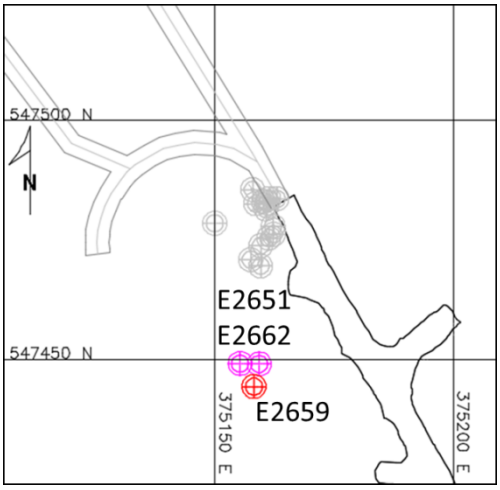

Event 2659
June 5, 2005
Magnitude = -1.5
NN Distance = 31.4m
Events on June 5: 15
Average NN Distance June 5: 6.3m

Events 2651 and 2662 are close to E2659 horizontally but further above. The area becomes inactive after June 5.

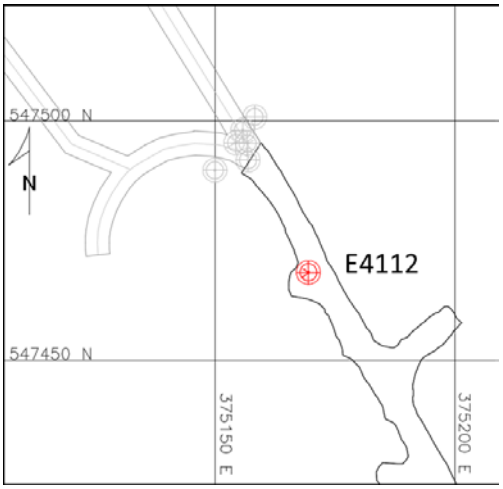

Event 4112
June 17, 2005
Magnitude = -2.9
NN Distance = 29.6m
Events on June 17: 7
Average NN Distance June 17: 10.9m

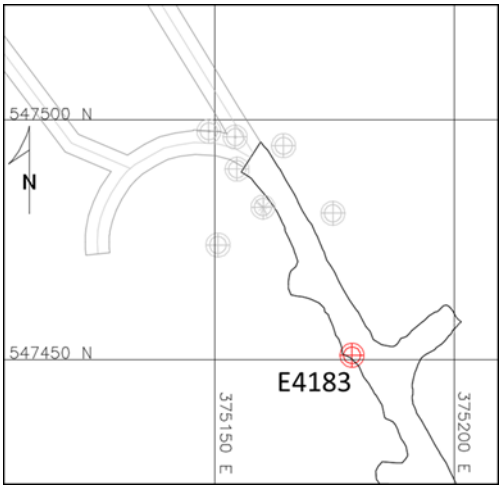

Event 4183
June 18, 2005
Magnitude = -2.1
NN Distance = 40.3m
Events on June 18: 8
Average NN Distance June 18: 18.6m

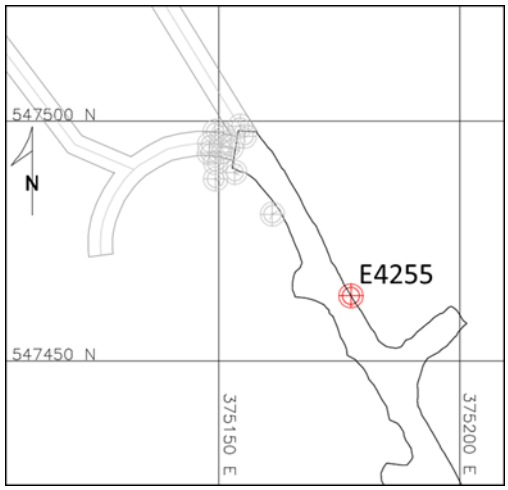

Event 4255
June 19, 2005
Magnitude = -3.5
NN Distance = 26.2m
Events on June 19: 14
Average NN Distance June 19: 5.8m

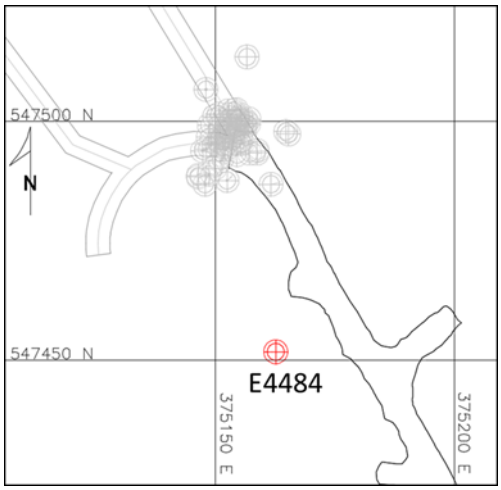

Event 4484
June 21, 2005
Magnitude = -2.7
NN Distance = 37.4m
Events on June 21: 66
Average NN Distance June 21: 3.1m

Event 4787
June 23, 2005
Magnitude = -2.7
NN Distance = 37.4m
Events on June 23: 66
Average NN Distance June 23: 3.1m

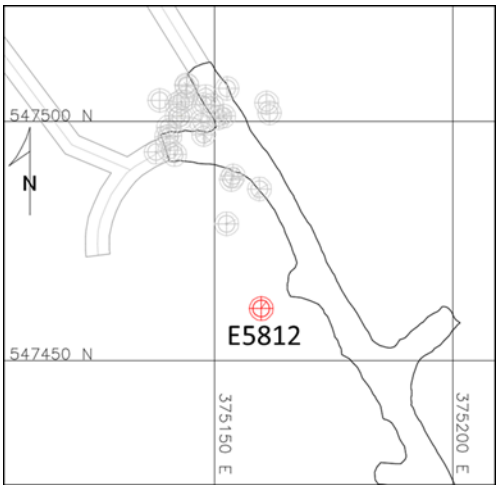

Event 5812
July 3, 2005
Magnitude = -1.7
NN Distance = 23.2m
Events on July 3: 29
Average NN Distance July 3: 5.5m

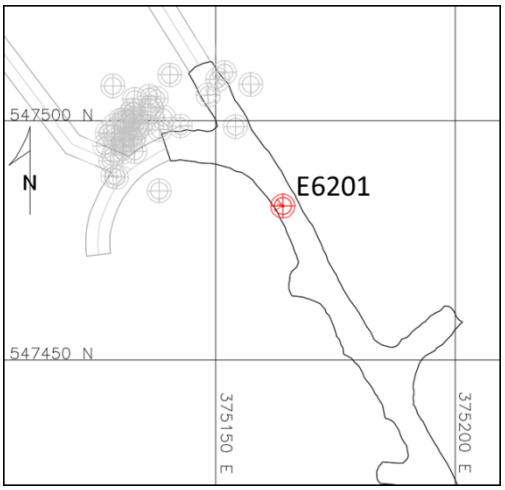

Event 6201
July 9, 2005
Magnitude = -2.6
NN Distance = 28.2m
Events on July 9: 53
Average NN Distance July 9: 4.2m

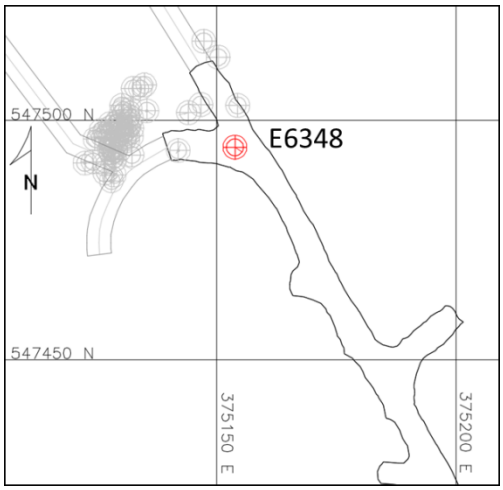

Event 6348
July 11, 2005
Magnitude = -2.7
NN Distance = 23.3m
Events on July 11: 60
Average NN Distance July 11: 3.4m

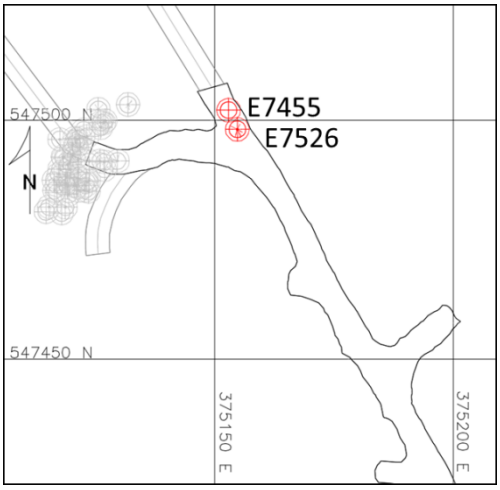

Event 7455 **Event 7526**
July 23, 2005
Mag = -2.8 M(R) = -2.5
NN Distance = 26.6m NN($_{dist}$)=24.1m
Events on July 23: 54
Average NN Distance July 23: 3.7m

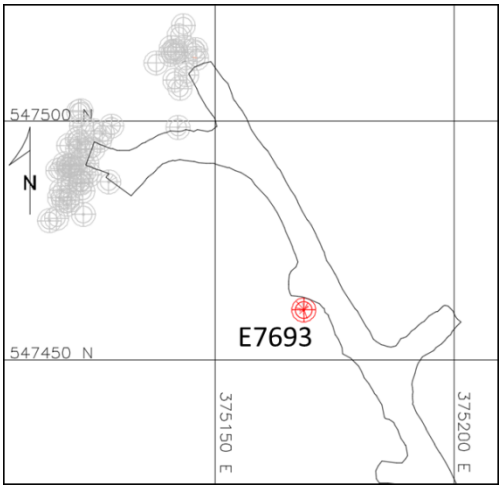

Event 7693
July 26, 2005
Magnitude = -2.7
NN Distance = 46.4m
Events on July 26: 64
Average NN Distance July 26: 3.8m

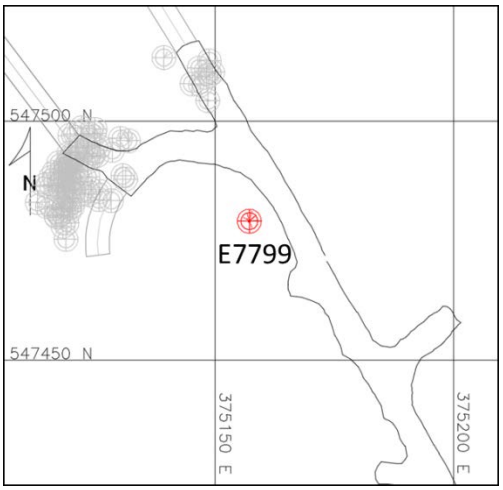

Event 7799
July 27, 2005
Magnitude = -2.2
NN Distance = 27.5m
Events on July 27: 99
Average NN Distance July 27: 3.0m

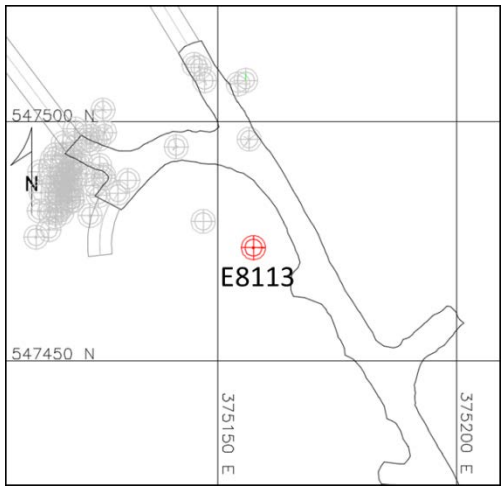

Event 8113
July 28, 2005
Magnitude = -2.5
NN Distance = 26.8m
Events on July 27: 79
Average NN Distance July 27: 3.8m

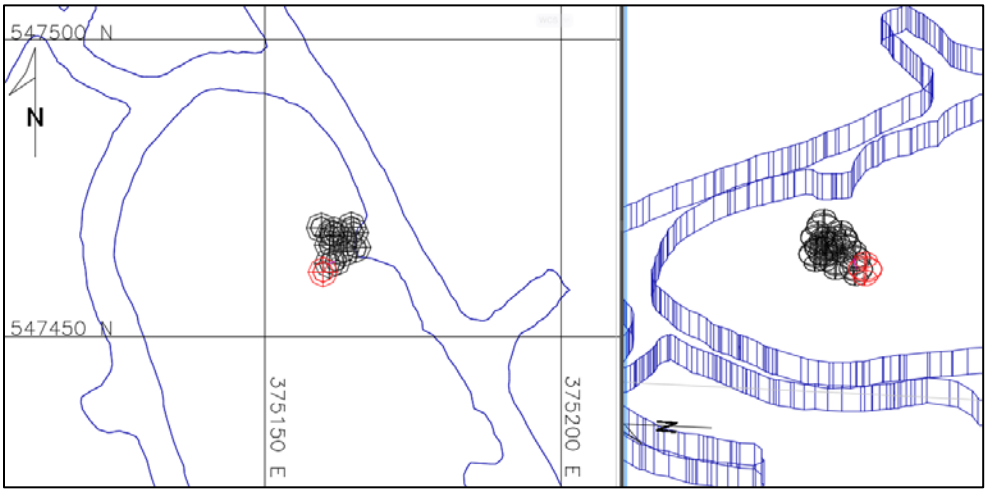

Figure 102: The proximity test identified Event 5812 (red) is one of fourteen events (black) in C1239. C1239 is located just below the safety bay and is more than 2.42 metres away from the main ramp cluster (C263). This cluster could be a small geological structure just below the ramp or a change in rock type.

Appendix II
Cluster Sizes in a Failing Pillar

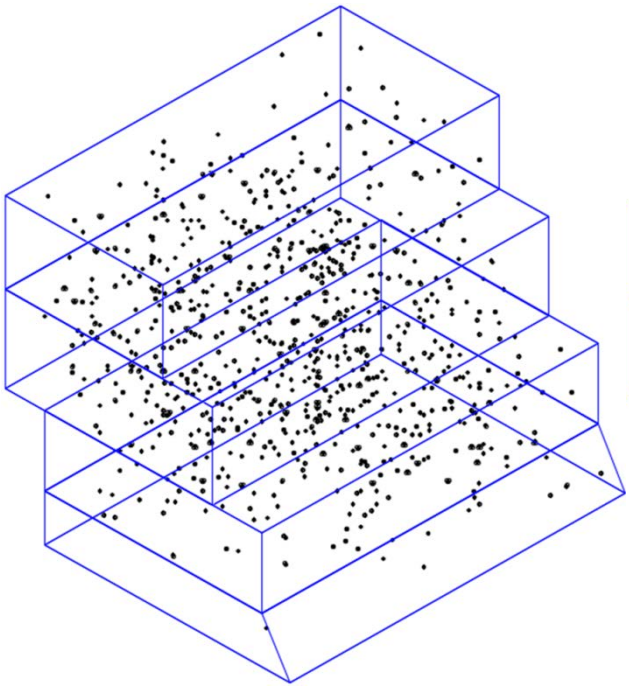

Single Events

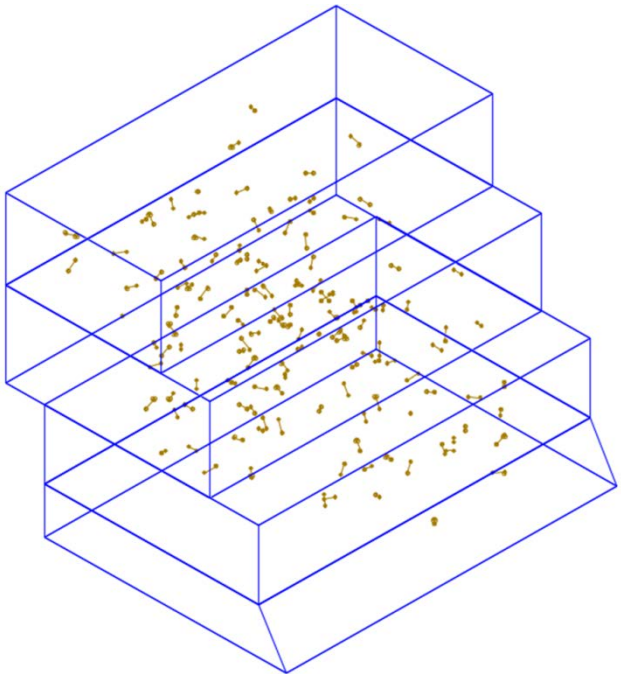

2 Event Clusters

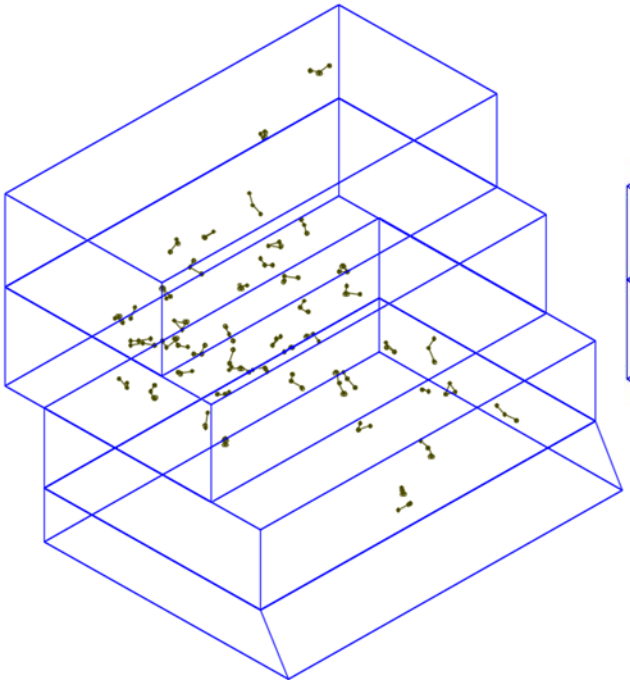

3 Event Clusters

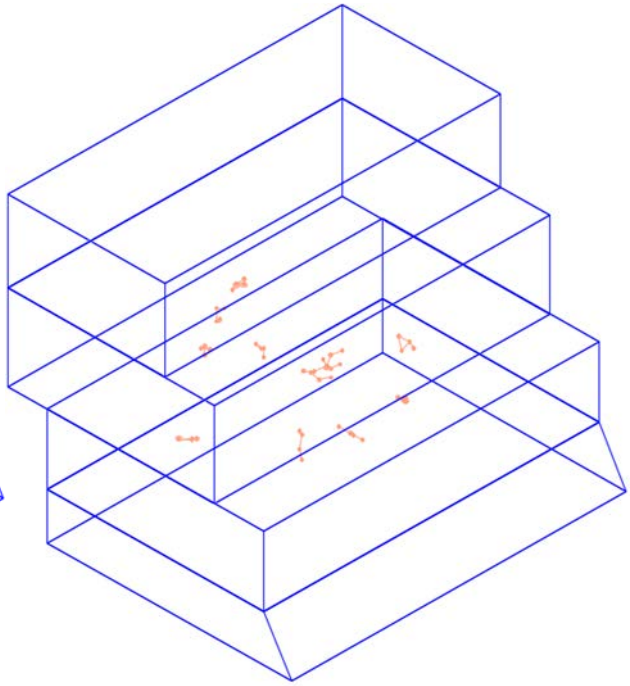

4 Event Clusters

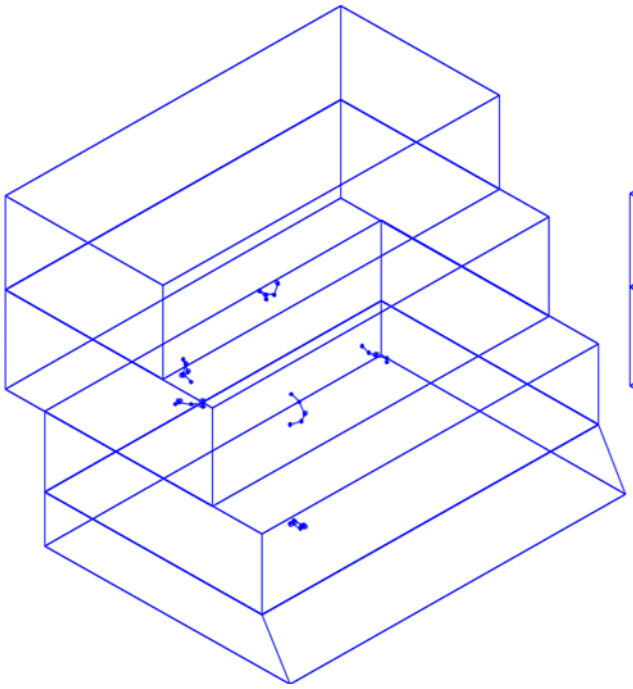

5 Event Clusters

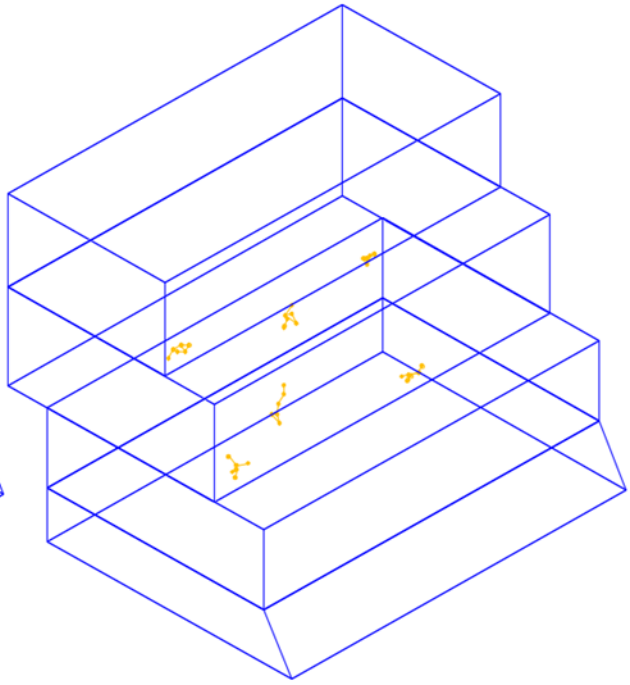

6 Event Clusters

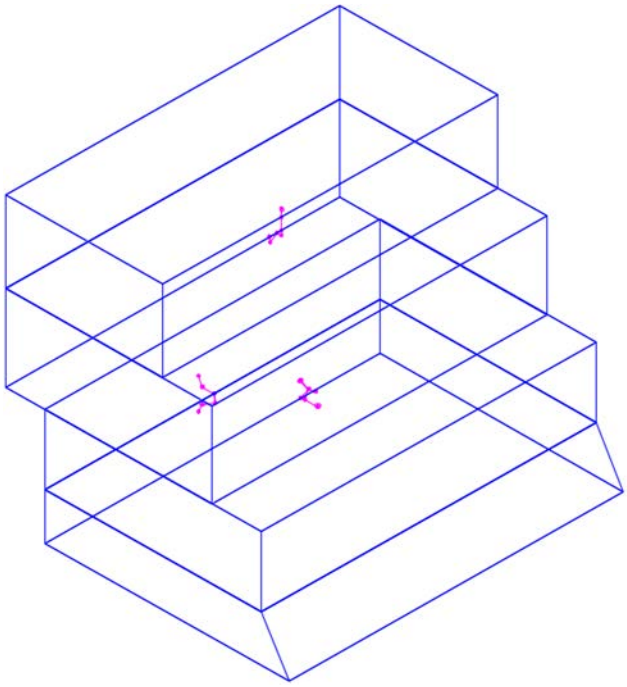

7 Event Clusters

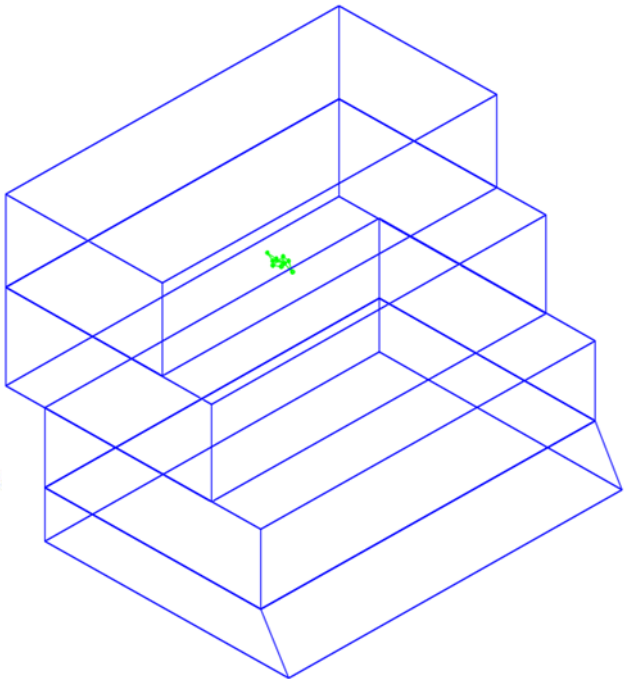

9 Event Cluster

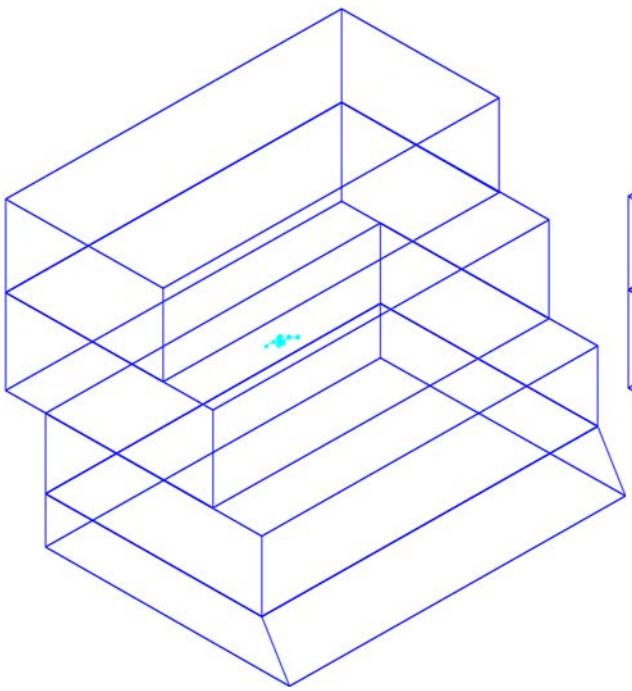

10 Event Cluster

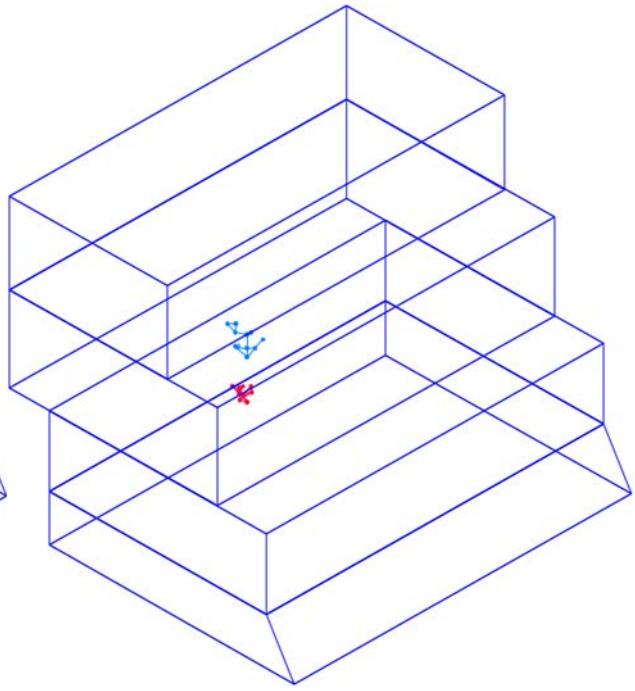

11 Event Clusters

Appendix III
Probability of Nearest Neighbour Distances

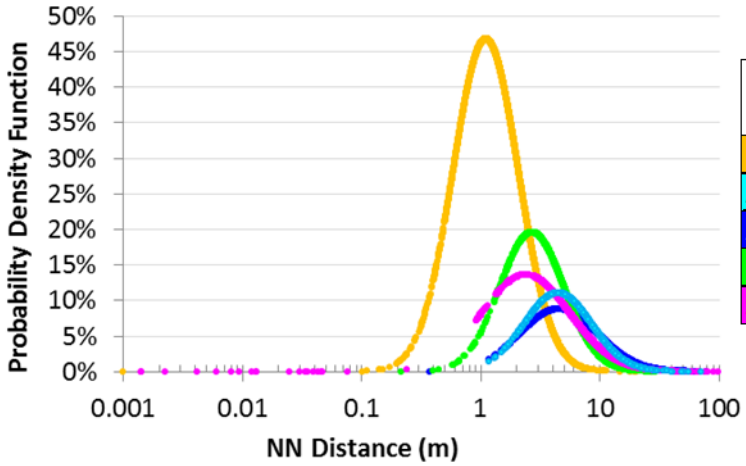

Case	# Events	NN Distance (m)	
		Mode	Mean
Ramp	3704	1.1	1.7
Abutment	710	4.5	6.8
Abutment	1350	4.5	8.0
Pillar	1368	2.7	4.0
Shear	4548	2.4	4.9

Figure 98 (previously shown)

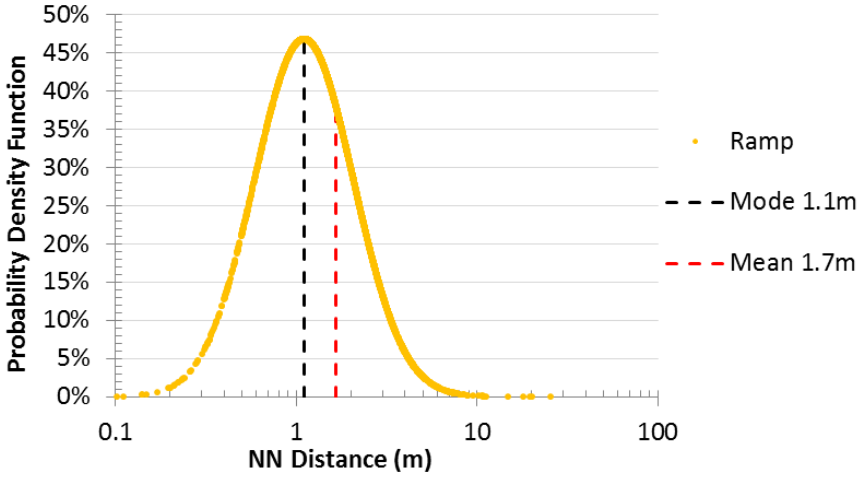

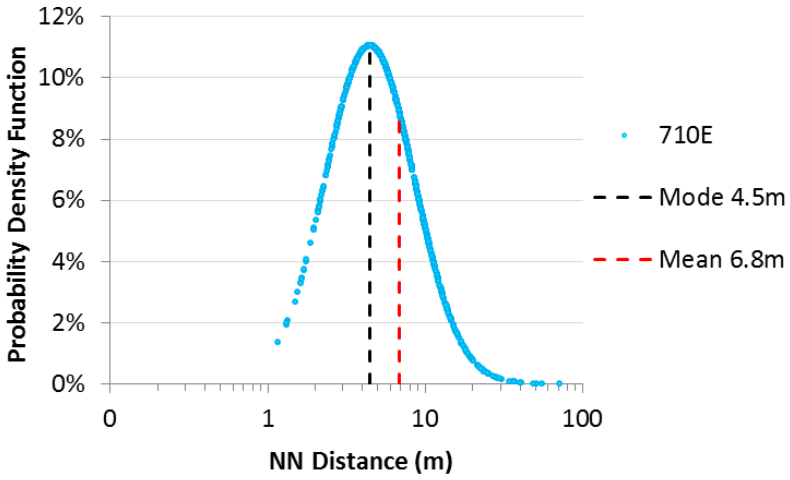
12%
10%
8%
6%
4%
2%
0%
Probability Density Function
0
1
10
100
NN Distance (m)
710E
Mode 4.5m
Mean 6.8m

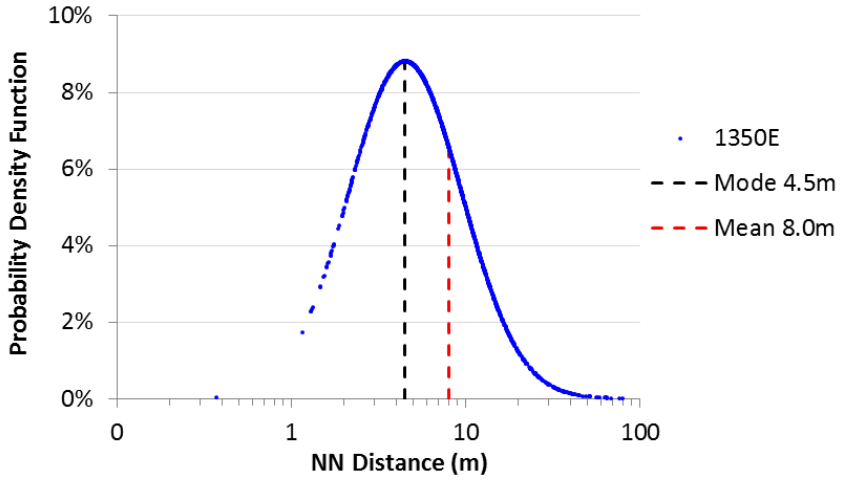
10%
8%
6%
4%
2%
0%
Probability Density Function
0
1
10
100
NN Distance (m)
1350E
Mode 4.5m
Mean 8.0m

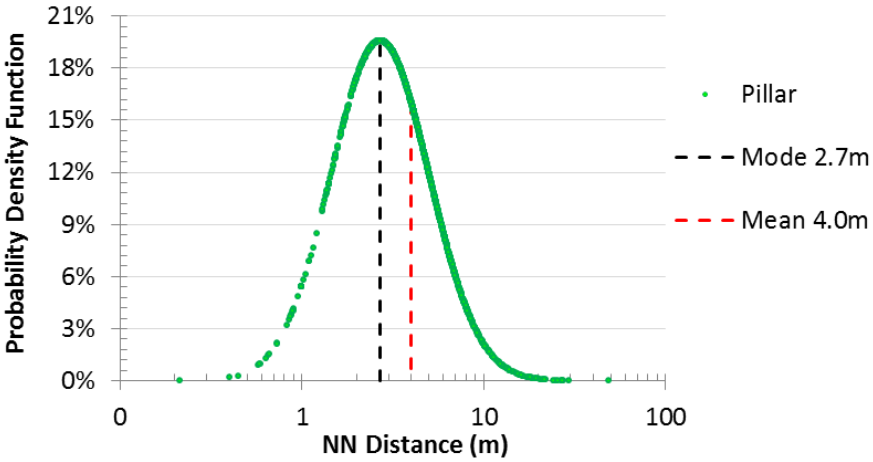
21%
18%
15%
12%
9%
6%
3%
0%
Probability Density Function
0
1
10
100
NN Distance (m)
Pillar
Mode 2.7m
Mean 4.0m

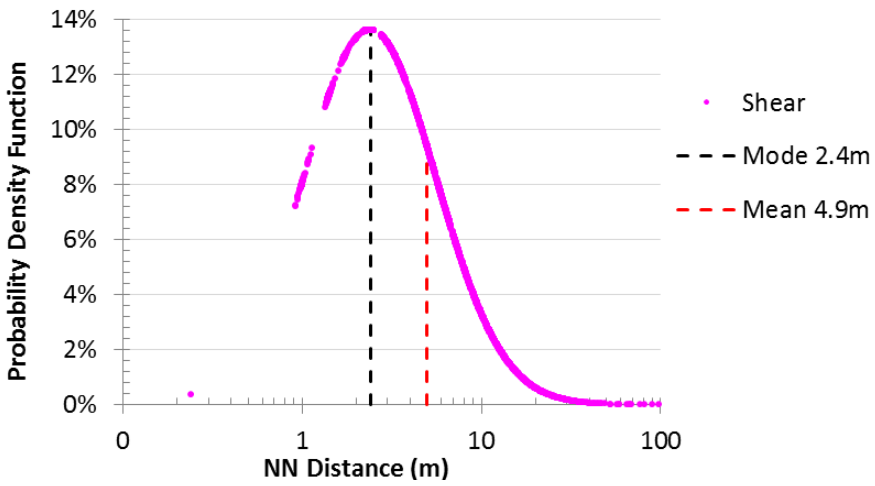
14%
12%
10%
8%
6%
4%
2%
0%
Probability Density Function
0
1
10
100
NN Distance (m)
Shear
Mode 2.4m
Mean 4.9m

Appendix IV
Ramp – Fractal Dimension of NN Distances by Magnitude Range

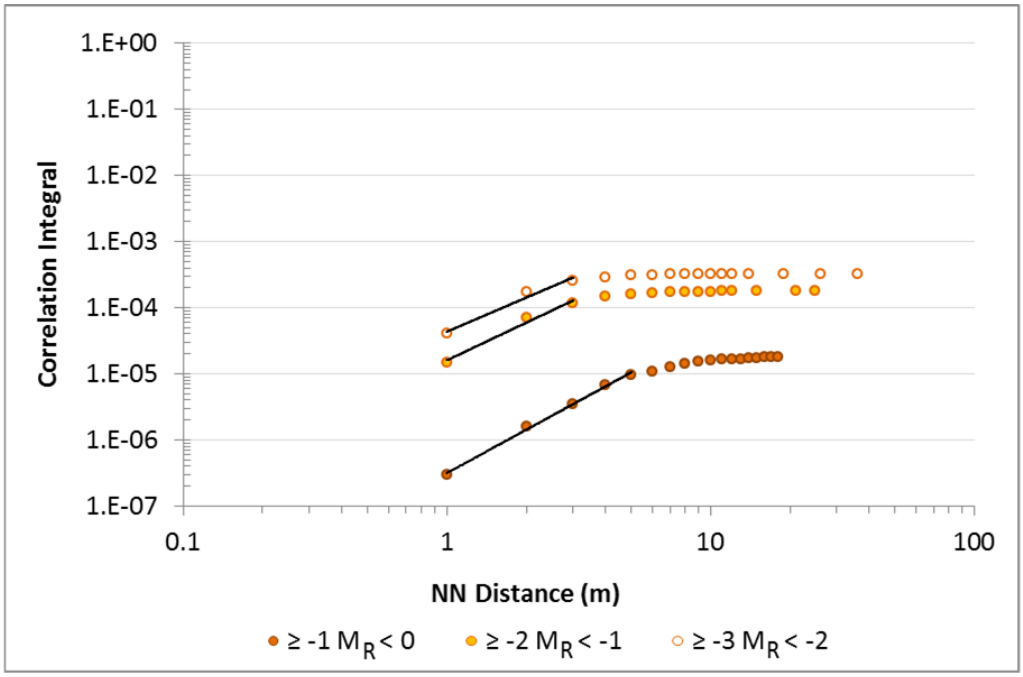

Mag R Range	FD	R^2	NN (m) Range		Max
-1 to 0	2.18	99.6%	1	5	18
-2 to -1	1.71	96.8%	1	3	25
-3 to -2	1.71	96.8%	1	3	36

Figure 55 (previously shown)

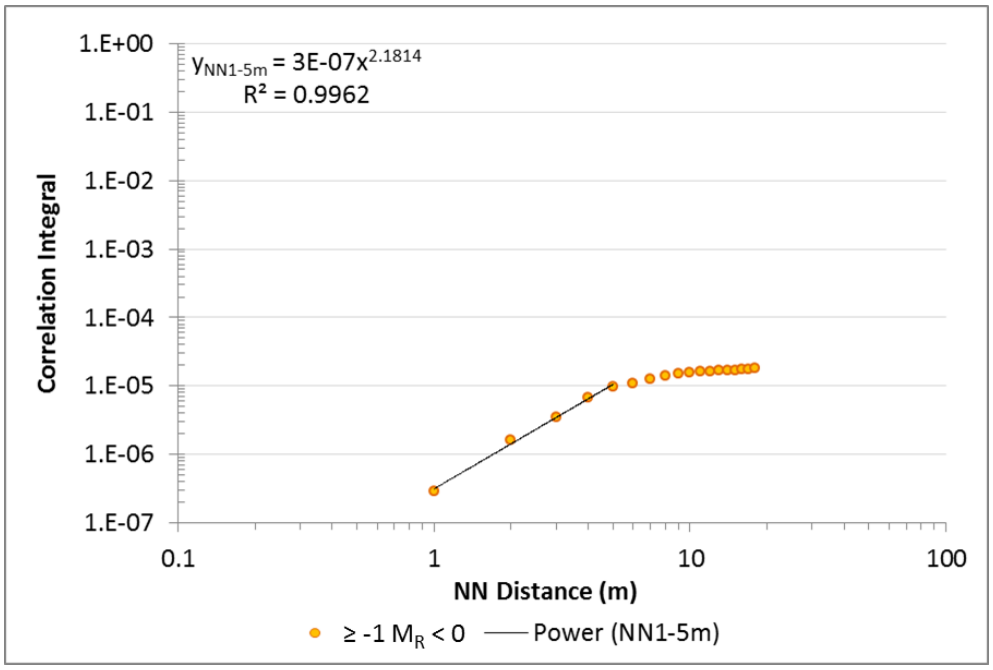
$y_{NN1-5m} = 3E-07x^{2.1814}$
$R^2 = 0.9962$
1.E+00
1.E-01
1.E-02
1.E-03
1.E-04
1.E-05
1.E-06
1.E-07
Correlation Integral
0.1
1
10
100
NN Distance (m)
≥ -1 M_R < 0
Power (NN1-5m)

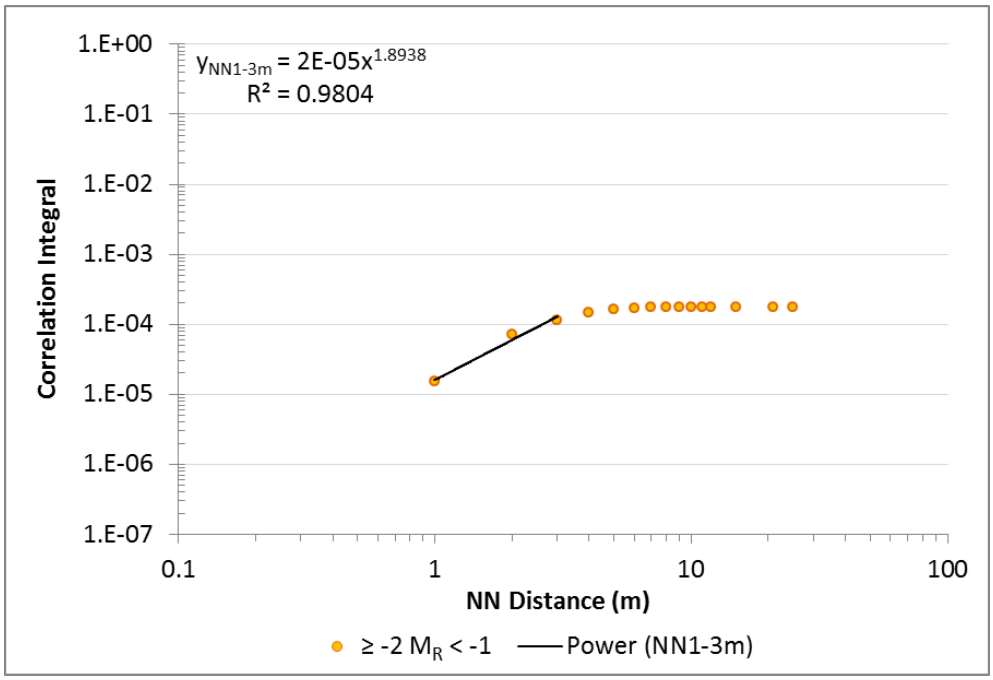
$y_{NN1-3m} = 2E-05x^{1.8938}$
$R^2 = 0.9804$
1.E+00
1.E-01
1.E-02
1.E-03
1.E-04
1.E-05
1.E-06
1.E-07
Correlation Integral
0.1
1
10
100
NN Distance (m)
≥ -2 M_R < -1
Power (NN1-3m)

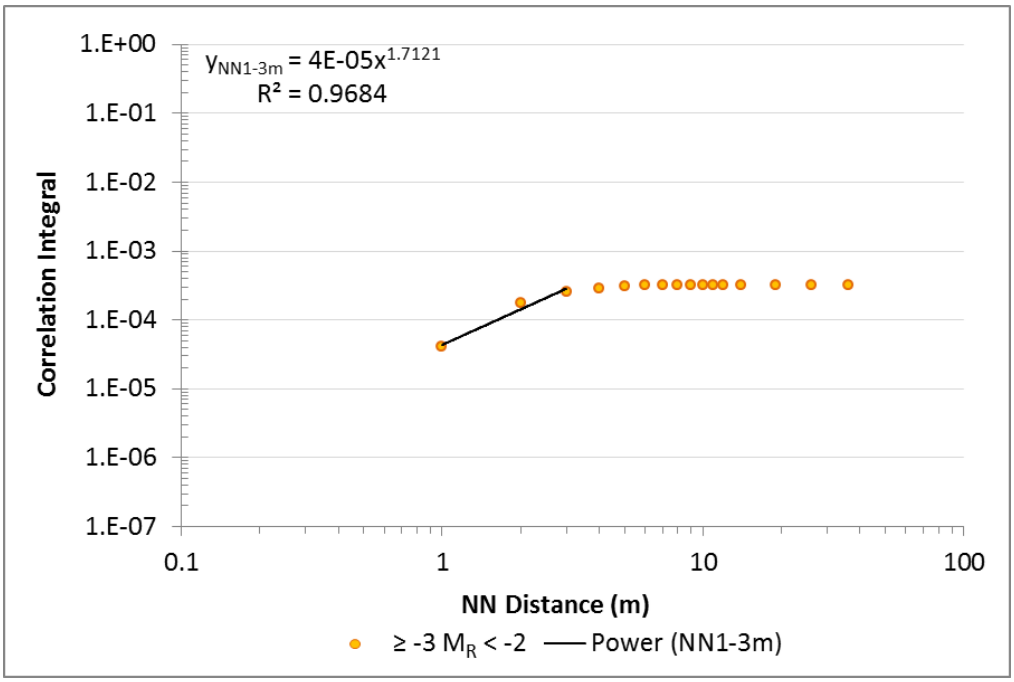
$y_{NN1-3m} = 4E-05x^{1.7121}$
$R^2 = 0.9684$
1.E+00
1.E-01
1.E-02
1.E-03
1.E-04
1.E-05
1.E-06
1.E-07
Correlation Integral
0.1
1
10
100
NN Distance (m)
≥ -3 M_R < -2
Power (NN1-3m)

Appendix V
Ramp – Fractal Dimension of Time Between NN by Magnitude Range

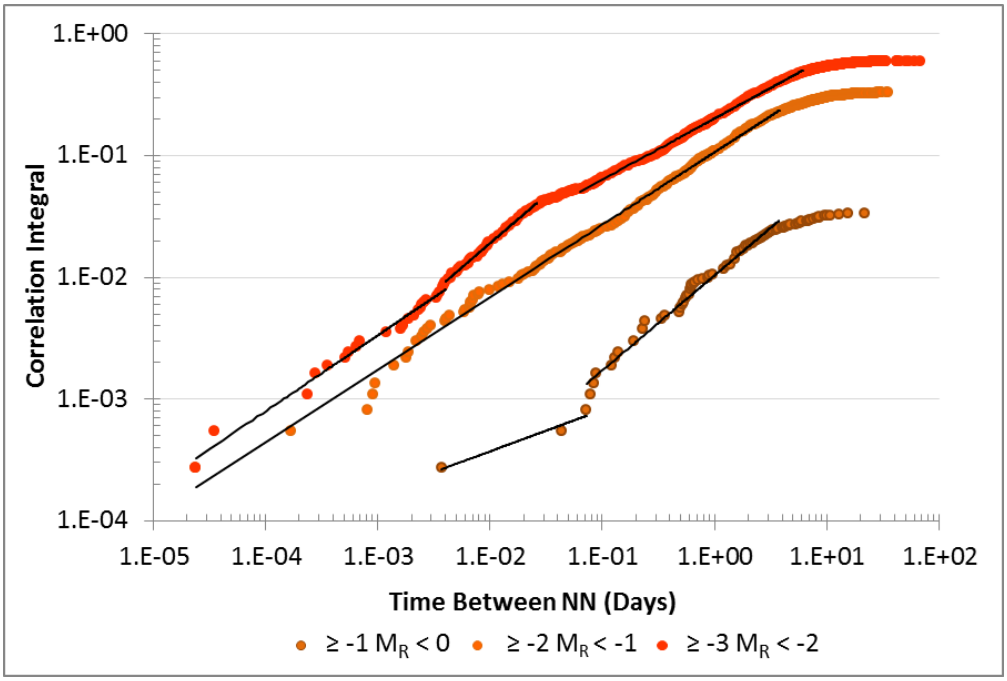

Magnitude Range	FD	R^2	Time Period	Max
0 to -1	0.34	95.32	5.3 min to 1.7 hrs	21.6 days
	0.78	98.26	1.7 hrs to 6.8 days	
-1 to -2	0.59	99.56	14.7sec to 3.8 days	35.4 days
-2 to -3	0.62	98.36	2 sec to 6.2 min	68.1 days
	0.79	99.72	6.2 to 37.4 min	
	0.50	99.80	1.5 hr to 6.7 days	

Figure 57 (previously shown)

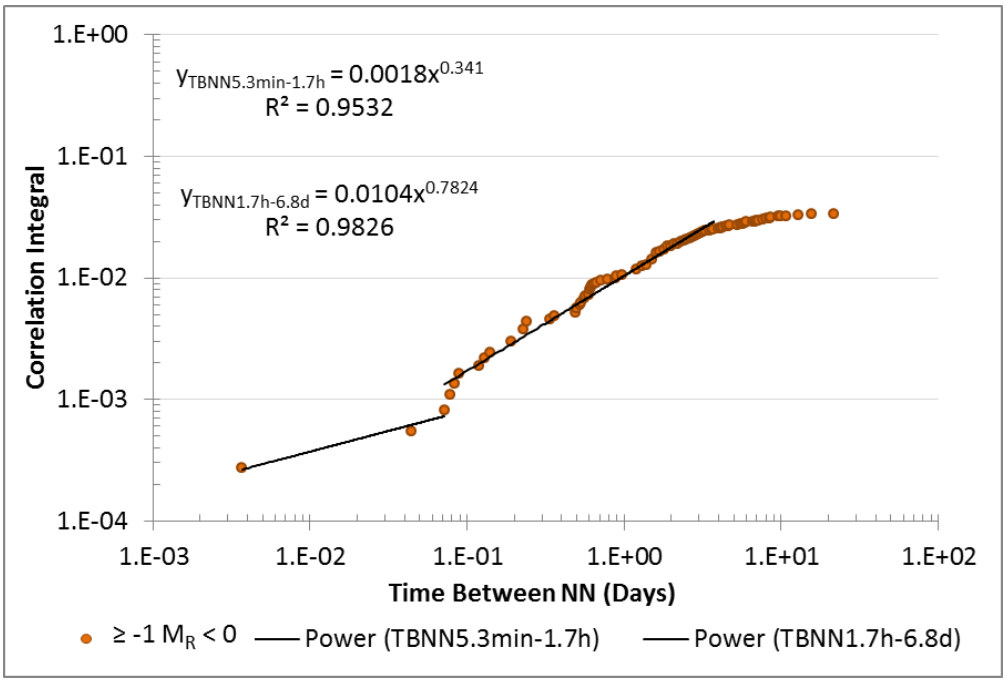
1.E+00
1.E-01
1.E-02
1.E-03
1.E-04
Correlation Integral
$y_{TBNN5.3min-1.7h} = 0.0018x^{0.341}$
$R^2 = 0.9532$
$y_{TBNN1.7h-6.8d} = 0.0104x^{0.7824}$
$R^2 = 0.9826$
1.E-03
1.E-02
1.E-01
1.E+00
1.E+01
1.E+02
Time Between NN (Days)
≥ -1 M_R < 0
Power (TBNN5.3min-1.7h)
Power (TBNN1.7h-6.8d)

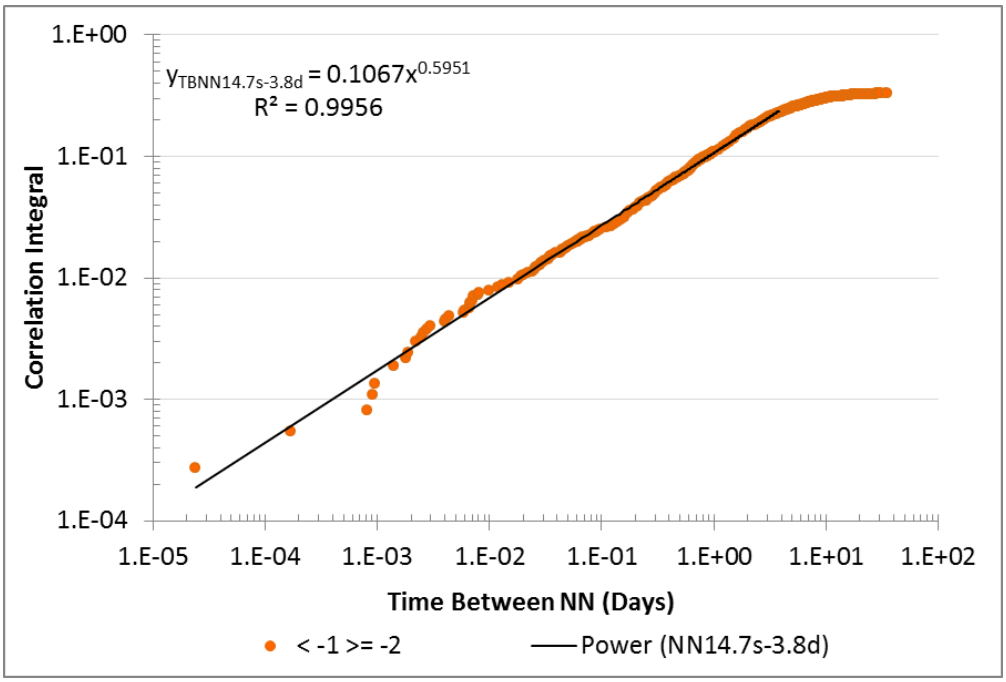
1.E+00
1.E-01
1.E-02
1.E-03
1.E-04
Correlation Integral
$y_{TBNN14.7s-3.8d} = 0.1067x^{0.5951}$
$R^2 = 0.9956$
1.E-05
1.E-04
1.E-03
1.E-02
1.E-01
1.E+00
1.E+01
1.E+02
Time Between NN (Days)
< -1 >= -2
Power (NN14.7s-3.8d)

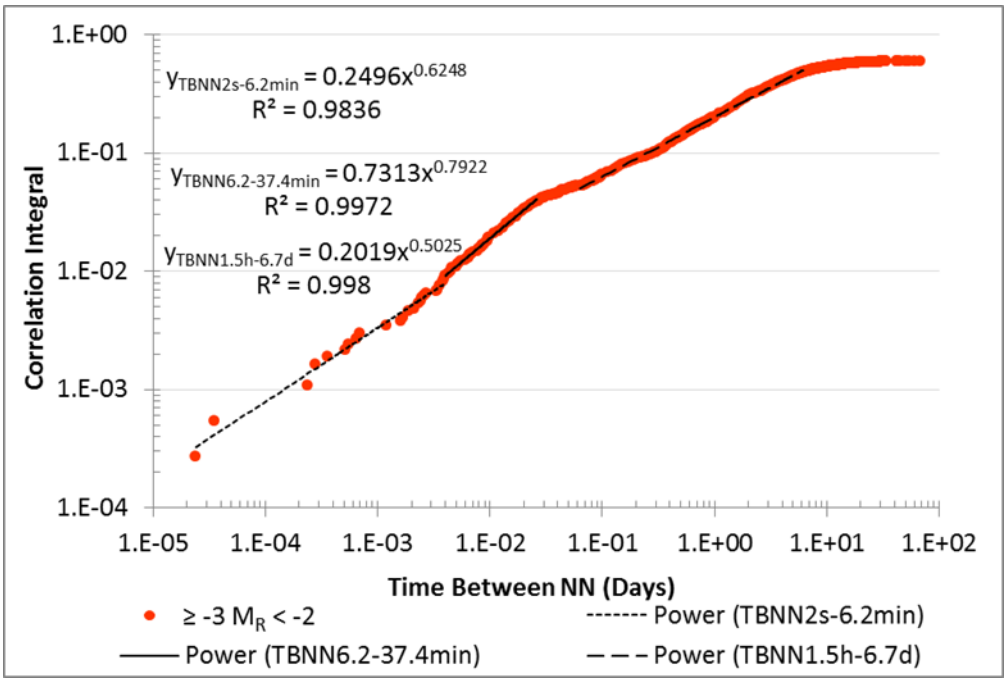
1.E+00
1.E-01
1.E-02
1.E-03
1.E-04
Correlation Integral
$y_{TBNN2s-6.2min} = 0.2496x^{0.6248}$
$R^2 = 0.9836$
$y_{TBNN6.2-37.4min} = 0.7313x^{0.7922}$
$R^2 = 0.9972$
$y_{TBNN1.5h-6.7d} = 0.2019x^{0.5025}$
$R^2 = 0.998$
1.E-05
1.E-04
1.E-03
1.E-02
1.E-01
1.E+00
1.E+01
1.E+02
Time Between NN (Days)
≥ -3 M_R < -2
Power (TBNN2s-6.2min)
Power (TBNN6.2-37.4min)
Power (TBNN1.5h-6.7d)

Appendix VI
Abutment 1350E – Fractal Dimension of NN Distances by Magnitude Range

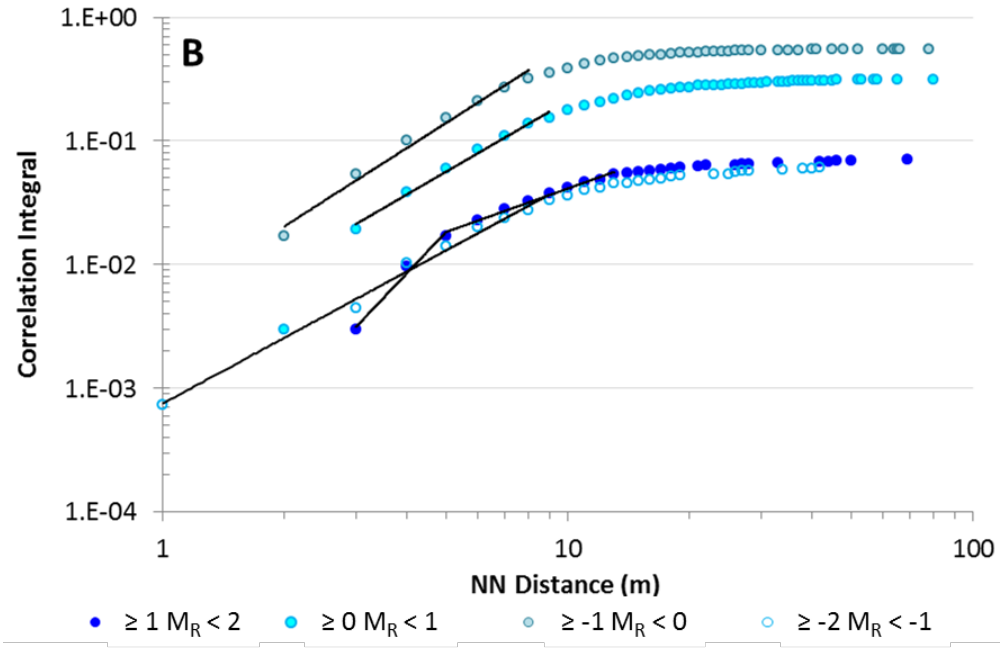

1350 Events						
Mag R Range	FD	R^2	NN (m) Range		Max	# NN
1 to 2	3.46	98.4%	3	5	69	95
	1.17	98.8%	5	13	69	95
0 to 1	1.90	99.0%	3	9	119	427
-1 to 0	2.09	98.4%	2	8	125	745
-2 to -1	1.77	99.2%	1	9	42	82

Figure 71: Image B (previously shown)

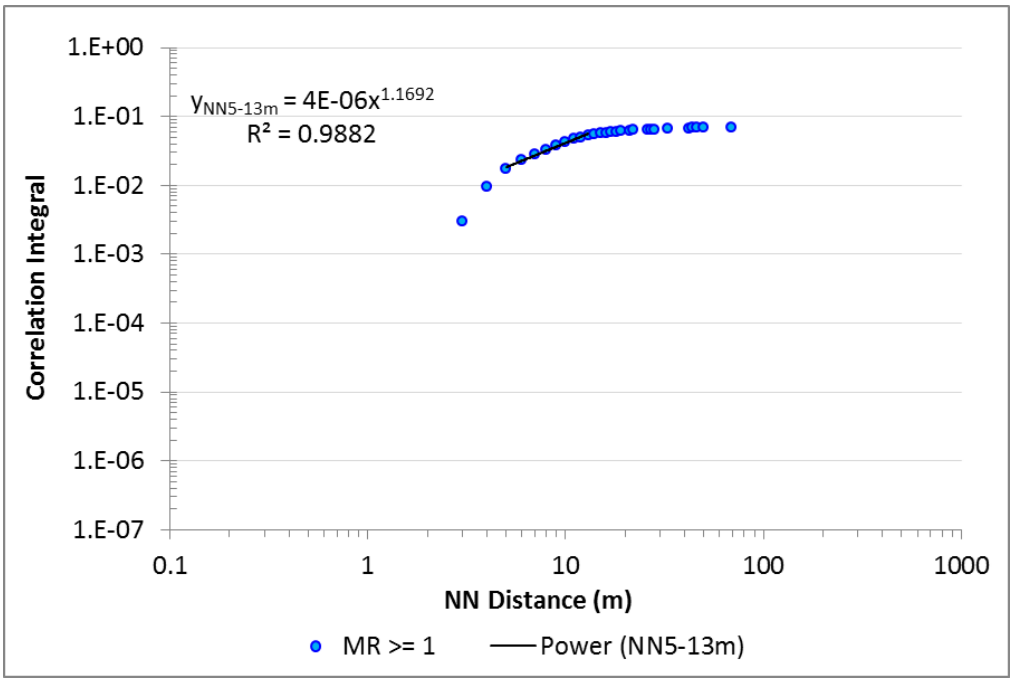
1.E+00
1.E-01
1.E-02
1.E-03
1.E-04
1.E-05
1.E-06
1.E-07
Correlation Integral
$y_{NN5-13m} = 4E-06x^{1.1692}$
$R^2 = 0.9882$
0.1
1
10
100
1000
NN Distance (m)
MR >= 1
Power (NN5-13m)

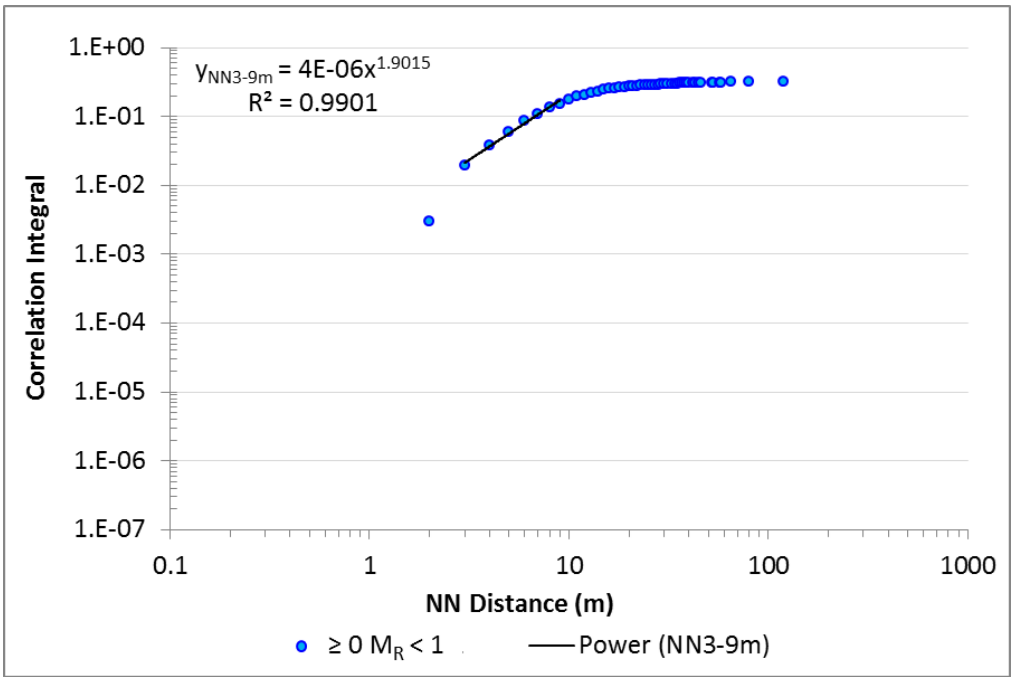
1.E+00
1.E-01
1.E-02
1.E-03
1.E-04
1.E-05
1.E-06
1.E-07
Correlation Integral
$y_{NN3-9m} = 4E-06x^{1.9015}$
$R^2 = 0.9901$
0.1
1
10
100
1000
NN Distance (m)
≥ 0 M_R < 1
Power (NN3-9m)

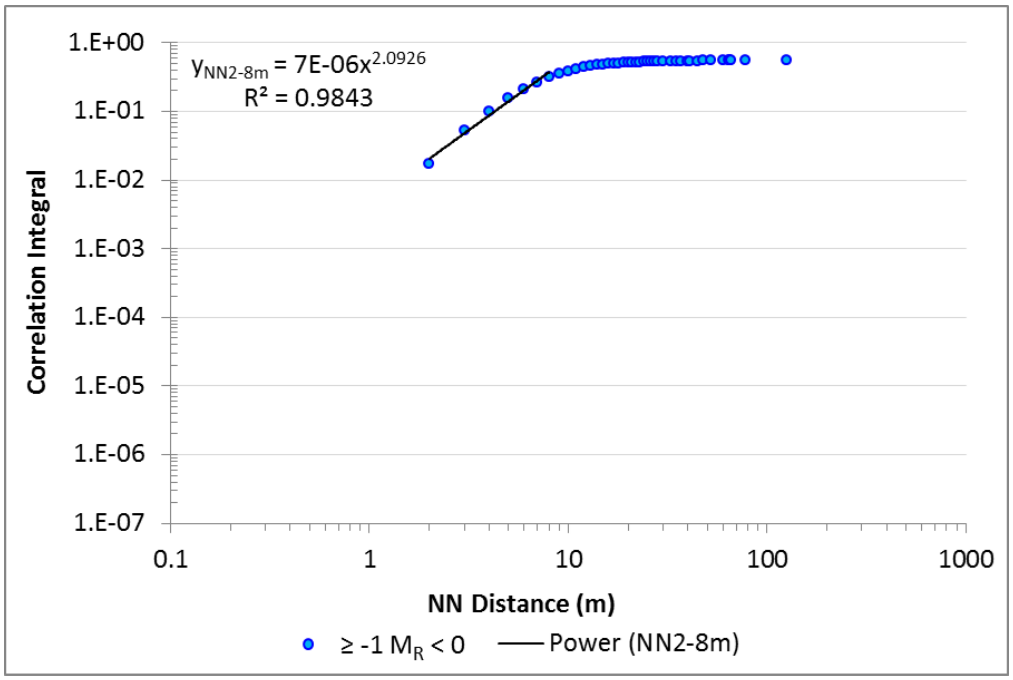
y_{NN2-8m} = 7E-06$x^{2.0926}$
R^2 = 0.9843
Correlation Integral
1.E+00
1.E-01
1.E-02
1.E-03
1.E-04
1.E-05
1.E-06
1.E-07
0.1
1
10
100
1000
NN Distance (m)
≥ -1 M_R < 0
Power (NN2-8m)

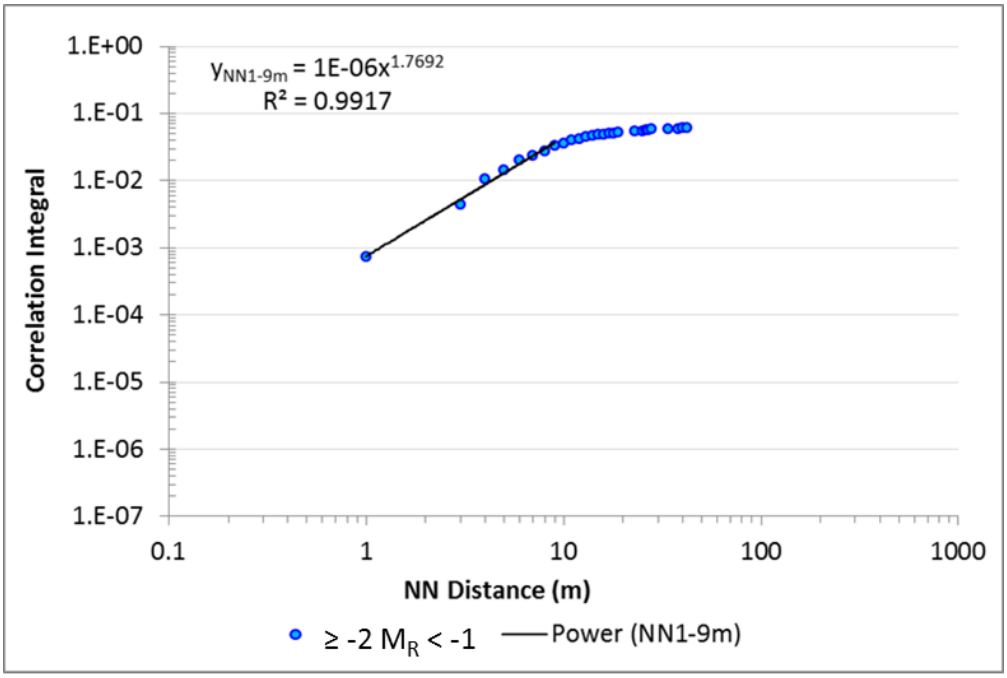
y_{NN1-9m} = 1E-06$x^{1.7692}$
R^2 = 0.9917
Correlation Integral
1.E+00
1.E-01
1.E-02
1.E-03
1.E-04
1.E-05
1.E-06
1.E-07
0.1
1
10
100
1000
NN Distance (m)
≥ -2 M_R < -1
Power (NN1-9m)

Appendix VII
Abutment 710E – Fractal Dimension of NN Distances by Magnitude Range

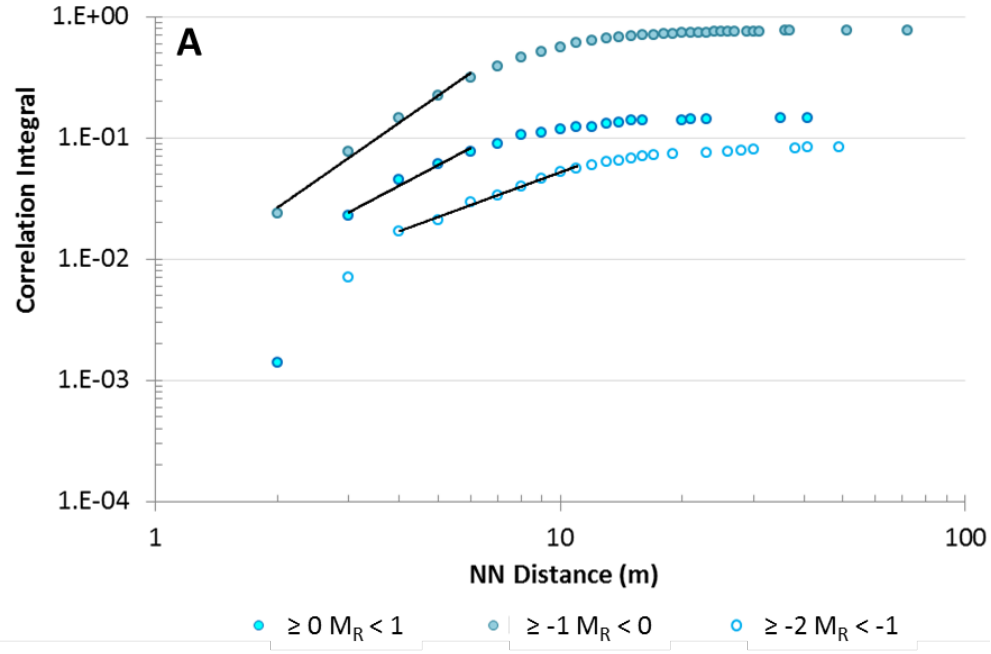

710 Events					
Mag R Range	FD	R^2	NN (m) Range		Max
>1	-	-	-	-	-
0 to 1	1.76	97.4%	3	6	29
-1 to 0	2.33	99.0%	2	6	72
-2 to -1	1.22	99.4%	4	11	49

Figure 71: Image A (previously shown)

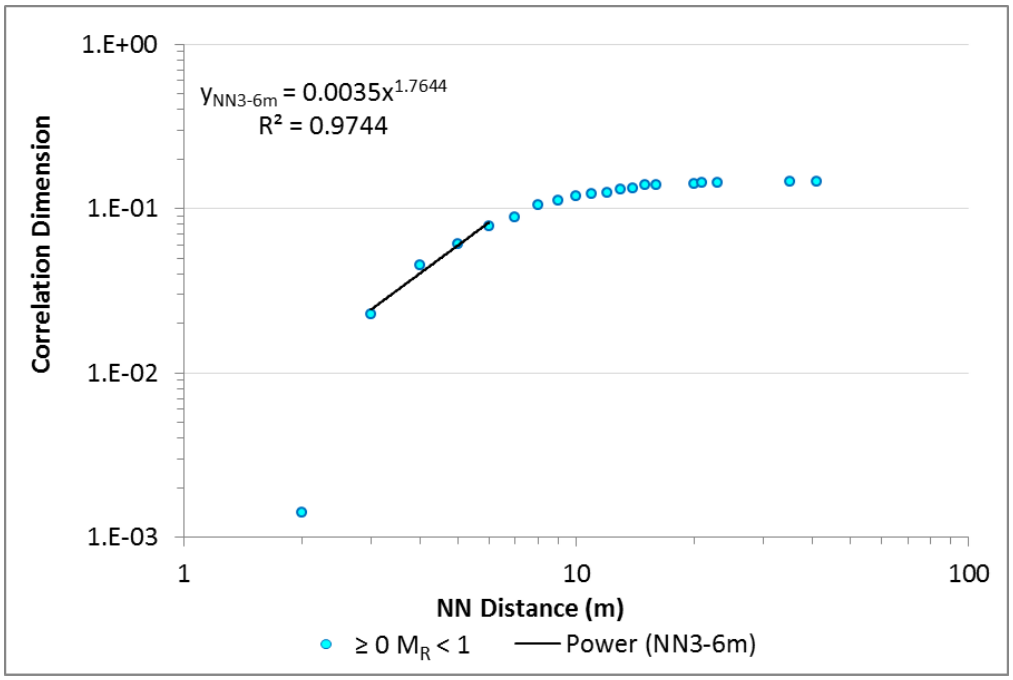
1.E+00
1.E-01
1.E-02
1.E-03
Correlation Dimension
$y_{NN3-6m} = 0.0035x^{1.7644}$
$R^2 = 0.9744$
1
10
100
NN Distance (m)
≥ 0 M_R < 1
Power (NN3-6m)

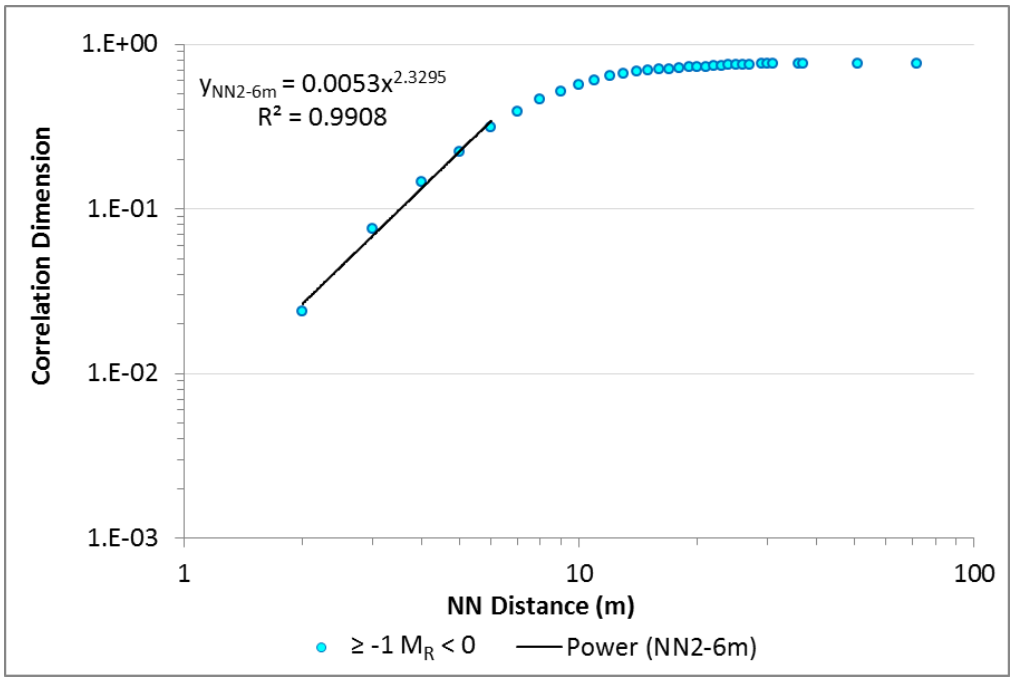
1.E+00
1.E-01
1.E-02
1.E-03
Correlation Dimension
$y_{NN2-6m} = 0.0053x^{2.3295}$
$R^2 = 0.9908$
1
10
100
NN Distance (m)
≥ -1 M_R < 0
Power (NN2-6m)

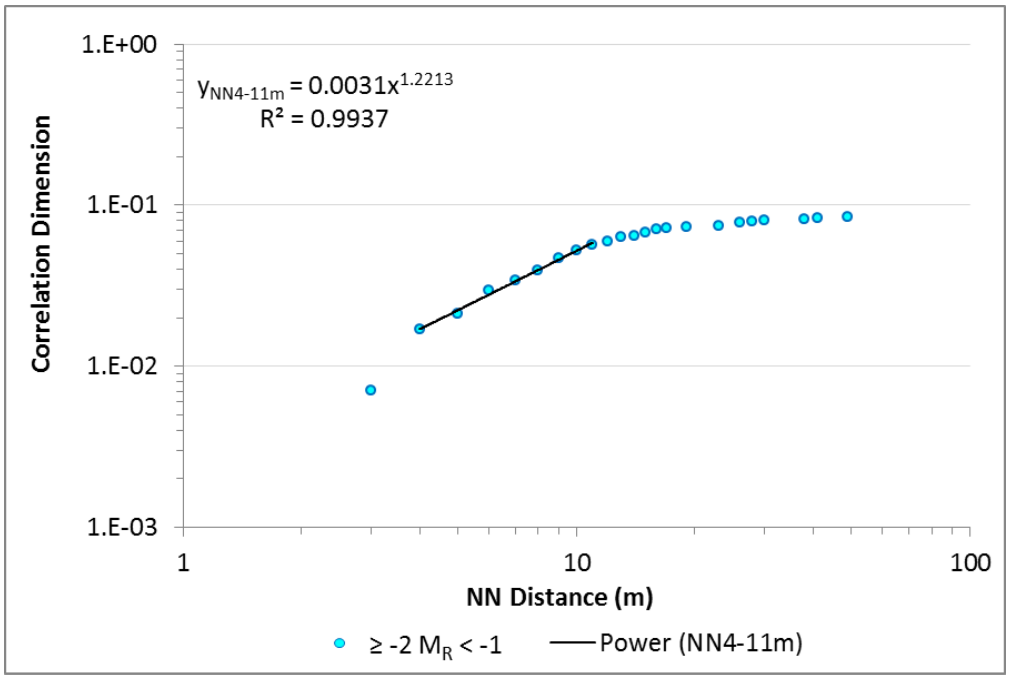
1.E+00
1.E-01
1.E-02
1.E-03
Correlation Dimension
$y_{NN4-11m} = 0.0031x^{1.2213}$
$R^2 = 0.9937$
1
10
100
NN Distance (m)
≥ -2 M_R < -1
Power (NN4-11m)

Appendix VIII
Abutment 1350E - FD of Time Between NN by Magnitude Range

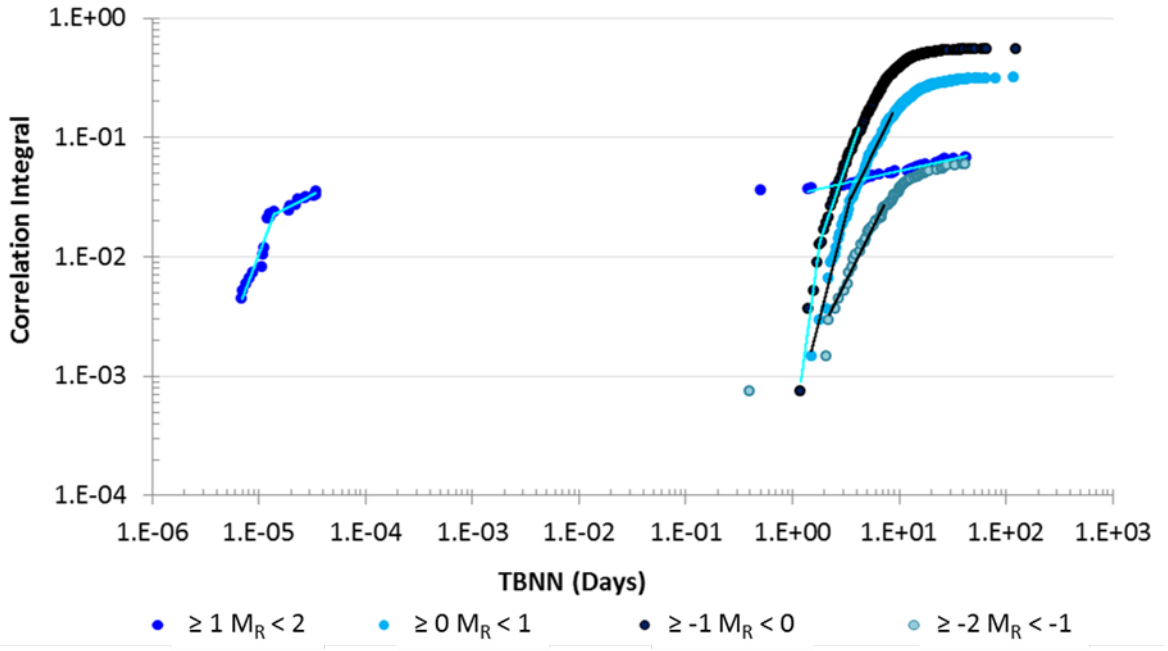

Magnitude Range	FD	R^2	TBNN Range	TBNN Max(d)
1 to 2	2.03	99.9%	0.6-0.8s	64
	0.19	97.9%	1.3-63.5d	
0 to 1	3.52	97.5%	1.5-3.5d	119
	1.83	99.4%	3.5-8.7d	
-1 to 0	6.59	95.5%	1.2-1.8d	125
	2.60	99.3%	1.8-4.2d	
-2 to -1	1.79	97.8%	2.2-7.2d	41

Figure 73 (previously shown)

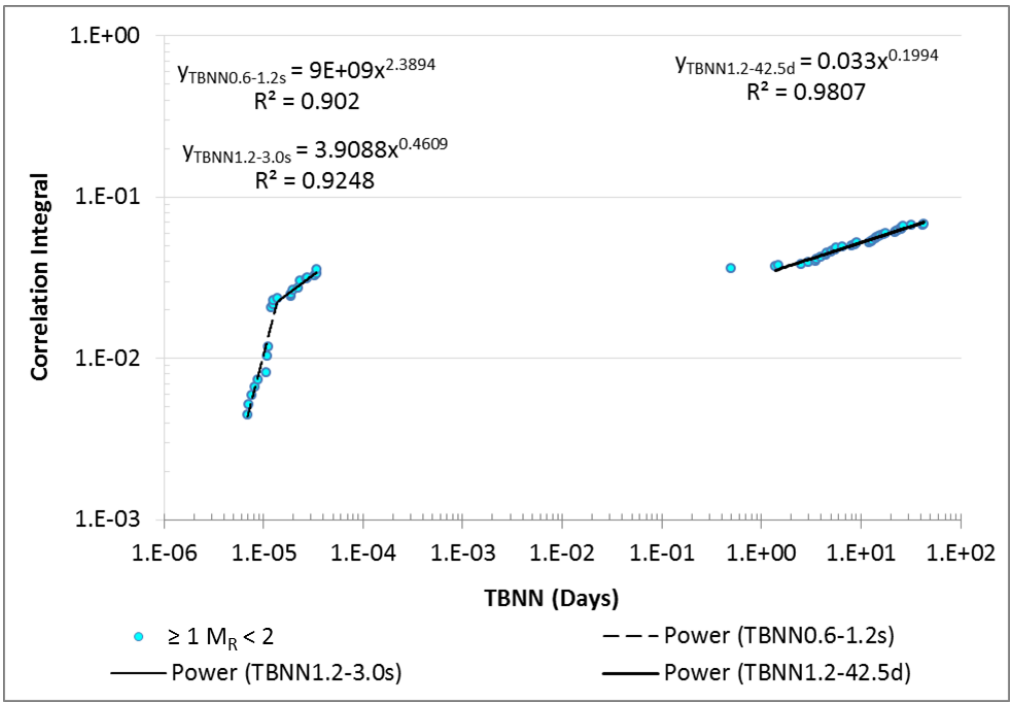
1.E+00
1.E-01
1.E-02
1.E-03
Correlation Integral
$y_{TBNN0.6-1.2s} = 9E+09x^{2.3894}$
$R^2 = 0.902$
$y_{TBNN1.2-3.0s} = 3.9088x^{0.4609}$
$R^2 = 0.9248$
$y_{TBNN1.2-42.5d} = 0.033x^{0.1994}$
$R^2 = 0.9807$
1.E-06
1.E-05
1.E-04
1.E-03
1.E-02
1.E-01
1.E+00
1.E+01
1.E+02
TBNN (Days)
≥ 1 M_R < 2
Power (TBNN0.6-1.2s)
Power (TBNN1.2-3.0s)
Power (TBNN1.2-42.5d)

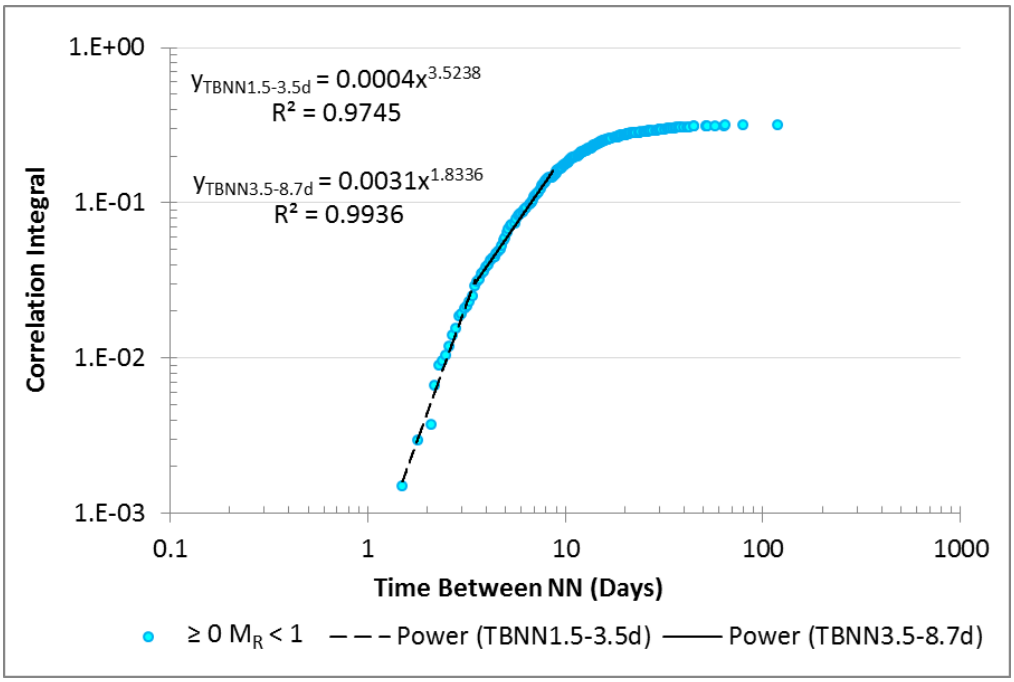
1.E+00
1.E-01
1.E-02
1.E-03
Correlation Integral
$y_{TBNN1.5-3.5d} = 0.0004x^{3.5238}$
$R^2 = 0.9745$
$y_{TBNN3.5-8.7d} = 0.0031x^{1.8336}$
$R^2 = 0.9936$
0.1
1
10
100
1000
Time Between NN (Days)
≥ 0 M_R < 1
Power (TBNN1.5-3.5d)
Power (TBNN3.5-8.7d)

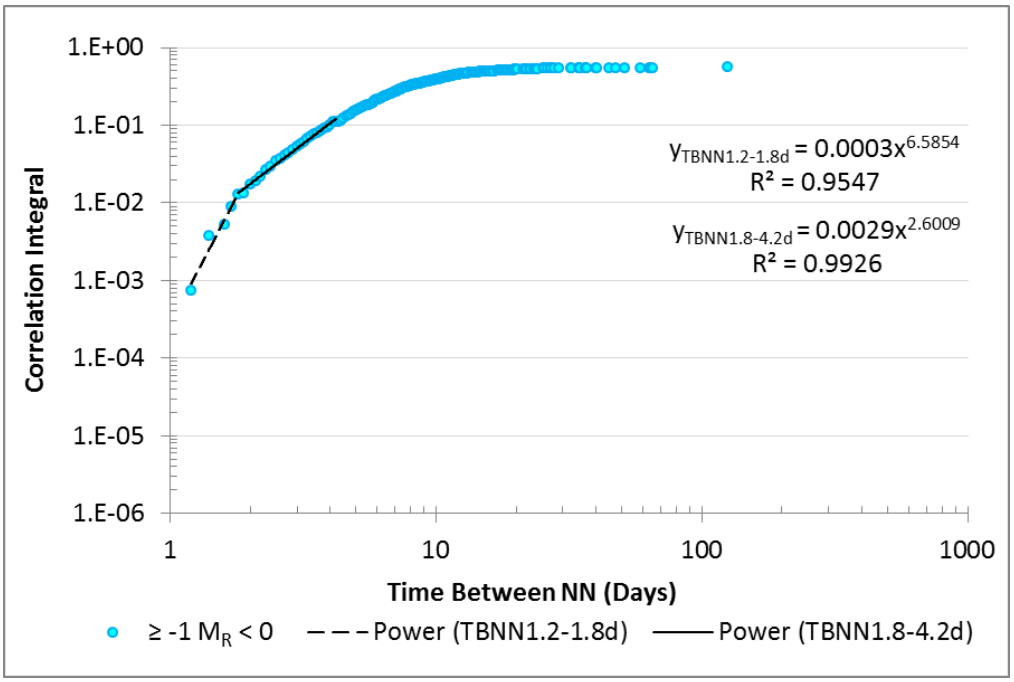
1.E+00
1.E-01
1.E-02
1.E-03
1.E-04
1.E-05
1.E-06
Correlation Integral
1
10
100
1000
Time Between NN (Days)
$y_{TBNN1.2-1.8d} = 0.0003x^{6.5854}$
$R^2 = 0.9547$
$y_{TBNN1.8-4.2d} = 0.0029x^{2.6009}$
$R^2 = 0.9926$
≥ -1 M_R < 0
Power (TBNN1.2-1.8d)
Power (TBNN1.8-4.2d)

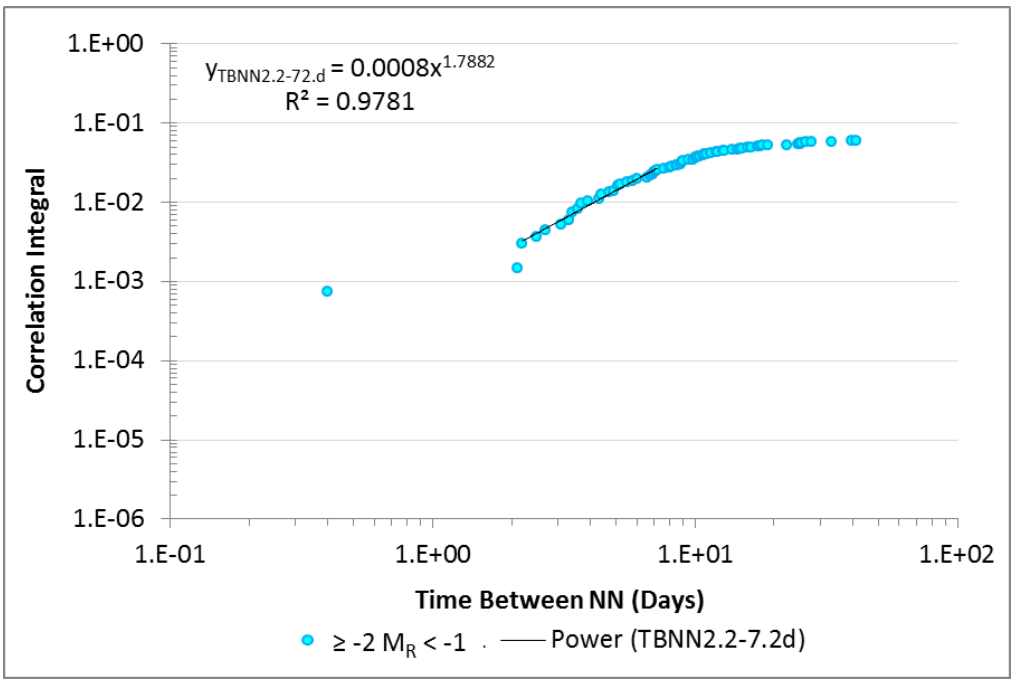
1.E+00
1.E-01
1.E-02
1.E-03
1.E-04
1.E-05
1.E-06
Correlation Integral
1.E-01
1.E+00
1.E+01
1.E+02
Time Between NN (Days)
$y_{TBNN2.2-72.d} = 0.0008x^{1.7882}$
$R^2 = 0.9781$
≥ -2 M_R < -1
Power (TBNN2.2-7.2d)

Appendix IX
Abutment 710E - FD of Time Between NN by Magnitude Range

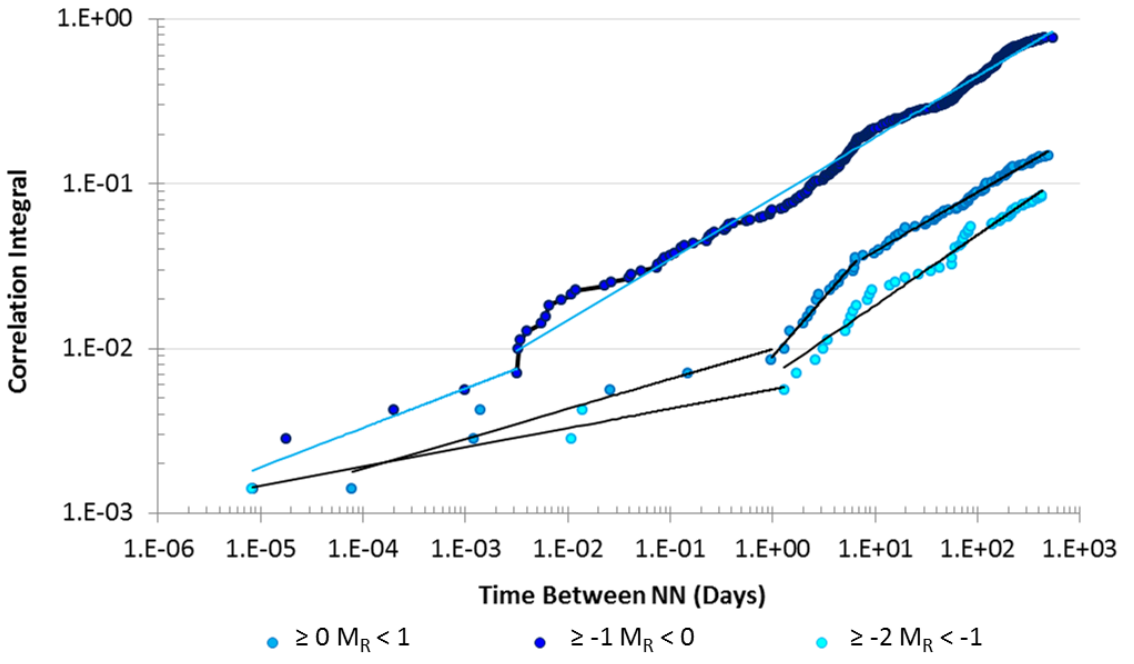

Magnitude Range	FD	R^2	TBNN Range	TBNN Max
>= 0 < 1	0.18	90.6%	6.8s-23.5h	489d (1.3y)
	0.71	98.2%	23.5h-6.5d	
	0.36	99.2%	7.6d-1.3y	
>= -1 < 0	0.24	91.2%	0.7s-4.6min	542d (1.5y)
	0.37	99.1%	4.6min-1.5y	
>= -2 < -1	0.12	93.2%	0.7s-1.3d	426d (1.2y)
	0.43	97.8%	1.3d-1.2y	

Figure 75 (previously shown)

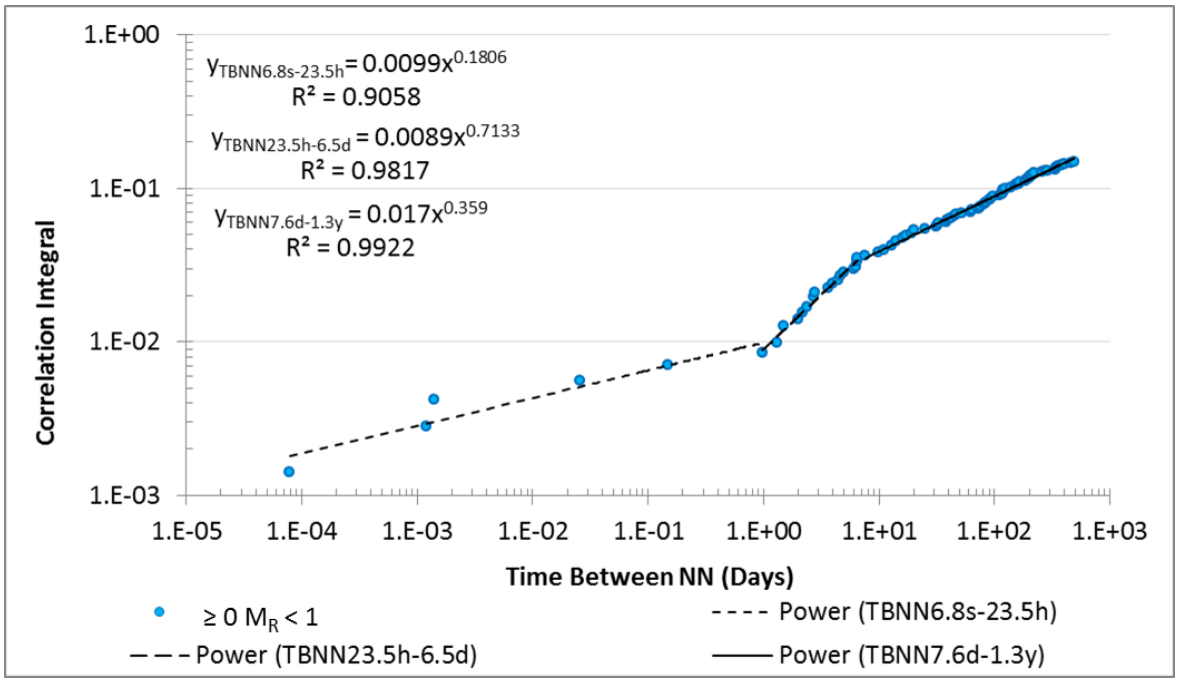
1.E+00
1.E-01
1.E-02
1.E-03
Correlation Integral
$y_{TBNN6.8s-23.5h} = 0.0099x^{0.1806}$
$R^2 = 0.9058$
$y_{TBNN23.5h-6.5d} = 0.0089x^{0.7133}$
$R^2 = 0.9817$
$y_{TBNN7.6d-1.3y} = 0.017x^{0.359}$
$R^2 = 0.9922$
1.E-05
1.E-04
1.E-03
1.E-02
1.E-01
1.E+00
1.E+01
1.E+02
1.E+03
Time Between NN (Days)
≥ 0 M_R < 1
Power (TBNN6.8s-23.5h)
Power (TBNN23.5h-6.5d)
Power (TBNN7.6d-1.3y)

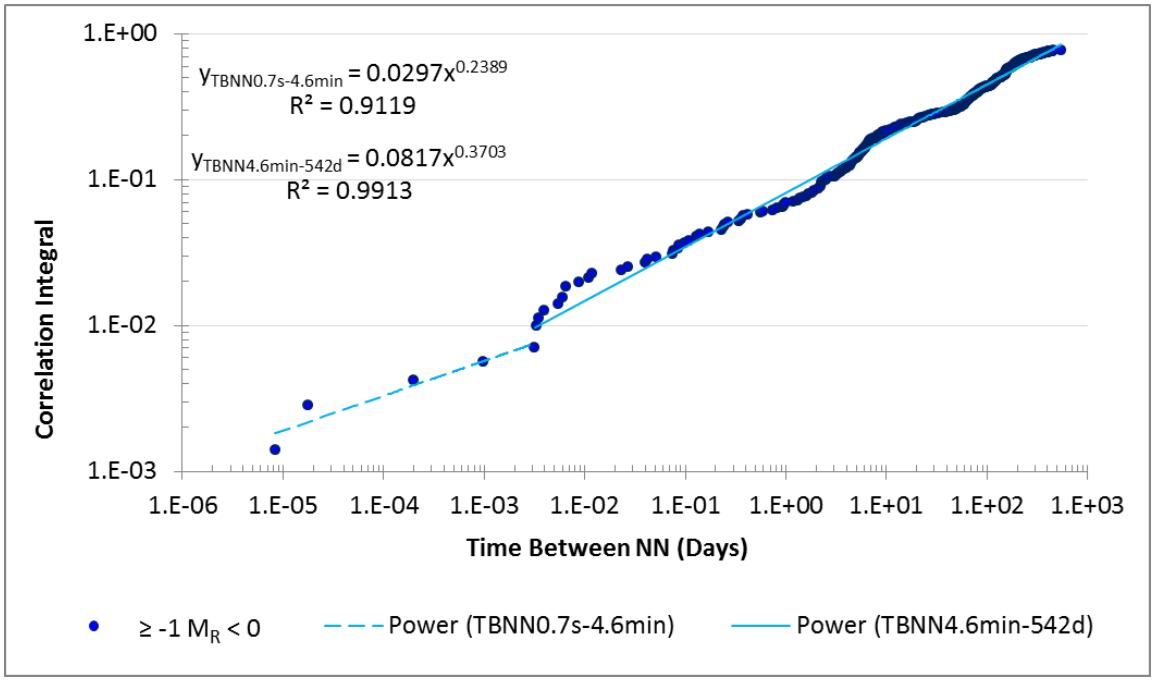
1.E+00
1.E-01
1.E-02
1.E-03
Correlation Integral
$y_{TBNN0.7s-4.6min} = 0.0297x^{0.2389}$
$R^2 = 0.9119$
$y_{TBNN4.6min-542d} = 0.0817x^{0.3703}$
$R^2 = 0.9913$
1.E-06
1.E-05
1.E-04
1.E-03
1.E-02
1.E-01
1.E+00
1.E+01
1.E+02
1.E+03
Time Between NN (Days)
≥ -1 M_R < 0
Power (TBNN0.7s-4.6min)
Power (TBNN4.6min-542d)

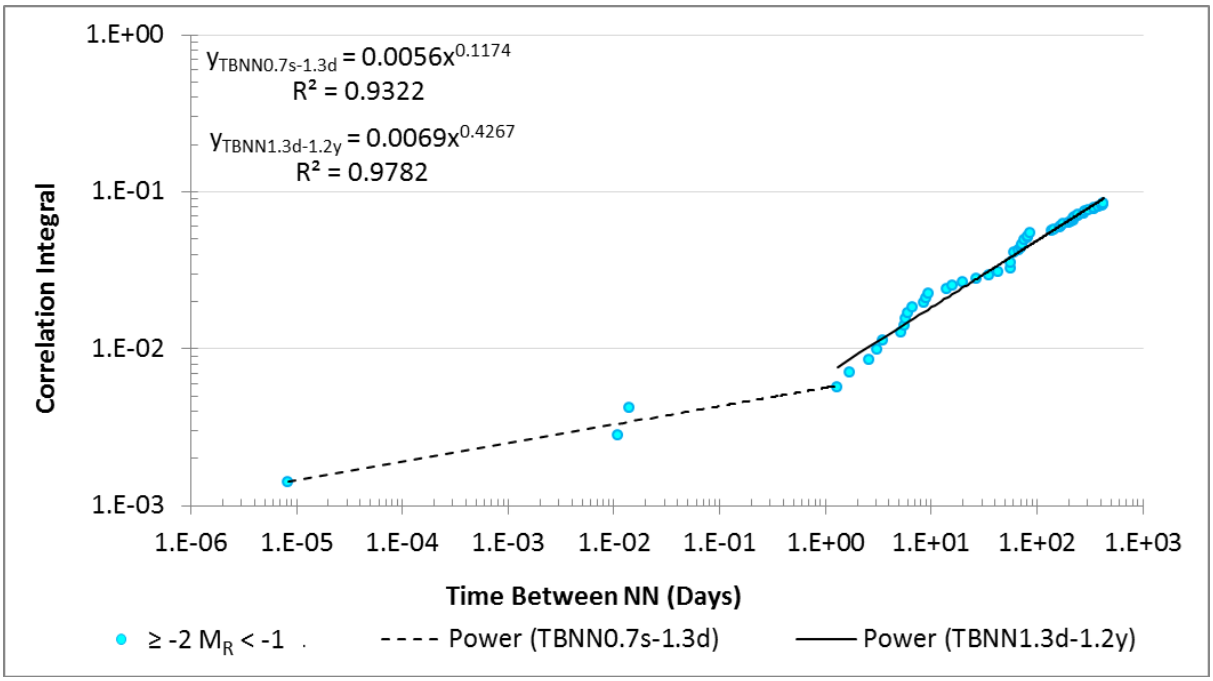
1.E+00
1.E-01
1.E-02
1.E-03
Correlation Integral
$y_{TBNN0.7s-1.3d} = 0.0056x^{0.1174}$
$R^2 = 0.9322$
$y_{TBNN1.3d-1.2y} = 0.0069x^{0.4267}$
$R^2 = 0.9782$
1.E-06
1.E-05
1.E-04
1.E-03
1.E-02
1.E-01
1.E+00
1.E+01
1.E+02
1.E+03
Time Between NN (Days)
≥ -2 M_R < -1
Power (TBNN0.7s-1.3d)
Power (TBNN1.3d-1.2y)

Appendix X
Pillar – Fractal Dimension of NN Distances by Magnitude Range

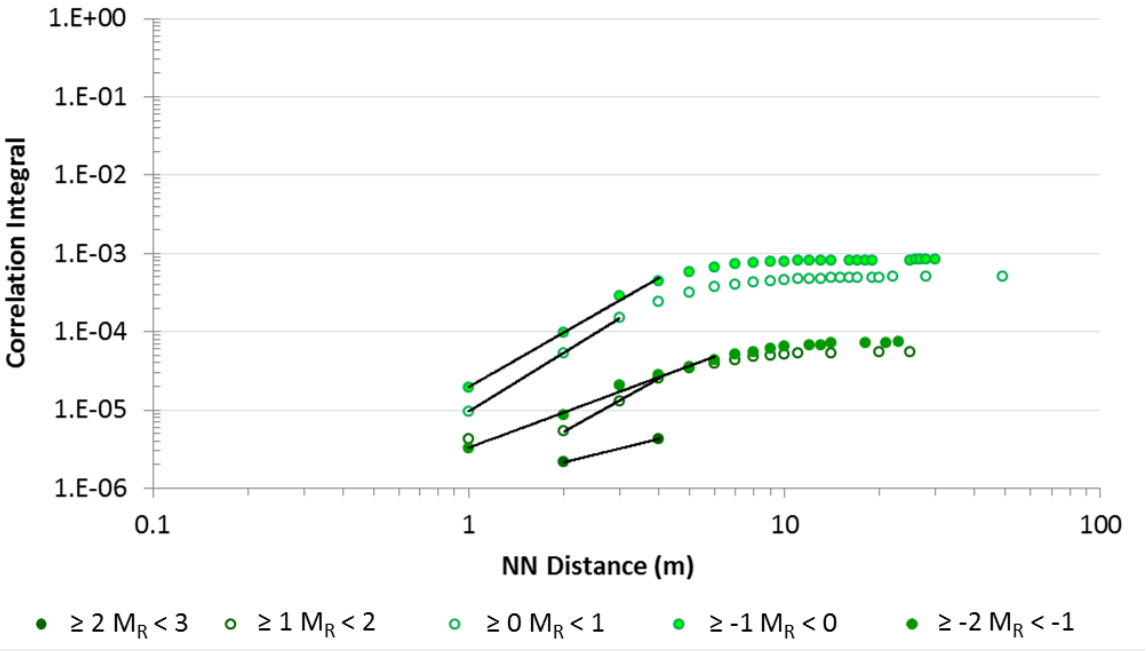

Mag R Range	FD	R^2	NN Distance (m)		
			Range		Max
>2	1.00	100.0%	2	4	4
1 to 2	2.26	99.9%	2	4	25
0 to 1	2.49	100.0%	1	3	49
-1 to 0	2.31	99.4%	1	4	30
-2 to -1	1.49	99.0%	1	6	23

Figure 85 (previously shown)

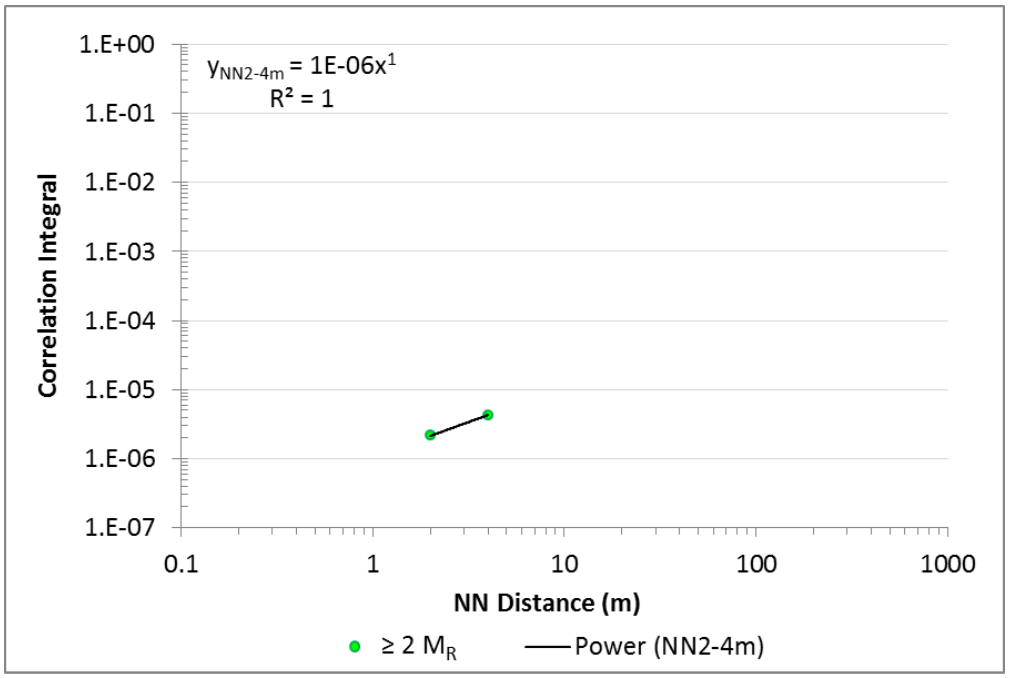
$y_{NN2-4m} = 1E-06x^{1}$
$R^2 = 1$
1.E+00
1.E-01
1.E-02
1.E-03
1.E-04
1.E-05
1.E-06
1.E-07
Correlation Integral
0.1
1
10
100
1000
NN Distance (m)
≥ 2 M_R
Power (NN2-4m)

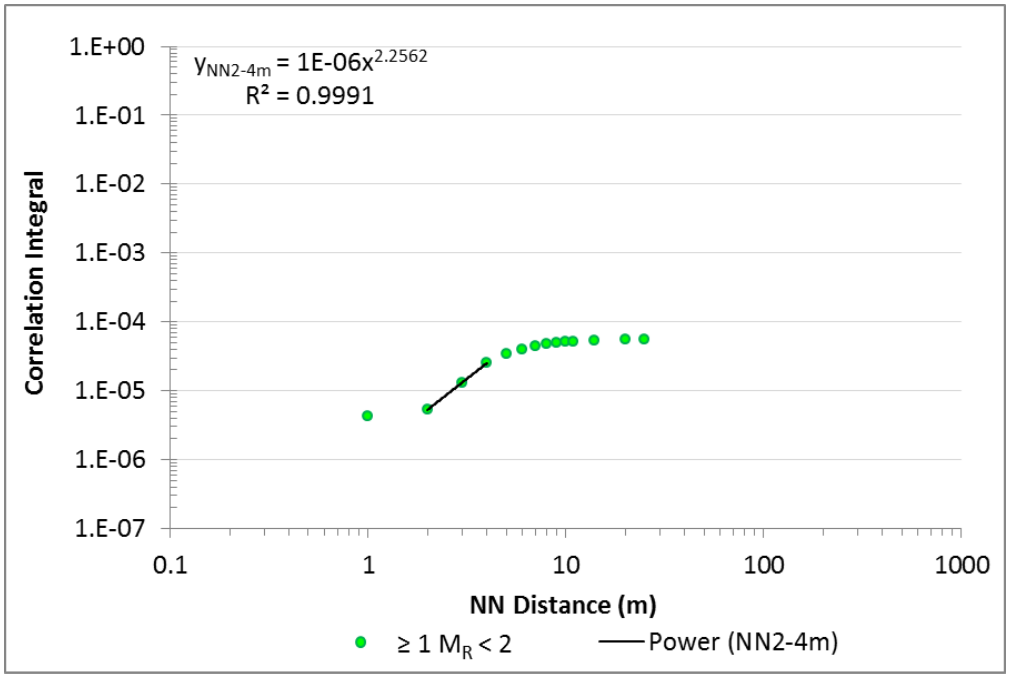
$y_{NN2-4m} = 1E-06x^{2.2562}$
$R^2 = 0.9991$
1.E+00
1.E-01
1.E-02
1.E-03
1.E-04
1.E-05
1.E-06
1.E-07
Correlation Integral
0.1
1
10
100
1000
NN Distance (m)
≥ 1 M_R < 2
Power (NN2-4m)

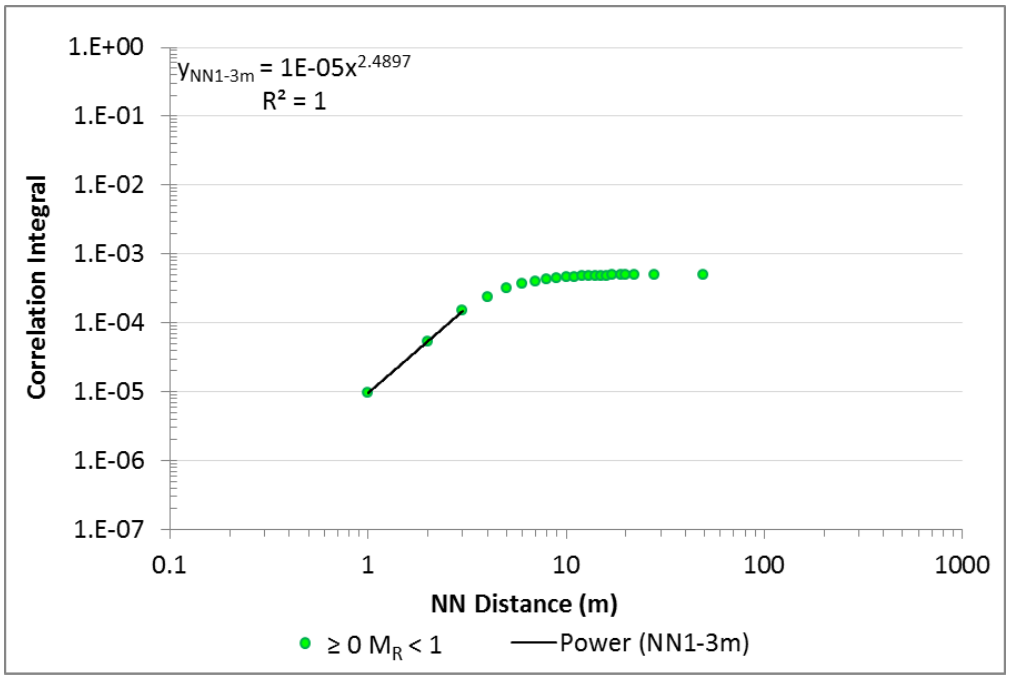
$y_{NN1-3m} = 1E-05x^{2.4897}$
$R^2 = 1$
Correlation Integral
1.E+00
1.E-01
1.E-02
1.E-03
1.E-04
1.E-05
1.E-06
1.E-07
0.1
1
10
100
1000
NN Distance (m)
≥ 0 M_R < 1
Power (NN1-3m)

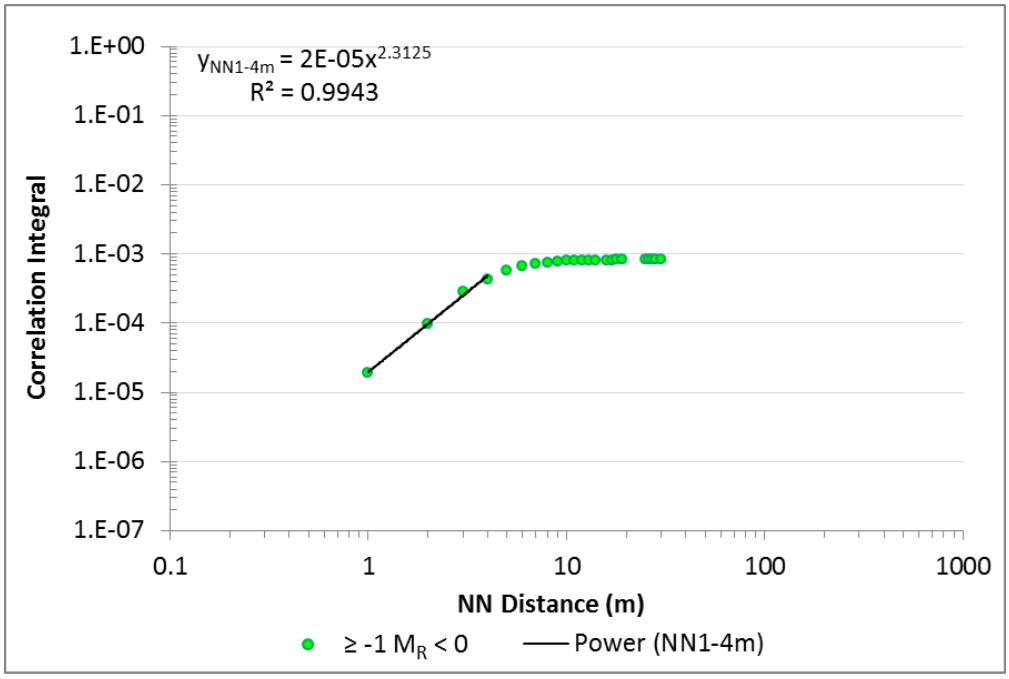
$y_{NN1-4m} = 2E-05x^{2.3125}$
$R^2 = 0.9943$
Correlation Integral
1.E+00
1.E-01
1.E-02
1.E-03
1.E-04
1.E-05
1.E-06
1.E-07
0.1
1
10
100
1000
NN Distance (m)
≥ -1 M_R < 0
Power (NN1-4m)

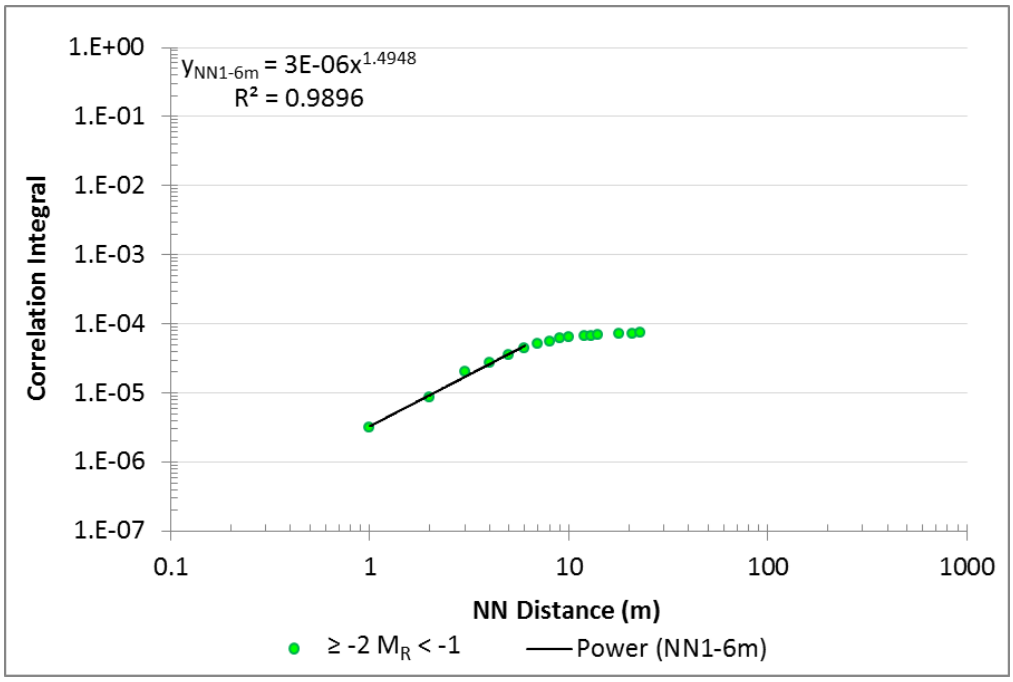
y_{NN1-6m} = 3E-06$x^{1.4948}$
R^2 = 0.9896
Correlation Integral
1.E+00
1.E-01
1.E-02
1.E-03
1.E-04
1.E-05
1.E-06
1.E-07
0.1
1
10
100
1000
NN Distance (m)
≥ -2 M_R < -1
Power (NN1-6m)

Appendix XI
Pillar – Fractal Dimension of Time Between NN by Magnitude Range

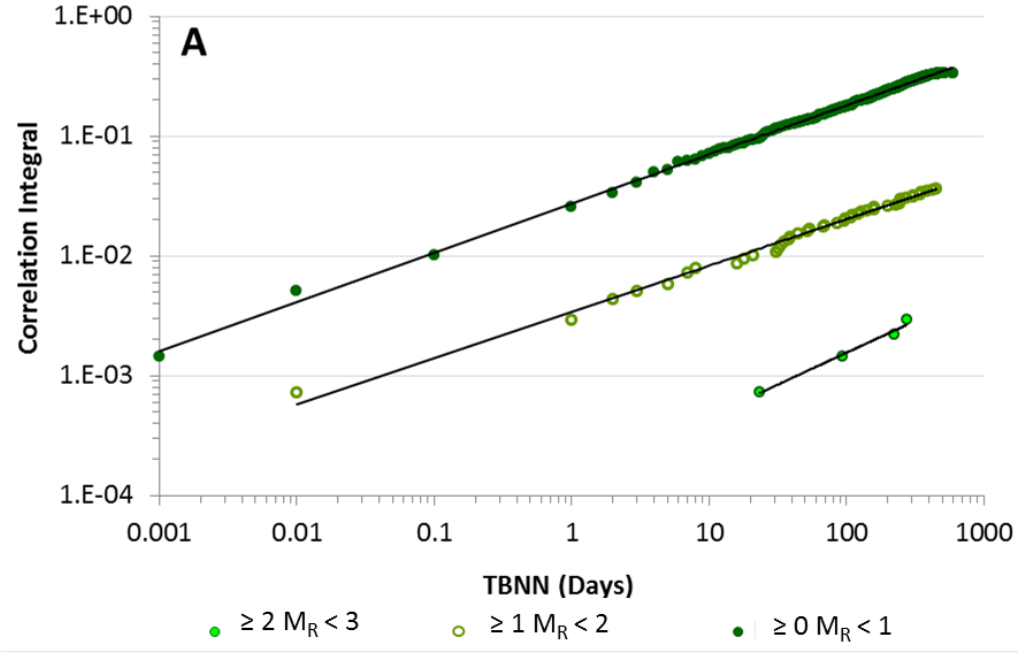

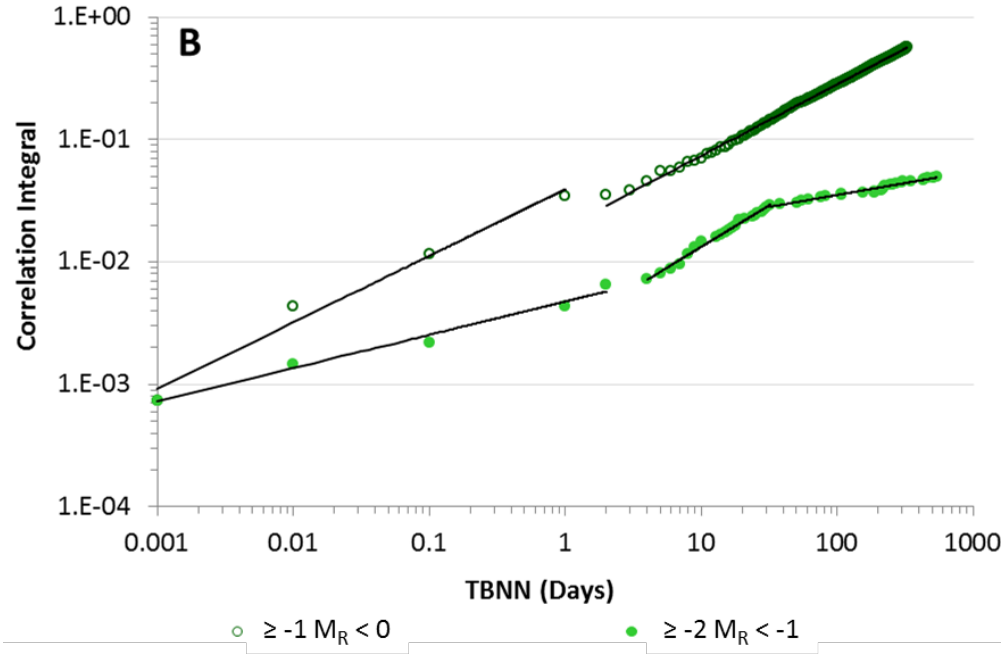

Figure 86 (previously shown)

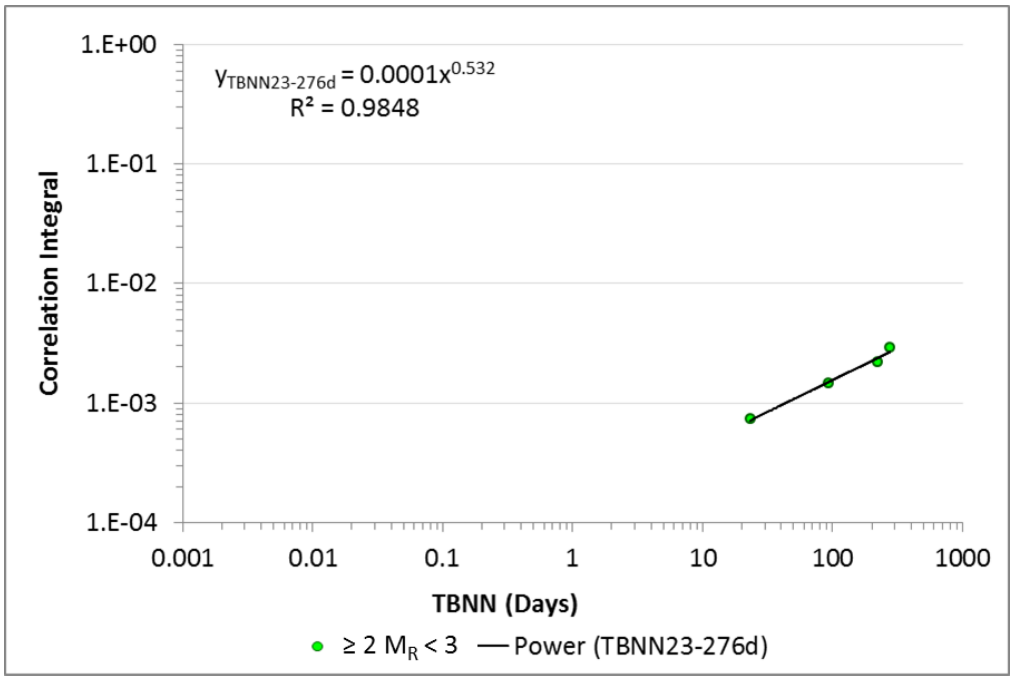
$y_{TBNN23-276d} = 0.0001x^{0.532}$
$R^2 = 0.9848$
1.E+00
1.E-01
1.E-02
1.E-03
1.E-04
Correlation Integral
0.001
0.01
0.1
1
10
100
1000
TBNN (Days)
≥ 2 M_R < 3
Power (TBNN23-276d)

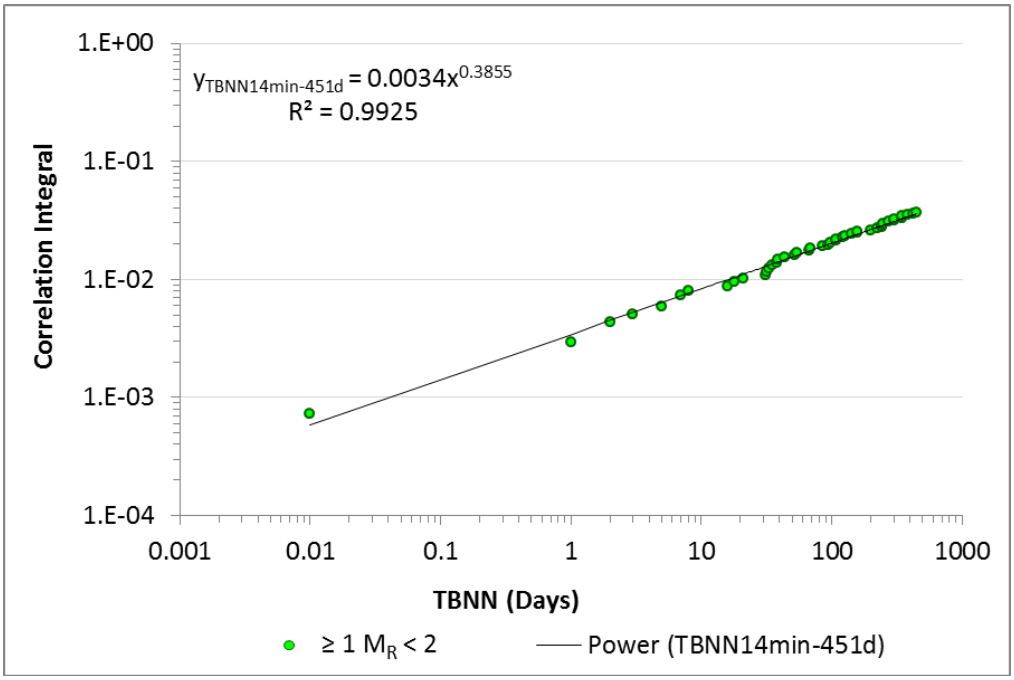
$y_{TBNN14min-451d} = 0.0034x^{0.3855}$
$R^2 = 0.9925$
1.E+00
1.E-01
1.E-02
1.E-03
1.E-04
Correlation Integral
0.001
0.01
0.1
1
10
100
1000
TBNN (Days)
≥ 1 M_R < 2
Power (TBNN14min-451d)

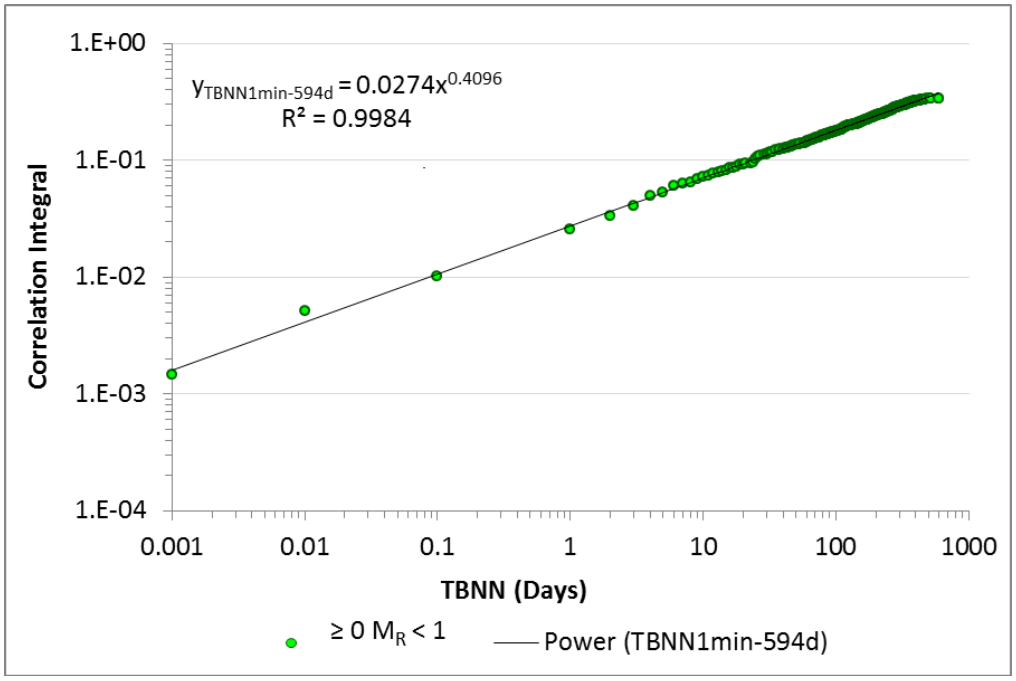
1.E+00
1.E-01
1.E-02
1.E-03
1.E-04
Correlation Integral
$y_{TBNN1min-594d} = 0.0274x^{0.4096}$
$R^2 = 0.9984$
0.001
0.01
0.1
1
10
100
1000
TBNN (Days)
≥ 0 M_R < 1
Power (TBNN1min-594d)

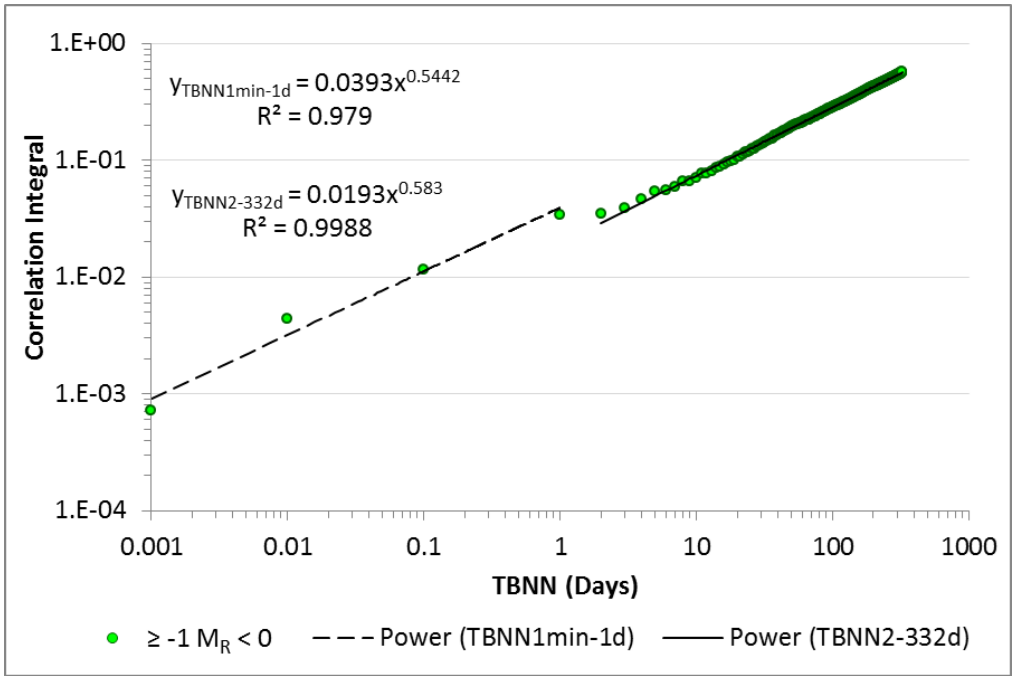
1.E+00
1.E-01
1.E-02
1.E-03
1.E-04
Correlation Integral
$y_{TBNN1min-1d} = 0.0393x^{0.5442}$
$R^2 = 0.979$
$y_{TBNN2-332d} = 0.0193x^{0.583}$
$R^2 = 0.9988$
0.001
0.01
0.1
1
10
100
1000
TBNN (Days)
≥ -1 M_R < 0
Power (TBNN1min-1d)
Power (TBNN2-332d)

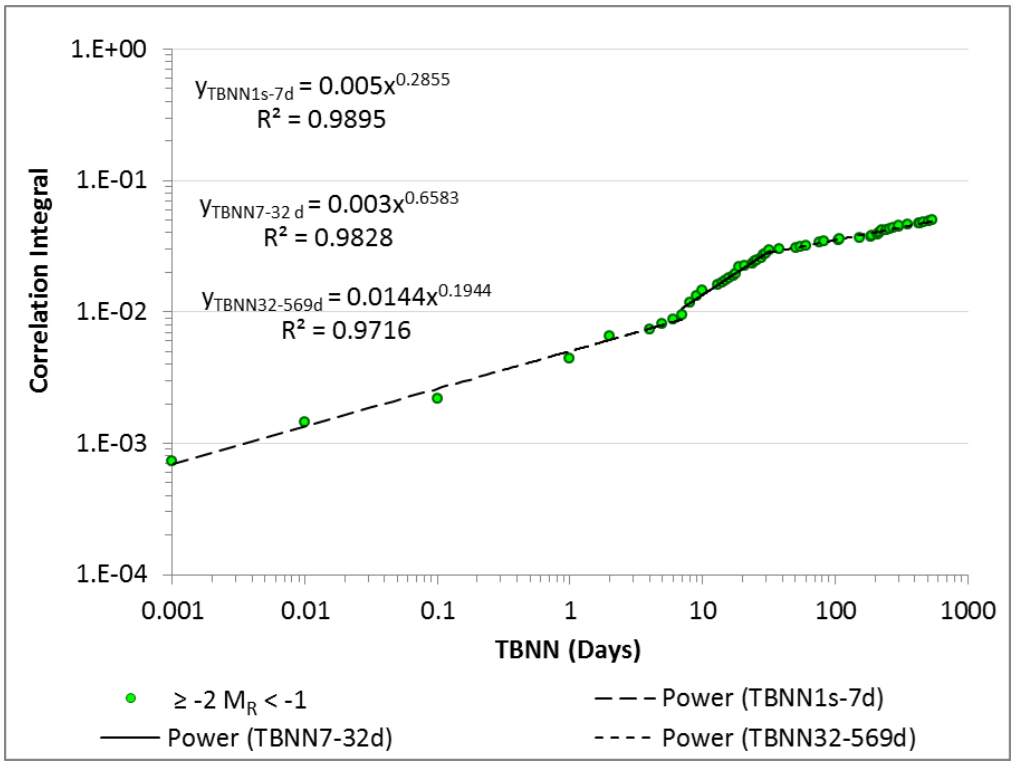
1.E+00
1.E-01
1.E-02
1.E-03
1.E-04
Correlation Integral
$y_{TBNN1s-7d} = 0.005x^{0.2855}$
$R^2 = 0.9895$
$y_{TBNN7-32\,d} = 0.003x^{0.6583}$
$R^2 = 0.9828$
$y_{TBNN32-569d} = 0.0144x^{0.1944}$
$R^2 = 0.9716$
0.001
0.01
0.1
1
10
100
1000
TBNN (Days)
≥ -2 M_R < -1
Power (TBNN1s-7d)
Power (TBNN7-32d)
Power (TBNN32-569d)

Appendix XII
Shear – Fractal Dimension of NN Distances by Magnitude Range

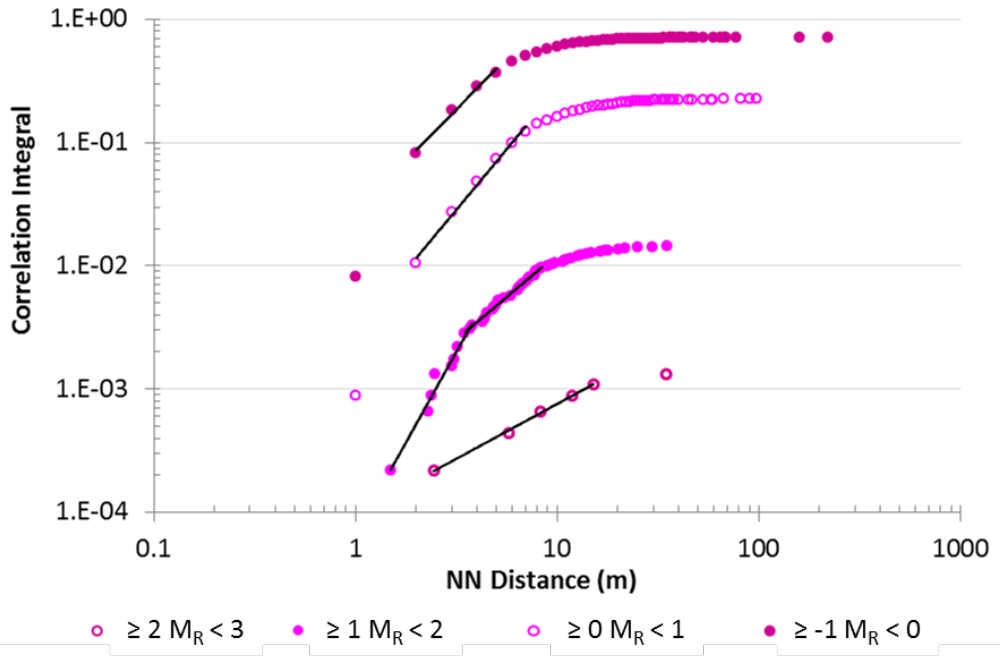

Magnitude Range	FD	R^2	NN (m)		
			Range		Max
>2	0.89	99.7%	2	16	35
1 to 2	2.94	97.9%	1	4	35
	1.38	99.3%	4	9	
0 to 1	1.97	99.3%	2	7	98
-1 to 0	1.67	98.8%	2	5	222

Figure 95 (previously shown)

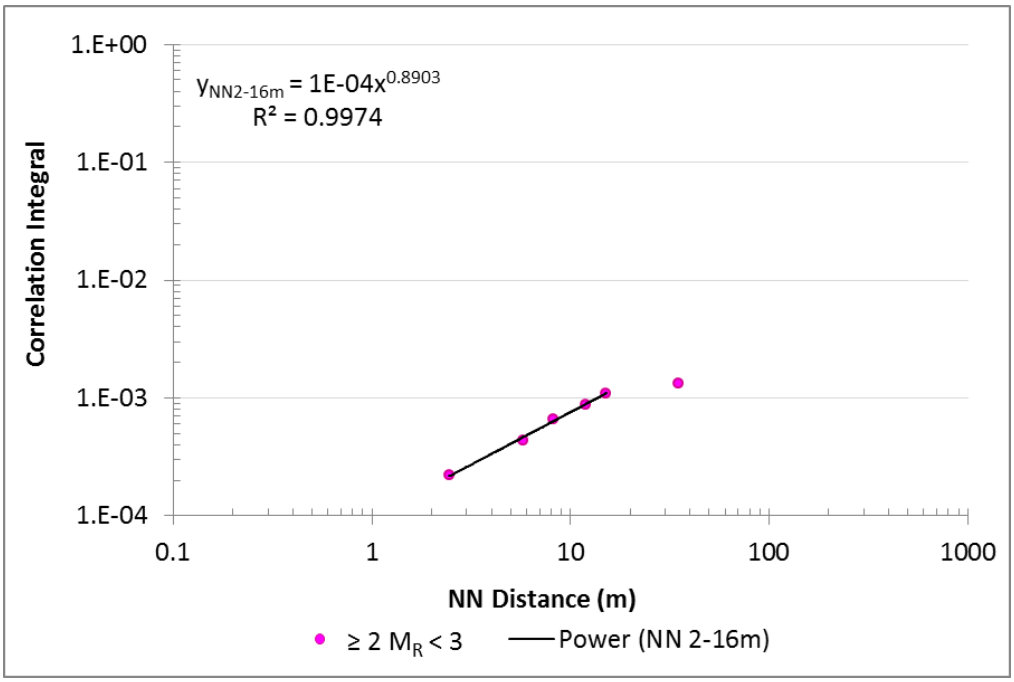
1.E+00
1.E-01
1.E-02
1.E-03
1.E-04
Correlation Integral
$y_{NN2-16m} = 1E-04x^{0.8903}$
$R^2 = 0.9974$
0.1
1
10
100
1000
NN Distance (m)
≥ 2 M_R < 3
Power (NN 2-16m)

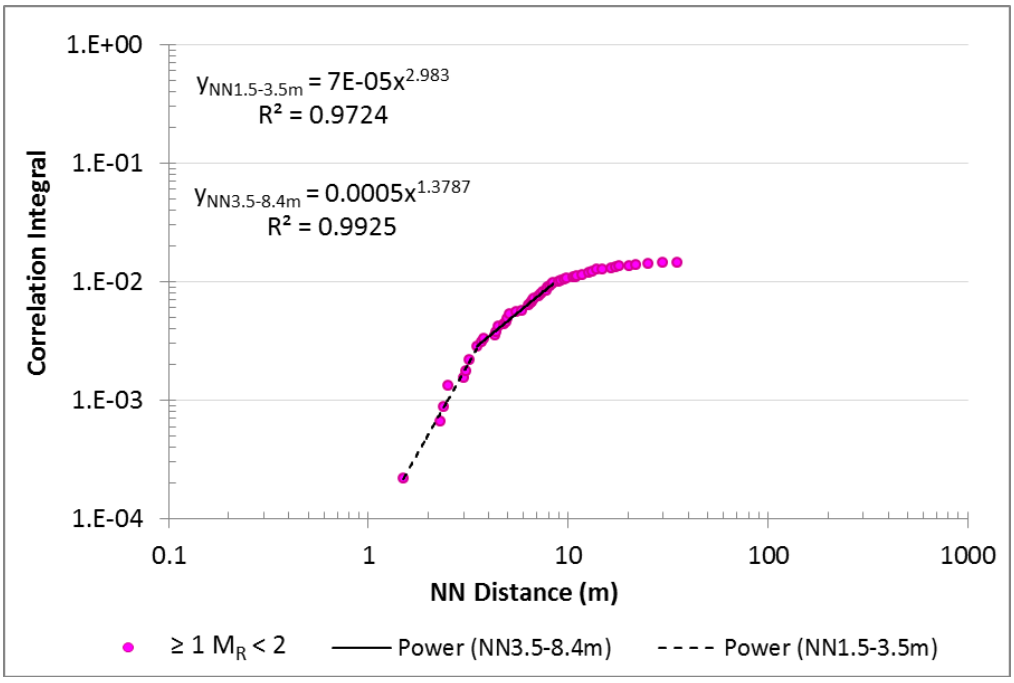
1.E+00
1.E-01
1.E-02
1.E-03
1.E-04
Correlation Integral
$y_{NN1.5-3.5m} = 7E-05x^{2.983}$
$R^2 = 0.9724$
$y_{NN3.5-8.4m} = 0.0005x^{1.3787}$
$R^2 = 0.9925$
0.1
1
10
100
1000
NN Distance (m)
≥ 1 M_R < 2
Power (NN3.5-8.4m)
Power (NN1.5-3.5m)

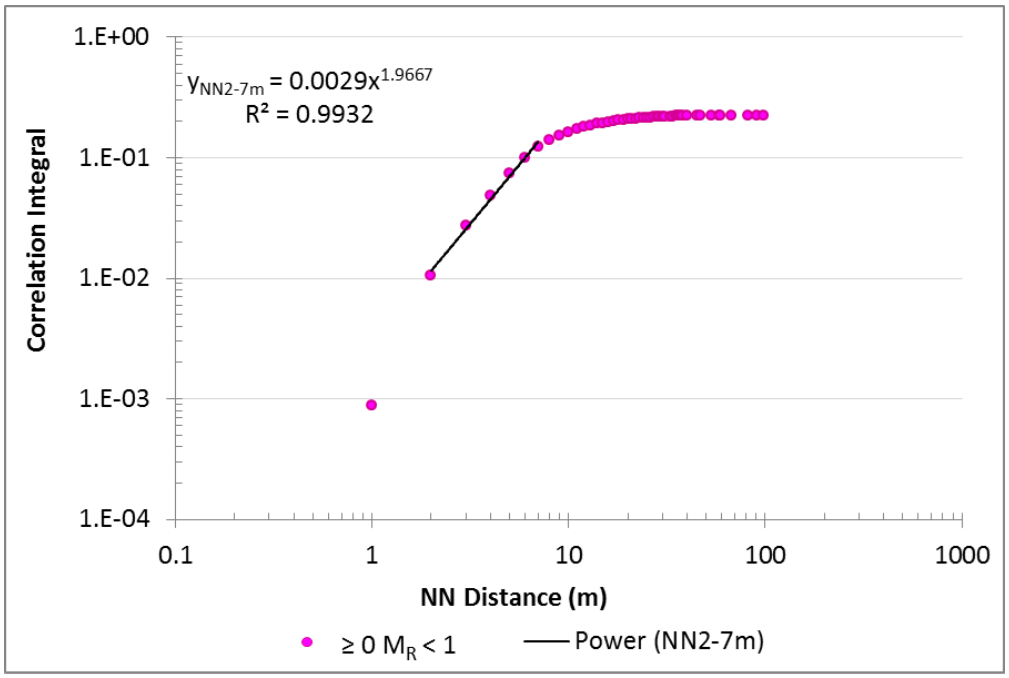
1.E+00
1.E-01
1.E-02
1.E-03
1.E-04
Correlation Integral
$y_{NN2-7m} = 0.0029x^{1.9667}$
$R^2 = 0.9932$
0.1
1
10
100
1000
NN Distance (m)
≥ 0 M_R < 1
Power (NN2-7m)

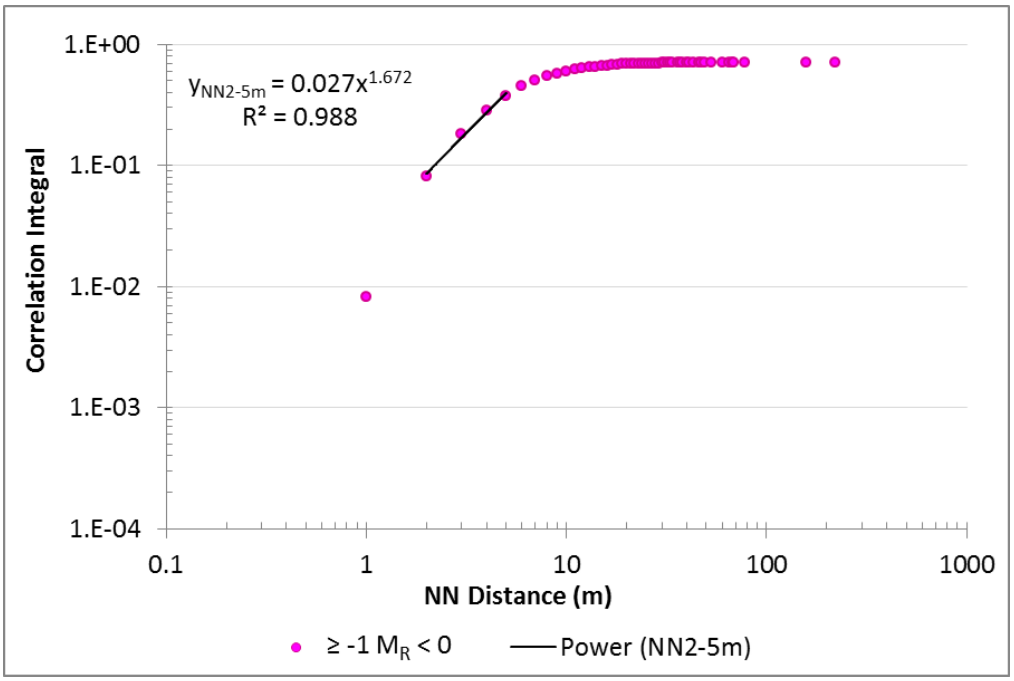
1.E+00
1.E-01
1.E-02
1.E-03
1.E-04
Correlation Integral
$y_{NN2-5m} = 0.027x^{1.672}$
$R^2 = 0.988$
0.1
1
10
100
1000
NN Distance (m)
≥ -1 M_R < 0
Power (NN2-5m)

Appendix XIII
Shear – Fractal Dimension of Time Between NN by Magnitude Range

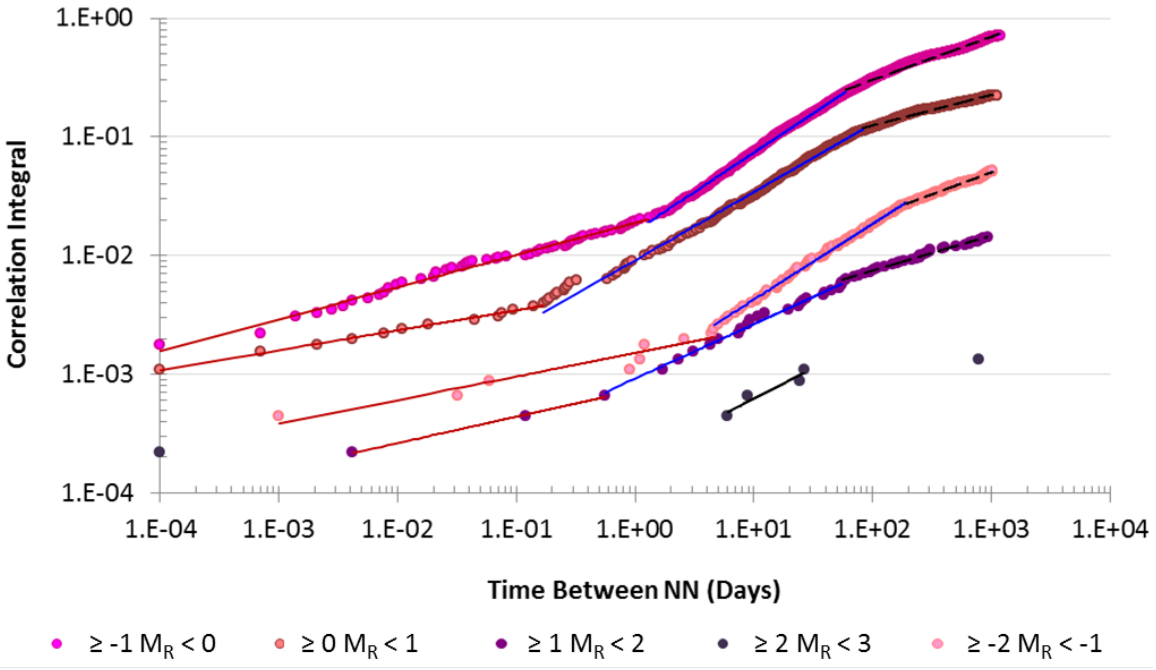

Magnitude Range	FD	R^2	TBNN Range
>2	0.51	91.7%	6-26 days
1 to 2	0.22	99.6%	6min-13.4hr
	0.46	99.0%	13.4hr-55d
	0.30	98.9%	55-933d
0 to 1	0.17	99.3%	8.6s-4.1h
	0.57	99.5%	4.1h-82d
	0.26	98.2%	82d-3y
-1 to 0	0.27	99.0%	8.6s-1.3d
	0.66	99.8%	1.3-59d
	0.36	98.9%	59d-3.1y
-2 to -1	0.20	92.4%	8.6min-4.6d
	0.64	99.8%	4.6-189d
	0.37	99.3%	189d-2.8y

Figure 96 (previously shown)

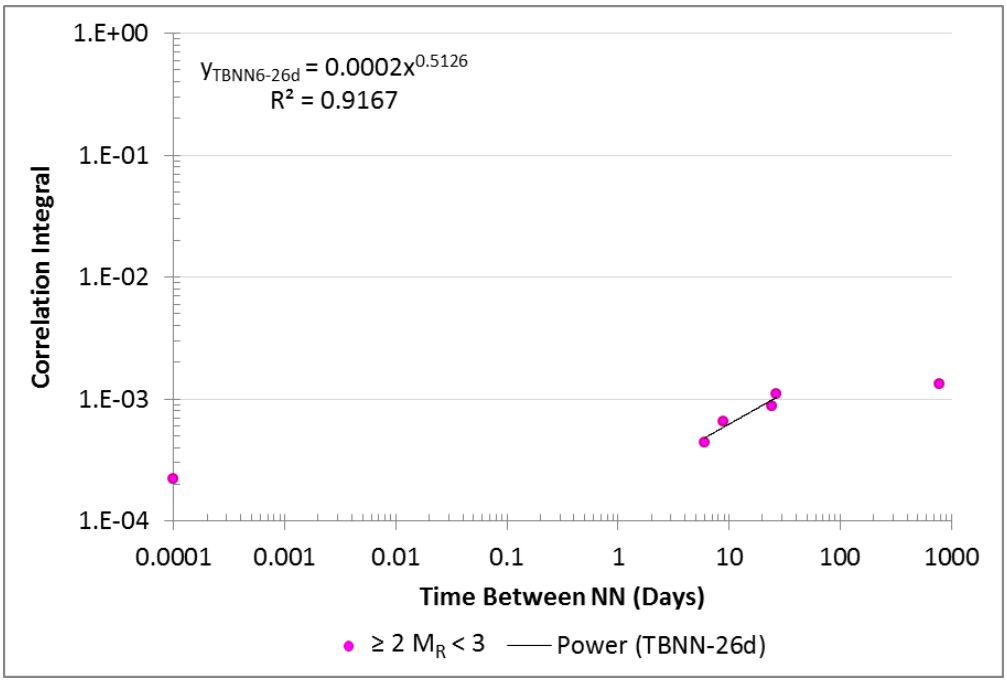
1.E+00
1.E-01
1.E-02
1.E-03
1.E-04
Correlation Integral
$y_{TBNN6-26d} = 0.0002x^{0.5126}$
$R^2 = 0.9167$
0.0001
0.001
0.01
0.1
1
10
100
1000
Time Between NN (Days)
≥ 2 M_R < 3
Power (TBNN-26d)

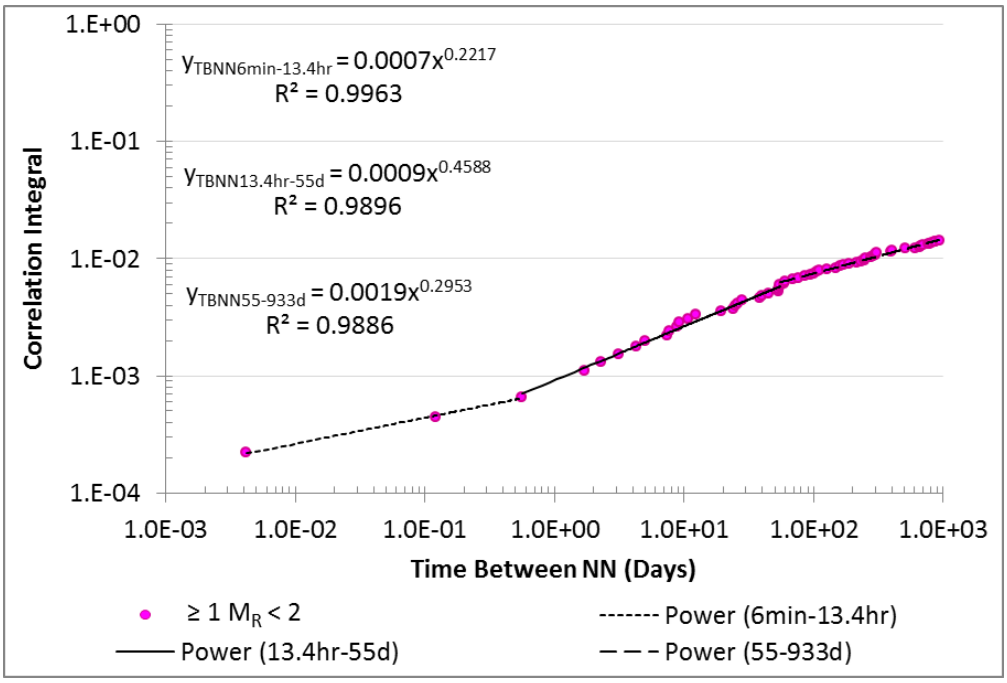
1.E+00
1.E-01
1.E-02
1.E-03
1.E-04
Correlation Integral
$y_{TBNN6min-13.4hr} = 0.0007x^{0.2217}$
$R^2 = 0.9963$
$y_{TBNN13.4hr-55d} = 0.0009x^{0.4588}$
$R^2 = 0.9896$
$y_{TBNN55-933d} = 0.0019x^{0.2953}$
$R^2 = 0.9886$
1.0E-03
1.0E-02
1.0E-01
1.0E+00
1.0E+01
1.0E+02
1.0E+03
Time Between NN (Days)
≥ 1 M_R < 2
Power (6min-13.4hr)
Power (13.4hr-55d)
Power (55-933d)

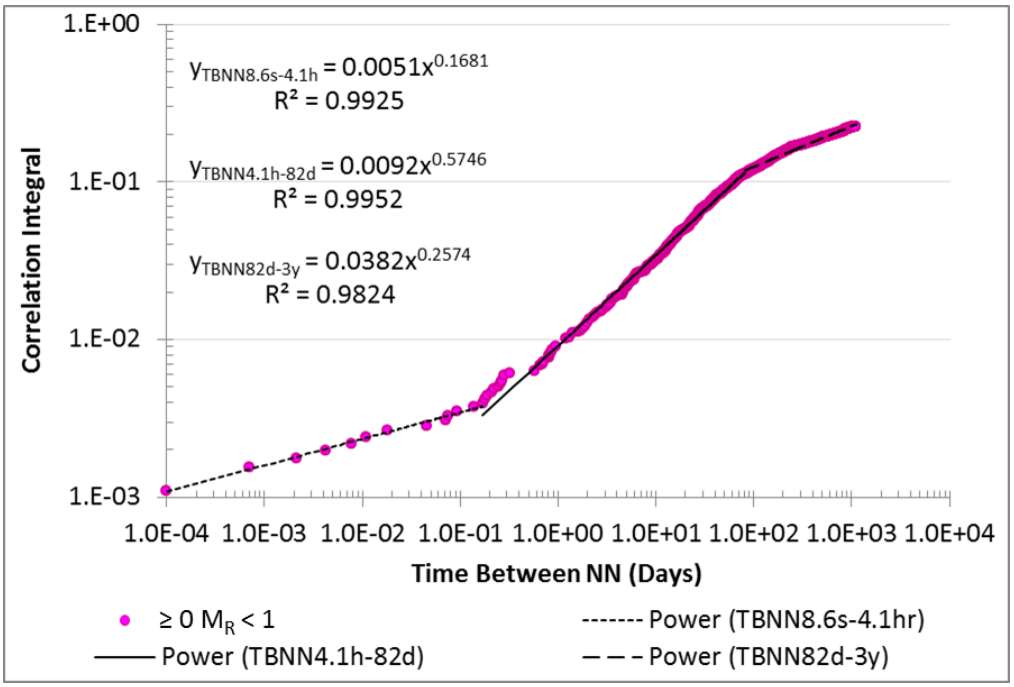
1.E+00
1.E-01
1.E-02
1.E-03
Correlation Integral
$y_{TBNN8.6s-4.1h} = 0.0051x^{0.1681}$
$R^2 = 0.9925$
$y_{TBNN4.1h-82d} = 0.0092x^{0.5746}$
$R^2 = 0.9952$
$y_{TBNN82d-3y} = 0.0382x^{0.2574}$
$R^2 = 0.9824$
1.0E-04 1.0E-03 1.0E-02 1.0E-01 1.0E+00 1.0E+01 1.0E+02 1.0E+03 1.0E+04
Time Between NN (Days)
≥ 0 M_R < 1
Power (TBNN4.1h-82d)
Power (TBNN8.6s-4.1hr)
Power (TBNN82d-3y)

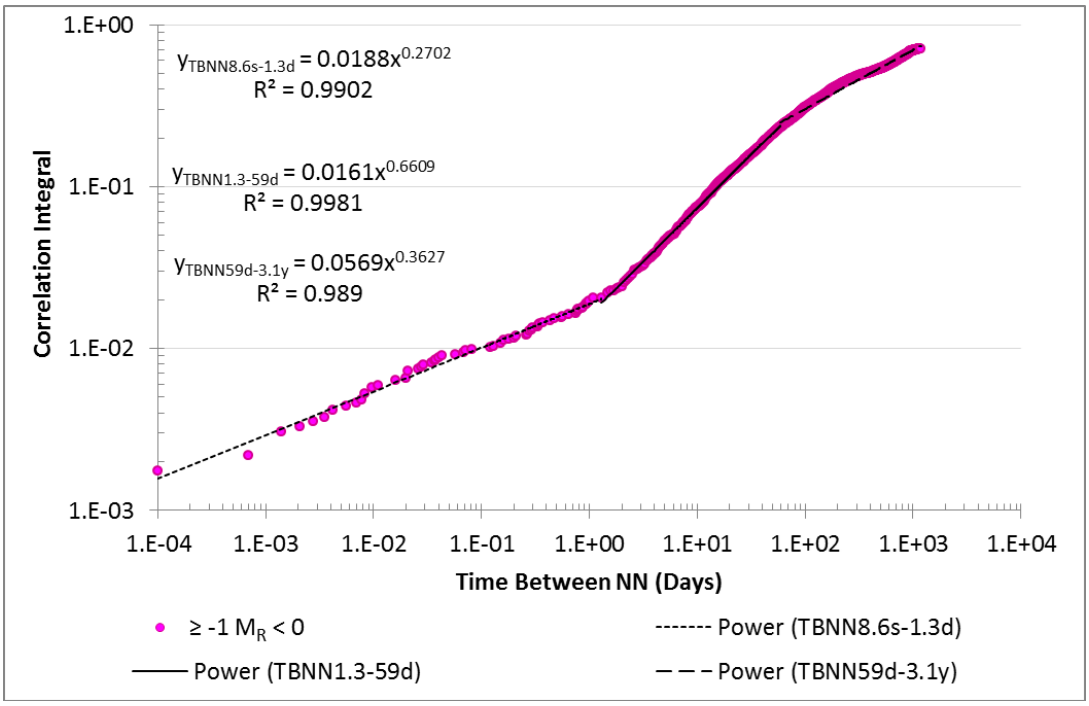
1.E+00
1.E-01
1.E-02
1.E-03
Correlation Integral
$y_{TBNN8.6s-1.3d} = 0.0188x^{0.2702}$
$R^2 = 0.9902$
$y_{TBNN1.3-59d} = 0.0161x^{0.6609}$
$R^2 = 0.9981$
$y_{TBNN59d-3.1y} = 0.0569x^{0.3627}$
$R^2 = 0.989$
1.E-04 1.E-03 1.E-02 1.E-01 1.E+00 1.E+01 1.E+02 1.E+03 1.E+04
Time Between NN (Days)
≥ -1 M_R < 0
Power (TBNN1.3-59d)
Power (TBNN8.6s-1.3d)
Power (TBNN59d-3.1y)

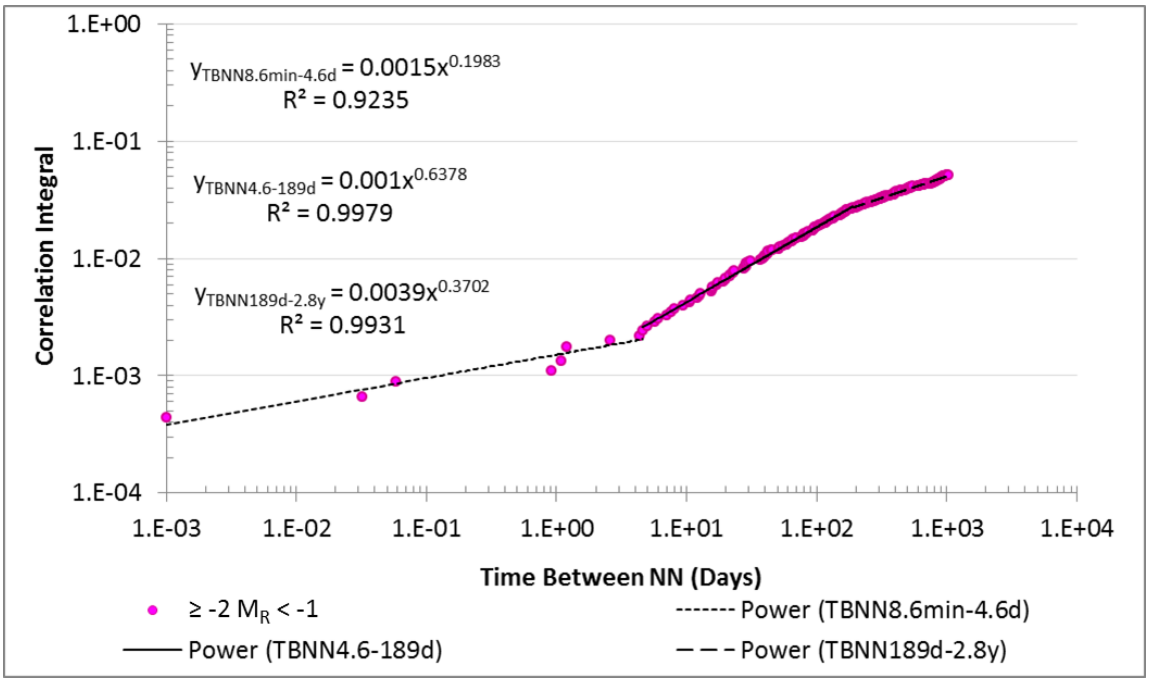
1.E+00
1.E-01
1.E-02
1.E-03
1.E-04
Correlation Integral
$y_{TBNN8.6min-4.6d} = 0.0015x^{0.1983}$
$R^2 = 0.9235$
$y_{TBNN4.6-189d} = 0.001x^{0.6378}$
$R^2 = 0.9979$
$y_{TBNN189d-2.8y} = 0.0039x^{0.3702}$
$R^2 = 0.9931$
1.E-03
1.E-02
1.E-01
1.E+00
1.E+01
1.E+02
1.E+03
1.E+04
Time Between NN (Days)
≥ -2 M_R < -1
Power (TBNN8.6min-4.6d)
Power (TBNN4.6-189d)
Power (TBNN189d-2.8y)

Appendix XIV
Comparison of Changing FD (NN Distance & Magnitude) by Seismic Source

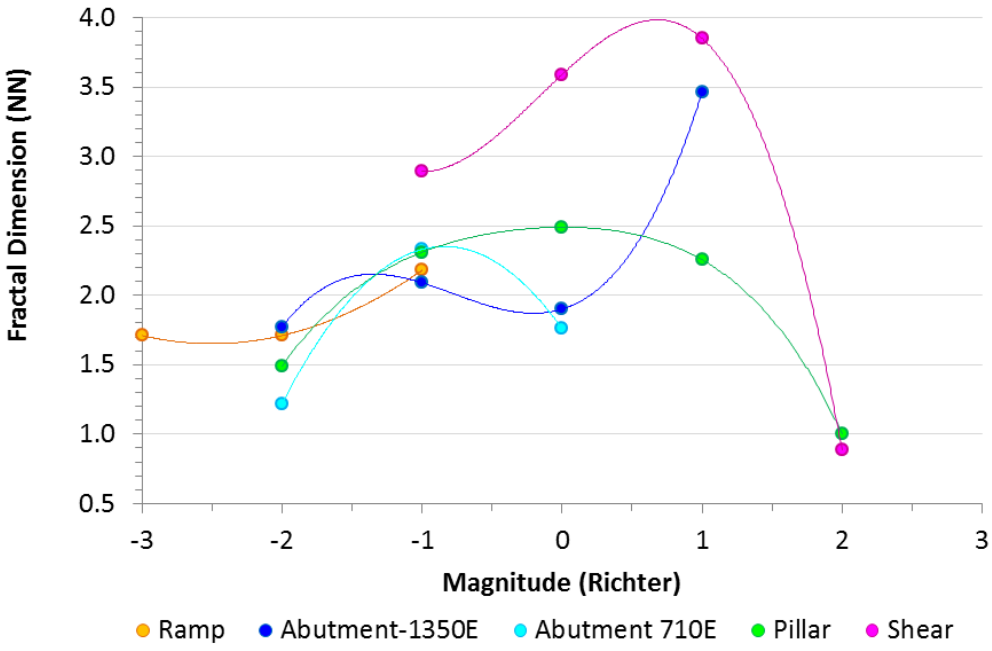

Magnitude Range	Fractal Dimension (NN)				
	Ramp	710E	1350E	Pillar	Shear
>2				1.00	0.89
1 to 2			3.46	2.26	3.85
0 to 1		1.76	1.90	2.49	3.59
-1 to 0	2.18	2.33	2.09	2.31	2.89
-2 to -1	1.71	1.22	1.77	1.49	
-3 to -2	1.71				

Figure 96 (previously shown)

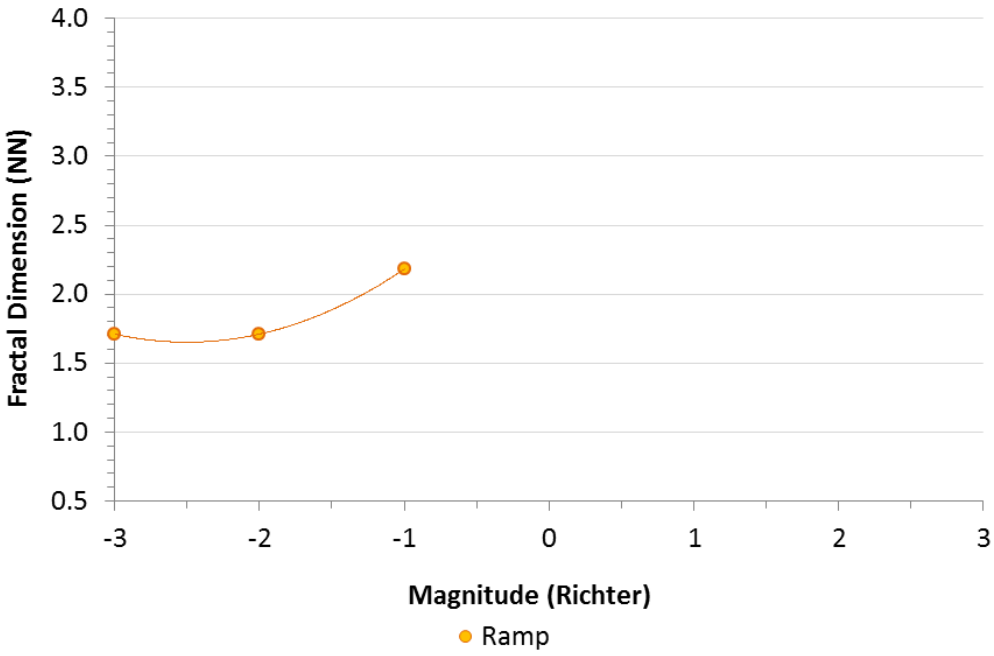
4.0
3.5
3.0
2.5
2.0
1.5
1.0
0.5
Fractal Dimension (NN)
-3
-2
-1
0
1
2
3
Magnitude (Richter)
Ramp

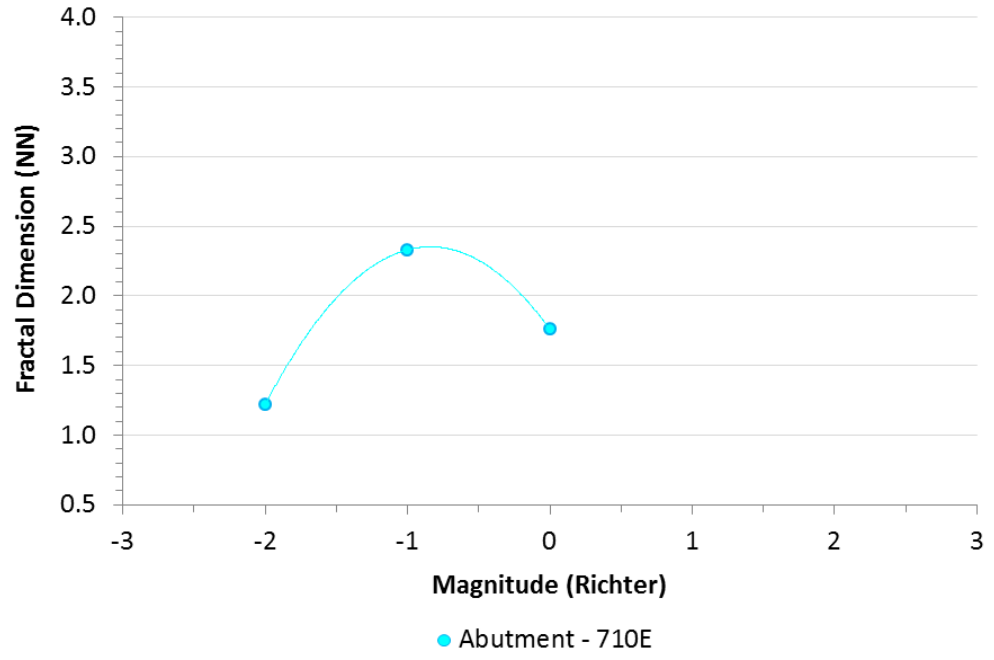
4.0
3.5
3.0
2.5
2.0
1.5
1.0
0.5
Fractal Dimension (NN)
-3
-2
-1
0
1
2
3
Magnitude (Richter)
Abutment - 710E

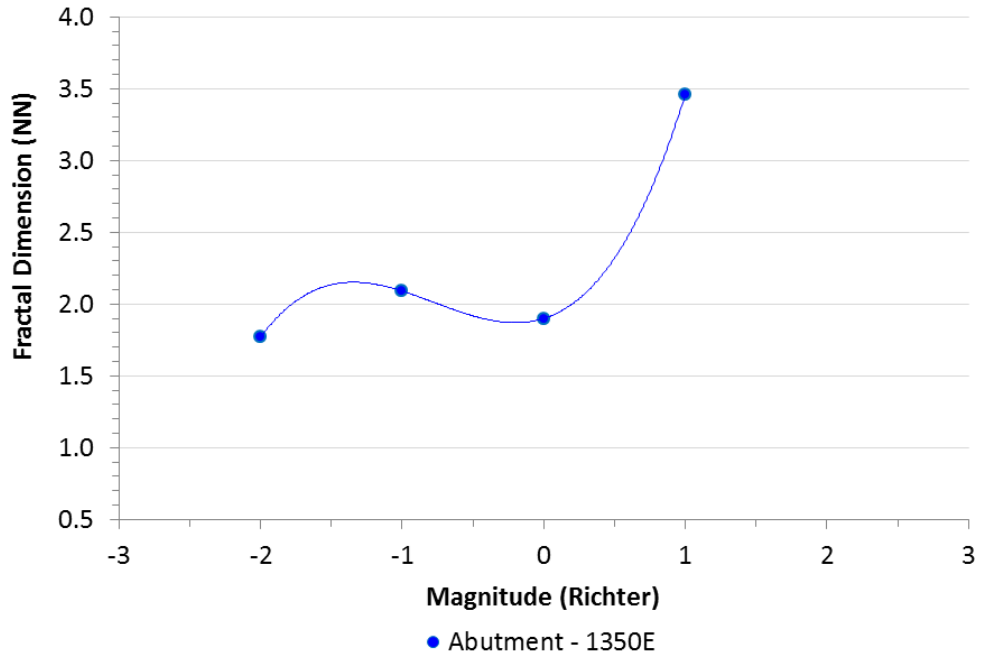
4.0
3.5
3.0
2.5
2.0
1.5
1.0
0.5
Fractal Dimension (NN)
-3
-2
-1
0
1
2
3
Magnitude (Richter)
Abutment - 1350E

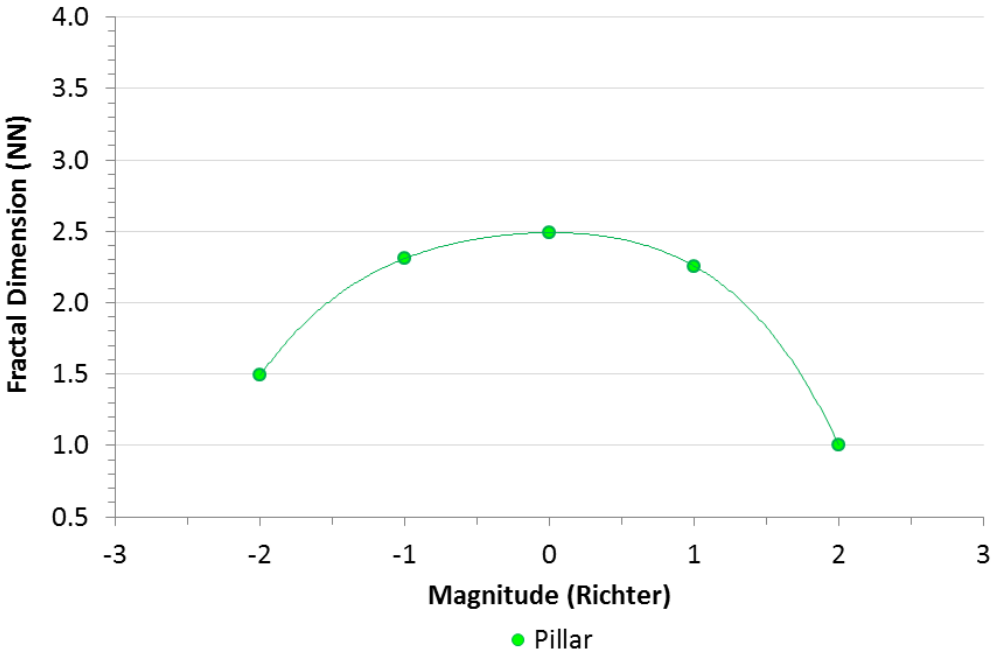
4.0
3.5
3.0
2.5
2.0
1.5
1.0
0.5
Fractal Dimension (NN)
-3
-2
-1
0
1
2
3
Magnitude (Richter)
Pillar

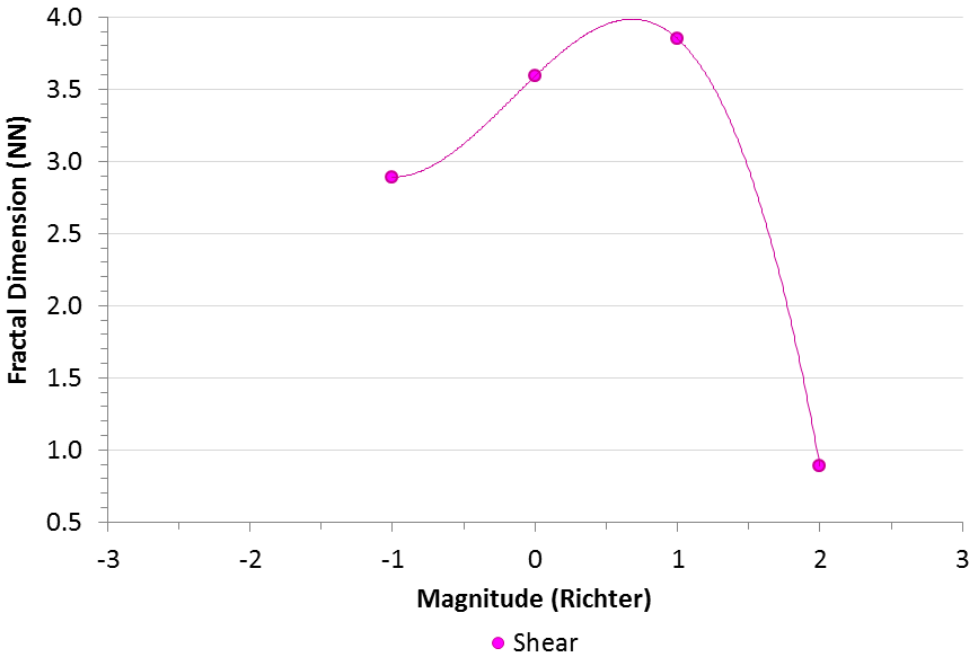
4.0
3.5
3.0
2.5
2.0
1.5
1.0
0.5
Fractal Dimension (NN)
-3
-2
-1
0
1
2
3
Magnitude (Richter)
Shear

Appendix XV
Comparison of Changing FD (TBNN & Magnitude) by Seismic Source

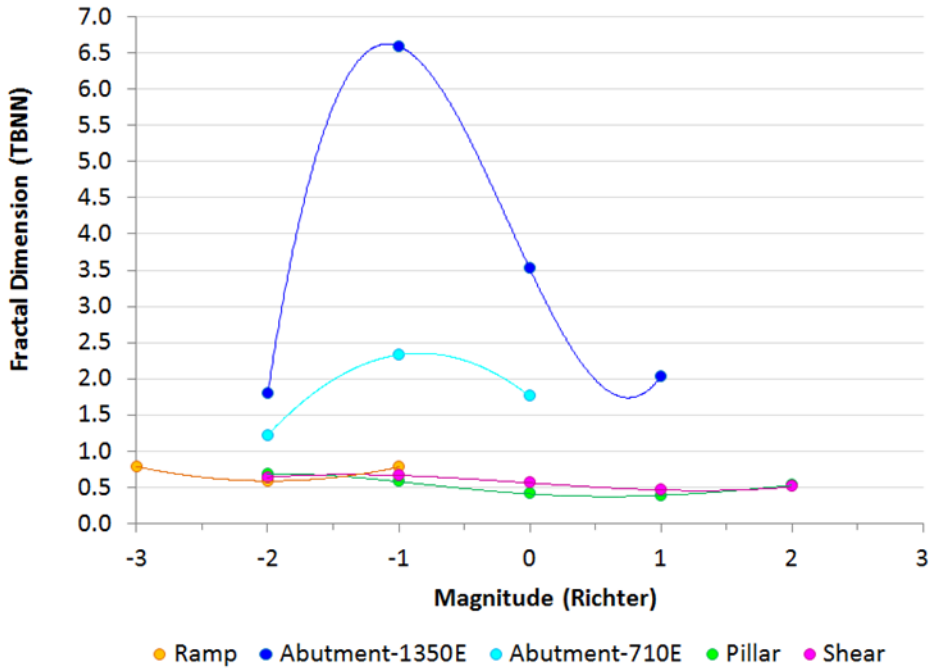

Magnitude Range	Magnitude Range	Fractal Dimension (TBNN)				
		Ramp	710E	1350E	Pillar	Shear
>2	2				0.53	0.51
1 to 2	1			2.03	0.39	0.46
0 to 1	0		1.76	3.52	0.41	0.57
-1 to 0	-1	0.78	2.33	6.59	0.58	0.66
-2 to -1	-2	0.59	1.22	1.79	0.68	0.64
-3 to -2	-3	0.79				

Figure 97 (previously shown)

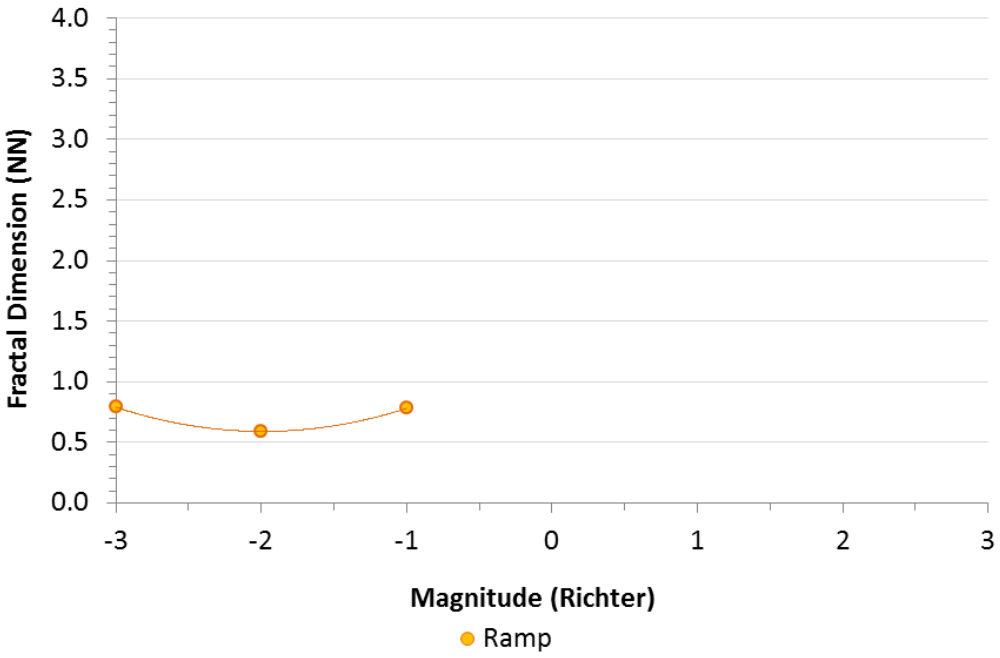
4.0
3.5
3.0
2.5
2.0
1.5
1.0
0.5
0.0
Fractal Dimension (NN)
-3
-2
-1
0
1
2
3
Magnitude (Richter)
Ramp

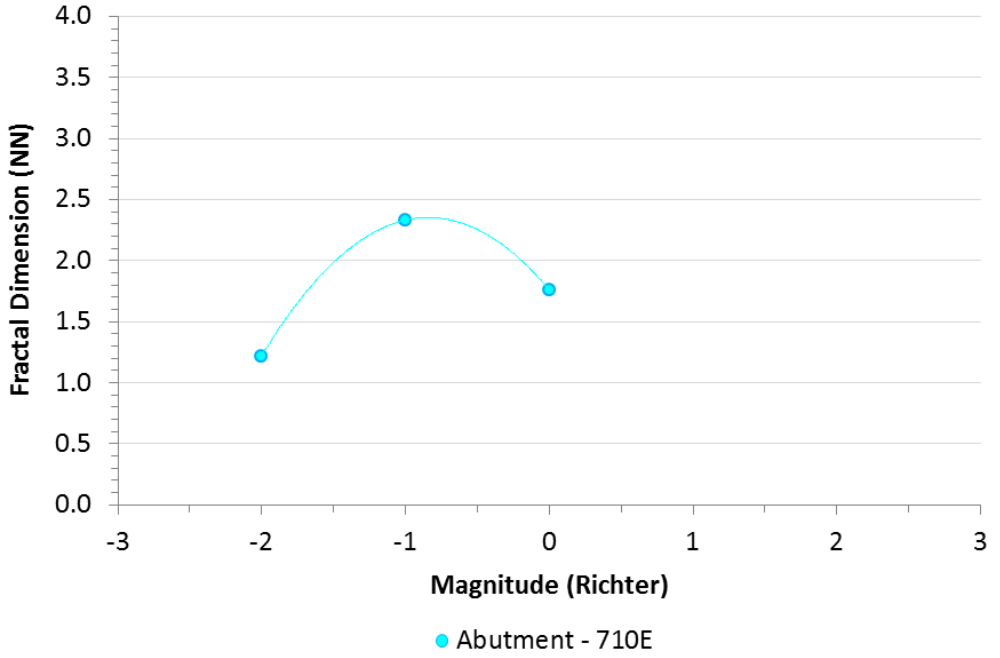
4.0
3.5
3.0
2.5
2.0
1.5
1.0
0.5
0.0
Fractal Dimension (NN)
-3
-2
-1
0
1
2
3
Magnitude (Richter)
Abutment - 710E

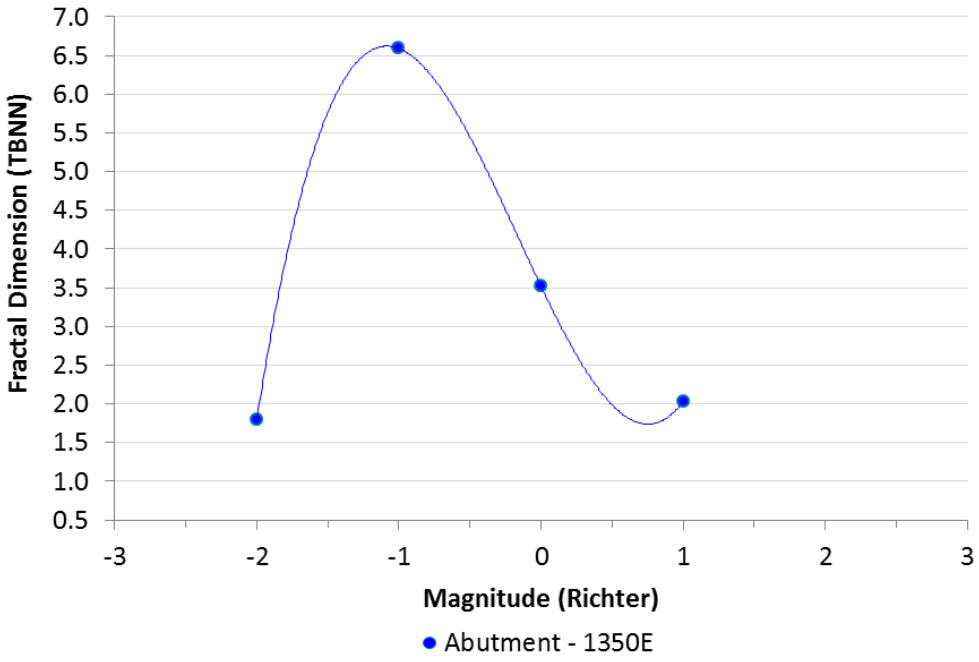
Fractal Dimension (TBNN)
7.0
6.5
6.0
5.5
5.0
4.5
4.0
3.5
3.0
2.5
2.0
1.5
1.0
0.5
-3
-2
-1
0
1
2
3
Magnitude (Richter)
Abutment - 1350E

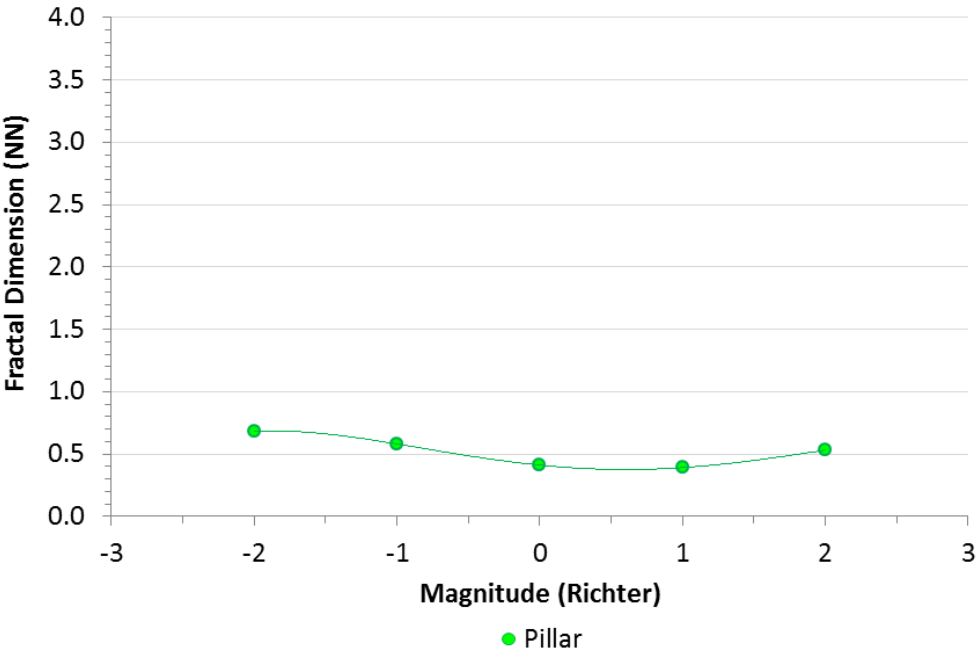
Fractal Dimension (NN)
4.0
3.5
3.0
2.5
2.0
1.5
1.0
0.5
0.0
-3
-2
-1
0
1
2
3
Magnitude (Richter)
Pillar

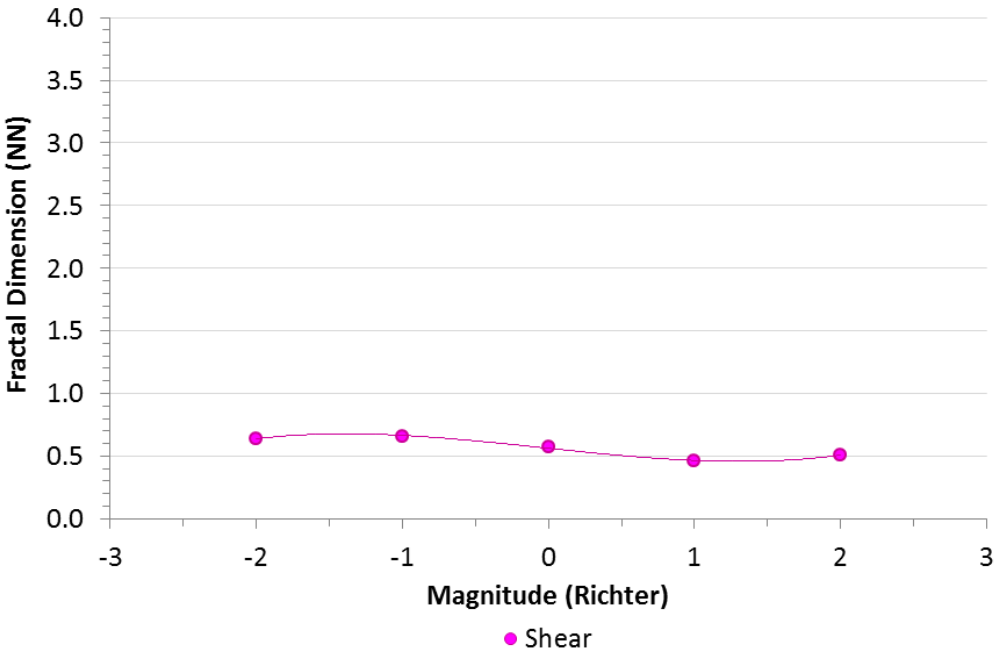
4.0
3.5
3.0
2.5
2.0
1.5
1.0
0.5
0.0
Fractal Dimension (NN)
-3
-2
-1
0
1
2
3
Magnitude (Richter)
Shear

Appendix XVI
Seismic Sensor Locations for each Case Study

The array of seismic sensors is only available for two case studies, Case 2 – Abutment and Case 4 – Shear.

Case 2 – Abutment

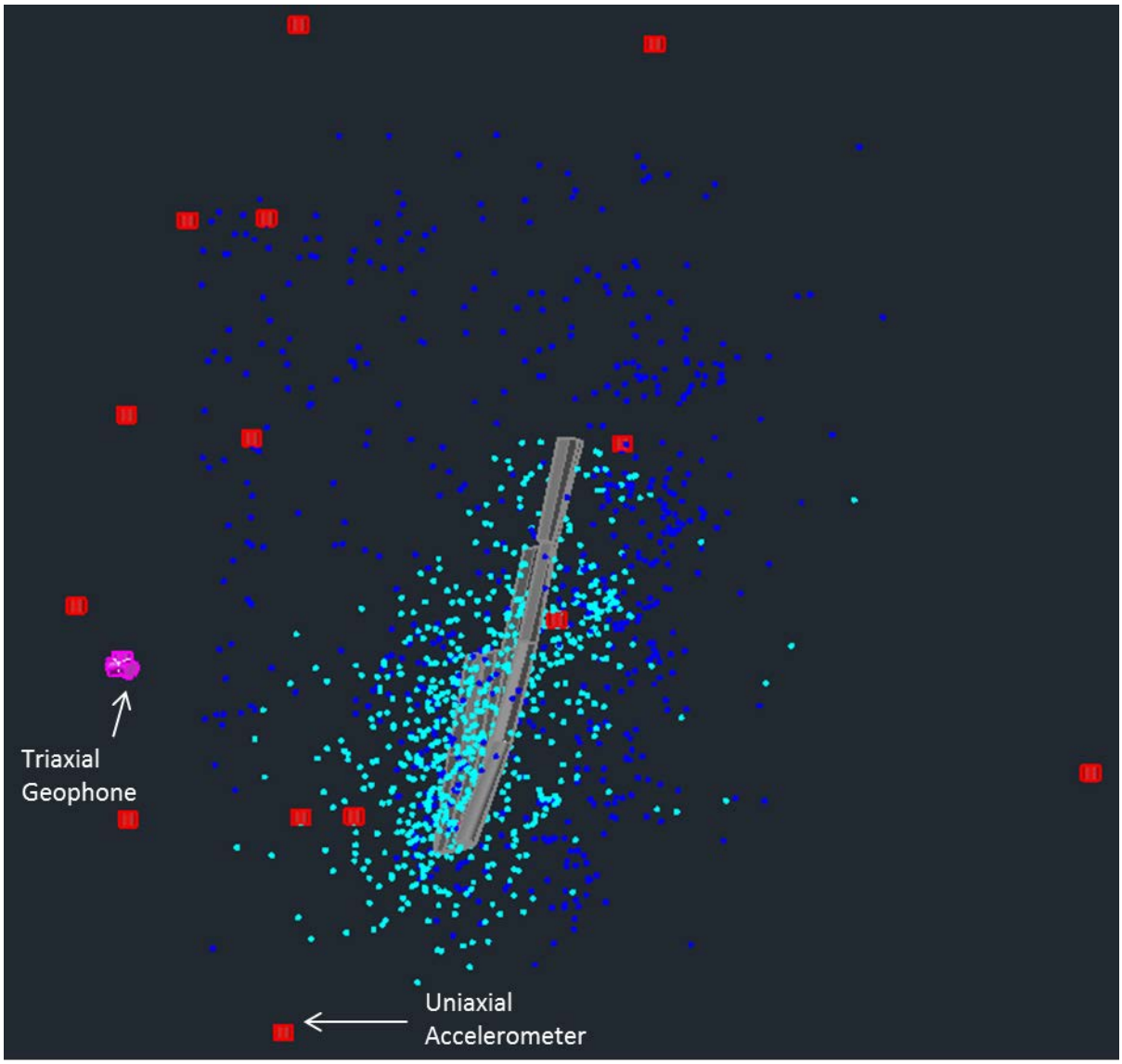

Figure 103: Seismic array around the abutments

Case 4 - Shear

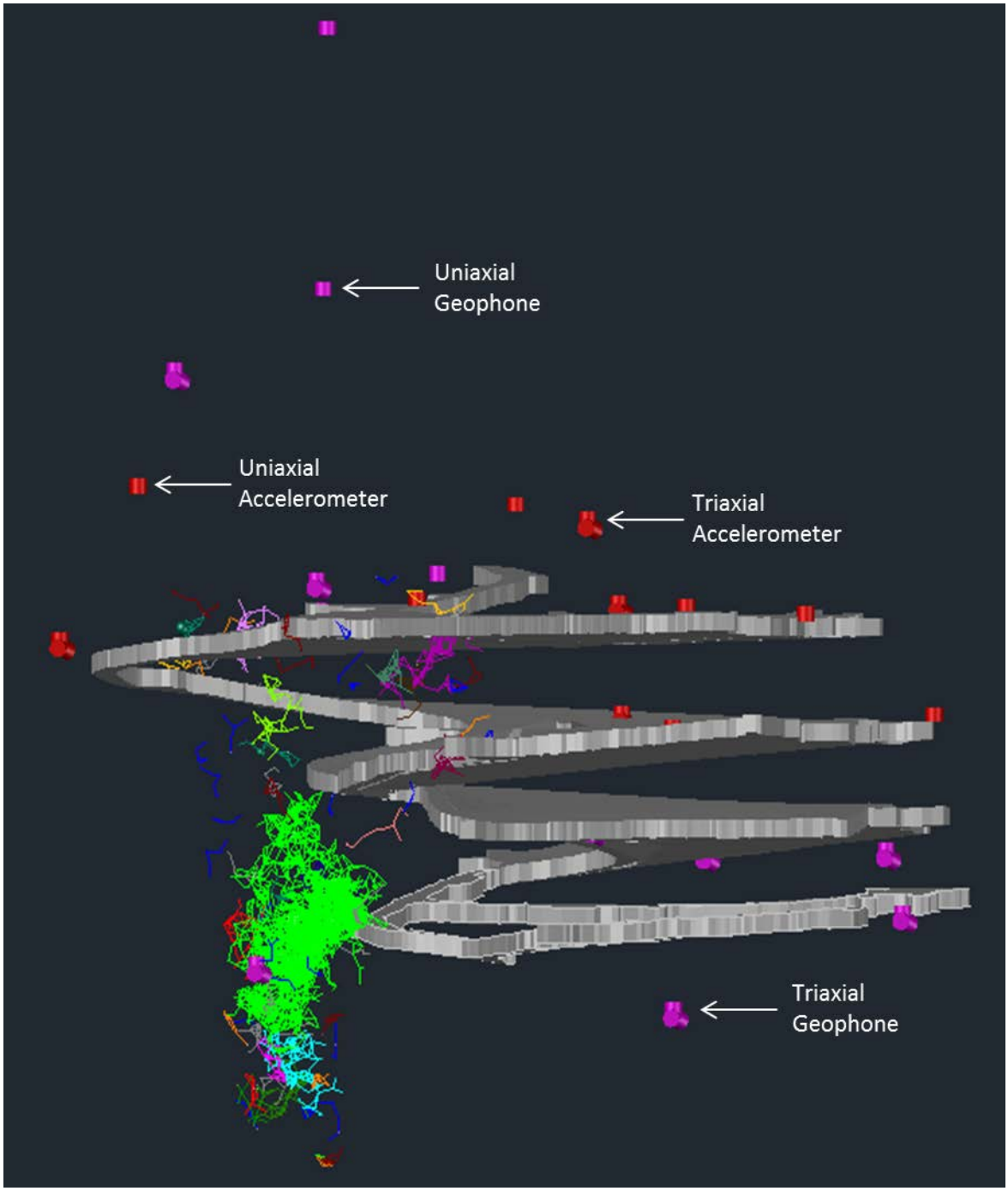

Figure 104: Seismic array around the shear